Technical University of Denmark

Mechatronics Applied to Fluid Film Bearings: Towards More Efficient Machinery

Cerda Varela, Alejandro Javier; Santos, Ilmar

Publication date:
2013

Document Version
Publisher's PDF, also known as Version of record

Mechatronics Applied to Fluid Film Bearings: Towards More Efficient Machinery

Alejandro Cerda Varela

Technical University of Denmark
Mechanical Engineering Department, Solid Mechanics Section
Building 404, DK-2800 Kongens Lyngby, Denmark

“El hombre no está hecho para la derrota. Se puede matar a un hombre, pero no derrotarlo” (E.Hemingway, El Viejo y el Mar)

A la memoria de mi Tata, Justo Edmundo Varela Alvarez

Summary (English)

The current trends regarding turbomachinery design and operation demand for an expansion of the operational boundaries of these mechanical systems, regarding production rate, reliability and adaptability. In order to face the new requirements, it is necessary to migrate towards a new concept, where the machine is defined as a mechatronic system. This integrated approach comprises the usage of machine elements capable of modifying their characteristics, by using in a combined way mechanical elements, sensors, processing units and actuators.

The research project entitled "Mechatronics Applied to Fluid Film Bearings: Towards more Efficient Machinery" was aimed at improving the state of the art regarding the usage of fluid film bearings as "smart" machine elements. Specifically, this project dealt with a tilting pad journal bearing design that features a controllable lubrication system, capable of modifying the static, thermal and dynamic properties of the bearing, depending on the operational requirements at hand.

The research activities carried out during the project included both theoretical as well as experimental investigations, using a test rig consisting of a rigid rotor supported by a tilting pad bearing featuring the controllable lubrication technology. These investigations were aimed at three main objectives: firstly, the improvement of the existing theoretical model for the tilting pad journal bearing with controllable lubrication; secondly, the experimental validation of the available theoretical model, regarding its capability of predicting the static, thermal and dynamic behavior of the controllable bearing; and lastly, the experimental evaluation of the feasibility of using the controllable bearing as a calibrated actuator.

Within these areas, the main original contributions and results achieved during

this research project are: the obtention of a theoretical model for the studied bearing, featuring a controllable thermoelastohydrodynamic regime; the expansion of the theoretical model for the hydraulic system associated with the controllable bearing, by including the effect of the pipelines dynamics; the experimental confirmation of the validity of the theoretical model, regarding the prediction of static and thermal characteristics of the controllable bearing; the experimental characterization of the active oil film forces generated by the bearing in the frequency domain; and the successful experimental application of this controllable machine element as a calibrated shaker, for rotordynamics parameter identification purposes.

The theoretical model of the studied controllable bearing proves to be adequate to predict the static and thermal behavior of the bearing. Furthermore, it is suitable to characterize the dynamic behavior of the bearing in the low frequency range, regarding the magnitude and phase of the active fluid film forces with respect to the control signal. However, the experimental characterization of the active fluid film forces generated by the controllable bearing revealed the existence of additional dynamic effects in the system, apart from the ones related to the servovalve and pipelines. These additional dynamics become specially relevant for applications where the controllable bearing must generate active forces in the high frequency range. Specifically, a phase lag effect was observed between the pressure in the injection nozzle and the active fluid film force acting over the rotor. This effect is not included in the current theoretical model of the controllable bearing, and it could arise from dynamic effects within the oil flow in the injection nozzle and bearing clearance. Consequently, new research fronts are opened within the field of controllable fluid film bearings.

Resumé (Dansk)

Den seneste tendens indenfor design og drift af turbomaskineri stiller i større udstrækning krav om udvidelse af de operationelle grænseområder for de mekaniske systemer hvad angår produktionen, driftssikkerheden og omstillingsevnen. For at imødekomme disse behov, er det nødvendigt at benytte et nyt koncept hvori maskinen er definereret som et mekatronisk system. Denne integrerede metode inkluderer brugen af maskinelementer som er i stand til at modificere egenskaberne ved at kombinere mekaniske elementer, sensorer, behandlingsenheder samt aktuatorer.

Formålet med forskningsprojektet "Mechatronics Applied to Fluid Film Bearings: Towards more Efficient Machinery" har været at forbedre den nyeste metode med hensyn til at benytte oliefilmslejer som "intelligente" maskinelementer. Dette projekt har i særdeleshed omhandlet design af et vippeskoleje som indeholder et regulerbart smørringssystem der er i stand til at modificere de statiske, termiske, og dynamiske lejeegenskaber afhængig af de operative krav som stilles. De forskningsaktiviteter som er udført i projektet inkluderer både teoretiske og eksperimentelle undersøgelser ved, at benytte en teststand bestående af en ubøjelig rotor understøttet af vippeskolejer som indeholder den regulerbare smørringsteknologi. Disse undersøgelser var rettet mod tre hovedformål. Det første hovedformål var, at forbedre den eksisterende teoretiske model for vippeskolejet med regulerbar smørring. Det andet hovedformål var, at validere den tilgængelige teoretiske model eksperimentelt med hensyn til at forudsige den statiske, termiske og dynamiske opførsel af det regulerbare leje. Det tredje hovedformål var, at evaluere egenskaberne eksperimentelt ved brugen af det regulerbare leje som en kalibreret aktuator.

Indenfor disse formål, er de største originale bidrag og resultater i projektet følgende. Udarbejdelse af en teoretisk model for det undersøgte leje, som indeholder

et regulerbart termoelastisk hydrodynamisk regime; udvidelse af den teoretiske model for det hydrauliske system som er tilknyttet det regulerbare leje ved at inkludere effekterne fra rørledningsdynamikken; eksperimentel karakterisering af de aktive oliefilmskrafter genereret af lejet i frekvensdomænet, og succesfuld eksperimentel implementering af det regulerbare maskinelement som en kalibreret ryster ved rotordynamiske identifikationsformål.

Det er bevist at den teoretiske model for det regulerbare leje er tilstrækkelig til at forudsige den statiske og termiske opførsel af lejet. Desuden er det passende at karakterisere den dynamiske opførsel af lejet i det lave frekvensområde, med hensyn til størrelsen og fasen af de aktive oliefilmskrafter i forbindelse med kontrolsignalet. Det viser sig dog, at den eksperimentelle karakterisering af de aktive oliefilmskrafter genereret af det regulerbare leje, afslørede eksistensen af øvrige dynamiske effekter i systemet foruden dem som er tilknyttet servoventilen og rørledningerne. Denne ekstra dynamik bliver særlig relevant ved implementeringerne, hvor det regulerbare leje er nødsaget til at generere aktive krafter i det høje frekvensområde. En faseforsinkelseseffekt var navnlig observeret mellem trykket i indsprøjtningsdysen og den aktive oliefilmskraft, som virker på rotoren. Denne effekt er ikke inkluderet i den nuværende teoretiske model for det regulerbare leje. Den kan opstå fra de dynamiske effekter indenfor olietilstrømningen i indsprøjtningsdysen og lejeklaringen. Som følge af dette, er nye forskningsområder opstået indenfor regulerbare oliefilmslejer.

Preface

This thesis was prepared at the department of Mechanical Engineering, Solid Mechanics Section (MEK-FAM) at the Technical University of Denmark in partial fulfillment of the requirements to obtain a Ph.D degree in Construction, Production, Civil Engineering and Transport. The research activities were carried out from the 1st of September 2009 to the 1st of December 2012, under the supervision of Professor Dr. Ing. Ilmar Ferreira Santos. I would like to thank Andreas Jauernik Voigt, Said Lahriri, Jon Steffen Larsen and Jorge Gonzalez for their valuable contribution concerning the improvement of the thesis document, as well as regarding general discussion of the topics covered on it.

Part of the research work was carried out during an external stay period, at the GMSC department, Institut Pprime, University of Poitiers, under the guidance of Dr. Ing. Michel Fillon. I would like to thank him and everyone at the GMSC department for a very warm welcome and an overall great experience, from the professional and personal perspective.

Professor Ilmar Santos has been pivotal for the completion of the work contained in this thesis, by providing both technical guidance and personal support during the last three years. I have no doubts whatsoever that one of the main reasons that made the development of this research project such a rewarding experience was the fact that he was my supervisor. For these reasons, and for the chance of coming to Denmark, I am truly indebted to him.

After three years at DTU, I am grateful for the chance of meeting some great individuals, and for developing relationships that go beyond the mere professional interaction. My gratitude, for their support and friendship in different stages of this long run, goes to: Edgar Estupiñan, Stefano Morosi, Asger Martin Haugaard, Said Lahriri, Emil Bureau, Simon Brow Warburg, Ramin Moslemian, Ze Pedro Blasques, Bo Bjerregaard Nielsen, Andreas Jauernik Voigt, Jon Steffen Larsen, Stefan Jaeger, Miguel Pichart Mocholi, Jorge Gonzalez, Fabian Pierart,

Konstantinos Poulios, Sergio de Almeida, Shravan Janakiraman, Christian Kim Christiansen. Also, I would like to thank Maria Bayard Dühring, Ricardo Alzugaray, Traudy Wandersleben, Miguel Peña Espinoza and Paula Cavada Hrepich for their support in difficult times and for the good moments shared together.
Finally, I would like to dedicate the last lines to my parents, Hector Cerda Rojas and Marcia Varela Aburto, to thank them for being a constant source of support during these years, despite the physical distance between us. Their sacrifices for giving me the best education possible, and the will to live and to overcome adversity that emanate from their life story...these are without any doubt the most fundamental reasons and inspirations for me being here today.

Lyngby,Denmark, 15-December-2012

Alejandro Cerda Varela

Nomenclature

α_{Π}	Coefficient of linear thermal expansion of the pad material
β	Equivalent bulk modulus of the pipeline oil flow
$\boldsymbol{\epsilon}$	Strain vector
$\boldsymbol{\Psi}$	Surface traction on the pad surface solid domain
$\boldsymbol{\sigma}$	Stress vector
ϵ	Normal strain
ϵ_{α}	Strain due to thermal deformation
η	Parameter for calculation of the oil viscosity variation with temperature
γ	Shear strain
γ_i	Oil modal flow for the pipeline modal analysis
$\hat{x}_0, \hat{z}_0$	Coordinates of the center of the injection hole
κ	Oil thermal conductivity
κ_{pad}	Thermal conductivity of the pad material
Λ	Surface boundary of the pad tridimensional solid domain
$(\hat{x}, \hat{y}, \hat{z})$	Local curvilinear reference frame of the fluid film domain
(x, y, z)	Global cartesian reference frame of the bearing model
μ	Oil film viscosity

μ^*	Oil viscosity at reference temperature
ν	Poisson ratio of the pad material
Ω	Journal rotational speed
ω_i	Pipeline acoustic natural frequencies
ω_V	Servovalve natural frequency for the linearized second order model
Π	Pad tridimensional solid domain
ρ	Oil density
ρ_Π	Density of the pad material
σ	Normal stress
τ	Shear stress
$\mathbf{f}_s$	Loading vector of the pad finite element model
g	Injection hole shape function
$\mathbf{G}(f)$	Controllable bearing global transfer function
$\mathbf{K}_s$	Stiffness matrix of the pad finite element model
$\mathbf{M}_s$	Mass matrix of the pad finite element model
$\mathbf{P}$	Servovalve supply pressure
$\mathbf{S}_{oil}, \mathbf{S}_{pad}$	Heat flux between oil and pad surface
$\mathbf{T}$	Servovalve oil reservoir pressure
$\mathbf{u}$	Displacement field of the pad solid domain
$\mathbf{u}_s$	Displacement vector of the pad finite element model
$\mathbf{u}_s^*$	Modal coordinates vector of the pad finite element model
$\mathbf{V}_s$	Pseudo modal matrix of the pad finite element model
ξ_V	Servovalve damping factor for the linearized second order model
A_{pipe}	Pipeline cross section area
c_0	Speed of sound of the pipeline flow
C_{pipe}	Pipeline radial compliance
C_p	Oil thermal heat capacity

d_0	Diameter of the injection nozzle
d_{pipe}	Equivalent damping coefficient for the pipeline flow modal analysis
E_Π	Elasticity modulus of the pad material
F_{active}	Oil film active force acting over the rotor
F_{ext}	External forces acting over the pipeline flow
h	Oil film thickness
H_∞	Free convection coefficient for pad thermal model
H_i	Acoustic normal modes for the pipeline flow modal analysis
K_{pq}	Servovalve load pressure - load flow coefficient
K_V	Servovalve spool position - load flow coefficient
l_0	Lenght of the injection nozzle
l_{pipe}	Length of the pipeline
p	Oil film pressure field
$p_{A,B}$	Oil pressure in the injection nozzle
p_{clear}	Oil film pressure in one point of the clearance
p_{inj}	Injection pressure measured experimentally
p_L	Servovalve load pressure
$q_{A,B}$	Oil flow in the injection nozzle
$q'_{A,B}$	Oil flow in the servovalve ports A and B
q_{leak}	Servovalve leakage flow
q_L	Servovalve load flow
q_V	Servovalve driven flow
R	Journal Radius
r	Air percentage contained in the pipeline oil volume
R_V	Servovalve static gain factor for the linearized second order model
S_0	Injection hole surface
S_q	Sink or source pipeline flow

T Oil film temperature

t Time

T^* Oil reference temperature for viscosity variation with the temperature

T_∞ Temperature of the surroundings for the pad thermal model

$T_{journal}$ Journal temperature

T_{pad} Pad temperature field

T_{ref} Reference temperature for calculating pad thermal expansion

u_V Servovalve control signal

V Oil volume

v Oil film velocity field

v_{inj} Velocity of the injection oil flow

x_{pipe} Pipeline longitudinal position

x_V Servovalve spool position

$G_i\left(f\right)$ Controllable bearing component transfer function

$S_{uu}\left(f\right)$ Power spectral density of the signal u

$S_{uv}\left(f\right)$ Cross spectral density between signal u and signal v

ETHD Elastothermohydrodynamic lubrication

TPJB Tilting-pad journal bearing

Contents

Summary (English) iii

Resumé (Dansk) v

Preface vii

Nomenclature xii

1 Introduction 1
- 1.1 Mechatronics and Rotating Machinery . . . 1
- 1.2 Fluid Film Bearings: The Tilting-Pad Journal Bearing Design . . 2
- 1.3 Mechatronic Tilting-Pad Journal Bearing Designs . . . 5
- 1.4 The Tilting-Pad Journal Bearing with Controllable Lubrication . 6
- 1.5 About This Research Project . . . 8
  - 1.5.1 Original Contributions . . . 8
  - 1.5.2 Experimental Facilities . . . 9
- 1.6 Structure Of This Thesis . . . 10

2 Controllable TPJB: Mathematical Model 13
- 2.1 Passive TPJB: Mathematical Model . . . 14
  - 2.1.1 Modeling The Hydrodynamic Effect: The Reynolds Equation . . . 14
  - 2.1.2 Modeling The Thermal Effects: The Oil Film Energy Equation And Fourier Law For The Pad Heat Conduction . . . 16
  - 2.1.3 Modeling The Pad Flexibility: Virtual Work Principle And Pseudo Modal Reduction . . . 20
  - 2.1.4 Modeling The Pad Pivot Flexibility . . . 22
- 2.2 Controllable TPJB: Mathematical Model . . . 23

2.2.1 Modeling The Servovalve 24
2.2.2 The Influence Of The Injection Pipeline Over The Controllable TPJB Dynamics 29
2.2.3 Linking The Hydraulic System With The Oil Film Pressure Field: The Modified Reynolds Equation 32
2.2.4 The Modified Oil Film Energy Equation 35
2.3 Summary: The Coupled Model For The Controllable TPJB . . . 37
2.4 Closure 38

3 Controllable TPJB: Numerical Implementation Of The Mathematical Model 39
3.1 Numerical Solution Of The Mathematical Model Partial Differential Equations: The Finite Element Method 40
3.1.1 Weak Form Formulation 40
3.1.2 Discretization 41
3.1.3 Finite Element Mesh Convergence Analysis 42
3.1.4 Numerical Stability Of The Finite Element Solution For The Oil Film Energy Equation: Test Case Analysis 44
3.2 Closure 48

4 Passive TPJB: Model Validation 49
4.1 Model Validation in Hydrodynamic Lubrication Regime 50
4.1.1 Validation against Someya 50
4.1.2 Validation against Nicholas *et al.* 51
4.1.3 Validation against Allaire *et al.* 51
4.2 Model Validation in Elastothermohydrodynamic Lubrication Regime 51
4.2.1 Validation against Taniguchi *et al.* 52
4.2.2 Validation against Fillon *et al.* 52
4.2.3 Validation against Ha and Yang 53
4.2.4 Validation against Brockwell *et al.* 54
4.3 Closure 54

5 Controllable TPJB: Results 65
5.1 Publication 1: Stability Analysis of an Industrial Gas Compressor Supported by Tilting-Pad Bearings Under Different Lubrication Regimes 66
5.2 Publication 2: Performance Improvement of Tilting-Pad Journal Bearings by means of Controllable Lubrication 78
5.3 Publication 3: On the Simplifications for the Thermal Modeling of Tilting-Pad Journal Bearings under Thermoelastohydrodynamic Regime 95
5.4 Publication 4: Steady State Characteristics of a Tilting Pad Journal Bearing with Controllable Lubrication: Comparison between Theoretical and Experimental Results 109

5.5 Publication 5: Actively Lubricated Bearings Applied as Calibrated Shakers to Aid Parameter Identification in Rotordynamics 123

6 Controllable TPJB: Characterization of Dynamic Behavior 137
6.1 Experimental Setup and Procedure . . . 138
6.2 Experimental Results: Transfer Functions Characterization . . . 140
6.2.1 Servovalve Transfer Function $G_1(f)$ . . . 140
6.2.2 Pipeline Transfer Function $G_2(f)$ . . . 141
6.2.3 Oil Film Transfer Function $G_3(f)$ . . . 142
6.2.4 Global Transfer Function $\mathbf{G}(f)$ . . . 143
6.3 Closure . . . 156

7 Conclusions and Future Aspects 159

A Derivation of the Reynolds Equation 163

B Derivation of the Oil Film Energy Equation 169
B.1 Rate of variation of internal energy . . . 170
B.2 Heat flux through boundaries . . . 171
B.3 Work of surface forces . . . 171
B.4 Energy Equation for the Passive TPJB . . . 171
B.5 Energy Equation for the Controllable TPJB . . . 173

C Mathematical Model of the Pipeline Dynamics 175
C.1 Governing equations: The Continuity and Navier-Stokes Equations 175
C.2 Introducing the Boundary Conditions . . . 177
C.3 Solution by using the Separation of Variables method . . . 178

Bibliography 181

Chapter 1

Introduction

1.1 Mechatronics and Rotating Machinery

The last part of the 20th century and the beginning of the current one have witnessed some extraordinary advances in the fields of electronics and informatics. The minituarization of computers, processors and electronic components, together with an increase in their capabilities, have been the cause of their introduction and implementation in devices related to every single aspect of our daily lifes.
At the same time, the challenges related to the design and operation of rotating machinery for industrial applications, such as energy extraction, conversion and power generation, are steadily increasing. The need for constantly increasing production and improving efficiency demands for a review of the traditional way in which rotating machinery is designed and operated.
Most components for rotating machines are designed and built using a "classical", purely mechanical approach. At the design stage, the most critical operational conditions are determined, and the machine elements necessary for complying with those design requirements are completely defined. In this case, the final product corresponds to a rotating machine capable of handling the operational conditions defined at the design stage, but with a limited capability to adapt to a new operational scenario characterized by new requirements. This scenario could be the result of an unexpected failure on one of the machine components,

or the modification of the demands for the production process. To face this problem, a highly invasive approach must be used, involving the redesign or replacement of mechanical components.
In order to monitor the mechanical condition of a rotating machine, it is desirable to have the possibility to perform parameter identification procedures “in situ”. For instance, the existence of cracks or mechanical losseness problems in the machine can be related to a modification of its stiffness and damping properties, which can be determined by analyzing an experimentally obtained frequency response function. Performing a parameter identification test on an industrial machine becomes a cumbersome task, if it involves stopping its normal operation in order to install the required sensors and actuators. Taking into account this scenario, it becomes desirable to include in the machine design some elements capable of acting as calibrated actuators, in order to perform this kind of test in a non-invasive way.
Taking into account these challenges, it is desirable to design machine elements that feature some “smart” capabilities. By linking the purely mechanical design approach with the highly developed electronic components that are available nowadays, one could obtain a mechatronic machine element. This concept comprises the inclusion of sensors capable of measuring physical variables related to the current operational condition of the machine, a processing unit capable of analyzing this information and generating control signals, and mechanical actuators capable of transducing the control signals into physical actions, capable of modifying the machine behavior by applying calibrated forces over it.
When designing rotating machinery, the specification of the bearings is of uttermost importance. These mechanical elements, together with providing support to the rotor, are one of the main sources of damping and stiffness in the machine. Consequently, their design will be crucial for determining the dynamic behavior of the machine as a whole. Therefore, it is natural to select them as objectives for implementing the mechatronic approach for smart machine elements design.

1.2 Fluid Film Bearings: The Tilting-Pad Journal Bearing Design

For applications where high loads and speeds are imposed over the rotor, fluid film bearings are the support elements of choice. There are several possible configurations for these machine elements. In this work, the focus is set on analyzing a particular one: the tilting-pad journal bearing. This design is widely used in turbomachinery, due to its improved stability characteristics when compared to other fluid film bearings alternatives [1, 2].
The highly succesful application of this bearing design is a result of the knowl-

edge accumulated over almost 60 years regarding its static and dynamic characteristics. Two major breakthroughs were achieved in this period, that correspond to the cornerstones of our current understanding and modeling approach of the dynamic behavior of this bearing design. Firstly, Lund [3] obtained a theoretical model for the equivalent linearized stiffness and damping coefficients of a tilting-pad bearing, based on a pad assembly method. A good review of this method and its implications on the development of rotordynamics is given by Nicholas [4]. The original work from Lund relied on assuming a condensation frequency in order to link the degrees of freedom corresponding to the journal and the pads when performing the perturbation analysis. At that time, the journal rotational frequency was chosen as the condensation frequency. This assumption enabled to obtain a set of eight synchronously reduced dynamic coefficients related to the journal degrees of freedom, that implicitly contained the contribution from each pad degree of freedom. Later on, Allaire *et al.* [5] expanded this approach, by introducing a pad perturbation method that eliminated the need for assuming a common perturbation frequency for all the bearing degrees of freedom when calculating the dynamic coefficients. Consequently, the so called full set of dynamic coefficients are obtained by this method, which explicitly included the contribution from the pads degrees of freedom. This set of coefficients can be reduced to the eight component form by using a dynamic condensation procedure. A long controversy was held about the election of the frequency used to perform this condensation, and its implications for stability calculation purposes. Nowadays, it is recognized that using the synchronously reduced coefficients is the right choice when calculating the rotor unbalance response, whereas for stability calculation purposes the full set of dynamic coefficients must be used [6, 7], or the reduced ones using the eigenfrequency of the mode approaching unstable behavior as the condensing frequency [8].
Based on the work of Lund and Allaire, it is possible to link in a straightforward manner the “local” dynamic behavior of the tilting-pad bearing, with the “global” rotor behavior. The connection between these two domains is done by using the bearing dynamic coefficients. Since the bearing stiffness and damping coefficients significantly alter the rotordynamics, it becomes fundamental to accurately predict them in the design stage. The advances in the field of modeling are inherently related to the comparison between theoretical results and the ones provided by experimental investigations.Regarding the experimental identification of TPJB dynamic coefficients, a long list of authors have made contributions. A complete review of these publications can be found in [9]. The works from Brockwell and Kleinbub [10] , Ha and Yang [11], Dmochowski [12], Childs and Carter [13] are good examples concerning experimental identification procedures.
The parameter identification techniques developed by these authors enable the experimental identification of the reduced set of dynamic coefficients, associated to the journal degrees of freedom. The experimental results presented in the literature reveal an important dependency of these coefficients on the excitation

frequency chosen for perturbing the system. Such frequency dependency can have important consequences in applications where non-synchronous or broad frequency range excitations are expected. Some divergence is found in the way the different authors deal with this issue. Some of them keep the frequency dependent form of the reduced stiffness and damping coefficients, for instance Dmochowski [12], whereas others like Childs [13] use a set of equivalent frequency independant added mass, stiffness and damping coefficients to represent the bearing dynamic behavior. This approach has been criticized by some authors regarding its ability to fully capture the bearing dynamics, its implications on the calculation of the stability margin of the rotor-bearings system, as well as considering the value of the added mass coefficients calculated by this method, when compared to the mass of the tested bearing [6, 7].
The comparison with experimental results have lead to a continuous improvement of the available theoretical models for the tilting-pads journal bearing. Since the bearing exhibits non-linear behavior, the accuracy in the linearization of the oil film forces necessary for obtaining the set of equivalent dynamic coefficients is highly dependant on the prediction of the static equilibrium position. Consequently, an accurate model must exhibit an acceptable degree of precision when calculating both the static and dynamic behavior of the bearing.
Nowadays, the state of the art regarding tilting-pad journal bearing modeling establishes that elastothermohydrodynamic (ETHD) lubrication regime must be included within the model in order to accurately represent its static and dynamic properties. This conclusion is the direct result of the work of several authors regarding bearing modeling through the years. For the sake of briefness, the publications cited here correspond to the ones that have influenced the development of the model presented in this work.
Lund and Pedersen [14] were among the first ones to include the effect of the pad and pivot flexibility, using a simplified model that calculated a modification of the bearing preload equivalent to the bending deformation of the pad. They demonstrated that these elastic deformations are equivalent to an increment in the preload of the bearing, with the resulting damping reduction. Ettles [15, 16] included both elastic deformations and thermal effects in his model, implementing a pad flexibility model based on beam theory. He used the "full bearing" approach, where all the pads are simultaneously included in the model, in contrast to the pad assembly method used previously, where a single pad is modelled and the global solution is obtained by superimposing the contribution from each pad. The assembly method was an elegant solution to deal with the limited amount of computing power available at the time. Brockwell and Dmochowski [17] implemented a similar model, and validated it against experimental results. They made some interesting analyses regarding the separate contribution of thermal and flexibility effects over the bearing static behavior. Fillon *et al.* [18, 19] and Palazzolo *et al.* [20, 21, 22, 23] were among the first authors to take advantage of the finite element method to develop thermoelastohydrodynamic models. Fillon *et al.* [19, 24] also provided some interesting

sets of experimental results regarding the temperature field in tilting-pad bearings. Palazzolo *et al.* implemented sophisticated finite element models for the tilting-pad bearing, including pivot flexibility using explicit contact boundary conditions [20, 21], upwinding formulation for avoiding numerical instability when solving the oil film energy equation [22], and a modal reduction scheme to determine the bearing dynamic properties including the pad flexibility in a reduced manner [23]. For pads featuring a socket pivot arrangement, some authors like Wygant *et al.* [25, 26] and Kim [27] have studied experimentally and theoretically the influence of the pivot friction over the cross-coupled stiffness coefficients.

1.3 Mechatronic Tilting-Pad Journal Bearing Designs

Several strategies can be followed in order to transform the tilting-pad bearing into a mechatronic machine element. In that regard, the current knowledge regarding the static and dynamic properties of this bearing provides some ideas. One of the key variables on the design phase of a fluid film bearing correspond to the preload, i.e. the relationship between the manufacturing clearance and the assembly clearance between the journal and the pad surface. This parameter is suitable to be modified during the operation of the machine, by placing actuators in the back of the pad that regulate the clearance between journal and pad surface. As a result, the clearance and the preload could be modified during operation, with the resulting modification of the bearing static and dynamic characteristics. Hence, a mechatronic tilting-pad bearing design is obtained.
This idea has been explored theoretically and experimentally by a number of authors. The first known implementation is attributed to Ulbrich and Althaus [28]. It featured the usage of piezoelectric actuators in order to perform the clearance adjustment. No control loop was implemented, because the required clearance for optimum rotor performance was defined beforehand. Another approach was implemented theoretically and experimentally by Santos [29, 30], considering the installation of hydraulic chambers in the back of the pads and a proportional valve to regulate the pressure within the chambers. This design faced some practical difficulties regarding the strain applied on the actuator chambers by the high pressure values required to modify the oil film thickness of the bearing. Regarding the design of controllers for mechatronic tilting-pad bearings, some theoretical studies have been carried out by Deckler *et al.* [31] and Wu and De Queiroz [32], regarding the usage of linear actuators in the back of the pad and also rotational actuators, acting directly over the tilting angle of the pad. Wu and De Queiroz applied some of their ideas experimentally, by building and testing a tilting-pad bearing design featuring controllable pushers

in the back of the pads [33].
This approach to obtain a controllable bearing modify the clearance geometry, with the resulting alteration of the oil film pressure field. A more direct approach to obtain a controllable configuration for the tilting-pad design would be to directly modify the oil flow pattern within the clearance, in order to perturb the pressure field and the resulting forces over the rotor. This concept, refered to as tilting-pad journal bearing with controllable lubrication, is the focus of the research project presented here.

1.4 The Tilting-Pad Journal Bearing with Controllable Lubrication

The tilting-pad journal bearing with controllable lubrication was first introduced in 1994 by Santos [29]. This controllable design modifies the pad geometry to include a nozzle located across the pad in the radial direction, capable of injecting pressurized oil directly into the bearing clearance. By doing this, the oil film pressure field is altered, as a function of the injected pressurized oil flow. The injected oil flow can be modified by means of a servovalve, which is controlled by an electric signal generated in a processing unit (controller or computer). Since the static and dynamic properties of the bearing are a function of the pressure field developed in the oil film, by feeding a suitable control signal into the servovalve, it becomes possible to alter the bearing behavior, according to the requirements at hand.
Since the introduction of this technology, there has been a constant effort dealing with the improvement of the theoretical model of this controllable bearing. Firstly, Santos and Russo [34] presented in a thorough way the Modified Reynolds Equation for Active Lubrication, which enables to calculate the oil film pressure field considering the effect of the radial oil injection. The effect of the servovalve is included in a simplified way, using a reduced modeling approach that includes dynamic effects by means of an equivalent second order transfer function. The effect of the pipeline connecting servovalve and the injection nozzle is neglected. A rigid-pad, isothermal modeling assumption was established for the analysis performed in this work, where the feasibility of modifying the oil film pressure field was theoretically demonstrated. Then, Santos and Nicoletti [35, 36] introduced an energy equation for the calculation of the oil film temperature field, including the effect of the oil injection. This model assumed an adiabatic regime for the oil film temperature calculation, thus neither heat transfer towards the pad or shaft, nor resulting thermal growth of those elements was considered. The rigid-pad assumption was kept at that time. Hence, the bearing model achieved a controllable thermohydrodynamic regime, being suitable to show the possibility of modifying the bearing thermal behavior by

using the oil injection system. Later on, Haugaard and Santos [37, 38] developed a finite element model for the fluid and solid domain of the active bearing, which enabled the inclusion of the pad flexibility effects using a modal reduction scheme. The pad pivot was modelled as a rigid support point. A study on the bearing dynamics was then performed, with focus on stability limits. The servovalve model was not modified from the original formulation presented by Santos [34], and the pipelines effect were also neglected. No thermal effects were included for this work, hence the model considered only a controllable elastohydrodynamic regime.

The available theoretical models for the tilting-pad bearing with controllable lubrication have been used in a number of publications, in order to show the benefits of applying the controllable lubrication concept in an industrial rotor system using different control schemes [39, 40, 41, 42]. Such benefits include: reduction of the vibrations when crossing critical speeds and increase of the rotor stability margin.

Regarding experimental results associated with the application of the tilting-pad journal bearing with controllable lubrication, a number of publications are available. The feasibility of modifying the tilting-pad bearing dynamic coefficients by using the active lubrication system was proven experimentally by Santos [43]. In this work, a comparison against theoretical results by using the model available at the time (controllable hydrodynamic lubrication regime) was presented, which yielded better results for the prediction of the stiffness coefficients than for the damping coefficients. Aditionally, the experimental results shown in [44, 45] include an experimental characterization of the active forces generated by a tilting-pad bearing featuring the controllable lubrication system. The characterization is performed in a quasi static way, neglecting the dependency of the active forces with the frequency of the control signal. The results of this experimental calibration procedure were then used to design controllers to modify the frequency response function of a test rig consisting of a flexible rotor. Similarly, the results shown in [39, 40] proved the feasibility of modifying the frequency response function as well as to reduce the vibrations amplitude of a rotor test rig by using the actively lubricated bearing as the actuator in a control loop.

It is noted that, with the sole exception of [43], there is a shortage of published results dealing with the direct comparison of the experimental results with the ones delivered by the available theoretical model, in order to validate it. Although there are experimental results that prove the validity of the concept of controllable lubrication applied to a tilting-pad bearing, those results correspond to the "system-level" approach, i.e they depict the modification of the global dynamic behavior of the rotor mounted on the controllable bearing. The "component-level" approach is missing, where the experimental investigation is focused in measuring the behavior of the controllable bearing itself, regarding its thermal and dynamic properties.

1.5 About This Research Project

The research project entitled "Mechatronics Applied to Fluid Film Bearings: Towards more Efficient Machinery" was aimed at improving the state of the art regarding the usage of fluid film bearings as smart machine elements, capable of improving the adaptability and availability of rotating machinery. Specifically, this project dealt with a tilting pad journal bearing design with controllable lubrication, as already described in the previous section.
The research activities were aimed at three main objectives: firstly, the improvement of the existing theoretical model for the tilting pad journal bearing with controllable lubrication; secondly, the experimental validation of the available theoretical model, regarding its capability of predicting the static, thermal and dynamic behavior of the controllable bearing; and lastly, the experimental evaluation of the feasibility of using the controllable bearing as a calibrated actuator.

1.5.1 Original Contributions

Within the previously established framework, the main original contributions achieved during the research project are:

1. Coupling of the available elastohydrodynamic and thermohydrodynamic theoretical models for the studied bearing into a single one, featuring a controllable thermoelastohydrodynamic lubrication regime.
2. Improvement of the available thermal model, by explicitly introducing the heat transfer effect between oil film and pad surface and the calculation of the pads temperature field.
3. Improvement of the available pad flexibility model, by introducing the effect of the pad pivot flexibility and the pad thermal deformations.
4. Expansion of the theoretical model for the hydraulic system associated to the controllable bearing, by introducing the effect of the pipelines connecting the servovalve with the injection nozzles in the pads.
5. Experimental validation of the theoretical model of the studied controllable bearing, regarding its thermal and static characteristics.
6. Experimental characterization of the active forces generated by the controllable bearing, and the analysis of the validity of the theoretical model to predict them.

7. The experimental confirmation of the feasibility of using the controllable bearing as a calibrated shaker, to perform parameter identification tests of a rotor system “in-situ”.

1.5.2 Experimental Facilities

The experimental activities were carried out in a test rig designed and built by Nielsen and Santos [46]. The test rig, which is shown in Figure 1.1, consists of a test bearing and a rigid rotor supported by a tilting frame. The rotor is driven by a belt transmission connected to an electric motor. The electric motor is equipped with a frequency converter and speed control. A single servovalve controls the pressurized oil flow towards each one of the injection points in the bearing pads. A computer equipped with a DSpace 1103 data acquisition and control card is available for recording and processing the data generated by the sensors mounted in the test rig.
The bearing case is divided in a top and a bottom half, with a tilting pad resting on each one of them through a rocker pivot. Calibrated separation plates are installed between these two halves, enabling to control the clearance and resulting preload on the test bearing. The test bearing itself consists of two tilting pads located above and below the rotor, which support it in the vertical direction. The rotor is prevented from movement in the horizontal direction, by the frame in which the rotor is mounted. Since the frame is allowed to tilt around its pivoting point, only a single degree of freedom is required to describe the position of the rotor, related to its vertical displacement. This can be measured by means of a displacement sensor. Furthermore, it is possible to fix the vertical position of the rotor by using an adjustment bolt located at the frame free end, and to measure the resulting forces over it, using a load cell associated with the adjustment bolt, see Figure 1.2.
A closer view of the tilting pad and its instrumentation can be seen in Figure1.3. It can be equipped with thermocouples, pressure transducers and a force transducer in the back of the pad, enabling the measurement of the resulting forces in the radial direction over the pad. The most important component within the tilting pads design is the nozzle, through which high pressure oil can be injected into the gap between the tilting pad and the rotor, thus rendering the bearing “controllable”. The oil flow towards the injection nozzle in each tilting pad is controlled by means of a single servo valve, which is connected to a high pressure oil supply pump. The position of the servovalve spool can be measured using its built-in displacement transducer.

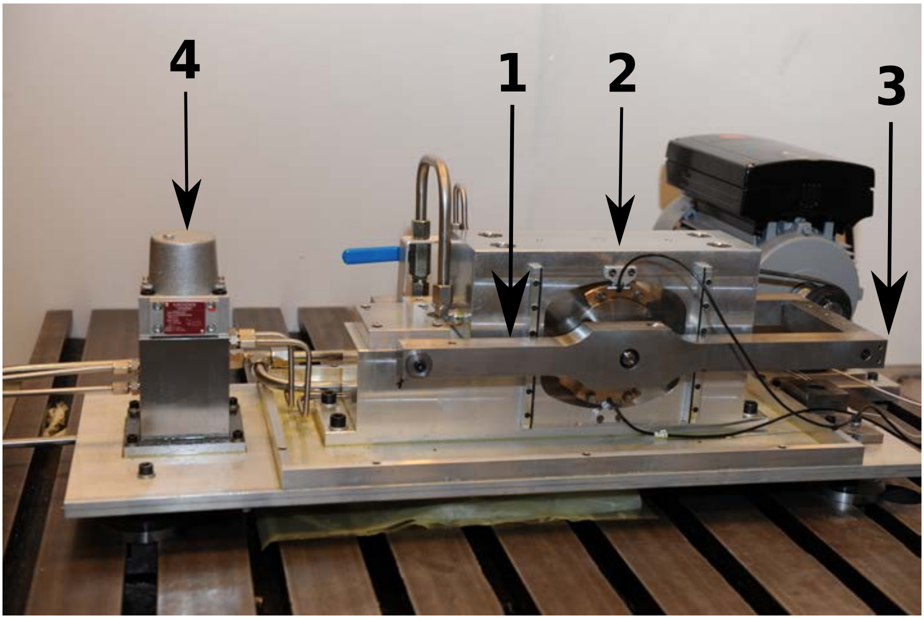

Figure 1.1: *Test rig of the tilting-pad bearing with controllable lubrication; the arrangement consists of a test bearing with two tilting-pads and a rigid rotor (2), supported by a tilting frame pivoted in one end (1). The tilting frame free end (3) can be used to apply load over the bearing, or to fix the rotor vertical position using an adjustment bolt. A servovalve (4) controls the pressurized oil flow towards the injection nozzle on each pad.*

1.6 Structure Of This Thesis

Regarding the structure of this thesis, Chapter 2 deals with the presentation of the theoretical model for the tilting-pad journal bearing with controllable lubrication. Chapter 3 presents an overview of the numerical methods used for solving the set of equations describing the controllable bearing. Chapter 4 provides a validation of the theoretical model on passive configuration (no injection bores), against some well known set of theoretical and experimental results available in the literature. Chapter 5 contains the results from this research project, in the form of five journal and conference publications. Chapter 6 provides an

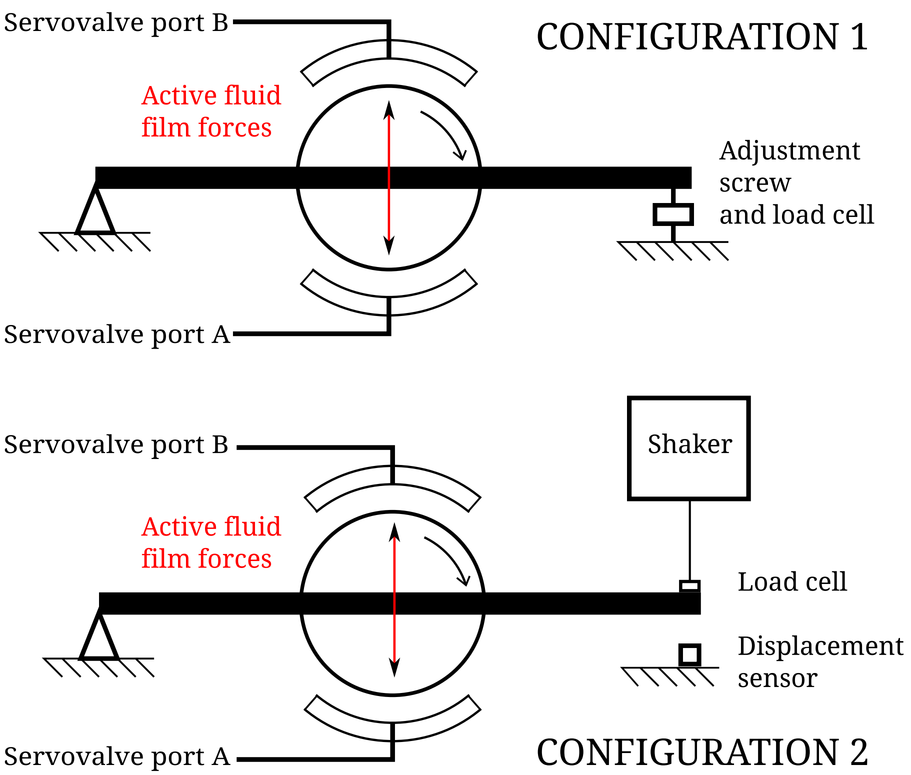

Figure 1.2: *Test rig configurations: measurement of the oil film forces by fixing the rotor-leverer arm vertical position (Configuration 1, upper), and measurement of the rotor-leverer arm displacement when a static or dynamic force is applied to the arm (Configuration 2, lower)*

experimental study on the characterization of the transfer function between servovalve control signal and the active force generated in the controllable TPJB. Finally, Chapter 7 states the conclusions of the research project, as well as the future aspects related to the general improvement of this technology.

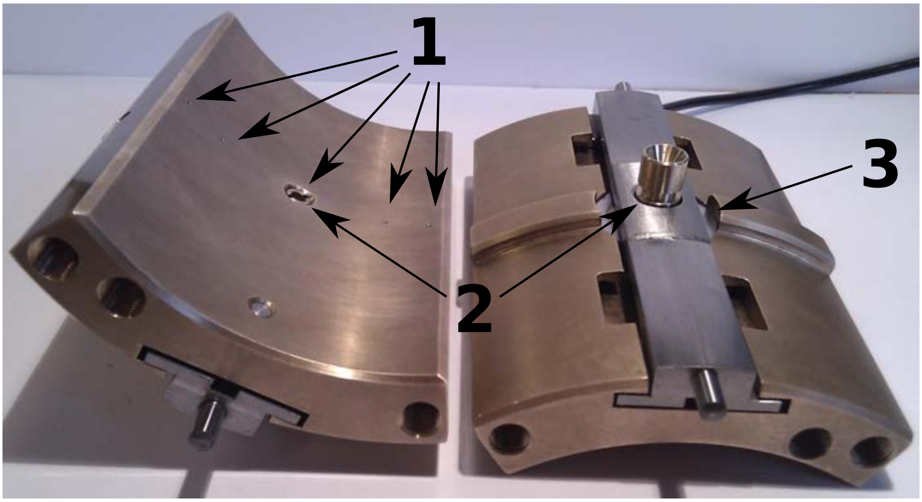

Figure 1.3: *Tilting pads installed in the test rig; (1) shows the position of the thermocouples or pressure transducers measurement points, (2) shows the high pressure injection nozzle, (3) shows the location of the load cell for measuring oil film resulting radial force*

Chapter 2

Controllable TPJB: Mathematical Model

In this chapter, the mathematical model for the TPJB with Controllable Lubrication is presented. The extent of this chapter is constrained with the objective of making this thesis as self-contained as possible. Special emphasis is directed towards clearly stating the simplifications introduced into the model to keep its formulation within a manageable complexity, while including the relevant physical phenomena for the studied controllable bearing. The reader is advised to refer to the cited references and appendices in this thesis, if a full mathematical presentation is required.

The oil injection process that renders controllable the TPJB design under study, can be considered as a perturbation acting over the oil film pressure and temperature fields, resulting in a modification of the bearing behavior. Hence, all the physical phenomena that are relevant for a passive TPJB (no injection bores in the pads) must also be included in the formulation of the controllable TPJB model. Consequently, the first section of this chapter is devoted to presenting the mathematical model of a passive TPJB. Followingly, the controllable TPJB configuration is introduced, by stating the way in which the oil injection process is included in the oil film pressure field and temperature field models. Additionally, the link between those effects and the behavior of the rest of the elements that compose the controllable TPJB (servovalve and injection pipelines) is included into the formulation.

2.1 Passive TPJB: Mathematical Model

According to the literature review carried out for this thesis, the state of the art regarding the mathematical modeling of a passive TPJB dictates that an elastothermohydrodynamic formulation is required, in order to predict the static and dynamic properties of the bearing with sufficient accuracy. Consequently, these effects have been included in the mathematical model, following the approach stated in this section.

2.1.1 Modeling The Hydrodynamic Effect: The Reynolds Equation

The load carrying capability of the TPJB is the result of the pressure field developed within the oil film during its operation, due to the hydrodynamic effect. The mathematical model commonly used to describe this pressure build-up process is known as the Reynolds Equation. A good presentation of the way this equation is derived can be found in [47]. For the sake of completeness, its derivation is included in Appendix A.
The Reynolds equation is a simplification of the Navier-Stokes equations, obtained through the analysis of the characteristics of the oil flow generated within the clearance during bearing operation. Provided that the oil film thickness is much smaller than all the other dimensions of the problem (journal and pad radius), the following simplificatory assumptions are introduced:

- *The fluid is considered newtonian and incompressible*
- *The fluid inertia effects can be neglected (laminar regime)*
- *The variation of the fluid film pressure and viscosity along the radial direction of the bearing clearance is negligible*

A curvilinear reference frame $(\hat{x}, \hat{y}, \hat{z})$ is defined on the surface of the bearing pad, in order to analyze the fluid film domain, see Figure 2.1. The axis are aligned with the circumferential $\hat{x}$, radial $\hat{y}$ and axial $\hat{z}$ directions in the surface of the pad. The oil film thickness function $h\left(\hat{x}, \hat{z}, t\right)$ can be obtained based on geometrical considerations, whereas the oil film viscosity $\mu\left(\hat{x}, \hat{z}\right)$ is stated as position dependent, for the sake of generality. Hence, the oil film pressure field $p\left(\hat{x}, \hat{z}, t\right)$ can be calculated solving the Reynolds Equation stated as:

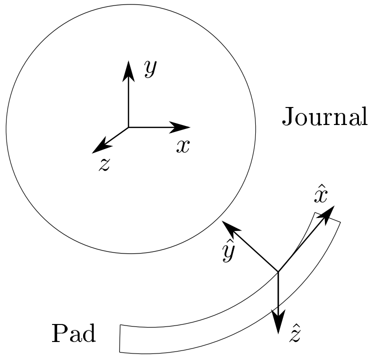

Figure 2.1: *Reference frames for the passive TPJB mathematical model; (x, y, z) correspond to the global cartesian reference frame, for the pads solid domain, and $(\hat{x}, \hat{y}, \hat{z})$ corresponds to the curvilinear reference frame for the fluid film domain*

$$\frac{\partial}{\partial \hat{x}}\left(\frac{h^3}{\mu}\frac{\partial p}{\partial \hat{x}}\right)+\frac{\partial}{\partial \hat{z}}\left(\frac{h^3}{\mu}\frac{\partial p}{\partial \hat{z}}\right)=6\Omega R\frac{\partial h}{\partial \hat{x}}+12\frac{\partial h}{\partial t} \tag{2.1}$$

According to Equation (2.1), two physical mechanisms are responsible for the pressure build-up within the oil film, and are represented by their corresponding source terms:

- *Wedge effect* $6\Omega R\frac{\partial h}{\partial \hat{x}}$
  This source term states mathematically that if the oil film thickness h presents a gradient in the circumferential direction $\hat{x}$, and the journal surface presents a tangential speed given by ΩR, it is possible to generate pressure within the oil film. This term depends on the journal tangential speed, the position of journal and tilting of the pads, that define the oil film thickness function. Hence, this pressure generation mechanism is related to the stiffness properties of the bearing.

- *Squeeze effect* $12\frac{\partial h}{\partial t}$
  If the relative velocity in the normal radial direction between the journal and the pad surface is different from zero, then it is possible to generate pressure in the oil film. This physical process is responsible for providing the damping properties associated to the bearing.

The boundary conditions for the Reynolds Equation are:

- Pressure is set to zero on the boundaries of the fluid film domain.
- The Gumbell model is applied in the event of cavitation, i.e. the oil film pressure is set to zero if cavitation occurs.

2.1.2 Modeling The Thermal Effects: The Oil Film Energy Equation And Fourier Law For The Pad Heat Conduction

As it can be seen in the Reynolds Equation, see Equation (2.1), the pressure developed in the oil film is a function of the oil viscosity μ. Consequently, an accurate characterization of this parameter is required. The dependency between oil temperature and viscosity is commonly described using an exponential law, as follows:

$$\mu (T) = \mu^* e^{-\eta(T-T^*)} \tag{2.2}$$

In Equation (2.2), the oil viscosity at a certain temperature $\mu (T)$ can be obtained using a reference viscosity value taken at a reference temperature $\mu^* (T^*)$, and the η parameter which is a characteristic of the chosen oil type.
If the oil film temperature is assumed to be constant over the entire surface of the bearing pads, then the oil viscosity can be assumed constant in the Reynolds Equation. A model stated using this assumption is defined as isothermal. However, any rise in the oil film temperature during bearing operation entails a reduction in the oil viscosity, consequently reducing the bearing load carrying capability and damping properties. The literature shows that modeling this oil temperature build-up effect is fundamental for a precise characterization of the bearing properties.
Consequently, a thermal model must be formulated in order to obtain the oil film temperature field $T (\hat{x}, \hat{y}, \hat{z})$, resulting in a precise characterization of the oil film viscosity $\mu (\hat{x}, \hat{z})$. For this work, the analysis is constrained to steady state behavior, hence the time dependency of the oil film temperature field is neglected. Regarding the definition of the domain for the analysis, experimental results available in the literature [19] show that the variation of the oil film temperature in the bearing axial direction $\hat{z}$ is negligible, when compared to the radial and circumferential direction. Hence, for a passive TPJB it is possible to model the oil temperature field considering a two dimensional domain $T (\hat{x}, \hat{y})$, defined in the radial and circumferential direction.
However, the passive TPJB model developed here will be expanded later to predict the behavior of a bearing featuring a controllable lubrication system. The perturbation introduced by the oil injection process entails that the assumption

of constant oil film temperature in the axial direction is not valid. Hence, to keep a two dimensional domain for the oil film thermal model, the temperature field is defined in the circumferential and axial direction $T(\hat{x},\hat{z})$, while a constant value is assumed in the radial direction across the oil film thickness.
Taking into account the previous considerations, the oil film temperature field $T(\hat{x},\hat{z})$ can be modeled using an energy equation formulation introduced in [35, 36] and stated in steady state as:

$$\kappa h \frac{\partial^2 T}{\partial \hat{x}^2} + \kappa h \frac{\partial^2 T}{\partial \hat{z}^2} + \left(\frac{\rho C_p h^3}{12\mu} \frac{\partial p}{\partial \hat{x}} - \frac{\rho C_p \Omega R h}{2} \right) \frac{\partial T}{\partial \hat{x}} +$$
$$\frac{\rho C_p h^3}{12\mu} \frac{\partial p}{\partial \hat{z}} \frac{\partial T}{\partial \hat{z}} + (\Omega R)^2 \frac{\mu}{h} + \frac{h^3}{12\mu} \left(\left(\frac{\partial p}{\partial \hat{x}} \right)^2 + \left(\frac{\partial p}{\partial \hat{z}} \right)^2 \right) + \mathbf{S}_{oil} = 0 \qquad (2.3)$$

Equation (2.3) shows that the oil temperature field $T(\hat{x},\hat{z})$ becomes a function of inherent oil properties, such as density ρ, thermal heat capacity C_p and thermal conductivity κ, and the oil film pressure field $p(\hat{x},\hat{z})$, thickness $h(\hat{x},\hat{z})$ and viscosity $\mu(\hat{x},\hat{z})$. Refer to Appendix B for the full mathematical procedure to obtain this equation. The physical phenomena included in this formulation are:

- *Diffusion effect* $\kappa h \frac{\partial^2 T}{\partial \hat{x}^2} + \kappa h \frac{\partial^2 T}{\partial \hat{z}^2}$
These terms consider the energy transport due to the oil thermal conductivity κ, and the oil film temperature field gradient in the axial and circumferential direction.
- *Convection effect* $\left(\frac{\rho C_p h^3}{12\mu} \frac{\partial p}{\partial \hat{x}} - \frac{\rho C_p \Omega R h}{2} \right) \frac{\partial T}{\partial \hat{x}} + \frac{\rho C_p h^3}{12\mu} \frac{\partial p}{\partial \hat{z}} \frac{\partial T}{\partial \hat{z}}$
These terms represent the energy transport associated with the oil mass flow in the axial and circumferential direction. Such mass flow includes the "journal-driven" Couette flow $\frac{\rho C_p \Omega R h}{2}$ and the "pressure gradient-driven" Pouiseuille flow $\frac{\rho C_p h^3}{12\mu} \frac{\partial p}{\partial \hat{x}}$ and $\frac{\rho C_p h^3}{12\mu} \frac{\partial p}{\partial \hat{z}}$
- *Work performed by viscous shear forces due to the flow in the axial and circumferential direction* $(\Omega R)^2 \frac{\mu}{h} + \frac{h^3}{12\mu} \left(\left(\frac{\partial p}{\partial \hat{x}} \right)^2 + \left(\frac{\partial p}{\partial \hat{z}} \right)^2 \right)$
- *Heat transfer between oil film and pad and journal surface* $\mathbf{S}_{oil}$

In order to properly define the source term related to the heat transfer towards pad and journal surface $\mathbf{S}_{oil}$, the temperature field of those elements must also be modeled.

Regarding the journal temperature, a single value $T_{journal}$ is used to describe the journal temperature, implicitly assuming that it is spatially constant. Such temperature can be set to be equal to an experimentally determined value, or calculated as the average value of the oil film temperature, following the approach established in [19, 48]. Physically, this calculation procedure entails that the global heat flux between the oil film and the journal is nil.
The pad temperature distribution can be calculated using the Fourier Law for heat conduction. Let (x, y, z) be the global cartesian reference frame for the pad solid domain, see Figure 2.1, and κ_{pad} the thermal conductivity of the pad material. Then, the pad temperature field $T_{pad}(x, y, z)$ is determined by:

$$\kappa_{pad}\left(\frac{\partial^2 T_{pad}}{\partial x^2}+\frac{\partial^2 T_{pad}}{\partial y^2}+\frac{\partial^2 T_{pad}}{\partial z^2}\right)$$
$$+H_{\infty}\left(T_{pad}-T_{\infty}\right)|_{boundary}+\mathbf{S}_{pad}=0 \tag{2.4}$$

The source terms included in Equation (2.4) represent two different heat transfer processes taking place on the pad boundaries:

- *Heat transfer to the surroundings* $H_{\infty}\left(T_{pad}-T_{\infty}\right)|_{boundary}$
  A free convection coefficient H_{∞} is used to model the cooling effect due to the heat transfer towards the surroundings, taking place in the pad faces that are not in contact with the oil film responsible for bearing load carrying capacity. The temperature of the surroundings T_{∞} is assumed constant.

- *Heat transfer to/from the oil film* $\mathbf{S}_{pad}$

In order to complete the definition of the thermal model for the passive TPJB, the heat transfer terms $\mathbf{S}_{oil}$ and $\mathbf{S}_{pad}$ must be defined. The standard approach for modeling this process corresponds to using the oil film temperature field, to calculate the heat flux at the boundary between oil film and journal surface, and oil film and pad surface. Hence, in general:

$$\mathbf{S}_{oil}=-\mathbf{S}_{pad}=\kappa\left.\frac{\partial T}{\partial \hat{y}}\right|_{boundary} \tag{2.5}$$

Since the present thermal model does not account for the oil film radial temperature distribution, the temperature gradient required in Equation (2.5) is not readily available. Hence, some simplificatory assumptions must be introduced. A throughout study on this issue was performed in Publication 3, appended to this thesis, see section 5.3. As a result of the study presented in Publication 3, the approach introduced by Knight and Barrett [49] is used here. In order to calculate the temperature gradient required for defining the heat transfer term, Equation (2.5), the oil film temperature profile in the radial direction is assumed to be parabolic. Hence, a second order polynomial can be used to approximate the radial oil temperature distribution, as follows:

$$\begin{aligned} T(\hat{y}) = T_{pad}|_{boundary} &+ 2\left(3T - 2T_{journal} - 2\,T_{pad}|_{boundary}\right)\frac{\hat{y}}{h} \\ &+3\left(T_{journal} - 2T + T_{pad}|_{boundary}\right)\left(\frac{\hat{y}}{h}\right)^2 \end{aligned} \tag{2.6}$$

According to Equation (2.6), the oil film temperature distribution in the radial direction $\hat{y}$ is characterized by three values: the journal temperature $T_{journal}$ at $\hat{y} = h$, the oil temperature at $\hat{y} = \frac{h}{2}$, and the pad temperature in the interface with the oil film $T_{pad}|_{boundary}$ at $\hat{y} = 0$. The oil temperature at the middle of the bearing clearance is taken to be equal to the oil film temperature T calculated by Equation (2.3). Consequently, the heat flux term in Equation (2.5) can be rewritten as:

$$\mathbf{S}_{oil} = -\mathbf{S}_{pad} = \frac{\kappa}{h}\left(3T - 2T_{journal} - 2\,T_{pad}|_{boundary}\right) \tag{2.7}$$

A similar approach is followed to model the heat transfer effect from the oil film towards the journal. Hence, the thermal model, including the coupling terms between the different domains that compose the bearing, is defined. The boundary conditions for this model are defined as follows:

- The oil film temperature T is prescribed along the leading edge of each pad, assuming that it is constant in the axial direction. The prescribed value corresponds to the experimentally measured one, or the one obtained performing an energy and mass balance in the space between two consecutive pads, as explained in [35, 36].
- For the pad heat conduction model, the temperature on the leading edge is prescribed, using the same approach stated above. The temperature of the surroundings T_∞ and the free convection coefficient H_∞ are also prescribed.

- The journal temperature $T_{journal}$ is set equal to the experimentally measured value or the one calculated as the average of the oil film temperature T, using the approach already presented.

- The influence of cavitation within the thermal behavior of the bearing is not incorporated in the current model.

2.1.3 Modeling The Pad Flexibility: Virtual Work Principle And Pseudo Modal Reduction

The oil film thickness function $h(\hat{x}, \hat{z}, t)$ must be defined in order to calculate the oil film pressure field using the Reynolds Equation. If a rigid pad assumption is utilized, then this variable is a function of the journal position and the tilting angle of each pad. However, the state of the art regarding the modeling of the TPJB states the need for including the elastic deformations of the pads within the model formulation, along with the resulting modification of the oil film thickness function.
This effect was throughly studied by Haugaard and Santos, resulting in its implementation in the context of the controllable TPJB model [37, 38, 50]. The pad flexibility model used here is the one developed by these authors. It corresponds to a tridimensional formulation, where the solid is taken to be linearly elastic and isotropic. Let Π be the pad tridimensional solid domain, and Λ the surface corresponding to the boundary of the pad solid domain. If no body forces are considered, and the loading corresponds only to the surface tractions $\boldsymbol{\Psi} = [\Psi_x, \Psi_y, \Psi_z]^T$ applied over the pad surface by the oil film pressure field, then the virtual work principle can be applied to yield:

$$\int_{\Pi} \left(\{\delta \mathbf{u}\}^T \rho_{\Pi} \{\delta \ddot{\mathbf{u}}\} + \{\delta \boldsymbol{\epsilon}\}^T \{\ \boldsymbol{\sigma}\} \right) d\Pi = \int_{\Lambda} \{\delta \mathbf{u}\}^T \{\boldsymbol{\Psi}\}\, d\Lambda \tag{2.8}$$

In Equation (2.8), one introduces the density of the pad material ρ_{Π}, the displacement vector $\mathbf{u}(x, y, z, t) = [u_x, u_y, u_z]^T$, the stress vector $\{\boldsymbol{\sigma}\} = [\sigma_x, \sigma_y, \sigma_z, \tau_{xy}, \tau_{yz}, \tau_{zx}]^T$, and the strain vector $\{\boldsymbol{\epsilon}\} = [\epsilon_x, \epsilon_y, \epsilon_z, \gamma_{xy}, \gamma_{yz}, \gamma_{zx}]^T$. No energy dissipation effects are considered within the solid domain, hence no velocity dependent terms $\delta \dot{\mathbf{u}}$ are included in Equation (2.8).
Considering linear isotropic behavior for the pad material, let E_{Π} be the elasticity modulus and ν the Poisson ratio of the pad material. Then, the stress-strain relationship given by the constitutive 6x6 matrix $\mathbf{C}$ holds:

$$
\begin{aligned}
&\{\boldsymbol{\sigma}\} = \mathbf{C}\{\boldsymbol{\epsilon}\} \\
&\mathbf{C}_{11} = \mathbf{C}_{22} = \mathbf{C}_{33} = \frac{(1-\nu)\,E_{\Pi}}{(1+\nu)\,(1-2\nu)} \\
&\mathbf{C}_{44} = \mathbf{C}_{55} = \mathbf{C}_{66} = \frac{E_{\Pi}}{2\,(1+\nu)} \\
&\mathbf{C}_{12} = \mathbf{C}_{21} = \mathbf{C}_{13} = \mathbf{C}_{31} = \mathbf{C}_{23} = \mathbf{C}_{32} = \frac{\nu E_{\Pi}}{(1+\nu)\,(1-2\nu)}
\end{aligned} \tag{2.9}
$$

Considering small strains and rotations, the strain-displacement relationship is given by:

$$
\{\boldsymbol{\epsilon}\} = \boldsymbol{\partial}\{\mathbf{u}\}
$$

$$
\boldsymbol{\partial} = \begin{bmatrix} \frac{\partial}{\partial x} & 0 & 0 \\ 0 & \frac{\partial}{\partial y} & 0 \\ 0 & 0 & \frac{\partial}{\partial z} \\ \frac{\partial}{\partial y} & \frac{\partial}{\partial x} & 0 \\ 0 & \frac{\partial}{\partial z} & \frac{\partial}{\partial y} \\ \frac{\partial}{\partial z} & 0 & \frac{\partial}{\partial x} \end{bmatrix} \tag{2.10}
$$

Using Equations (2.9) and (2.10) it is possible to state the Virtual Work Principle in terms of the nodal displacements $\mathbf{u}$ and the applied surface tractions $\boldsymbol{\Psi}$, originating from the oil film pressure field.
Regarding the boundary conditions for the pad flexibility model, a pivot boundary condition is established. It consists of restricting the displacement of some nodes on each pad, so that their movement is constrained to a rotation around a fixed point. i.e the pad pivot. More details are given in [37, 38, 50].
By applying the Bubnov-Galerkin method to the Virtual Work Principle stated in Equation 2.8, one can reduce the original problem to an equivalent discrete formulation [51]:

$$
\mathbf{M}_s\ddot{\mathbf{u}}_s + \mathbf{K}_s\mathbf{u}_s = \mathbf{f}_s \tag{2.11}
$$

where $\mathbf{u}_s$ correspond to the displacement degrees of freedom for each node of the pad finite element model, $\mathbf{M}_s$ and $\mathbf{K}_s$ correspond to the inertia and stiffness matrix for the pads and $\mathbf{f}_s$ represent the loads over the pads due to the pressure field in the oil film.

The system defined in Equation (2.11) in its homogeneous form, i.e. $\mathbf{f}_s = [0]^T$, is suitable for calculating the associated eigenvalues and eigenvectors from the each pad. The calculation of the pad eigenmodes does not consider the effect of the oil film. By selecting the eigenmodes considered relevant for the analysis of the bearing behavior, the pseudo-modal matrix $\mathbf{V}_s$ can be constructed, containing in its columns the selected eigenmodes. Hence Equation (2.11) can be rearranged as follows:

$$\begin{aligned}\mathbf{V}_s^T\mathbf{M}_s\mathbf{V}_s\ddot{\mathbf{u}}_s^* + \mathbf{V}_s^T\mathbf{K}_s\mathbf{V}_s\mathbf{u}_s^* &= \mathbf{V}_s^T\mathbf{f}_s \\ \mathbf{u}_s &= \mathbf{V}_s\mathbf{u}_s^*\end{aligned} \tag{2.12}$$

By using the reduction scheme shown in Equation (2.12), the system is reduced and consequently defined by the modal coordinates vector $\mathbf{u}_s^*$, where there are as many degrees of freedom as eigenmodes were included into the pseudo-modal matrix $\mathbf{V}_s$. It corresponds to a pseudo-modal reduction, since only the eigenmodes which are relevant are included into the analysis. If only the first eigenmode is included, then a rigid pad model is established, and the corresponding modal coordinate measures the tilting of the pad around the pivot. The use of higher eigenmodes enables the inclusion of the flexibility of the pads.
Since the model developed in this work includes thermal effects, the temperature distribution in the pad solid domain is readily available, as it was shown in section 2.1. Hence, considering the pad temperature field T_{pad} and a reference temperature T_{ref} where the nominal geometry is defined, the deformation related to the thermal growth of the pads can be calculated using a coefficient of linear termal expansion α_{Π} as follows:

$$\epsilon_{x\alpha} = \epsilon_{y\alpha} = \epsilon_{z\alpha} = \alpha_{\Pi}\left(T_{pad} - T_{ref}\right) \tag{2.13}$$

A similar approach can be followed to obtain the thermal expansion of the journal, using the available value that characterizes its temperature $T_{journal}$. Consequently, these thermal deformations can be included in the determination of the oil film thickness function.

2.1.4 Modeling The Pad Pivot Flexibility

The pad flexibility model developed by Haugaard and Santos did not include the effect of the pivot flexibility. The boundary condition implemented at that time corresponds to a rigid pivot point, around which the nodes are restricted to exhibit rotational movement. The importance of including the pivot flexibility for an accurate prediction of the bearing dynamic properties has been well established, hence it is desirable to expand the current flexibility model to include this effect.
The modeling approach implemented in this work takes advantage of the pseudo

modal reduction method already introduced by Haugaard and Santos. When solving the eigenvalue problem for the pad flexibility model, the calculated eigenmodes do not exhibit pivot flexibility, due to boundary condition applied to the finite element model. However, it can be considered that the pivot flexibility effect would generate an additional eigenmode, characterized by rigid body motion of the pad, in the radial direction. Since such motion can not be achieved by a "calculated" eigenmode, this assumed pivot mode is linearly independent with the rest of the eigenmodes. Consequently, it is suitable for being included within the pseudo modal matrix $\mathbf{V}_s$.
The modal mass and stiffness matrix can be modified to accomodate the assumed pivot flexibility mode. For doing so, the corresponding modal mass is assumed to be equal to the pad mass, whereas the modal stiffness is set to be equal to the pivot stiffness value obtained experimentally.

2.2 Controllable TPJB: Mathematical Model

Having defined the mathematical model for the TPJB in its passive configuration, the ground is set to define the model for the bearing in its controllable configuration.
All the physical phenomena that were included in the passive TPJB model, are also relevant effects when modeling the TPJB in its controllable configuration. Hence, the terms already included in the constitutive equations for calculating the oil film pressure field, temperature field and pad flexibility are kept here. However, extra terms must be included in order to model the perturbation introduced by the oil injection into the bearing clearance. Furthermore, the oil injection demands for the addition of some new elements into the original bearing design, namely servovalves and injection pipelines. The influence of these elements must also be included within the mathematical model.
Although the model presented here can be extended to controllable TPJB with different number of pads and injection holes, this presentation is constrained to a bearing featuring a two-pad, load on pad arrangement, that features a single injection hole on each pad. Both injection points are connected using pipelines to a single servovalve. This is done in order to simplify the mathematical formulation and to make a direct link to the experimental setup used in this work.

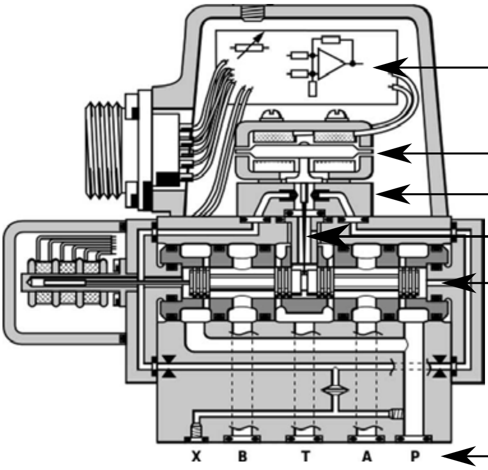

Figure 2.2: *Servovalve Moog D765 cross-section view, with its main components labelled (drawing taken from Moog Datasheet "Servovalves with integrated electronics D765 series, ISO 10372 Size 04").*

2.2.1 Modeling The Servovalve

When dealing with the controllable TPJB as a mechatronic system, the mathematical model has to include the element that links the electronic components (controller) with the mechanical system. In this case, this element is the servovalve. This electromechanical device enables control of the oil flow towards the injection point on each pad of the bearing, as a function of a control voltage signal. This flow imposes a modification of the oil film pressure field. Hence, the static and dynamic bearing properties become a function of the servovalve control signal, rendering the TPJB a controllable mechatronic system.
A good reference to obtain more information about hydraulic valves and servovalves in general can be found in [52]. Although a number of configurations are possible for these devices, here the focus is put on presenting the mathematical model for the servovalve used in the experimental setup, model Moog D765, consisting of a four ways, spool valve configuration, see Figure 2.2.
In brief, the servovalve operational principle is based on connecting or disconnecting the ports A and B (load ports, in this case connected to the lower and upper pad injection points), to the ports connected to the high pressure supply **P** and the reservoir **T**, see Figure 2.2. Hence, at any time, three different states are possible: A closed and B closed, A=**P** and B=**T**, or A=**T** and B=**P**. The switching between these states is performed by the movement of the spool, whose lands can connect or disconnect the different ports. The spool movement is governed by the pressure applied on each end of it, which is defined at the

valve pilot stage. At the pilot stage, two nozzles are located opossed to each other, and are blocked or opened by the movement of the flapper connected to the torque motor, as a result of the command signal sent to it. If the torque motor rotates clockwise, then the flapper moves to the left, closing the left nozzle and opening the right one. Consequently, the left end of the spool receives flow from the high pressure supply port, resulting in a spool movement from left to right. This will cause a deformation of the feedback spring, generating a counteracting moment over the flapper-torque motor, that returns the system to static equilibrium state. For modern servovalves like the one under study here, the feedback is performed not only by mechanical means, i.e. the deformation of the feedback spring, but also by a built-in controller, that directly measures the spool position and compares it with the reference signal. This is done in order to avoid non linear effects (for example, stick-slip friction phenomena).
Although the previous presentation portrayed a static usage of the servovalve to describe its operational principle, this device is meant to be used in applications where quick changes of the flow and pressure over the load ports are required. The dynamic behavior of the servovalve is often represented by means of a frequency response function, relating the output flow with the input signal amplitude and frequency. Figure 2.3 depicts the frequency response function for the studied servovalve. It can be seen that, depending on the frequency of the control signal, a phase lag between input signal and resulting flow can manifest. Moreover, it can be seen that above the servovalve resonant frequency, the flow and control signal tend to be in counterphase. This phase shift effect has significant consequences when using the servovalve for control purposes, as it is intended in the controllable TPJB. Hence, the effort in obtaining an adequate model for this device is justified.

From the brief presentation given above, it becomes evident that the modeling of this electromechanical device involves the coupling of several physical phenomena, such as electromagnetism (torque motor), solid and fluid mechanics (spool movement, feedback spring deformation, flows in the pilot and spool stage), electronics (built-in controller). To avoid an excessive complexity of the controllable TPJB model, a reduced approach is desirable to include the dynamics of the servovalve into the global model. Consequently, the model implemented by Santos and Russo [34] is kept here.
Consider Figure 2.4 for the following analysis. The oil flow q_L through the spool stage of the servovalve can be analyzed as the flow through an orifice of variable area, using Bernoulli equation and mass conservation principle [52], resulting in the following expression:

$$q_L = C_d A_{orifice} \sqrt{\frac{(\mathbf{P} - p_L)}{\rho}} \tag{2.14}$$

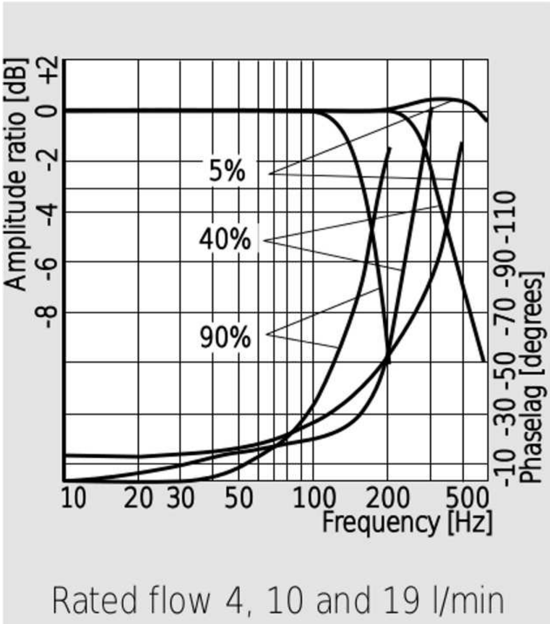

Figure 2.3: *Servovalve Moog D765 frequency response function, for different amplitudes of the control signal and supply pressure 210 bar (taken from Moog Datasheet "Servovalves with integrated electronics D765 series, ISO 10372 Size 04")*

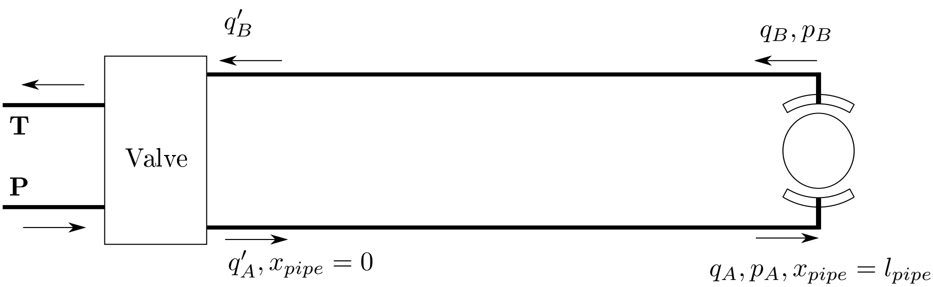

Figure 2.4: *Nomenclature used for the servovalve and pipeline dynamics analysis*

Where $A_{orifice}$ corresponds to the area of the orifice, **P** corresponds to the supply pressure of the hydraulic system, $p_L = p_A - p_B$. Furthermore, C_d or discharge coefficient incorporates the ratio between the pipe and orifice areas, and empirical coefficients related to the orifice flow losses.
The area of the orifice $A_{orifice}$ is a function of the spool position x_V. Considering

that the supply pressure **P** remains constant, the behavior of the flow towards the injection points A and B q_L can be defined as [52]:

$$q_L := q_L\left(x_V, p_L\right) \tag{2.15}$$

Equation (2.14) establish a non-linear dependence between the different parameters considered. In order to analyze the system dynamics, it becomes convenient to linearize the behavior of this system, by assuming that the system stays "in the vicinities" of a certain operational condition. By considering an infinitesimal variation of the spool position x_V and load pressure p_L around the servovalve operating point $*$, Equation (2.15) can be approximated in steady state using a Taylor series expansion as:

$$q_L = q_L^* + \left.\frac{\partial q_L}{\partial x_V}\right|_* \delta x_V + \left.\frac{\partial q_L}{\partial p_L}\right|_* \delta p_L + ... \tag{2.16}$$

By neglecting higher order terms, Equation (2.16) can be stated as a linearized first order approximation as follows:

$$\begin{aligned} q_L = q_L^* + K_V \Delta x_V + K_{pq} \Delta p_L \\ K_V := \frac{\partial q_L}{\partial x_V} \\ K_{pq} := \frac{\partial q_L}{\partial p_L} \\ \Delta x_V = x_V - x_V^* \\ \Delta p_L = p_L - p_L^* \end{aligned} \tag{2.17}$$

Where the valve coefficients K_V and K_{pq} have been introduced. These coefficients are dependant on the servovalve operating point $*$ where the linearization is performed. In this case, the operational point considered for the subsequent analysis corresponds to $x_V^* = 0$, i.e. the spool is centered. Using the controllable TPJB for control purposes entails that quick changes in the direction of the active force over the rotor are required. Consequently, the direction of the injection flow must be reverted quickly, which is obtained by small movements of the spool position around its centered position.

Additional assumptions must be imposed to complete the analysis, regarding the null point servovalve behavior. Firstly, the valve is considered as underlapped,

meaning that $q_L \neq 0$ for $x_V = 0$. This assumption correspond to the behavior of real servovalves, due to manufacturing clearances and wear [52]. Secondly, the analysis is restricted for small spool displacements, hence the valve coefficients K_V and K_{pq} are assumed constant. This condition holds true if the control signal for the servovalve u_v is much smaller than the maximum possible value ($\frac{1}{10}$ of the maximum value [53]). Thirdly, it is assumed that $p_L^* = p_A^* - p_B^* = 0$, implying that both injection points have the same pressure for $x_V^* = 0$.
Taking into account the preceding analysis, Equation (2.17) can be reduced for the null point linearized analysis as follows:

$$q_L = q_L^* + K_V x_V + K_{pq} p_L \quad \textit{for } x_V^* = 0 \tag{2.18}$$

Since the valve is underlapped, the flow at the null point q_L^* is assumed equal to the leakage flow q_{leak}. Hence:

$$q_L^* = q_{leak} \Rightarrow q_L = q_{leak} + K_V x_V + K_{pq} p_L \quad \textit{for } x_V^* = 0 \tag{2.19}$$

Consequently, the linearized model for the flow through the servovalve contains three terms:

- A leakage flow q_{leak}, to model the flow observed when the spool is centered $x_V = 0$.
- A spool driven flow $q_V = K_V x_V$, dependent on the spool position.
- A load pressure driven flow $q_p = K_{pq} p_L$, dependent on the pressure difference between the injection points in the pads $p_L = p_A - p_B$.

So far, only the spool stage flow have been included within the analysis. Since the pilot stage, torque motor, feedback spring and built in controller determine the position of the spool x_V, the effect of those elements can be included within the spool position dependent flow q_V. It has been established [53, 54, 55] that the dynamic behavior of the servovalve driven flow $q_V(t)$ can be modeled using a second-order ordinary differential equation:

$$\ddot{q}_V + 2\xi_V \omega_V \dot{q}_V + \omega_V^2 q_V = \omega_V^2 R_V u_V \tag{2.20}$$

Where $u_V(t)$ corresponds to the signal used to control the servovalve, and ω_V, ξ_V, R_V are characteristic parameters of the servovalve. Equation (2.20) implicitly contains the effect of the pilot stage, torque motor, feedback spring and controller over the valve dynamics, and it is capable of capturing the frequency dependant amplitude and phase behavior for the flow $q_V(t)$ with respect to the control signal $u_V(t)$, as seen in Figure 2.3.
Consequently, Equation (2.19) can be rewritten as:

$$q_L = q_{leak} + q_V(t) + K_{pq} p_L \quad \text{for } x_V^* = 0 \tag{2.21}$$

By convention, the flow towards the injection points on each pad is considered as positive. Consequently, one obtains expressions for the flow in the servovalve ports A and B:

$$\begin{aligned} q'_A(t) &= q_{leak} + q_V(t) + K_{pq}(p_A(t) - p_B(t)) \\ q'_B(t) &= q_{leak} - q_V(t) - K_{pq}(p_A(t) - p_B(t)) \\ \ddot{q}_V + 2\xi_V\omega_V\dot{q}_V + \omega_V^2 q_V &= \omega_V^2 R_V u_V \end{aligned} \tag{2.22}$$

2.2.2 The Influence Of The Injection Pipeline Over The Controllable TPJB Dynamics

Prior to the start of this research project, the state-of-the-art mathematical model for the TPJB with controllable lubrication considered the servovalve as the only element that introduced a frequency dependent transfer function between input control signal and the resulting injection flow at the bearing pad [29, 34]. The effect of the pipeline was neglected, by assuming that the first acoustic natural frequency of the oil within the pipeline was much higher than the servovalve natural frequency ω_V. Hence, the contribution from the pipeline dynamics to the overall behavior of the controllable bearing could be neglected, entailing that $q'_A = q_A$ and $q'_B = q_B$, see Figure 2.4.
The acoustic natural frequencies in the pipeline are functions of the compressibility of the fluid running through it. A measure of the compressibility of a fluid is given by its bulk modulus. The relationship between applied pressure and resulting change of fluid volume V is given by the bulk modulus β, defined as:

$$\beta = V\frac{\partial p}{\partial V} \tag{2.23}$$

Considering the oil flow through the pipeline, its equivalent bulk modulus β can be determined as [52]:

$$\beta = \left[\frac{1-r}{\beta_{oil}} + \frac{r}{\beta_{air}} + C_{pipe} \right]^{-1} \tag{2.24}$$

In Equation (2.24), r is the percentage of air in the total volume of fluid, β_{air} and β_{oil} the bulk modulus of air and oil respectively, and C_{pipe} the radial compliance of the pipe. This last parameter enables to include the contribution from the pipe flexibility into the oil flow bulk modulus.
The bulk modulus of air is approximately ten thousand times smaller than the one from the oil. If the oil flow does not contain any air, thus $r = 0$ in Equation (2.24), meaning that the resulting flow can be analyzed as incompressible, and the controllable TPJB can be analyzed considering negligible contribution from the pipeline dynamics. However, any real hydraulic system contains a small fraction of air within the working fluid, which can decrease dramatically the magnitude of the acoustic natural frequencies [52, 56]. Experimental results obtained during this research project, see Publication 5 in section 5.5, revealed significant phase lag between the servovalve response and the active force over the rotor. One of the contributions to this time delay can originate from the pipeline acoustic modes. Hence, it is necessary to expand the mathematical model to explicitly include the effect of the injection pipeline.
The relevance of including compressibility effects for the modeling of hydraulic systems is well understood [57, 58, 59]. This effect is included when modeling the behavior of the hydraulic fluid contained within the servovalve, actuator chambers as well as in the connection pipelines. For the analysis presented here, the compressibility effects are only considered for the flow contained in the pipeline, being neglected within the servovalve chambers and within the oil film.
Due to its relevance for the design and modeling of fluid power systems, the dynamic behavior of the oil within the pipeline is throughly studied by a number of authors. A good summary of the available theoretical models and numerical methods used for analyzing this problem can be found in [60, 61]. In the present work, the approach presented in [62] is followed. A complete presentation of the mathematical procedure followed for obtaining the pipeline dynamic model can be found in Appendix C.
For analyzing the flow within the pipeline, its behavior is characterized in terms of the volumetric flow rate $q\left(x_{pipe}, t\right)$ and pressure $p\left(x_{pipe}, t\right)$ along the longitudinal position x_{pipe}. By assuming that the density of the flow remains constant,

the continuity equation for a differential pipeline element can be stated as:

$$\frac{\partial p}{\partial t} + \frac{\rho c_0^2}{A_{pipe}} \frac{\partial q}{\partial x_{pipe}} = \frac{\rho c_0^2}{A_{pipe}} S_q$$
$$c_0 = \sqrt{\frac{\beta}{\rho}} \tag{2.25}$$

Where c_0 is the speed of sound in the flow, and A_{pipe} is the pipe cross section area. Furthermore, the Navier-Stokes equations can be reduced to the following form to analyze the pipeline flow:

$$\frac{\partial q}{\partial t} + \frac{A_{pipe}}{\rho} \frac{\partial p}{\partial x_{pipe}} = \frac{F_{ext}}{\rho} \tag{2.26}$$

The simultaneous solution of Equation (2.25) and Equation (2.26), enables obtaining the volumetric flow rate $q\left(x_{pipe}, t\right)$ and pressure $p\left(x_{pipe}, t\right)$ in the pipeline. The continuity equation is stated considering the variation of flow rate along the pipeline due to compressibility effects and sources or sinks S_q in the pipeline. Furthermore, the reduced form of the Navier-Stokes equation accounts for the variation of linear momentum of the flow due to the pressure gradient and applied forces F_{ext}, such as the ones arising from viscous effects.
The system of equations defined by Equation (2.25) and (2.26) is solved using the separation of variables method, see Appendix C. The boundary conditions correspond to the flow in the servovalve port, $q\left(x_{pipe} = 0, t\right) = q'_{A,B}$, and the pressure in the injection nozzle $p\left(x_{pipe} = l_{pipe}, t\right) = p_{A,B}$. Then, the flow in each pad injection nozzle $q_{A,B}$ can be modeled as:

$$q_{A,B}\left(t\right) = \sum_{i=1}^{n} H_i\left(x_{pipe} = l_{pipe}\right) \gamma_i\left(t\right) \tag{2.27}$$

where:

$$H_i\left(x_{pipe} = l_{pipe}\right) = sin\left(\frac{\omega_i l_{pipe}}{c_0}\right)$$
$$\omega_i = \frac{\left(2i-1\right)\pi c_0}{2 l_{pipe}}$$
$$\ddot{\gamma}_i + d_{pipe}\dot{\gamma}_i + \omega_i^2 \gamma_i = c_0\, \omega_i\, q'_{A,B} - \frac{A_{pipe}}{\rho} \dot{p}_{A,B} \left(-1\right)^{i+1} \tag{2.28}$$

From Equation (2.28), it can be seen that the resulting flow in the injection nozzle $q_{A,B}$ depends on the pipeline acoustic natural frequencies ω_i, acoustic

normal modes H_i and modal flows γ_i. These functions depend on the speed of sound in the flow c_0, the length and cross section area of the pipe l_{pipe}, A_{pipe}, and an equivalent damping coefficient d_{pipe} accounting for the viscous losses in the system. The forcing terms introduced in the second order differential equations that model the modal flows γ_i become a function of the flow in the servovalve port $q'_{A,B}$ and the pressure in the injection nozzle $p_{A,B}$.
The number of acoustic modes n to be considered in Equation (2.27) depends on the number of acoustic natural frequencies that lie within the frequency range selected for analyzing the dynamic behavior of the controllable bearing. For instance, if $n = 2$, then Equation (2.27) reduces to:

$$\begin{aligned} q_{A,B}(t) &= \gamma_1 - \gamma_2 \\ \ddot{\gamma}_1 + d_{pipe}\dot{\gamma}_1 + \left(\frac{\pi c_0}{2l_{pipe}}\right)^2 \gamma_1 &= \frac{\pi c_0^2}{2l_{pipe}} q'_{A,B} - \frac{A_{pipe}}{\rho}\dot{p}_{A,B} \\ \ddot{\gamma}_2 + d_{pipe}\dot{\gamma}_2 + \left(\frac{3\pi c_0}{2l_{pipe}}\right)^2 \gamma_2 &= \frac{3\pi c_0^2}{2l_{pipe}} q'_{A,B} + \frac{A_{pipe}}{\rho}\dot{p}_{A,B} \end{aligned} \tag{2.29}$$

2.2.3 Linking The Hydraulic System With The Oil Film Pressure Field: The Modified Reynolds Equation

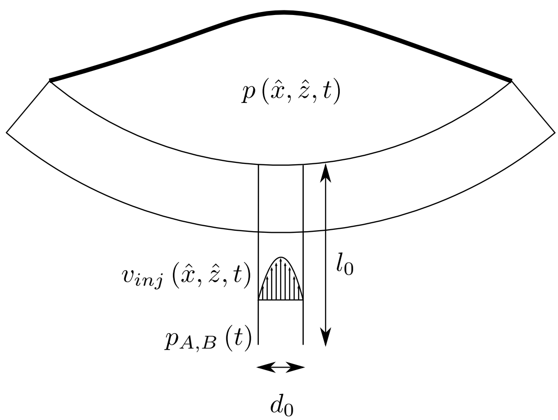

Figure 2.5: *The simplified model for including the effect of the oil injection within the Reynolds Equation*

In the preceding sections, an expression for the oil flow towards each injec-

tion point $q_A(t)$ and $q_B(t)$ was obtained, by analyzing the servovalve dynamics around the null operating point and the pipeline contribution to the overall dynamic behavior. At this point, it becomes necessary to link those results with the oil film behavior within the bearing.
Figure 2.5 depicts a schematic for the situation under analysis. The pipe connected to the injection hole in the pad exhibits pressure $p_{A,B}(t)$ in one end, as previously defined, and $p(\hat{x}, \hat{z}, t)$ in the other end, corresponding to the pressure developed within the oil film. By assuming a fully developed laminar flow within the circular injection nozzle (Hagen-Poiseuille flow) [34], the velocity of the injected oil in the radial direction $v_{inj}(\hat{x}, \hat{z}, t)$ can be described by:

$$v_{inj}(\hat{x}, \hat{z}, t) = \frac{1}{4\mu_{inj}} \left(\frac{p_{A,B}(t) - p(\hat{x}, \hat{z}, t)}{l_0} \right) \left(\frac{d_0^2}{4} - (\hat{x} - \hat{x}_0)^2 - (\hat{z} - \hat{z}_0)^2 \right) \tag{2.30}$$

Where d_0, l_0 stand for the diameter and length of the injection pipe, and $\hat{x}_0, \hat{z}_0$ stand for the coordinates of the center of the injection hole in the curvilinear reference frame. By integrating the velocity profile over the orifice surface S_0, the injected oil flow is obtained as:

$$q_{A,B}(t) = \frac{1}{4\mu_{inj} l_0} \int_{S_0} \left(p_{A,B}(t) - p(\hat{x}, \hat{z}, t) \right) \left(\frac{d_0^2}{4} - (\hat{x} - \hat{x}_0)^2 - (\hat{z} - \hat{z}_0)^2 \right) dS \tag{2.31}$$

Equation (2.31) describe the flow in the injection points $q_A(t)$ and $q_B(t)$, hence it can be inserted in Equation (2.29) to link the servovalve and pipeline domain with the bearing fluid film domain.
In order to complete this formulation, the relationship between oil film pressure field $p(\hat{x}, \hat{z}, t)$ and injection point pressure $p_A(t), p_B(t)$ needs to be defined. For this purpose, the boundary conditions for the oil film velocity field $\mathbf{v}(\hat{x}, \hat{y}, \hat{z}, t)$ are modified [34]. For a passive TPJB, these boundary conditions are stated as follows:

$$\begin{aligned}
v_{\hat{x}}(\hat{x}, \hat{y} = 0, \hat{z}, t) &= 0 \\
v_{\hat{x}}(\hat{x}, \hat{y} = h, \hat{z}, t) &= \Omega R \\
v_{\hat{y}}(\hat{x}, \hat{y} = 0, \hat{z}, t) &= 0 \\
v_{\hat{y}}(\hat{x}, \hat{y} = h, \hat{z}, t) &= \frac{\partial h}{\partial t} \\
v_{\hat{z}}(\hat{x}, \hat{y} = 0, \hat{z}, t) &= 0 \\
v_{\hat{z}}(\hat{x}, \hat{y} = h, \hat{z}, t) &= 0
\end{aligned} \tag{2.32}$$

The boundary conditions for the oil film velocity field stated in Equation (2.32) correspond to the "no slip" condition on the surface of the pad and journal, for each one of the directions analyzed. These boundary conditions are modified within the injection hole. It is considered that the pad surface is not altered by the presence of the hole, meaning that the no-slip condition is kept in the circumferential and axial direction. However, the velocity profile of the injected oil is applied as boundary condition for the velocity field in the radial direction, as follows:

$$\begin{aligned}
v_{\hat{x}}\left(\hat{x}, \hat{y}=0, \hat{z}, t\right) &= 0 \\
v_{\hat{x}}\left(\hat{x}, \hat{y}=h, \hat{z}, t\right) &= \Omega R \\
v_{\hat{y}}\left(\hat{x}, \hat{y}=0, \hat{z}, t\right) &= v_{inj} \\
v_{\hat{y}}\left(\hat{x}, \hat{y}=h, \hat{z}, t\right) &= \frac{\partial h}{\partial t} \\
v_{\hat{z}}\left(\hat{x}, \hat{y}=0, \hat{z}, t\right) &= 0 \\
v_{\hat{z}}\left(\hat{x}, \hat{y}=h, \hat{z}, t\right) &= 0
\end{aligned} \tag{2.33}$$

Note that the no-slip assumption is kept in the axial and circumferential direction of the injection orifice. Inserting the boundary conditions stated in Equation (2.33) in the Navier-Stokes equation, see Appendix A for details, and keeping the hypotheses established for the Reynolds Equation in section 2.1.1, the oil film pressure field in the injection orifice can be described by:

$$\frac{\partial}{\partial \hat{x}}\left(\frac{h^3}{\mu}\frac{\partial p}{\partial \hat{x}}\right) + \frac{\partial}{\partial \hat{z}}\left(\frac{h^3}{\mu}\frac{\partial p}{\partial \hat{z}}\right) = 6\Omega R\frac{\partial h}{\partial \hat{x}} + 12\frac{\partial h}{\partial t} + 12 v_{inj} \tag{2.34}$$

In order to extend Equation (2.34) to be valid for the whole fluid film domain, the $g\left(\hat{x}, \hat{z}\right)$ function is defined as:

$$\begin{aligned}
g\left(\hat{x}, \hat{z}\right) = \frac{d_0^2}{4} - \left(\hat{x} - \hat{x}_0\right)^2 - \left(\hat{z} - \hat{z}_0\right)^2 \ \mathit{if}\ \left(\hat{x} - \hat{x}_0\right)^2 - \left(\hat{z} - \hat{z}_0\right)^2 &\le \frac{d_0^2}{4} \\
g\left(\hat{x}, \hat{z}\right) = 0 \ \mathit{if}\ \left(\hat{x} - \hat{x}_0\right)^2 - \left(\hat{z} - \hat{z}_0\right)^2 &> \frac{d_0^2}{4}
\end{aligned} \tag{2.35}$$

Then, by combining Equation (2.30),(2.34),(2.35), the Modified Reynolds Equation is obtained for pad A and B as:

$$\frac{\partial}{\partial \hat{x}}\left(\frac{h^3}{\mu}\frac{\partial p}{\partial \hat{x}}\right)+\frac{\partial}{\partial \hat{z}}\left(\frac{h^3}{\mu}\frac{\partial p}{\partial \hat{z}}\right)=6\Omega R\frac{\partial h}{\partial \hat{x}}+12\frac{\partial h}{\partial t}+3g\frac{(p-p_A)}{\mu_{inj}l_0}$$
$$\frac{\partial}{\partial \hat{x}}\left(\frac{h^3}{\mu}\frac{\partial p}{\partial \hat{x}}\right)+\frac{\partial}{\partial \hat{z}}\left(\frac{h^3}{\mu}\frac{\partial p}{\partial \hat{z}}\right)=6\Omega R\frac{\partial h}{\partial \hat{x}}+12\frac{\partial h}{\partial t}+3g\frac{(p-p_B)}{\mu_{inj}l_0} \tag{2.36}$$

Hence, the link between the oil film pressure field $p(\hat{x},\hat{z},t)$ and the pressure in the injection pipe $p_A(t), p_B(t)$ is established.

2.2.4 The Modified Oil Film Energy Equation

The inclusion of the oil injection effect within the Oil Film Energy Equation can be done in a simplified way, as proposed in [35, 36]. In section 2.2.3, an analytical expression for the oil injection velocity in the radial direction v_{inj} was obtained. Assuming that the temperature T_{inj} of the injected oil is known and constant within the injection orifice S_0, the oil injection effect can be included within the oil film energy equation as follows:

$$\kappa h\frac{\partial^2 T}{\partial \hat{x}^2}+\kappa h\frac{\partial^2 T}{\partial \hat{z}^2}+\left(\frac{\rho C_p h^3}{12\mu}\frac{\partial p}{\partial \hat{x}}-\frac{\rho C_p \Omega R h}{2}\right)\frac{\partial T}{\partial \hat{x}}+$$
$$\frac{\rho C_p h^3}{12\mu}\frac{\partial p}{\partial \hat{z}}\frac{\partial T}{\partial \hat{z}}+(\Omega R)^2\frac{\mu}{h}+\frac{h^3}{12\mu}\left(\left(\frac{\partial p}{\partial \hat{x}}\right)^2+\left(\frac{\partial p}{\partial \hat{z}}\right)^2\right)+\mathbf{S}_{oil}$$
$$+\left(\kappa\frac{T_{inj}-T}{l_0}+\rho C_p v_{inj}(T_{inj}-T)+p v_{inj}+\frac{4}{3}\frac{\mu}{h}v_{inj}^2\right)\Bigg|_{S_0}=0 \tag{2.37}$$

In Equation (2.37), the additional terms related to the oil injection are evaluated only within the injection orifice S_0. Refer to Appendix B for more details about their derivation. The physical meaning of each one of the additional terms related to the oil injection is:

- *Heat transfer due to thermal conductivity* $\kappa\frac{T_{inj}-T}{l_0}$
  This term represents the heat transfer between the oil within the injection pipe and the oil in the bearing clearance, due to their temperature difference and the thermal conductivity.

- *Convective heat transport* $\rho C_p v_{inj} \left(T_{inj} - T\right)$
  This term represents the heat carried into the bearing clearance by the injected oil flow.

- *Work performed by pressure and viscous forces considering the injected flow in the radial direction* $p v_{inj} + \frac{4}{3}\frac{\mu}{h} v_{inj}^2$

2.3 Summary: The Coupled Model For The Controllable TPJB

1. **Oil Flow and Pressure Within the System:**

Servovalve driven flow: $\ddot{q}_V + 2\xi_V \omega_V \dot{q}_V + \omega_V^2 q_V = \omega_V^2 R_V u_V$ (2.38)

Servovalve port A flow: $q'_A = q_{leak} + q_V + K_{pq}(p_A - p_B)$ (2.39)

Servovalve port B flow: $q'_B = q_{leak} - q_V - K_{pq}(p_A - p_B)$ (2.40)

1st modal flow pipe A: $\ddot{\gamma}_{1A} + d_{pipe}\dot{\gamma}_{1A} + \left(\frac{\pi c_0}{2l_{pipe}}\right)^2 \gamma_{1A} = \frac{\pi c_0^2}{2l_{pipe}} q'_A - \frac{A_{pipe}}{\rho}\dot{p}_A$ (2.41)

2nd modal flow pipe A: $\ddot{\gamma}_{2A} + d_{pipe}\dot{\gamma}_{2A} + \left(\frac{3\pi c_0}{2l_{pipe}}\right)^2 \gamma_{2A} = \frac{3\pi c_0^2}{2l_{pipe}} q'_A + \frac{A_{pipe}}{\rho}\dot{p}_A$ (2.42)

1st modal flow pipe B: $\ddot{\gamma}_{1B} + d_{pipe}\dot{\gamma}_{1B} + \left(\frac{\pi c_0}{2l_{pipe}}\right)^2 \gamma_{1B} = \frac{\pi c_0^2}{2l_{pipe}} q'_B - \frac{A_{pipe}}{\rho}\dot{p}_B$ (2.43)

2nd modal flow pipe B: $\ddot{\gamma}_{2B} + d_{pipe}\dot{\gamma}_{2B} + \left(\frac{3\pi c_0}{2l_{pipe}}\right)^2 \gamma_{2B} = \frac{3\pi c_0^2}{2l_{pipe}} q'_B + \frac{A_{pipe}}{\rho}\dot{p}_B$ (2.44)

Pouiseuille flow injection nozzle A: $\gamma_{1A} - \gamma_{2A} =$

$$\frac{1}{4\mu_{inj} l_0}\int_{S_0} (p_A - p(\hat{x},\hat{z},t))\left(\frac{d_0^2}{4} - (\hat{x}-\hat{x}_0)^2 - (\hat{z}-\hat{z}_0)^2\right) dS \tag{2.45}$$

Pouiseuille flow injection nozzle B: $\gamma_{1B} - \gamma_{2B} =$

$$\frac{1}{4\mu_{inj} l_0}\int_{S_0} (p_B - p(\hat{x},\hat{z},t))\left(\frac{d_0^2}{4} - (\hat{x}-\hat{x}_0)^2 - (\hat{z}-\hat{z}_0)^2\right) dS \tag{2.46}$$

Oil film pressure pad A: $\frac{\partial}{\partial \hat{x}}\left(\frac{h^3}{\mu}\frac{\partial p}{\partial \hat{x}}\right) + \frac{\partial}{\partial \hat{z}}\left(\frac{h^3}{\mu}\frac{\partial p}{\partial \hat{z}}\right) =$

$$6\Omega R\frac{\partial h}{\partial \hat{x}} + 12\frac{\partial h}{\partial t} + 3g\frac{(p - p_A)}{\mu_{inj} l_0} \tag{2.47}$$

Oil film pressure pad B: $\frac{\partial}{\partial \hat{x}}\left(\frac{h^3}{\mu}\frac{\partial p}{\partial \hat{x}}\right) + \frac{\partial}{\partial \hat{z}}\left(\frac{h^3}{\mu}\frac{\partial p}{\partial \hat{z}}\right) =$

$$6\Omega R\frac{\partial h}{\partial \hat{x}} + 12\frac{\partial h}{\partial t} + 3g\frac{(p - p_B)}{\mu_{inj} l_0} \tag{2.48}$$

2. **Oil Film Temperature and Pad Temperature Field:**

$$\textit{Oil film temperature: } \kappa h \frac{\partial^2 T}{\partial \hat{x}^2} + \kappa h \frac{\partial^2 T}{\partial \hat{z}^2} + \left(\frac{\rho C_p h^3}{12\mu} \frac{\partial p}{\partial \hat{x}} - \frac{\rho C_p \Omega R h}{2} \right) \frac{\partial T}{\partial \hat{x}} + \frac{\rho C_p h^3}{12\mu} \frac{\partial p}{\partial \hat{z}} \frac{\partial T}{\partial \hat{z}} + (\Omega R)^2 \frac{\mu}{h} + \frac{h^3}{12\mu} \left(\left(\frac{\partial p}{\partial \hat{x}} \right)^2 + \left(\frac{\partial p}{\partial \hat{z}} \right)^2 \right) + \mathbf{S}_{oil} + \left(\kappa \frac{T_{inj} - T}{l_0} + \rho C_p v_{inj} \left(T_{inj} - T \right) + p v_{inj} + \frac{4}{3} \frac{\mu}{h} v_{inj}^2 \right) \Bigg|_{S_0} = 0 \tag{2.49}$$

$$\textit{Pad temperature field: } \kappa_{pad} \left(\frac{\partial^2 T_{pad}}{\partial x^2} + \frac{\partial^2 T_{pad}}{\partial y^2} + \frac{\partial^2 T_{pad}}{\partial z^2} \right) + H_\infty \left(T_{pad} - T_\infty \right) |_{boundary} + \mathbf{S}_{pad} = 0 \tag{2.50}$$

$$\textit{Heat transfer oil-pad: } \mathbf{S}_{oil} = -\mathbf{S}_{pad} = \frac{\kappa}{h} \left(3T - 2T_{journal} - 2 \left. T_{pad} \right|_{boundary} \right) \tag{2.51}$$

$$\textit{Oil temperature-viscosity relationship: } \mu(T) = \mu^* e^{-\eta (T - T^*)} \tag{2.52}$$

3. **Pad elastic and thermal deformations:**

$$\textit{Elastic deformations: } \mathbf{V}_s^T \mathbf{M}_s \mathbf{V}_s \ddot{\mathbf{u}}_s^* + \mathbf{V}_s^T \mathbf{K}_s \mathbf{V}_s \mathbf{u}_s^* = \mathbf{V}_s^T \mathbf{f}_s (p) \tag{2.53}$$

$$\textit{Thermal deformations: } \epsilon_{x\alpha} = \epsilon_{y\alpha} = \epsilon_{z\alpha} = \alpha_\Pi \left(T_{pad} - T_{ref} \right) \tag{2.54}$$

2.4 Closure

In this chapter, the mathematical model for the tilting-pad journal bearing with controllable lubrication has been presented. A presentation of the constitutive equations for each one of the domains (oil film, pads, pipelines and servovalve) that compose the controllable bearing has been given, with the corresponding simplificatory assumptions used for obtaining them. This set of equations include the relevant physical phenomena taking place within the bearing. The validity of this model, in its passive and controllable configuration, is examined in the following chapters of this thesis.

Chapter 3

Controllable TPJB: Numerical Implementation Of The Mathematical Model

The constitutive equations for each one element of the TPJB with controllable lubrication have been presented in the preceding chapter. The focus was set on analyzing the physical phenomena taking place within the studied system, and the simplifications introduced in order to obtain a manageable mathematical formulation for analyzing it. Since no analytical solution can be obtained for this set of equations, a numerical solving procedure must be implemented. This chapter provides a brief overview on this subject.

3.1 Numerical Solution Of The Mathematical Model Partial Differential Equations: The Finite Element Method

The Finite Element Method is the mathematical tool chosen here for solving the partial differential equations that define the behavior of the pad solid domain and the oil film fluid domain. More specifically, the equations solved are: Modified Reynolds Equation for the oil film pressure field, Oil Film Energy Equation and Fourier Law for heat conduction.
The selection of this method is justified due to the advantages that it presents to solve the partial differential equations originating from the Virtual Work Principle applied on the pad solid domain. Solving this problem using Finite Element Method is a well established procedure, with many references available, for instance [51]. Using the same numerical method for solving the remaining partial differential equations renders the communication between the different domains straightforward, from the numerical implementation point of view.
The implementation of the finite element method used in this work is based upon the work of Haugaard and Santos [37, 38]. A throughout presentation on this implementation is given in [50], hence it will not be repeated here. The finite element model developed by Haugaard and Santos contained the coupled solution of the Modified Reynolds Equation, for the oil film pressure field, and the Virtual Work Principle for the pad flexibility, which was later reduced to a pseudo modal reduction scheme. The same framework is used in this work for the coupled solution of the Oil film Energy Equation and Pad Fourier Law for heat conduction, in order to describe the thermal behavior of the analyzed controllable TPJB.

3.1.1 Weak Form Formulation

The first step for solving a partial differential equation using the finite element method is to obtain the weak form of the original problem. One of the assumptions introduced by Haugaard and Santos [37, 38, 50] is axial symmetry of the pressure field and pad displacements. Hence, only half of the pad in the axial direction is modeled. This approach is kept here. For each one of the partial differential equations that compose the problem, the obtention of the weak form is done according to the following guidelines:

- *Modified Reynolds Equation for the Oil Film Pressure Field* (Equation 2.36): The Bubnov-Galerkin method is used. The boundary conditions introduced to obtain the weak form correspond to: pressure equal to zero in the trailing and leading edge of the fluid domain, pressure equal to zero in the axial end of the fluid domain, symmetry condition (pressure gradient in the axial direction equals zero) in the boundary of the domain corresponding to the middle of pad in the axial direction.

- *Virtual Work Principle for the displacements of the Pad Solid Domain* (Equation 2.8): The Bubnov-Galerkin method is used. The symmetry condition is applied as a boundary condition for obtaining the weak form.

- *Fourier Law for Pad Heat Conduction* (Equation 2.4): The Bubnov-Galerkin method is used. The boundary conditions introduced for obtaining the weak form are: symmetry condition in the axial direction, heat flux equal to a free convection condition on the unloaded surfaces of the pad, heat flux equal to the heat transfer term with the oil film domain on the loaded pad surface.

- *Oil Film Energy Equation* (Equation 2.37): The strong dominance of convective effects over diffusive effects for the Oil Film Energy Equation implies numerical instability issues (wiggles) if the Bubnov-Galerkin method is applied. Hence, an streamline upwinded Petrov-Galerkin method is used for obtaining the weak form, following the method outlined by Brookes and Hughes [63].

3.1.2 Discretization

The tridimensional solid pad domain is discretized using twenty node serendipity second order elements. Hence, the numerical solution of the Pad Flexibility and Fourier Law equations are based on this discretization. The usage of second order elements is justified by the need to describe the geometry of the injection hole accurately, while keeping the number of elements within a manageable range.
The bidimensional oil film fluid domain used for modeling the pressure and temperature fields is discretized using eight node second order quadrilateral elements. Such element correspond to one face of the tridimensional finite elements used for discretizing the pad solid domain, hence linking the two domains is straightforward.

3.1.3 Finite Element Mesh Convergence Analysis

Performing a convergence analysis on the numerical solution of a partial differential equation should provide an idea of the discretization error, meaning the difference between the exact mathematical solution of the equation, and the approximated numerical solution using finite element method. Since an exact mathematical solution is not available for the equations that define the problem analyzed in this work, an approximated analysis is performed.
To perform this analysis, a single-pad bearing arrangement is considered. The pad geometry corresponds to the one used for the test rig featured in this work. The pad is discretized using different number of elements, as described in Table 3.1 and shown in Figure 3.1. For all the discretizations implemented, two elements are used in the radial direction of the pad.
The fluid domain is the two dimensional domain where the Modified Reynolds Equation and the Oil Film Energy Equation are solved. Furthermore, the solid domain is the tridimensional domain that considers the entire pad, and it is used for solving the pad flexibility equation and heat conduction using Fourier Law.
To measure the convergence of the numerical solution, the relative error is defined as follows:

$$\text{Relative error} = \frac{\left(\max\left(\lambda\right) - \max\left(\lambda_{ref}\right)\right)}{\max\left(\lambda_{ref}\right)} \tag{3.1}$$

In Equation (3.1), λ is the physical magnitude whose convergence is being analyzed as a function of the mesh discretization, whereas λ_{ref} is the value used as reference. Since no analytical results are available, numerical results obtained using a fine mesh discretization are used as a reference. Specifically, the results obtained using mesh number 7 are considered as the reference value, see Table 3.1, since that mesh presents the finest discretization possible with the computational power available.
The physical magnitudes considered for the convergence study are:

- **Pad Eigenvalues**: these results include implicitly both the stiffness and inertia properties of the pad, hence by analyzing their convergence it is possible to validate the numerical implementation of the pad flexibility model.

- **Oil film pressure field**: these results are used to validate the numerical solution of the Modified Reynolds Equation. In order to decouple these results from the convergence behavior of the other fields studied, a rigid-pad isothermal analysis is established.

- **Oil film temperature field**: these results are obtained from the coupled solution of the Oil Film Energy Equation and Pad Heat Conduction using Fourier Law. A rigid-pad assumption is established to decouple the results from the pad flexibility convergence. However, the results are inherently coupled to the solution of the Modified Reynolds Equation

Both a passive (no injection hole in the pad) and an active (injection system on) lubrication regime are established for obtaining the convergence analysis results.
The results of the convergence analysis for the pad eigenvalues are depicted in Figure 3.2. Convergence is observed for the three first pad flexible modes considered for this analysis. It is also observed that for each mesh the modes related to higher eigenvalues exhibit higher relative error, which was expected. The convergence behavior for oil film pressure and temperature field is shown in Figure 3.3 and 3.4, respectively. Lower relative errors for the pressure field is observed for the active case, when compared to the passive case. This is due to the maximum pressure value obtained in that case, occurring in the elements used for discretizing the oil injection hole. Within these elements, the pressure is "prescribed" by the injection pressure applied in the injection pipe, which entails a lower error. Regarding oil temperature field, no significant changes are observed when switching from a passive to an active configuration.

Table 3.1: *Number of elements of the mesh used for the convergence analysis; mesh number seven corresponds to the one used as reference for calculating the relative error*

Mesh	2-D fluid domain elements	3-D solid domain elements
1	72	144
2	162	324
3	288	576
4	450	900
5	648	1296
6	806	1612
7	**980**	**1960**

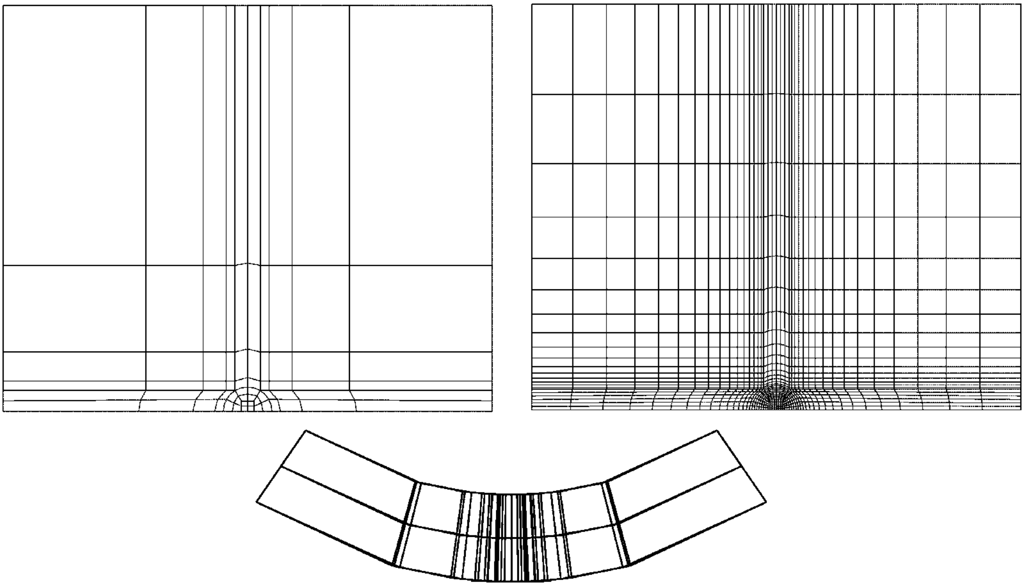

Figure 3.1: *Structure of the mesh for the convergence analysis: fluid domain discretization for mesh 1 (top left) and mesh 7 (top right); side view of the solid domain discretization for mesh 1 (bottom)*

3.1.4 Numerical Stability Of The Finite Element Solution For The Oil Film Energy Equation: Test Case Analysis

The weak form of the Oil Film Energy Equation is obtained by using an streamlined upstream Petrov Galerkin finite element formulation, as presented by Brooks and Hughes [63]. As explained previously, this is done in order to reduce the numerical instability or "wiggle" in the temperature results, arising from the strong dominance of convective over diffusive terms for the oil film thermal problem. This instability consists of an unphysical oscilation of the temperature results between adjacent nodes of the finite element mesh.
One of the test cases presented in [63] is used here to validate the numerical implementation of the upwinding method. It consists of a two dimensional square domain, with a mass flow $\mathbf{v}$ directed in a direction skewed relative to the cartesian reference system for the domain, as it is shown in Figure 3.5. The temperature of the flow T is the magnitude to be obtained. The temperature is prescribed on the boundaries of the square, and the flow is directed from "hot" boundaries towards "cold" boundaries. The two physical processes taking

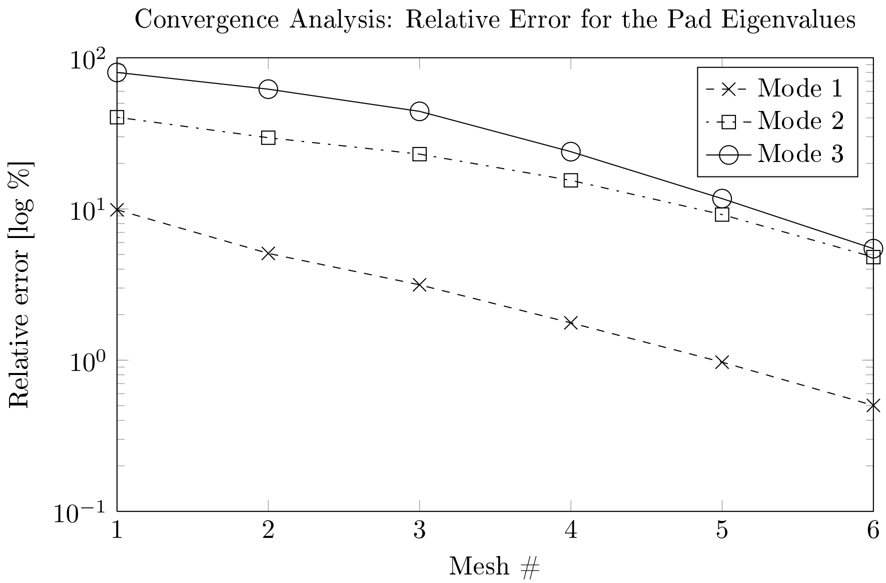

Figure 3.2: *Mesh convergence analysis results for the pad eigenvalues*

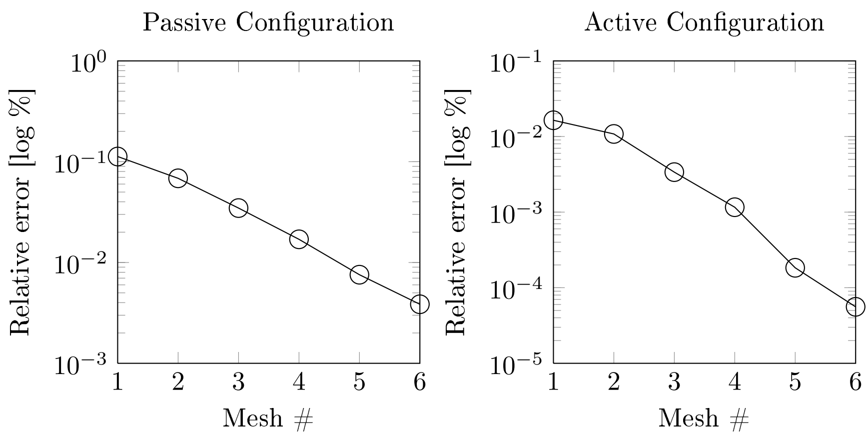

Figure 3.3: *Mesh convergence analysis results for the pressure field, for a passive configuration (no injection hole in the pad) and an active configuration (oil injection on)*

place in this problem are convection, considering the heat transport from "hot" boundaries to "cold" boundaries due to the mass flow, and diffusion, considering

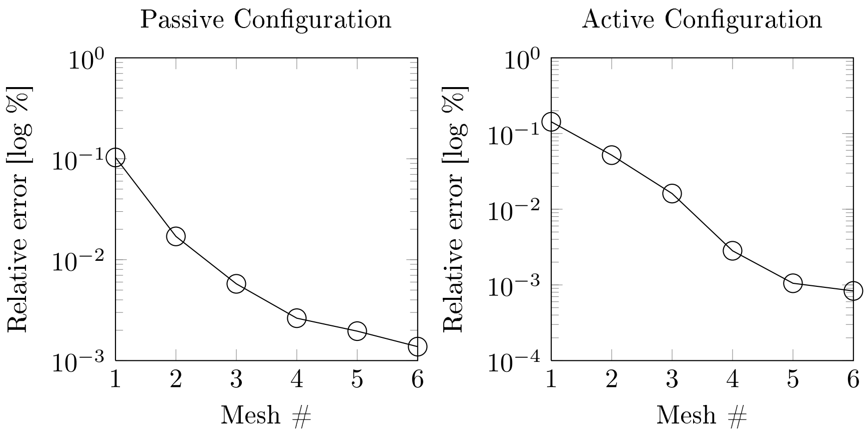

Figure 3.4: *Mesh convergence analysis results for the temperature field, for a passive configuration (no injection hole in the pad) and an active configuration (oil injection on)*

the cooling down of the flow in the vicinities of the "cold" boundaries due to the thermal conductivity κ of the fluid.
Mathematically, the problem is stated as:

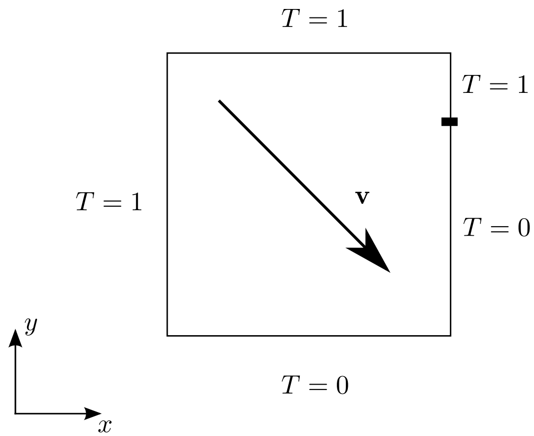

Figure 3.5: *Geometry and boundary conditions for the upwind formulation test case, as presented by Brooks and Hughes [63]*

$$\begin{aligned} f\mathbf{v} \cdot \nabla T &= \kappa \Delta T \\ \mathbf{v} &= [v_x, v_y]^T \end{aligned} \tag{3.2}$$

By setting the flow magnitude $|\mathbf{v}|$ to 1, and varying the flow thermal conductivity κ, it is possible to modify the Péclet number for the flow, which entails the variation of the ratio of magnitude between the convection and the diffusion terms in Equation (3.2), as defined by:

$$Pe = \frac{|\mathbf{v}|\, L}{\kappa} \tag{3.3}$$

Where $L = 1$ corresponds to the length of the side of the square domain. Then, the problem is solved using the finite element method, using both the Garlerkin and the streamline upwinded Petrov Galerkin approach for obtaining the weak form. The mesh is set up so that the orientation and shape of the quadrilateral elements is not regular. This is done in order to test the ability of the upwinding algorithm to determine the flow direction in the isoparametric local reference frame of each element, which is fundamental for the upwinding method.

Figure 3.6 depicts the results obtained for different Péclet numbers, when using the Galerkin method to obtain the weak form of the differential equation for the analyzed problem. It can be seen that for $Pe = 10000$ some spurious oscilations of the flow temperature value arise in the vicinities of the "cold" boundaries. In that area, an unphysical rise of the flow temperature is obtained. In other words, for a flow where the convection is the dominating effect, numerical instability takes place if no upwinding is implemented for solving the problem using the finite element method.

Figure 3.7 shows the results for the same problem, when the streamline upwinded Petrov Galerkin is implemented. It can be seen that even for $Pe = 10000$, the solution does not present wiggles, showing the expected physical behavior, which corresponds to the development of a thin "cold" fluid layer in the vicinities of those boundaries. This stable result is obtained despite the coarse discretization of the finite element mesh towards the boundaries. This result validates the implementation of the upwinding method for obtaining the weak form of the oil film energy equation.

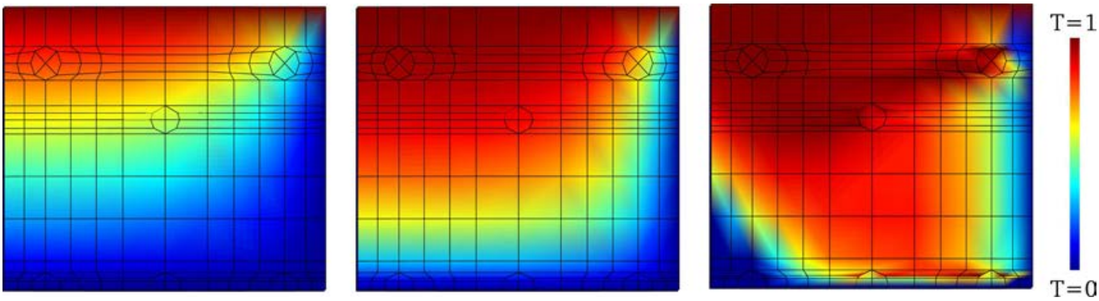

Figure 3.6: *Temperature results for the upwind formulation test case with different Péclet numbers, using Galerkin approach (no upwinding method); results for Pe=10 (left), Pe=100 (center), Pe=10000 (right)*

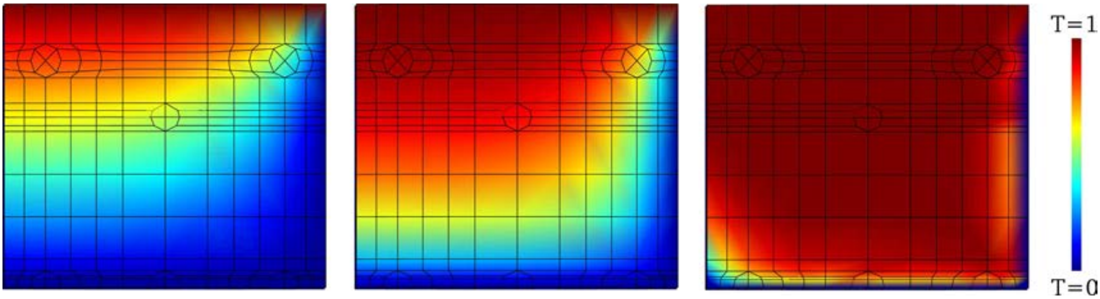

Figure 3.7: *Temperature results for the upwind formulation test case with different Péclet numbers, using Petrov Galerkin approach (upwinding method); results for Pe=10 (left), Pe=100 (center), Pe=10000 (right)*

3.2 Closure

The numerical method used for solving the controllable TPJB model has been presented, and the validity of the numerical implementation has been verified through convergence and numerical stability analysis. The accuracy of this model from the physical point of view will be discussed in the following chapters.

Chapter 4

Passive TPJB: Model Validation

In the previous chapter, the mathematical model for the tilting-pad journal bearing with controllable lubrication was presented. Additionally, the validity of the numerical implementation was verified, by analyzing convergence for different mesh discretizations, and by verifying the absence of numerical instability issues in the results. Consequently, the next step is to validate the available mathematical model from a physical point of view, by analyzing whether it is capable of predicting the physical behavior of the studied system for different operational conditions.

The system under analysis is the controllable version of the tilting-pad bearing. A first step consists of verifying the capability of the model to accurately predict the static and dynamic behavior of a passive tilting-pad bearing (no injection holes in the pad). The physical phenomena taking place within the bearing for the passive and controllable configuration are essentially identical, namely pressure build-up in the oil film due to hydrodynamic effect, temperature build-up within the oil film and heat transfer from and towards pad surface and journal, as well as elastic deformations in the pads and pivots. The difference between the two configurations stems from the perturbation introduced in those processes by the injection of high pressure oil into the bearing clearance. Thus, by validating the model for the bearing on its passive configuration a solid foundation is provided for the later work, consisting of validating the controllable TPJB model. Any divergence should then be explained by analyzing the oil

injection process and the way it is included in the model.
The model validation of the tilting-pad bearing in passive configuration is performed by relying on theoretical and experimental results available within the literature. Due to the wide spread usage of the tilting-pad bearing design in industrial turbomachinery, there is a significant amount of publications dealing with its static and dynamic characteristics, from a theoretical and experimental point of view. The data sets used for validating the model are among the most widely used or cited by the authors within the field.

4.1 Model Validation in Hydrodynamic Lubrication Regime

The early work concerning the modeling of the static and dynamic characteristics of tilting-pad bearings included solely the hydrodynamic effect within the model formulation, neglecting the effect of elastic deformation and thermal effects.
The results presented in this section compare theoretical results from the literature with the ones obtained using the model developed in this work, for passive tilting-pad bearings operating in hydrodynamic lubrication regime. A rigid pad, isothermal analysis assumption is utilized. The comparison includes journal equilibrium position (eccentricity) and synchronously reduced dynamic coefficients.

4.1.1 Validation against Someya

The “Journal-Bearing Databook” from Tsuneo Someya [64] (1988) provided a significant amount of data in terms of simulations and experimental results, regarding fluid film bearings static and dynamic characteristics. For the model validation process, two different set of results have been selected from the book: bearing number 27 (TPJB with four pads, load between pad, preload 0.75), and bearing number 49 (TPJB with five pads, load on pad, preload 0.5). The studied parameters are journal eccentricity and synchronously reduced dynamic coefficients. The comparison between the results from this book and the ones obtained with the available model are shown in Figure 4.1 and Figure 4.2. Very good agreement is obtained for the analyzed range of Sommerfeld number for both configurations.

4.1.2 Validation against Nicholas *et al.*

The work presented by Nicholas, Gunter and Allaire [65] in 1979 provided the first extensive study on the effect of changing preload, offset and pad loading configuration over the dynamic properties of a five pad tilting-pad bearing. For this study, the results concerning the preload effect over the synchronously reduced dynamic coefficients have been selected for validation purposes. Figure 4.3 presents the obtained results and compares them with the reference results; close agreement is observed for the analyzed range of Sommerfeld numbers.

4.1.3 Validation against Allaire *et al.*

Allaire, Parsell and Barrett [5] introduced in 1981 the pad perturbation method for obtaining the dynamic coefficients of tilting-pad bearings. Such method enables to obtain the full set of stiffness and dynamic coefficients, which can be later on reduced using a predetermined condensation frequency. If the journal rotational frequency is the chosen one for the condensation procedure, then the synchronously reduced coefficients are obtained.
The set of results presented by these authors enables to validate the perturbation analysis used for obtaining each one of the full dynamic coefficients. The comparison between benchmark results and the ones obtained using the available model are presented in Figure 4.4. Both the full and the reduced dynamic coefficients for the journal degrees of freedom x, y are presented, yielding good agreement.

4.2 Model Validation in Elastothermohydrodynamic Lubrication Regime

The state of the art regarding TPJB modeling dictates the need for including thermal and flexibility effects within the model, in order to obtain good agreement with experimental results. The literature shows that if only hydrodynamic effects are considered for the model formulation, a significant overprediction of the bearing damping properties will be obtained, with the potential catastrophic consequences in an industrial application context.
This section tests the validity of the available model when an elastothermohydrodynamic (ETHD) lubrication regime is imposed, by comparing its results against theoretical and experimental results from the literature.

4.2.1 Validation against Taniguchi *et al.*

The set of results obtained by Taniguchi, Makino, Takeshita and Ichimura [48] corresponds to the theoretical prediction and experimental measurements concerning the steady-state static and thermal behavior of a large 4 pad, load between pad, tilting-pad bearing operating in transition to turbulent regime. The authors develop a three dimensional thermohydrodynamic model for the bearing, including the effect of turbulence. No flexibility effects originating from pad or pivot elastic deformations are considered. Their set of experimental data is specially interesting, since they obtained the complete mapping of the oil film pressure field and oil film thickness in the axial center line of the bearing, by installing a pressure transducer and displacement pick-up in the rotor.
This set of results correspond to a bearing operating in the transition to turbulent regime. This condition falls outside of the range of application of the model developed in this work, which is limited to a bearing operating in laminar regime. However, a number of authors have taken advantage of this interesting set of results to validate their "laminar" models (among others, Fillon [19] and Palazzolo [22]). Hence, these results are included in this model validation analysis.
Figure 4.5 presents the comparison between the results from the reference and the ones obtained with the model developed in this work. Only the results for the highly loaded pads are shown, since the other two pads are completely cavitated. An elastothermohydrodynamic analysis is established for this model, considering pad flexibility, but neglecting pivot stiffness, since the authors do not provide information about its value for the analyzed bearing.
In general, good agreement with the reference results is obtained. Regarding oil fim thickness, the model predicts a thinner oil film than the value measured experimentally. It is likely that including the pivot flexibility, a better agreement between the model and the experimental results would be achieved. The experimental oil film pressure results feature a pressure peak towards the pad leading edge, consequence of the "ram" pressure developed within the oil when entering the thin clearance between pad surface and journal. Since neither of the theoretical models include this effect, the pressure is underestimated in that area. Regarding the pad surface temperature results, good agreement is obtained with the experimental results.

4.2.2 Validation against Fillon *et al.*

Fillon, Bligoud and Frene [19] presented in 1992 an extensive experimental study regarding the thermal behavior of tilting-pad bearings operating in laminar regime. Two different pad geometries were tested, and among the parameters measured were: circumferential and axial distribution of the pad surface tem-

perature, pad radial temperature distribution, journal temperature and housing temperature. These results were used by Palazzollo *et al.* [22, 23] to validate their elastothermohydrodynamic model.
Figure 4.6 presents the comparison between the pad surface temperature experimentally obtained by Fillon *et al.* [19] , compared against the oil film and pad surface temperature results obtained using the model developed in this work. The theoretical results include oil film temperature and pad surface temperature. It can be seen that the theoretical prediction for the oil film temperature exhibits a better overall agreement with the experiment than the pad surface temperature prediction. The pad surface temperature is slightly overpredicted in the highly loaded pads, and slightly underpredicted for the lightly loaded pads. This is a consequence of the assumption of a parabolic profile for the radial temperature distribution within the oil film, as described in the presentation of the mathematical model for the bearing, see Chapter 2.

4.2.3 Validation against Ha and Yang

Ha and Yang [11] published an experimental study on the issue of the frequency dependency of the reduced dynamic coefficients for the tilting-pad bearing. A comparison between the model results and their experimental results is provided in Figure 4.7. In these figures, the excitation frequency ratio corresponds to the ratio between excitation frequency for the parameter identification procedure and the journal rotational frequency.
In general, better agreement is observed for the prediction of the damping reduced coefficients than for the stiffness results. It is specially noteworthy that an almost perfect agreement is obtained for the direct damping coefficient in the loaded direction c_{yy}, whereas the stifness prediction in that direction k_{yy} is almost twice the experimental value. This suggests some kind of mistake in the plot for the experimentally obtained stiffness, since an overprediction of the stiffness value would certainly imply an underprediction of the damping value in that direction. It should also be noted that the model underestimate the cross-coupling stiffness k_{xy}, k_{yx} coefficients, when compared to the experimental results. These experimental results are coincident with the eccentricity and attitude angle results reported by the authors, which exhibit important cross-coupling effect (i.e attitude angle not equal to zero).
It has been shown both experimentally [25, 26] and theoretically [27] that neglecting the effect of the pivot friction over the tilting angle of the pads for the ball-socket pivot design implies a significant underestimation on the prediction of cross-coupled stiffness coefficients. This could explain the observed divergence between this model results, which neglects the pivot friction effect, and the ones reported in [11].

4.2.4 Validation against Brockwell *et al.*

Brockwell, Kleinbub and Dmochowski [10] presented in 1990 a set of experimental results regarding the experimental identification of synchronously reduced dynamic coefficients for a five-pad, load between pad, no preload tilting-pad journal bearing. These authors compare their experimental results against a theoretical model. This set of experimental results is also used in [23] to validate a ETHD model for the TPJB.
The comparison between the results obtained by the model developed in this work and these experimental results is given for two different journal rotational speeds in Figure 4.8 and Figure 4.9. Good agreement is obtained for the reduced stiffness and dynamic coefficients in the x, y directions. This accuracy was achieved by including the pivot flexibility in the calculations, using the value reported by the authors of [10]. If this effect is neglected, the result is a significant overprediction of the damping coefficients.

4.3 Closure

In this chapter, the model developed in this work for the tilting-pad journal bearing has been validated in passive configuration (no injection hole in the pad), using theoretical and experimental results available within the literature. The study evaluated the capability of the model to predict the static, thermal and dynamic properties of the bearing.
The results obtained show that the model is capable of predicting the bearing behavior with an acceptable degree of precision. Now that the model is validated in its passive configuration, it is possible to move on to its validation in its controllable configuration, which is one of the main objectives of this work.

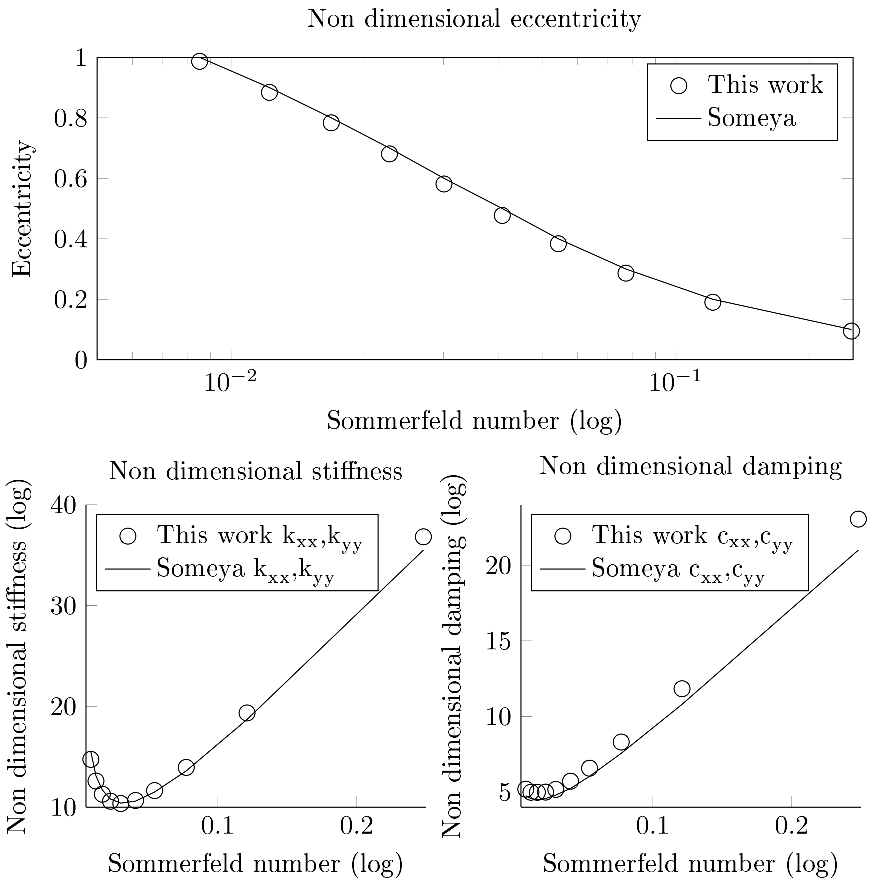

Figure 4.1: Validation against Someya [64] for bearing no. 27, journal eccentricity and synchronously reduced dynamic coefficients for different Sommerfeld numbers

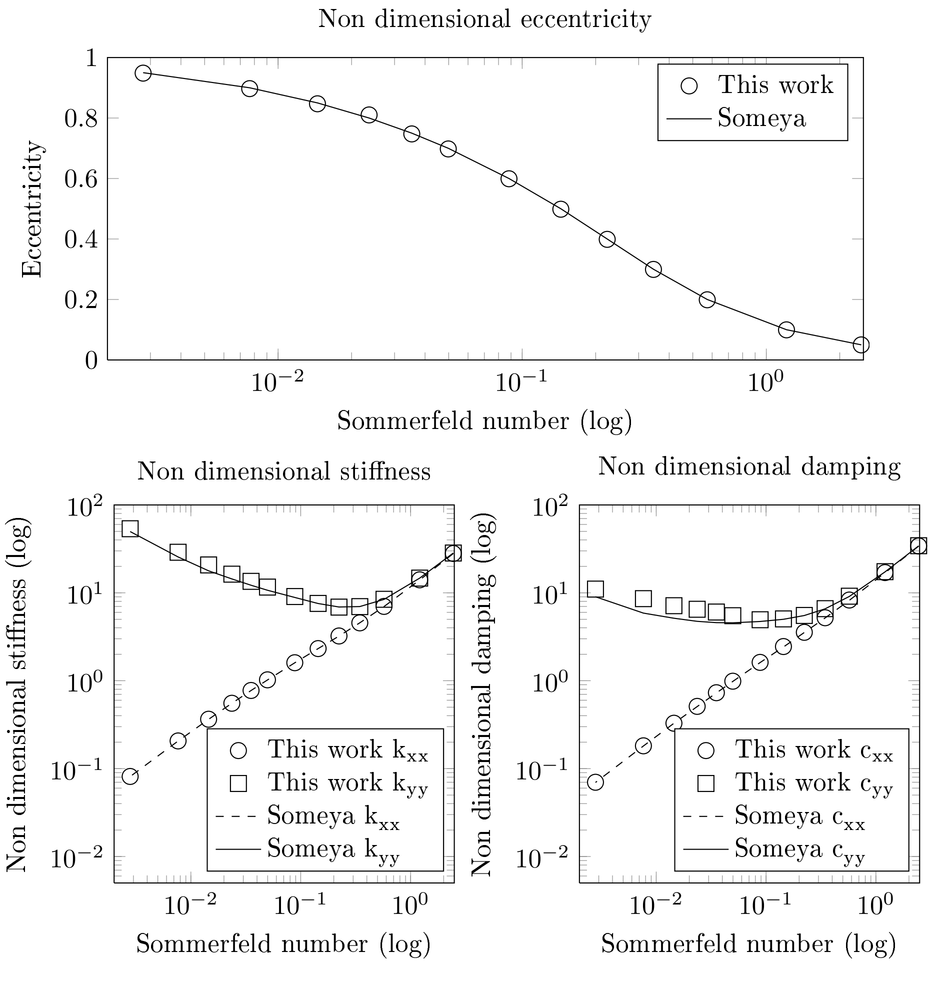

Figure 4.2: Validation against Someya [64] for bearing no. 49, journal eccentricity and synchronously reduced dynamic coefficients for different Sommerfeld numbers

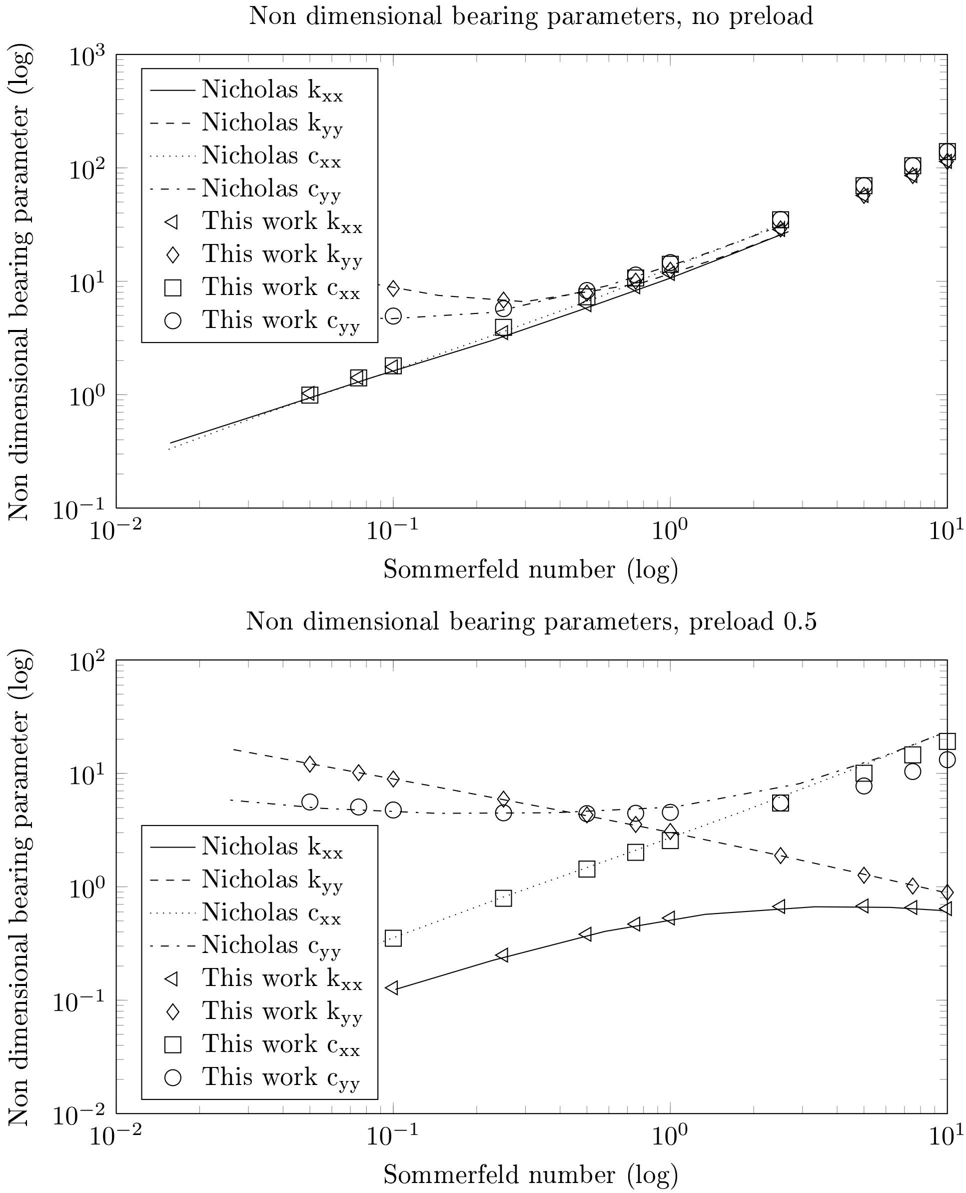

Figure 4.3: Validation against Nicholas *et al.* [65], synchronously reduced dynamic coefficients for different preloads

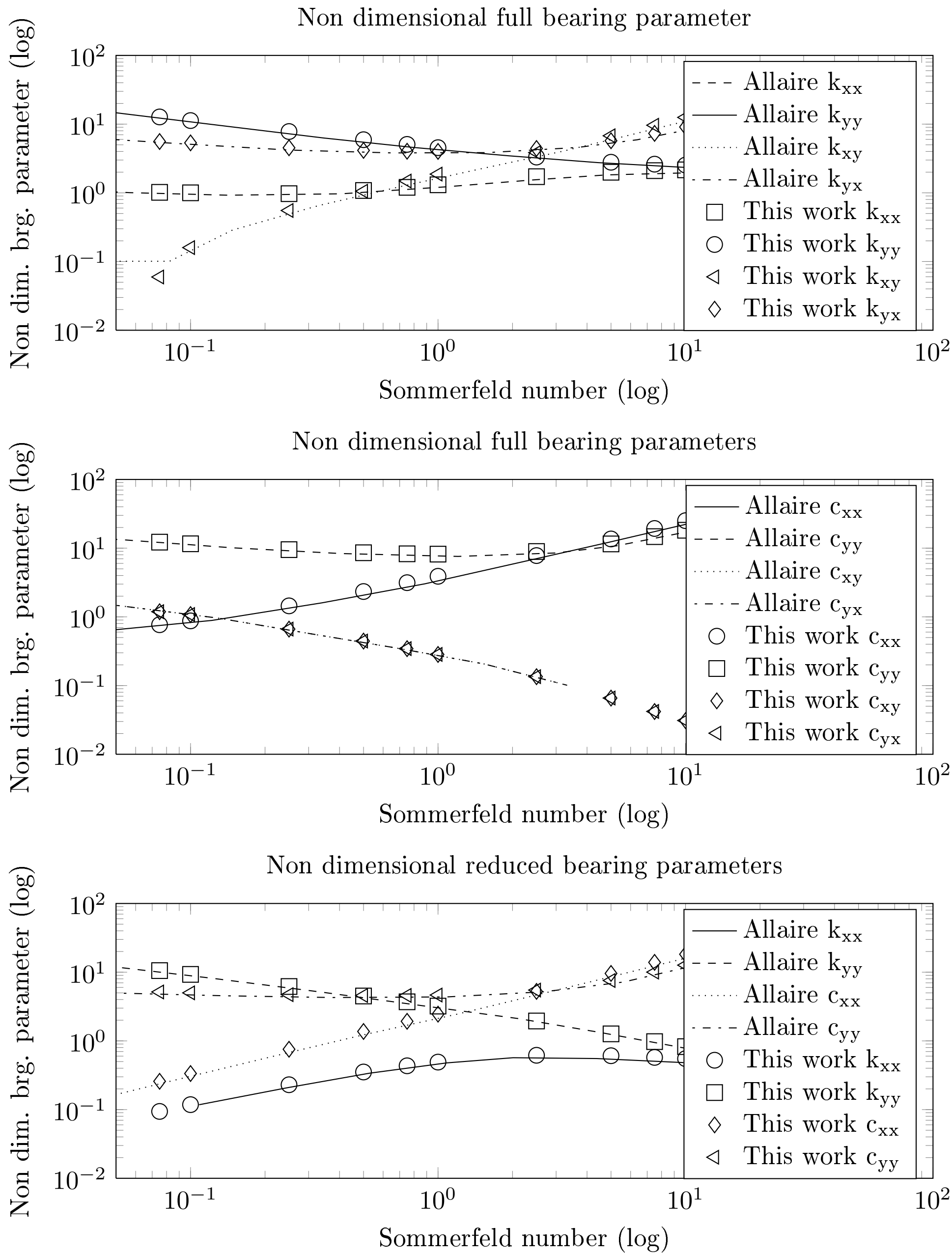

Figure 4.4: Validation against Allaire *et al.* [5], full and synchronously reduced dynamic coefficients

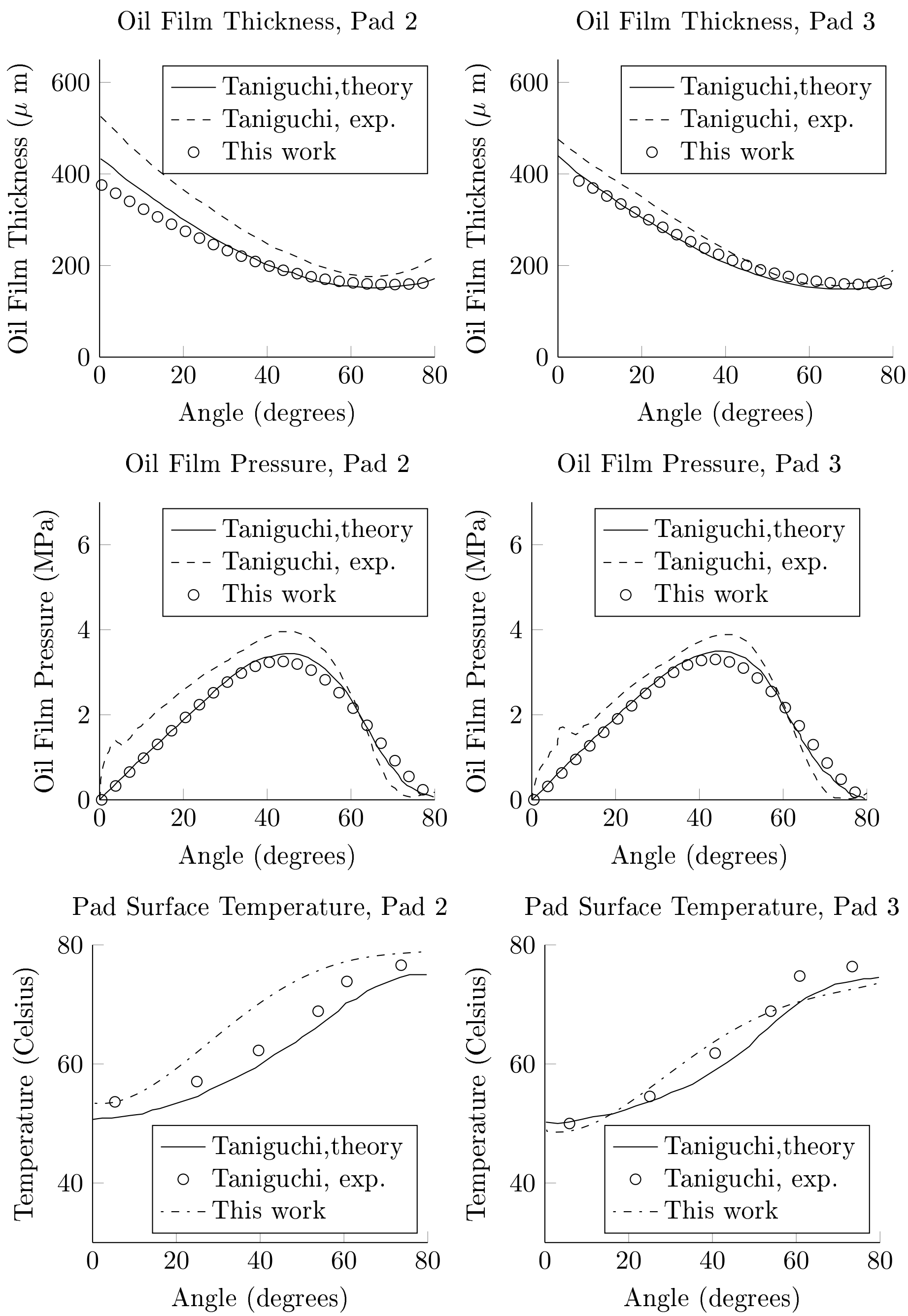

Figure 4.5: Validation against Taniguchi *et al.* [48], experimental and theoretical results for the oil film pressure, oil film thickness and pad surface temperature

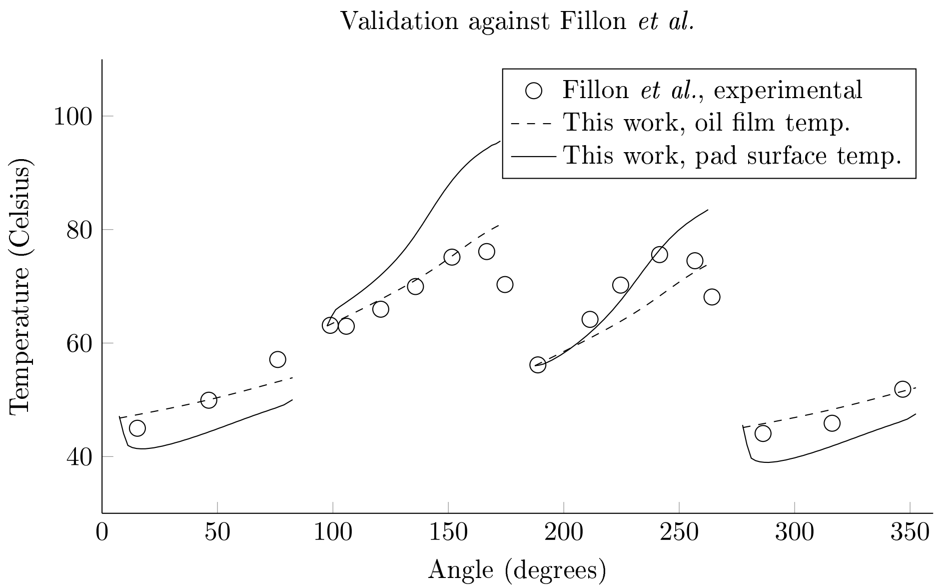

Figure 4.6: Validation against Fillon *et al.* [19], experimental results for the pad surface temperature

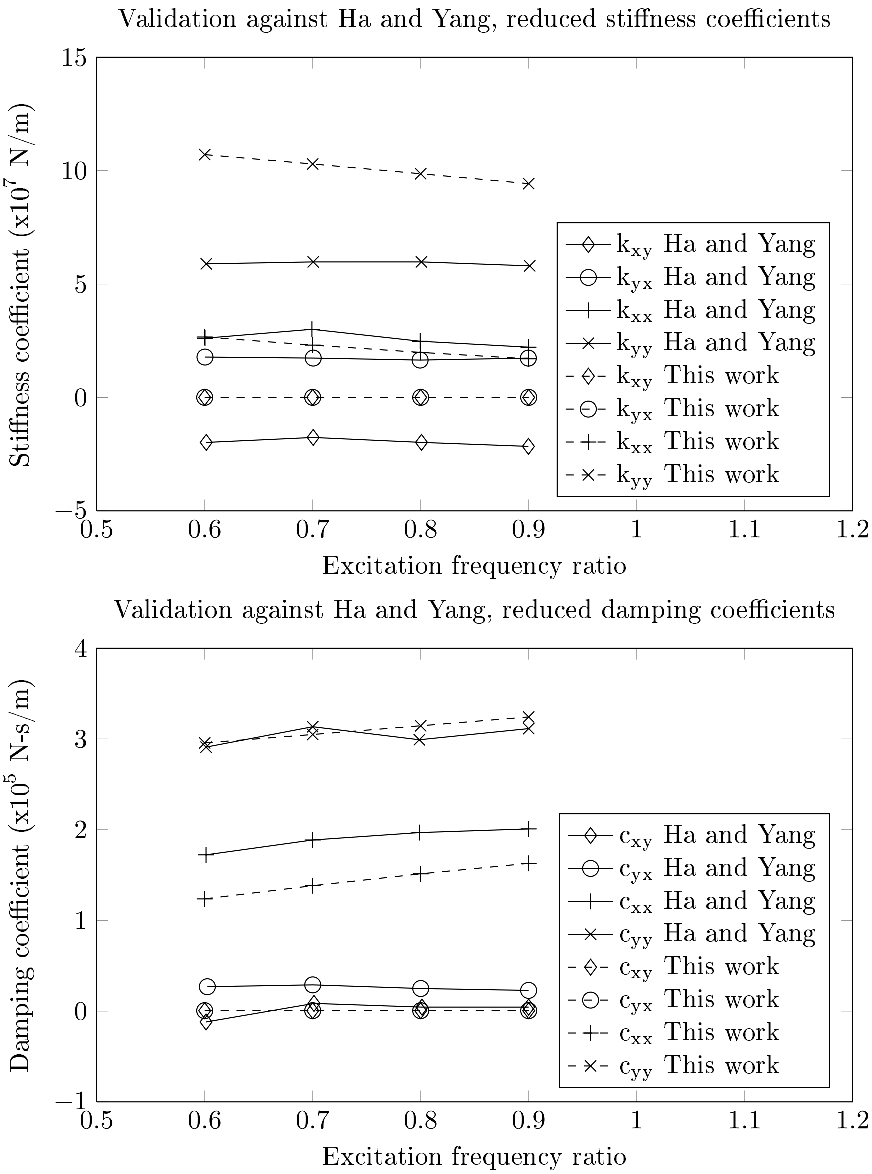

Figure 4.7: Validation against Ha and Yang [11], experimental results for the frequency dependency of reduced dynamic coefficients

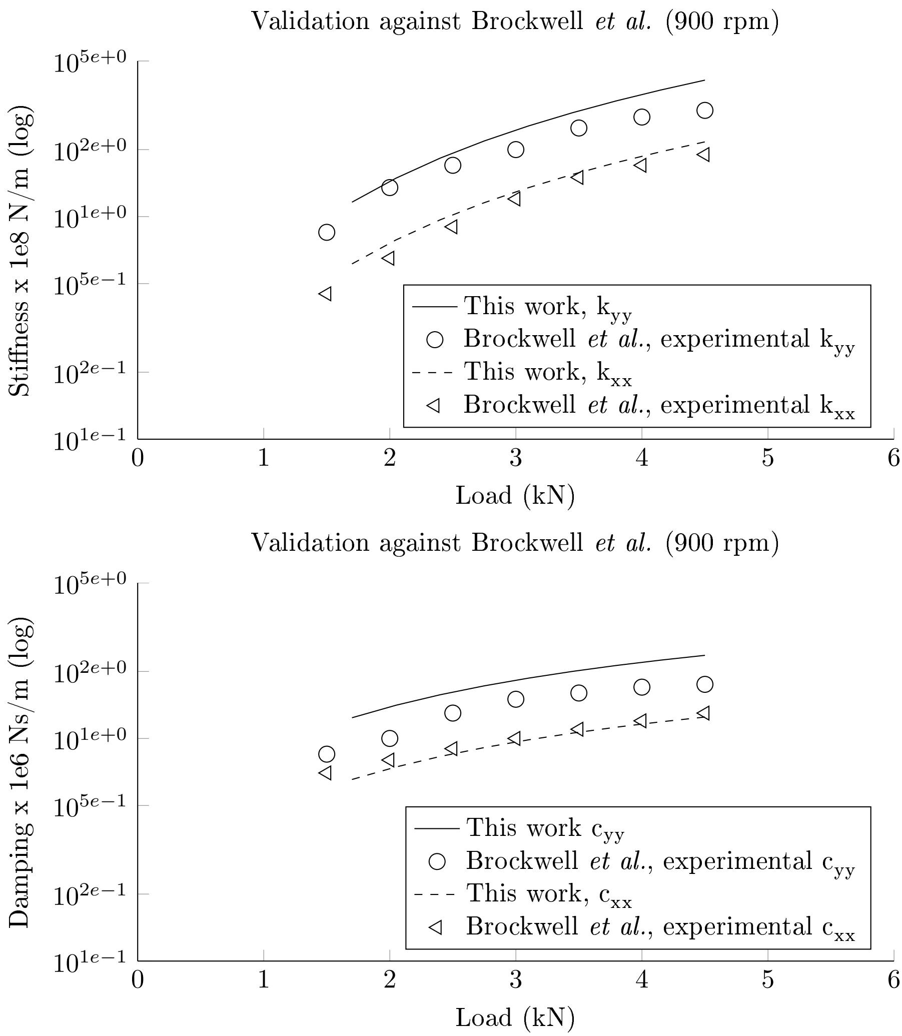

Figure 4.8: Validation against Brockwell *et al.* [10], experimental results for the synchronously reduced dynamic coefficients (900 RPM)

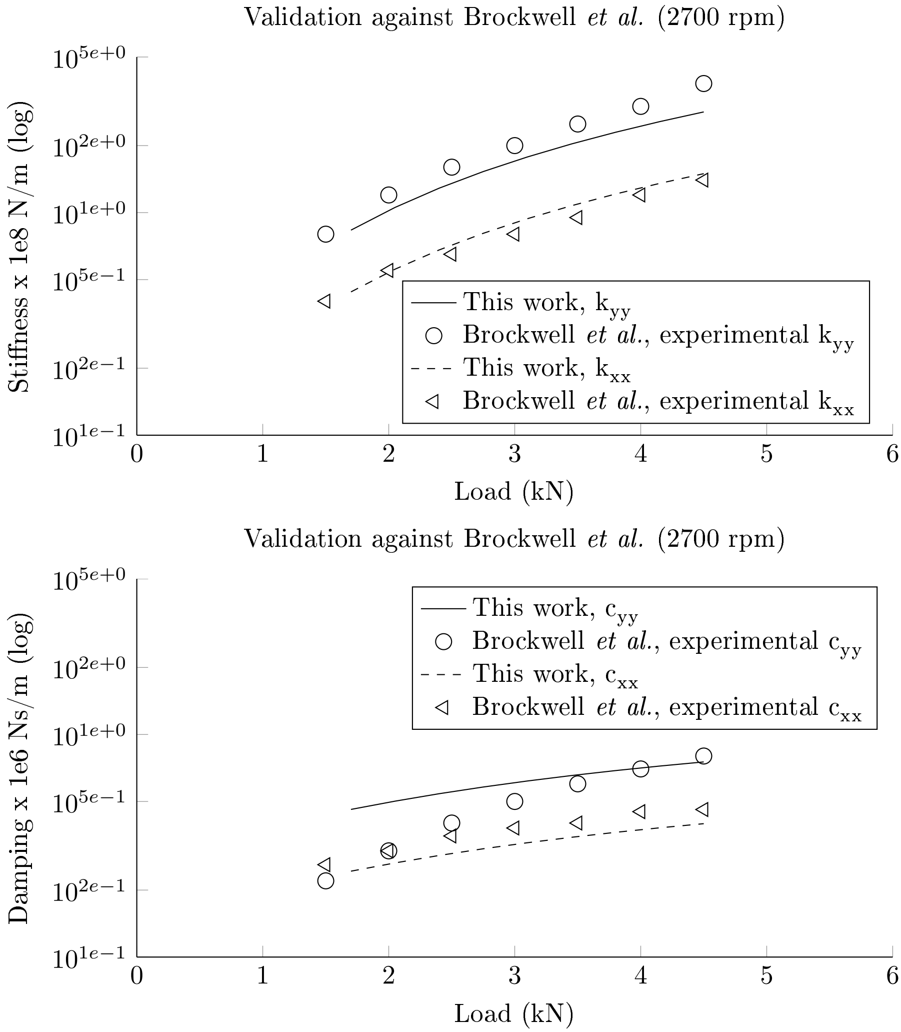

Figure 4.9: Validation against Brockwell *et al.* [10], experimental results for the synchronously reduced dynamic coefficients (2700 RPM)

Chapter 5

Controllable TPJB: Results

This chapter contains the results obtained during this research project, contained in the form of five journal and conference papers. A short outline of the topics covered on each one of these publications is given as follows:

1. Publication 1 focuses on theoretically studying the effect of applying different lubrication regimes for tilting-pad journal bearings (hydrodynamic, elastohydrodynamic, termohydrodynamic, controllable hydrodynamic), over the dynamic response of an industrial compressor.
2. Publication 2 presents the coupled thermoelastohydrodynamic model for the tilting-pad journal bearing with controllable lubrication, developed in this research project.
3. Publication 3 deals with the improvement of the thermal model for the controllable tilting-pad bearing, by studying simplified approaches to include explicitly the heat transfer effect betwen oil film and pad surface.
4. Publication 4 presents the experimental validation of the thermoelastohydrodynamic model for the tilting-pad journal bearing with controllable lubrication, regarding the prediction of static and thermal behavior.
5. Publication 5 studies experimentally the application of the controllable TPJB as a calibrated shaker for rotordynamic parameter identification purposes.

5.1 Publication 1: Stability Analysis of an Industrial Gas Compressor Supported by Tilting-Pad Bearings Under Different Lubrication Regimes

Stability Analysis of an Industrial Gas Compressor Supported by Tilting-Pad Bearings Under Different Lubrication Regimes

Alejandro Cerda Varela[1]
e-mail: acer@mek.dtu.dk

Ilmar Ferreira Santos
e-mail: ifs@mek.dtu.dk

Department of Mechanical Engineering,
Technical University of Denmark,
2800 Kgs. Lyngby, Denmark

This work is aimed at a theoretical study of the dynamic behavior of a rotor-tilting pad journal bearing (TPJB) system under different lubrication regimes, namely, thermohydrodynamic (THD), elastohydrodynamic (EHD), and hybrid lubrication regime. The rotor modeled corresponds to an industrial compressor. Special emphasis is put on analyzing the stability map of the rotor when the different lubrication regimes are included into the TPJB modeling. Results show that, for the studied rotor, the inclusion of a THD model is more relevant when compared to an EHD model, as it implies a reduction on the instability onset speed for the rotor. Also, results show the feasibility of extending the stable operating range of the rotor by implementing a hybrid lubrication regime.
[DOI: 10.1115/1.4004214]

1 Introduction

Tilting pad journal bearings are commonly used in rotating machinery due to their inherent stability properties [1,2] Hence, an important amount of effort has been put during the last four decades in order to improve the quality and accuracy of the available models for such devices.

Lund [3] was one of the first authors to solve the Reynolds equation for calculating theoretically the reduced dynamic coefficients of tilting-pad journal bearings. This work was later on extended by Allaire [4] in order to calculate the complete set of dynamic coefficients for the bearing. Malcher [5] and Klumpp [6] investigated theoretically and experimentally the behavior of the dynamic coefficients on the basis of advanced experiments. Jones and Martin [7] studied theoretically the influence of bearing geometry on the steady-state and dynamic behavior of these bearings. Springer [8,9], Rouch [10], and Parsell et al. [11] investigated theoretically the dynamic properties of these bearings for predicting rotor instabilities. Ettles [12] included pivot flexibility and thermal effects in one model and concluded that thermal effects can reduce the bearing damping properties. Such damping reduction effect was also observed when including pad flexibility in a simplified model [13] and when using the finite element method to include both pad flexibility and pivot stiffness [14,15]. Dmochowski [16] investigated theoretically as well as experimentally the behavior of damping and stiffness reduced coefficients as a function of the excitation frequency taking into consideration the influence of pivot flexibility. The tilting pad-journal bearings models have been expanded consistently from their basic hydrodynamic formulation to include other effects, currently reaching a thermoelastohydrodynamic formulation [17]. Also, experimental and theoretical effort has been extended to the study of the feasibility of achieving an active lubrication regime [18–21], where the TPJB can be used to apply controlled forces over the rotor, enabling to modify its dynamic behavior.

The rotor-bearing stability properties are strongly dependent on the bearing dynamic coefficients [22] due to their significant contribution to the stiffness and specially damping characteristics of the overall system. Hence, the stability analysis of a rotor supported by TPJBs is strongly dependent on the modeling of the bearings themselves; hence on the lubrication regime assumed.

The main original contribution of this paper is not focused on the actual modeling of the TPJB-rotor system, but on the comparison of the effect of different lubrication regimes over the rotor stability analysis. This work is aimed at investigating the stability of an industrial compressor supported by TPJBs. Three lubrication regimes (EHD, THD, hybrid) are separately imposed, in order to clearly identify their effect on the stability of the global system.

2 Modeling

For the modeling of the rotor-bearing system, this paper relies heavily on previous work on the subject. Hence, the mathematical models used to describe the behavior of the different components of the system are only presented in a brief way, for the sake of completeness of this paper. For a more complete description on the way such models were obtained, the reader should refer to the given references.

2.1 Modified Reynolds Equation. The theoretical stability analysis of an industrial rotor requires the existence of a mathematical model capable of representing accurately the inertia, stiffness, and damping properties of the studied system. The inclusion of the bearings into the model requires an adequate modeling of their stiffness and damping properties. Such properties, in the case of tilting pad journal bearings, depend on the pressure field developed within the oil film during the operation of the bearing. Hence, a suitable model for the oil film behavior is required.

The fluid film behavior in the land surfaces of finite oil film bearing is described by the Reynolds equation, deduced by using the Navier–Stokes and continuity equations, considering a laminar flow where the inertia of the fluid and the shear viscous forces in the radial direction are neglected. The nonslip boundary condition is applied at the surface of the rotor and the pads. The basic formulation for the Reynolds equation was extended [18] in order to

[1]Corresponding author.

Contributed by the International Gas Turbine Institute (IGTI) for publication in the Journal of Engineering for Gas Turbines and Power. Manuscript received April 27, 2011; final manuscript received May 3, 2011; published online December 20, 2011. Editor: Dilip R. Ballal.

include the effect of injecting oil into the bearing clearance using an orifice drilled through the surface of the pad, obtaining the modified Reynolds equation as shown in Eq. (1):

$$\frac{\partial}{\partial \bar{y}}\left(\frac{h^3}{\mu}\frac{\partial p}{\partial \bar{y}}\right)+\frac{\partial}{\partial \bar{z}}\left(\frac{h^3}{\mu}\frac{\partial p}{\partial \bar{z}}\right)-\frac{3}{\mu l_0}\sum_{i=1}^{n_0}F_i(\bar{y},\,\bar{z})\cdot p$$
$$=6U\frac{\partial h}{\partial \bar{y}}-12\frac{\partial h}{\partial t}-\frac{3}{\mu l_0}\sum_{i=1}^{n_0}F_i(\bar{y},\,\bar{z})\cdot P_{inj} \tag{1}$$

where $F_i(\bar{y},\bar{z})$ is defined as follows:

$$F_i(\bar{y},\bar{z})=\frac{d_0^2}{4}-(\bar{y}-\bar{y_i})^2-(\bar{z}-\bar{z_i})^2$$
$$\text{if } (\bar{y}-\bar{y_i})^2-(\bar{z}-\bar{z_i})^2\le\frac{d_0^2}{4}$$
$$F_i(\bar{y},\bar{z})=0 \tag{2}$$
$$\text{if } (\bar{y}-\bar{y_i})^2-(\bar{z}-\bar{z_i})^2\ge\frac{d_0^2}{4}$$

A number of publications [19–21] on the subject of actively lubricated tilting pad journal bearings base the modeling of the oil film under a hybrid lubrication regime on Eq. (1). The references included here only correspond to the earlier work on the subject. It can be seen that the function $F_i(\bar{y},\bar{z})$ is related to the orifice's position along the pad surface, given by the coordinates $(\bar{y_i},\,\bar{z_i})$, and the orifices diameter d_0. For a passive TPJB, $F_i(\bar{y},\bar{z})$ is equal to zero; hence the term P_{inj} corresponding to the oil injection pressure, vanishes.

From Eq. (1), it can be seen that pressure field $p(\bar{y},\bar{z})$ developed in the oil film is a function of rotor rotational speed ($U=\Omega R$), the oil viscosity μ, the oil film thickness h, which is a function of rotor journal position and the rotation of each bearing pad, and the injection pressure P_{inj} and injection hole geometry, in the case of a hybrid lubrication regime. Hence, this basic model can be extended in order to include other effects which vary any of these parameters, entailing a modification of the pressure profile and the resulting forces over the rotor, with the subsequent change in the behavior of the TPJBs-rotor system.

2.2 Thermohydrodynamic Model. The previously defined model for the oil film behavior corresponds to an isothermal formulation for the problem. It means that the effect of the temperature build up due to the viscous forces generated across the oil film during the operation of the bearing and the subsequent reduction of the oil film viscosity is neglected. If such effect is included into the modeling, then a THD model is obtained, as explained in Refs. [23,24]. To do so, one must solve the energy equation, stated in Eq. (3), in order to obtain the temperature field $T(\bar{y},\bar{z})$ across the oil film as a function of the bearing gap h.

$$\rho C_p h\frac{\partial T}{\partial t}+k_c h\frac{\partial^2 T}{\partial \bar{y}^2}+k_c h\frac{\partial^2 T}{\partial \bar{z}^2}+k_c\left.\frac{\partial T}{\partial \bar{x}}\right|_0 F_i$$
$$+\left(\frac{\rho C_p h^3}{12\mu}\frac{\partial p}{\partial \bar{y}}-\frac{\rho C_p U h}{2}\right)\frac{\partial T}{\partial \bar{y}}+\frac{\rho C_p h^3}{12\mu}\frac{\partial p}{\partial \bar{z}}\frac{\partial T}{\partial \bar{z}}$$
$$\rho C_p\left(V_{inj}-\frac{\partial h}{\partial t}\right)(T-T_{inj})=\frac{4}{3}\frac{\mu}{h}\left(V_{inj}-\frac{\partial h}{\partial t}\right)^2$$
$$p\left(V_{inj}-\frac{\partial h}{\partial t}\right)-U^2\frac{\mu}{h}-\frac{h^3}{12\mu}\left[\left(\frac{\partial p}{\partial \bar{y}}\right)^2+\left(\frac{\partial p}{\partial \bar{z}}\right)^2\right] \tag{3}$$

It must be noted that the THD model presented here corresponds to an adiabatic solution, meaning that no heat transfer takes place between the oil and the pads. Here, the injection velocity profile V_{inj} is determined as a completely developed laminar flow inside the injection orifice, using the following expression:

$$V_{inj}(\bar{y},\,\bar{z})=-\frac{1}{4\mu l_0}\left(P_{inj}-p\right)\cdot\sum_{i=1}^{n_0}F_i(\bar{y},\,\bar{z}) \tag{4}$$

Once Eq. (3) is solved and the temperature field $T(\bar{y},\bar{z})$ is obtained, one can calculate the viscosity across the oil film as a function of such temperature field.

2.3 Elastohydrodynamic Model. In this work, the inclusion of the pad flexibility is done following a pseudomodal reduction scheme, as exposed first in Ref. [25] and then used in Refs. [26,27] to study the EHD regime with hybrid lubrication. The pads are modeled using the finite element method. By using this method, the mathematical model for the pads is defined as

$$\mathbf{M}_s\ddot{q}_s+\mathbf{K}_s q_s=f_s \tag{5}$$

where q_s correspond to the degrees of freedom for each node of the finite element model, $\mathbf{M}_s$ and $\mathbf{K}_s$ correspond to the inertia and stiffness matrix for the pads, obtained using the finite element method, and f_s represent the loads over the pads due to the pressure profile in the oil film. By calculating the pseudomodal matrix $\mathbf{V}_s$ containing on its columns some of the eigenmodes of the pads, one can rearrange Eq. (5) as follows:

$$\mathbf{V}_s^T\mathbf{M}_s\mathbf{V}_s\ddot{q}_s^*+\mathbf{V}_s^T\mathbf{K}_s\mathbf{V}_s q_s^*=\mathbf{V}_s^T f_s$$
$$q_s=\mathbf{V}_s q_s^* \tag{6}$$

By using the reduction scheme exposed in Eq. (6), one ends working with a reduced system defined by the modal coordinates vector q_s^*, where there are as many degrees of freedom as eigenmodes were included into the modal matrix $\mathbf{V}_s$. It corresponds to a pseudomodal reduction, since only the eigenmodes which are relevant are included into the analysis. If only the first eigenmode is included, then a rigid pad model is established, and the corresponding modal coordinate measures the rotation of the pad around the pivot. The use of higher eigenmodes enables to include the flexibility of the pads into the results.

Since it is always possible to obtain the "true" displacements of the pads q_s based on the modal displacements q_s^*, one can determine the oil film thickness h in order to solve Reynolds equation. Hence, the link between pad deformation and pressure profile and the resulting loads over the rotor and pads is established. The use of the pseudomodal reduction is especially convenient when it comes to obtain the dynamic coefficients of the TPJB. If one uses the full finite element model of the pads in order to obtain the dynamic coefficients of the bearing, it is necessary to perturb analytically or numerically every single degree of freedom associated with the finite element model. By using the pseudomodal reduction scheme, only the modal coordinates q_s^* are perturbed, reducing the workload and making the results more manageable and easier to interpret on a physical way.

2.4 TPJB Dynamic Coefficients. The inclusion of the TPJBs into the global rotor model is performed by calculating the dynamic coefficients associated with the bearings. First introduced by Ref. [3] to obtain synchronously reduced dynamic coefficients and then extended by Ref. [4] to calculate the complete set of dynamic coefficients, the concept of the dynamic coefficients has become a cornerstone among the tools employed for analyzing the dynamic behavior of a rotor mounted over oil film bearings. It allows the analyst to avoid the computationally expensive operation of solving the Reynolds equation to determine the pressure profile and the resulting loads over the rotor journal and bearing pads. Instead, the behavior of such loads is linearized around the static equilibrium of the system, using a first order approximation. Hence, one can define the stiffness and damping coefficients for the TPJB as follows:

$$
\begin{aligned}
k_{ij} &= \frac{\partial F_i}{\partial \delta_j} \\
d_{ij} &= \frac{\partial F_i}{\partial \dot{\delta}_j}
\end{aligned}
\tag{7}
$$

where δ_j corresponds to the degrees of freedom associated with the journal-TPJB system. If a rigid pad model is used, then $i, j = 1, \ldots, 2 + n_s$, including the two translational degrees of freedom of the rotor journal and the rotations of each pad. If a flexible pad model is used, then $i, j = 1, \ldots, 2 + n_s \cdot n_{flex}$, where n_{flex} correspond to the number of modes for each pad included into the analysis, according to the pseudomodal reduction scheme. If $n_{flex} = 1$, then the flexible model is reduced to a rigid pad model.

Synchronously reduced coefficients are calculated in order to describe the general behavior of the stiffness and damping properties of the bearing when the different lubrication regimes are included. For analyzing the stability of the TPJBs-rotor system, the complete set of dynamic coefficients are used. Some results regarding the stability of the TPJB-rotor system are also obtained using the synchronously reduced dynamic coefficients of the bearings, in order to observe their effect into the overall stability behavior of the studied system.

2.5 Rotor Modeling. The finite element method is employed to model the rotor, using shaft elements, as proposed by Ref. [28]. Proportional damping is used in order to model the energy dissipation across the rotor. The proportional damping parameters are tuned in order to obtain a damping ratio equal to 0.001 for the two first natural frequencies of the rotor on free-free boundary conditions.

By using this method, the system can be represented mathematically as follows:

$$
\mathbf{M}_r \ddot{q}_r + (\mathbf{D}_r - \Omega \mathbf{G}_r)\, \dot{q}_r + \mathbf{K}_r q_r = f_r \tag{8}
$$

In Eq. (8), q_r represent the degrees of freedom of the nodes corresponding to the finite shaft model of the rotor, $\mathbf{M}_r$ is the rotor inertia matrix, $\mathbf{D}_r$ is the proportional damping matrix, $\mathbf{G}_r$ is the gyroscopic matrix, and $\mathbf{K}_r$ is the rotor stiffness matrix. Related to the loading term f_r, for this analysis the only loading applied to the system corresponds to the static load due to the weight of the rotor.

2.6 Stability Analysis for the TPJBs-Rotor System. So far, the mathematical models for the TPJBs and the rotor have been exposed separately. In order to analyze the stability, one must couple such models into a global system, which includes the degrees of freedom of the rotor and the bearing pads. By doing so, the model for the global system is defined as:

$$
\begin{gathered}
\mathbf{M}_g \ddot{q}_g + \left(\mathbf{D}_g - \Omega \mathbf{G}_g\right) \dot{q}_g + \mathbf{K}_g q_g = f_g \\
\text{where } q_g = \left\{ q_r \; q_s^* \right\}^T
\end{gathered}
\tag{9}
$$

The degrees of freedom for the global system q_g are defined by the rotor model degrees of freedom q_r and by the pads degrees of freedom q_s^*, derived from the pseudomodal reduction. If a rigid pad model is utilized, then there are n_s degrees of freedom associated with pads, corresponding to the rotations around the pivots. If a flexible model is used, then there are $n_s n_{flex}$ degrees of freedom associated with the pads, with the additional degrees of freedom related to the pad deformations. According to Eq. (9), in order to analyze the system it becomes necessary to define the global mass, damping and stiffness matrices. The use of the dynamic coefficients for representing the TPJBs in the global system enables to do such coupling in a straightforward fashion.

The procedure followed to analyze the stability of the rotor system is depicted as follows:

(1) Set a desired rotational speed for the rotor Ω.
(2) Using a Newton Raphson scheme, determine the static equilibrium position for the global system q_g^0. The Reynolds equation is solved in order to determine the pressure field on each pad. Then, direct integration of the pressure field is employed in order to determine the forces over the rotor and the pads surface by the fluid film.
(3) For the determined equilibrium position, using a perturbation method, one calculates the dynamic stiffness and damping coefficients for each TPJB, related to the rotor journal degrees of freedom and the pads degrees of freedom coming from the pseudomodal reduction scheme. By doing so, stiffness $\mathbf{K}_{b1}$, $\mathbf{K}_{b2}$ and damping matrices $\mathbf{D}_{b1}$, $\mathbf{D}_{b2}$ are obtained for each bearing.
(4) By assembling the stiffness and damping matrix from the rotor finite element model $\mathbf{K}_r$ and $\mathbf{D}_r$ with the ones coming from the bearings stiffness coefficients $\mathbf{K}_{b1}$, $\mathbf{K}_{b2}$ and damping coefficients $\mathbf{D}_{b1}$, $\mathbf{D}_{b2}$, one obtains the global matrices $\mathbf{K}_g$ and $\mathbf{D}_g$. As for the global mass matrix $\mathbf{M}_g$, only the inertia coming from the rotational degrees of freedom of the pads is included into the model.
(5) aving the global matrices completely defined, including both the presence of the rotor and the bearing pads, it is possible to calculate the eigenvalues and eigenmodes for the global system. The sign of the real part of the obtained eigenvalues is used to determine the stability of the system. If positive, it means that the rotor system presents unstable behavior.

3 Case Analysis: Industrial Compressor Modeling

In this section, the results obtained by using the previously defined mathematical model for studying an industrial case are presented. The system modeled corresponds to an industrial rotor system. Namely, the rotor corresponds to a gas compressor, composed of five impellers. It weighs 391 Kg, and it operates normally within the range of 6942 RPM and 10,170 RPM. The rotor is supported by two identical tilting pad journal bearings. Figure 1 shows the finite element model of such rotor, depicting also the location of the TPJB and the reference systems used on this study. The loading due to the rotor weight acts on the negative y direction; hence pad #4 becomes the most heavily loaded one. The impellers, seals and other machine elements are considered as rigid disks and are incorporated into the model by adding inertia to the respective nodes. Hence, in the model, the impellers are at nodes 20, 24, 28, 32, and 36. Bushes are at nodes 22, 26, 30, and 34. A thrust disk sleeve is located at node 3. A balance piston is

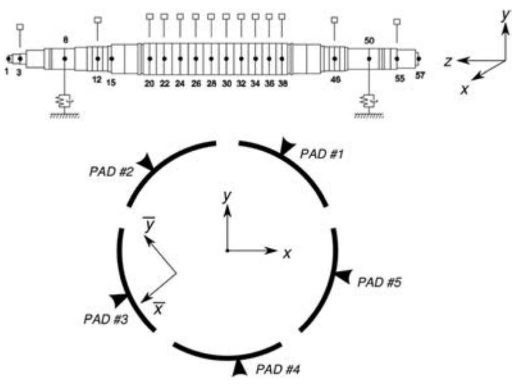

Fig. 1 Mechanical model of the compressor by shaft elements; global coordinate system (x, y, z) and pad local coordinate system ($\bar{x}$, $\bar{y}$, $\bar{z}$) used for the study

located at node 38. Seal bushes are located at nodes 12 and 46. Coupling is at node 55.

As for the TPJBs, they are located at nodes 8 and 50. From now on, the bearing located at node 8 will be referred as "bearing 1" and the one located at node 50 as "bearing 2." Table 1 depicts all the parameters that define the geometry of such bearings.

3.1 Numerical Results. The obtained results are presented in a way that enables to compare the effect of including different lubrication regimes models for the TPJBs on the overall behavior of the studied rotor-bearings system. Hence, only one effect is studied at the time, in order to identify clearly the consequences of including it into the modeling. The lubrication regimes to be studied are follow.

3.1.1 Elastohydrodynamic Lubrication Regime (EHD). In this section, the flexibility of the pads is included into the model by using the pseudomodal reduction method. The oil film is modeled using the Reynolds equation. No thermal effects are included into the oil film model. The bearings work in passive configuration, meaning that no oil injection into the bearing clearance is taking place.

3.1.2 Thermohydrodynamic Lubrication Regime (THD). In this section, the temperature build-up generated on the bearings oil film due to rotor operation is modeled using the THD model exposed previously. No pad flexibility effects are included, and no oil is injected into the bearing clearance.

3.1.3 Hybrid Lubrication Regime. in this section, the effect of injecting oil at different pressures into the bearing clearance is included. No thermal effects and no pad flexibility effects are taken into account.

The results analyzed include: static equilibrium position for the TPJB pads and rotor journals, dynamic coefficients for the TPJBs, stability map for the rotor-bearings system. Regarding the equilibrium position results, the eccentricity ratio is calculated as the ratio between shaft journal displacement and the assembled bearing gap (h_0). The results obtained are presented as a function of the rotor rotational speed in the range between 6000 RPM and 11,000 RPM.

Table 1 TPJB characteristics

Parameter	Value	Units
Journal radius (R)	50.800	mm
Number of pads (n_s)	5	–
Pad inner radius (R_s)	50.921	mm
Pad aperture angle (α_0)	60	deg.
Angular position pivot pad #1	60	deg.
Angular position pivot pad #2	132	deg.
Angular position pivot pad #3	204	deg.
Angular position pivot pad #4	276	deg.
Angular position pivot pad #5	348	deg.
Offset	0.6	–
Pad width (L)	44.450	mm
Pad thickness (Δs)	10.312	mm
Pad material elasticity modulus (E)	200	GPa
Pad material Poisson's ratio (ν)	0.3	–
Pad material density (ρ_s)	7800	Kg/m^3
Injection orifice length (l_0)	5.0	mm
Injection orifice diameter (d_0)	5.0	mm
Number of orifices per pad (n_0)	1,2	–
Assembled bearing gap (h_0)	102	μm
Oil viscosity (40°C) (μ)	0.028	Pa s
Oil viscosity (80°C) (μ)	0.007	Pa s
Oil density (ρ)	863.5	kg/m^3
Oil specific heat (C_p)	1900	J/kgK
Oil thermal conductivity (k_c)	0.13	W/mK
Oil supply temperature	50	°C

3.2 Elastohydrodynamic Regime Results. The behavior of the pressure field generated in a TPJB oil film is influenced, among other over variables, by the bearing clearance, namely, the distance existing between the pad and the journal surface. Such parameter is included into the Reynolds equation by the h parameter. When one considers the pads to be rigid, such parameter is only a function of the journal position and the pads angular rotation. However, if the pads are considered as flexible elements, then the clearance is also a function of the deformations on the pads due to the load exerted over them by the oil film pressure. Hence, one can expect that the pressure field, and the resulting forces over the rotor are affected by the pad flexibility effect. The question to be answered is how relevant is the inclusion of such effect into the overall modeling of the rotor dynamic behavior.

First, one can compare the static equilibrium position achieved by the rotor journal and the bearing pads when including the flexibility of the pads into the modeling. Figure 2 shows the eccentricity ratio and rotation of pad #4 as a function of the rotation speed of the rotor, for the rigid and the flexible pads. It can be seen that, by including the flexibility of the pads, the eccentricity ratio decreases over the studied rotational speed, and the tilt angle of the pad becomes higher. Hence, the equilibrium position of the system is altered. Since for all cases the same load is applied over the bearing (the one due to the weight of the rotor), one can state that by including the pad flexibility the bearing system actually becomes stiffer; in other words, for the same applied load over the rotor journal a lower displacement is obtained. Although the fact that by adding extra flexibility into the pads model entails a stiffer bearing system may seem unnatural at first glance, one must understand that the overall stiffness of the bearing system is highly influenced by the stiffness of the oil film. Such stiffness is a function of the bearing clearances, determined by the system equilibrium position and deformation of the pads. Hence, since the effect of the pad flexibility is to alter the bearing clearance, the stiffness of the oil film is modified, implying that the overall system becomes stiffer.

The previous statement can be confirmed by taking a look at Figs. 3 and 4. One can see that the inclusion of the pad flexibility entails a variation of the oil film thickness, which also implies that the pressure profile is modified. Such change is a consequence of the system new equilibrium position (rotor journal position and pad tilt) and the deformation of the pads. It is also seen that such effect is stronger for higher rotational speed, which is consistent on the higher pressure generated when operating at a higher speed, which implies higher deformation of the pads.

From the results presented so far, one can also note that the inclusion of modes 2 and 3 into the flexible model of the pad does not entail a relevant change in the behavior of the system, when compared to the effect of just including the first flexible mode. This means that the first flexible mode is dominating when it comes to obtaining the deformed shape of the pad under load. The deformation of the surface of the pad due to the first flexible mode can be seen in Fig. 5. It can be seen that the maximum deformation of the pad is about a 3% of the oil film minimum thickness, and it is obtained toward the edge of the pads. No deformation is obtained around the pivot of the pad, due to the fact that the included mode corresponds to a pure bending mode, where no pad surface deformation is included and where the nodes around the pivot have their displacement restricted. As expected, the deformation of the pads due to the first flexible mode is larger for higher rotational speed, and the deformations implies that, in practice, the curvature radius of the pads are increased. Such effect implies a higher "effective" preload factor into the system, which support the "stiffening" effect commented when looking at the results shown in Fig. 2.

The link between the TPJB "local" behavior, discussed so far, and the overall dynamic behavior of the rotor system comes from the dynamic coefficients, used to represent the bearing into the dynamic model. In order to present this information in a compact way, the synchronously reduced dynamic coefficients are obtained

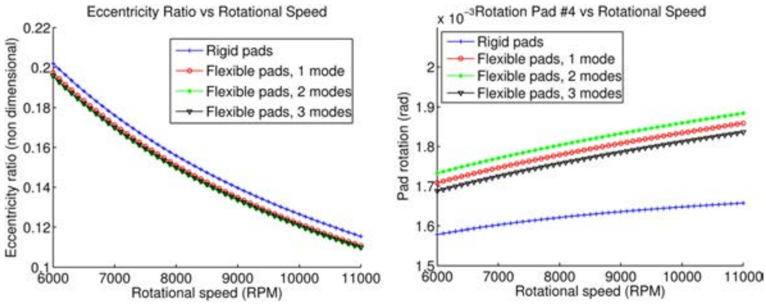

Fig. 2 Static equilibrium position for bearing 1, as a function of the rotational speed; results for the eccentricity ratio of the rotor journal and the rotation of pad #4

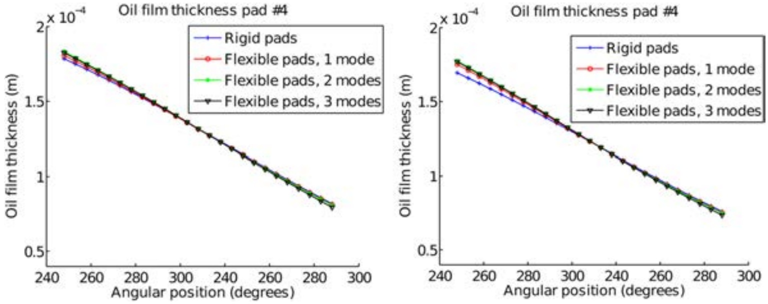

Fig. 3 Oil film thickness for bearing 1 pad #4 at equilibrium position; comparison of results for 6000 RPM (left) and 11,000 RPM (right). Results obtained at $\overline{Z} = 0$.

for the studied TPJB. The direct stiffness and damping coefficients in the vertical direction of bearing 1, as a function of the rotational speed, are shown in Fig. 6. On these results, the conclusions obtained so far from the equilibrium positions, oil film thickness and pressure profiles of the studied bearing are confirmed. First, one can note convergence behavior on the results obtained when including just the first flexible mode and the two other modes. Secondly, it can be seen that the results from the rigid pad and the flexible pad model approach each other for lower rotational speeds. This is consistent with the relationship between rotational speed, pressure profile, and deformations of the pads. Thirdly, it can be noted that the inclusion of the pad flexibility generates a stiffening of the overall bearing system. Lastly, one can see a reduction of the damping coefficient of the bearing when increasing the rotational speed and when including the flexibility of the pads. This result fits with the stiffening effect observed when increasing the rotational speed and when including the flexibility of the pads.

The stability map obtained using the TPJB complete dynamic coefficients is shown in Fig. 7. Results are shown for the rigid and flexible pad assumption. Once again, convergence on the behavior of the system when incorporating the different flexible modes for the pads is observed. It can be noted that the instability onset speed is not modified in a noticeable way by the inclusion of modes 2 and 3, when compared to the results obtained when only including the first flexible mode. When comparing the results obtained assuming rigid pads with those including the first flexible mode, it can be seen that the change in the instability onset speed

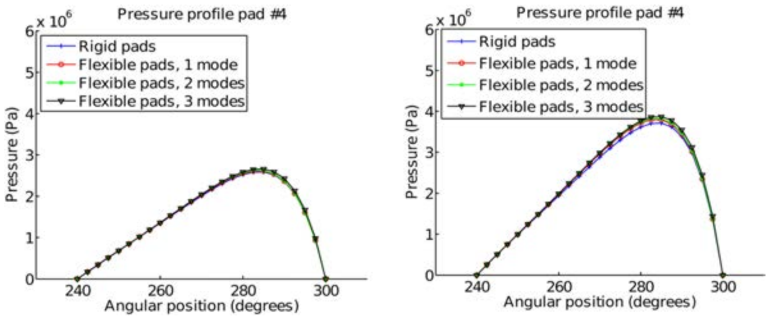

Fig. 4 Pressure profile at equilibrium position for bearing 1 pad #4; comparison of results for 6000 RPM (left) and 11,000 RPM (right). Result obtained at $\overline{Z} = 0$.

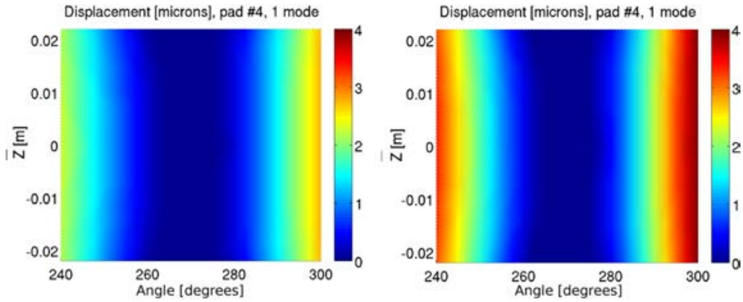

Fig. 5 Deformation of bearing 1 pad #4 at equilibrium position; comparison of results for 6000 RPM (left) and 11,000 RPM (right)

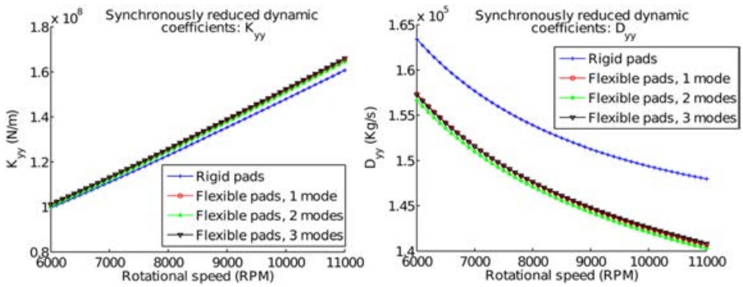

Fig. 6 Synchronously reduced direct stiffness and damping coefficients for bearing 1, vertical direction: comparison between rigid pads and flexible pads with different numbers of flexible modes included

is almost negligible. Putting this result in perspective, it means that for the specific rotor under study, under its particular operating conditions of load and speed, the effect of including the flexibility of the pads is not relevant when it comes to analyzing the stability of the rotor system.

3.3 Thermohydrodynamic Regime Results. The viscous friction forces generated across the TPJB oil film induce a temperature build up of the oil. Since the oil viscosity is a function of the temperature, such property of the lubricant is modified when including a thermal model in the modeling of the oil film behavior. From the Reynolds equation, it is evident that any change in the viscosity of the lubricant induces changes in the pressure profiles; hence in the overall behavior of the bearing.

By solving the THD model, one obtains nonuniform temperature and viscosity values for the oil film. Such results are shown in Fig. 8. From those results, it becomes clear the increase in the oil film temperature and the decrease of the oil viscosity for a higher rotational speed. Also, it can be seen that the highest temperature values (and lower viscosity) are obtained in the area where the oil film thickness is lower?

When looking at Fig. 9, one can see that the change in viscosity due to the oil temperature build up has clear effects on the equilibrium position of the bearing. The eccentricity ratio becomes higher for all rotational speeds analyzed, meaning the rotor journal achieves a lower equilibrium position. Also, the tilt of the pad becomes higher. This can be explained when analyzing the Reynolds equation. In order to equilibrate the static load applied over

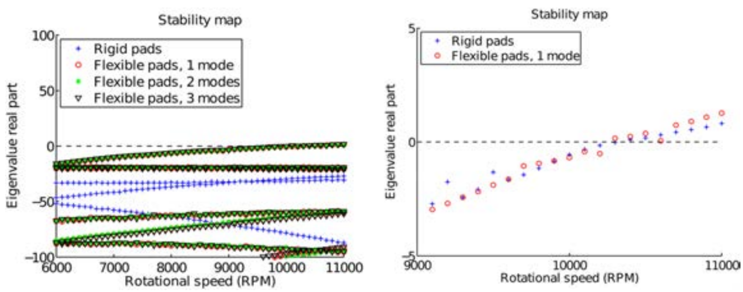

Fig. 7 Stability map for the compressor; comparison between rigid pads and flexible pads model, for different numbers of modes (figure to the right details the instability onset zone)

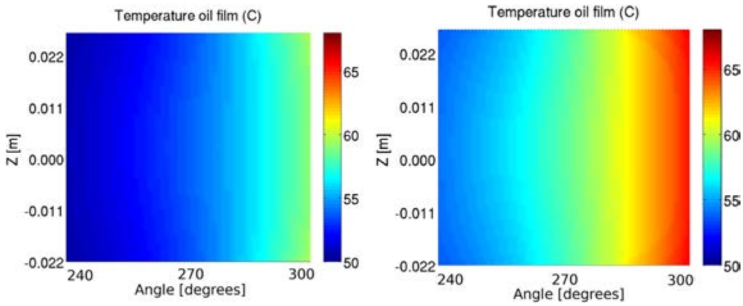

Fig. 8 Oil film temperature for bearing 1 pad #4 at equilibrium position; comparison of results for 6000 RPM (left) and 11,000 RPM (right)

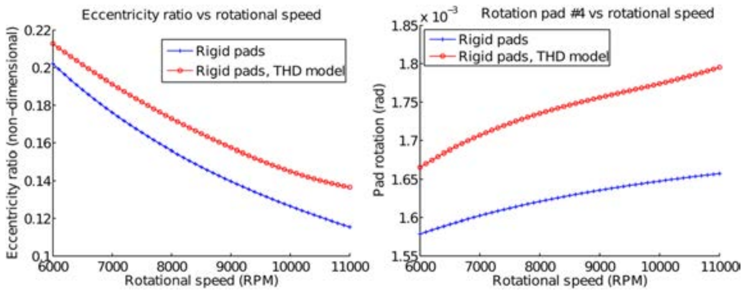

Fig. 9 Static equilibrium position for bearing 1, as a function of rotational speed; results for eccentricity ratio of the rotor journal and the rotation of pad #4

the rotor journal, a pressure profile must be obtained on each pad. The pressure profile, on static conditions, is a function of the gradient of the oil film thickness in the journal sliding direction. Since the viscosity is lower for higher temperatures, a higher oil film thickness gradient is necessary in order to generate the required pressure profile. This is obtained by a higher eccentricity and a higher tilt of the pads.

The change induced over the oil film thickness and the pressure profile by the oil film thermal effects entails a change in the bearing dynamic coefficients, as shown in Fig. 10. The overall effect consists in a reduction of the bearing stiffness and damping properties. Such reduction becomes more important as one increases the rotational speed, which is consistent with the fact that shear forces across the fluid film are a function of the rotational speed of the rotor.

When looking at the stability map shown in Fig. 11, it becomes clear that for the studied rotor, not including the thermal effects on the oil film modeling would induce an overestimation of the stability of the rotor. This is a relevant result, moreover because the load and operating speed of the studied system can be considered "low."

3.4 Stability Analysis Using the Synchronously Reduced Dynamic Coefficients for the Bearings. The stability results presented so far were obtained using the full set of dynamic coefficients to include the bearings into the rotor model. If one uses the synchronously reduced dynamic coefficients to represent the bearings, the results obtained for the stability map are shown in Fig. 12. By comparing these results with the ones already

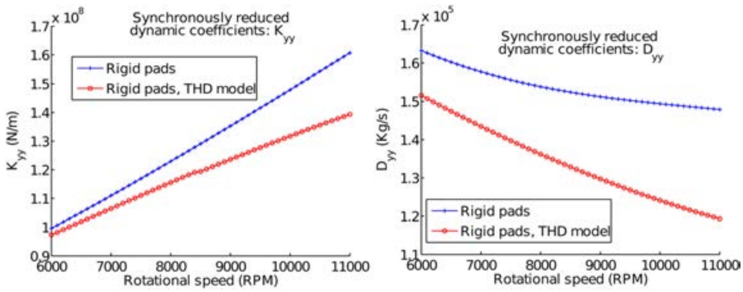

Fig. 10 Synchronously reduced direct stiffness and damping coefficients for bearing 1, vertical direction; effect of including THD model

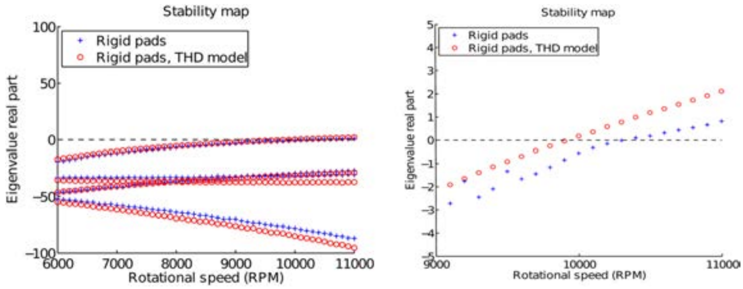

Fig. 11 Stability map for the compressor; effect of including the THD model for the oil film (figure to the right details the instability onset zone)

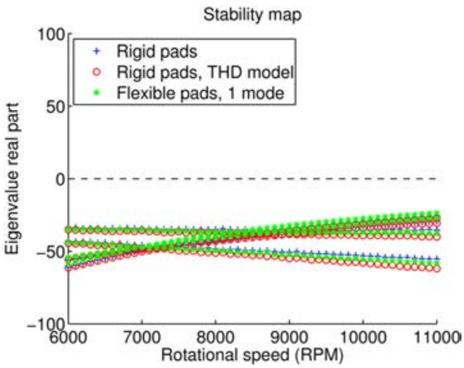

Fig. 12 Stability map for the compressor, calculated using the TPJBs synchronously reduced dynamic coefficients for different lubrication regimes

presented in Figs. 7 and 11, it becomes evident that such an approach induces an important overestimation of the stable operating range of the studied system, when compared to the results obtained using the full set of bearing dynamic coefficients.

3.5 Hybrid Lubrication Regime Results. When speaking of a hybrid lubrication regime, one refers to a system where high pressurized oil is injected through an orifice (or several orifices) on the pads directly into the bearing clearance. In contrast to an active lubrication regime, in the hybrid regime the injection pressure is fixed to a constant value. By doing so, it is possible to modify the oil film pressure profile, entailing a modification of the dynamic properties of the TPJB [19–21]. Hence, it is reasonable to think that by using a proper configuration for the hybrid system it should be possible to extend the rotor stable operating range.

A number of configurations (defined by position of injection holes on the pads) were tested using the available model for the rotor-TPJBs system. From those preliminary iterations, two configurations were chosen and are presented here. They provide satisfactory results regarding to an increase of the rotor stability range. Both configurations set the position of the injection holes towards the leading edge of the bearing pads. A scheme for the disposition of the injection holes is provided in the figures. It is important to highlight that the distribution of the holes is not symmetrical with respect to the pivot line (no holes are positioned close to the trailing edge).

In Fig. 13, it can be seen that by injecting pressurized oil into the bearing clearance the equilibrium position of the rotor journal and the bearing pads is greatly influenced. By injecting oil near the leading edge of the pads, one increases the pressure field on that region. In order to achieve its static equilibrium, the pressure near the trailing edge must be incremented; hence a higher tilt for the pads is observed. It can be seen that such an effect is a more pronounced force for the "two injection holes" configuration, which is consistent with the higher increase in the pressure field when compared to the "one hole" configuration.

The corresponding change in the oil film thickness and pressure profile entails modification of the bearing dynamic coefficients, as can be seen in Fig. 14. It can be noted that the expected decrease in the damping for the TPJB when increasing the rotor rotational speed is actually diminished when using the hybrid lubrication regime. A reduction in damping is obtained for this regime when compared to the passive configuration (no injection), but the damping characteristics remain more or less constant through the analyzed rotational speed range.

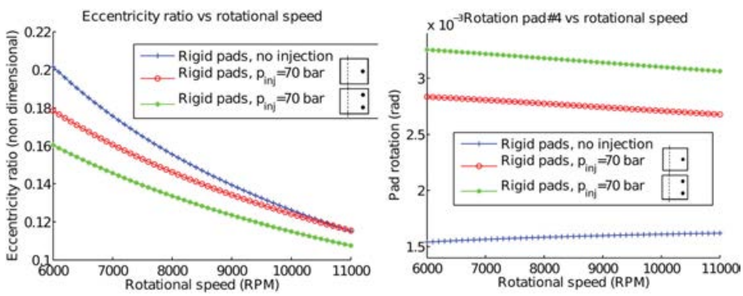

Fig. 13 Static equilibrium for bearing 1, as a function of rotational speed; results for the eccentricity ratio of the rotor journal and the rotation of pad #4, effect of oil injection for two configurations

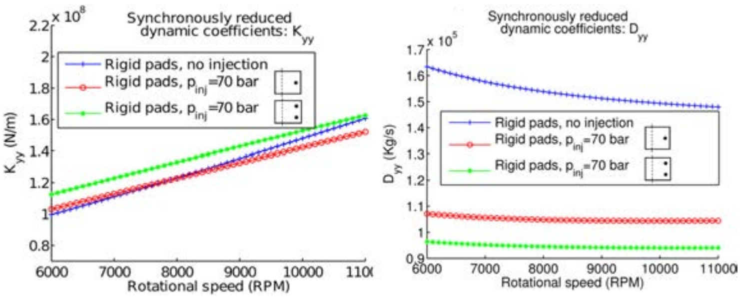

Fig. 14 Synchronously reduced direct stiffness and damping coefficients for bearing 1, vertical direction; effect of oil injection for two configurations

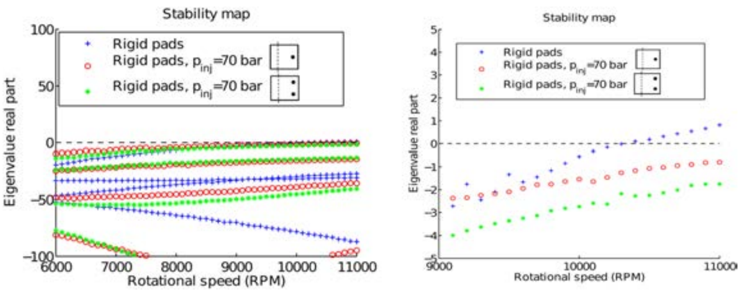

Fig. 15 Stability map for the compressor; effect of hybrid oil injection for two configurations (figure to the right details the instability onset zone)

When looking at the stability map depicted in Fig. 15, it can be seen that both configurations for the hybrid lubrication enable one to extend the stable operational range of the rotor. Although it can be seen that the real part of the eigenvalues gets closer to zero for the studied range when compared to the "no injection" case, the instability onset speed is increased for the hybrid lubrication regime. As for the effect of the injection pressure, from Fig. 16, it can be seen that even for a relatively low injection pressure (20 bar), it is possible to increase the instability onset speed of the rotor, when compared to the passive lubrication regime. Hence, it has been demonstrated that the use of a hybrid lubrication regime, with the proper positioning of the injection holes on the pads, can present advantages over a passive regime (no injection) when considering the stability of the system. Another benefit from this regime is the cooling effect, reducing the overall temperature of the oil film [23,24].

4 Conclusion

In this work, an industrial compressor mounted over TPJBs has been modeled and analyzed, in order to assess the effect of including different lubrication regimes in the dynamic behavior of the system. Results have been obtained in the form of equilibrium positions and dynamic coefficients for the TPJBs, and a stability map for the compressor. According to the numerical results obtained, one can state the following conclusions:

(1) The instability onset speed of the rotor-TPJB system studied is 10,300 RPM for the passive bearing for isothermal model with no pad flexibility effects included; 9900 RPM for the THD lubrication regime; 10,300 for the EHD lubrication regime; over 11,000 RPM for the hybrid lubrication regime.

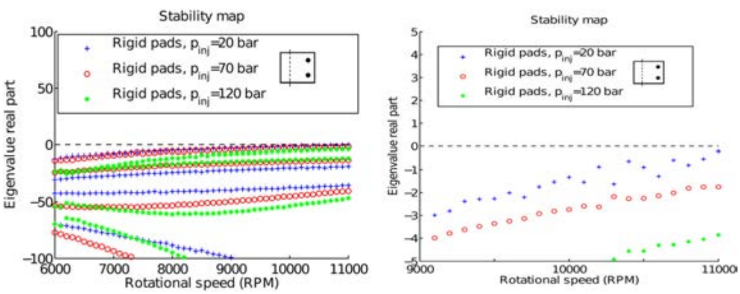

Fig. 16 Stability map for the compressor; effect of injection pressure for hybrid regime with "two holes" configuration (figure to the right details the instability onset zone)

(2) The results obtained for the stability map show that neglecting the temperature build up of the oil film due to viscous forces generated during the bearing operation would induce an overestimation of the instability onset speed for the rotor. Hence, according to these results, even for a rotor working with loading and speed conditions as the ones imposed on the model (which can be considered to be on the "low" range) it is relevant to include a THD modeling of the oil film behavior.
(3) The inclusion of the pad flexibility effect into the modeling, using a pseudomodal reduction scheme, presented a negligible effect on the instability onset speed for the analyzed rotor, when compared to the results obtained when including the THD model. Again, such result must be analyzed taking into account the particular operational conditions of the analyzed rotor.
(4) When analyzing the synchronously reduced dynamic coefficients for the TPJBs, it can be noted that the inclusion of the pad flexibility into the modeling induces an increase in the stiffness and a reduction on the damping of the bearing. Hence, a model for TPJB that neglects the pad flexibility will overestimate the damping of the bearing.
(5) The results obtained for equilibrium positions and dynamic coefficients for the bearings and stability map for the rotor show that the effect of including higher modes into the pseudomodal reduction scheme is negligible when compared to just including the first bending mode for the pads. Convergence behavior is observed when including higher modes into the modeling. Hence, according to these results it is enough to include the first bending mode in order to model the effect of flexibility of the pads.
(6) The results of the stability analysis of the rotor-TPJB system using the synchronously reduced dynamic coefficients showed an overestimation of the stable operating range of the rotor, when compared to the results obtained using the full set of dynamic coefficients.
(7) The theoretical results obtained show that when imposing a hybrid lubrication regime for the bearings, using a constant oil injection pressure, it is possible to extend the stable operational range for the rotor. The results obtained are dependent on the configuration for the injection holes on the pad and the oil injection pressure. From the obtained results, it can be concluded that a proper configuration for increasing the instability onset speed of the rotor must place the injection holes towards the leading edge of the pads.

Nomenclature

α_0 = TPJB pad apperture angle
Δs = TPJB pad thickness
μ = oil dynamic viscosity (Pa s)
ν = TPJB pad material Poisson's ratio
Ω = rotor rotational speed (rad/s)
$\bar{x}$ = pad local Cartesian coordinate system
$\bar{y}$ = pad local Cartesian coordinate system
$\bar{z}$ = pad local Cartesian coordinate system
ρ = oil density ($\mathrm{Kg/m^3}$)
ρ_s = TPJB pad material density
$\mathbf{D}_{b1}$ = damping matrix for the TPJB 1
$\mathbf{D}_{b2}$ = damping matrix for the TPJB 2
$\mathbf{D}_g$ = damping matrix for the TPJB-rotor global model
$\mathbf{D}_r$ = damping matrix for the rotor finite element model
$\mathbf{G}_g$ = gyroscopic matrix for the TPJB-rotor global model
$\mathbf{G}_r$ = gyroscopic matrix for the rotor finite element model
$\mathbf{K}_{b1}$ = stiffness matrix for the TPJB 1
$\mathbf{K}_{b2}$ = stiffness matrix for the TPJB 2
$\mathbf{K}_g$ = stiffness matrix for the TPJB-rotor global model
$\mathbf{K}_r$ = stiffness matrix for the rotor finite element model
$\mathbf{K}_s$ = stiffness matrix for the pad finite element model
$\mathbf{M}_g$ = inertia matrix for the TPJB-rotor global model
$\mathbf{M}_r$ = inertia matrix for the rotor finite element model
$\mathbf{M}_s$ = inertia matrix for the pad finite element model
$\mathbf{V}_s$ = pseudomodal matrix for the pad finite element model
F = positioning function for injection holes ($\mathrm{m^2}$)
C_p = oil specific heat (J/kg K)
d_0 = diameter of the oil injection hole (m)
d_{ij} = damping coefficients for the TPJB
E = TPJB pad material elasticity modulus
EHD = elastohydrodynamic lubrication regime
f_g = TPJB-rotor global model load vector
f_r = rotor finite element model load vector
f_s = pad finite element model load vector
h = oil film thickness (m)
k_c = oil thermal conductivity (W/m K)
k_{ij} = stiffness coefficients for the TPJB
L = TPJB pad width
l_0 = length of the oil injection hole (m)
n_0 = number of injection holes on each pad
n_{flex} = number of eigenmodes included into the pseudomodal matrix for the pad finite
n_s = number of pads on the TPJB
p = oil film pressure (Pa)
P_{inj} = oil injection pressure (Pa)
q_g = TPJB-rotor global model displacements vector
q_g^0 = TPJB-rotor global model static equilibrium vector
q_r = rotor finite element model displacements vector
q_s = pad finite element model displacements vector
q_s^* = modal displacements for the pad model pseudomodal reduction
R = rotor journal radius
R_s = TPJB pad inner radius
T = oil temperature (°C)
t = time (s)
THD = thermohydrodynamic lubrication regime
TPJB = tilting pad journal bearing
U = rotor journal tangential speed (m/s)
V_{inj} = injection velocity (m/s)
x = global Cartesian coordinate system
y = global Cartesian coordinate system
z = global Cartesian coordinate system

References

[1] Glienicke, J., 1987, "Stabilitatsprobleme bei Lagerung schnellaufender Wellen-Berechnung, Konstruktion und Verhalten von Mehrflchen- und Kippsegmentlagern," Technische Akademie Wuppertal, Germany.
[2] Flack, R. D., and Zuck, C. J., 1988, "Experiments on the Stability of Two Flexible Rotor in Tilting Pad Journal Bearing," Tribol. Trans., **31**(2), pp. 251–257.
[3] Lund, J., 1964, "Spring and Damping for the Tilting Pad Journal Bearings," ASLE Trans., **7**(4), pp. 342–352.
[4] Allaire, P., Parsell, J., and Barrett, L., 1981, "A Pad Perturbation Method for the Dynamic Coefficients of Tilting-Pad Journal Bearings," Wear, **72**, pp. 29–44.
[5] Malcher, L., 1975, "Die Federungs- und Dampfungseigenschaften von Gleitlagern fur Turbomaschinen – Experimentelle Untersuchungen von MGF- und Kippsegmentlagern," Ph.D. thesis, Technical University of Karlsruhe.
[6] Klumpp, R., 1976, "Die Eigenschaften von Kippsegment-Radiallagern," Konstruktion, **28**(8), pp. 320–324.
[7] Jones, G., and Martin, F., 1979, "Geometry Effects in Tilting Pad Journal Bearings," ASLE Trans., **22**(3), pp. 227–246.
[8] Springer, H., 1978, "Zur Berechnung Hydrodynamischer Lager mit Hilfe von Tschebyscheff-Polynomen," Forsch. Ing.-Wes., **44**(4), pp. 126–134.
[9] Springer, H., 1979, "Nichtlineare Schwingungen schwerer Rotoren mit vertikaler Welle und Kippsegmentradiallagern," Forsch. Ing.-Wes., **45**(4), pp. 119–132.
[10] Rouch, K., 1983, "Dynamic of Pivoted Pad Journal Bearings, Including Pad Translation and Rotation Effects," ASLE Trans., **26**(1), pp. 102–109.
[11] Allaire, P., Parsell, J., and Barrett, L., 1983, "Frequency Effects in Tilting Pad Journal Bearing Dynamic Coefficients," ASLE Trans., **26**(2), pp. 222–227.
[12] Ettles, C., 1980, "The Analysis and Performance of Pivoted Pad Journal Bearings Considering Thermal and Elastic Effects," J. Lubr. Tech., ASME Trans.,**102**(2), pp. 182–194.
[13] Lund, J., 1987, "The Influence of Pad Flexibility on the Dynamic Coefficients of a Tilting Pad Journal Bearing," ASME J. Tribol., **109**, pp. 65–70.
[14] Earles, L., Palazzolo, A., and Armentrout, R., 1990, "A Finite Element Approach to Pad Flexibility Effects in Tilting Pad Journal Bearings: Part I - Single Pad Analysis," ASME J. Tribol., **112**, pp. 169–177.

[15] Earles, L., Palazzolo, A., and Armentrout, R., 1990, "A Finite Element Approach to Pad Flexibility Effects in Tilting Pad Journal Bearings: Part II—Assembled Bearing and System Analysis," ASME J. Tribol., **112**, pp. 178–182.
[16] Dmochowski, W., 2007, "Dynamic Properties of Tilting-Pad Journal Bearings: Experimental and Theoretical Investigation of Frequency Effects due to Pivot Flexibility," ASME J. Eng. Gas Turbines Power, **129**, pp. 865–869.
[17] Fillon, M., Bligoud, J. C., and Frêne, J., 1992, "Experimental Study of Tilting-Pad Journal Bearings—Comparison with Theoretical Thermoelastohydrodynamic Results," ASME 1991 Modal Anal., Model., Diagn. Control Anal. Exp., **114**, pp. 579–588.
[18] Santos, I., 1994, "Design and Evaluation of Two Types of Active Tilting Pad Journal Bearings," *The Active Control of Vibration*, C. R. Burrows and P. S. Keogh, eds., Mechanical Engineering Publications, London, pp. 79–87.
[19] Santos, I., 1995, "Strategien fur die Erhohung der Dampfungsreserve von kippsegmentgelagerten Rotorsystemen," *Schwingungen in Rotierenden Maschinen*, Vol. 3, Nordmann, eds., Vieweg Verlag, Braunschweig, Germany, pp. 3–12.
[20] Santos, I., 1997, "Aktive Schmierung zur Regelung von Rotorsystemen," *Schwingungen in Rotierenden Maschinen*, Vol. 4, H. S. H. Krretier and R. Nordmann, eds., Vieweg Verlag, Braunschweig, Germany, pp. 37–47.
[21] Santos, I., and Russo, F., 1998, "Tilting-Pad Journal Bearings with Electronic Radial Oil Injection," J. Tribol., ASME Trans., **120**(3), pp. 583–594.
[22] Lund, J., 1974, "Stability and Damped Critical Speeds of a Flexible Rotor in Fluid-Film Bearings," ASME Trans., **73**, pp. 509–517.
[23] Santos, I., and Nicoletti, R., 1999, "THD Analysis in Tilting-Pad Journal Bearings Using Multiple Orifice Hybrid Lubrication," J. Tribol., ASME Trans., **121**, pp. 892–900.
[24] Santos, I., and Nicoletti, R., 2001, "Influence of Orifice Distribution on the Thermal and Static Properties of Hybridly Lubricated Bearings," Int. J. Solids Struct., **38**, pp. 2069–2081.
[25] Kim, J., Palazzolo, A., and Gadangi, R., 1995, "Dynamics Characteristics of TEHD Tilt Pad Journal Bearing Simulation including Multiple Mode Pad Flexibility," ASME J. Vib. Acoust., **117**(1), pp. 123–135.
[26] Haugaard, A., and Santos, I., 2010, "Multi-Orifice Active Tilting-Pad Journal Bearings-Harnessing of Synergetic Coupling Effects," Tribol. Int., **43**(8), pp. 1374–1391.
[27] Haugaard, A., and Santos, I., 2010, "Stability of Multi Orifice Active Tilting-Pad Journal Bearings," Tribol. Int., **43**(9), pp. 1742–1750.
[28] Nelson, H., and McVaugh, J., 1976, "The Dynamics of Rotor-Bearing Systems Using Finite Element," J. Eng. Ind., **98**, pp. 593–600.

5.2 Publication 2: Performance Improvement of Tilting-Pad Journal Bearings by means of Controllable Lubrication

Mechanics & Industry 13, 17–32 (2012)

DOI: 10.1051/meca/2012004
www.mechanics-industry.org

Mechanics & Industry

Performance improvement of tilting-pad journal bearings by means of controllable lubrication

Alejandro Cerda Varela[a] and Ilmar Ferreira Santos

Department of Mechanical Engineering, Technical University of Denmark, 2800 Kgs. Lyngby, Denmark

Received 28 July 2011, Accepted 3 November 2011

Abstract – Tilting-Pad Journal Bearings (TPJB) are commonly used on high-performance turbomachinery due to their excellent stability properties at high speed when compared to other designs for oil film bearings. Hence, efforts have been made to improve the accuracy for the available models for these mechanical devices, achieving nowadays an elasto-thermo-hydrodynamic formulation. On the other hand, the basic design of the Tilting-Pad Journal Bearing has been modified in order to transform it into a smart machine element. One approach to do so is to inject pressurized oil directly into the bearing clearance through holes drilled across the bearing pads. By adjusting the injection pressure, it is possible to modify the dynamic characteristics of the bearing. A controllable lubrication regime is obtained, allowing to expand the operational boundaries of the original design. This work focuses on presenting an elasto-thermo-hydrodynamic model (*ETHD*) for the Tilting-Pad Journal Bearing, including the effect of the controllable lubrication system. The basic model is validated by comparing its results against theoretical and experimental results available in the literature. Then, the validated code is used to show the benefits of applying a controllable lubrication regime, by means of the modification of the thermal and dynamic behaviour of the bearing.

Key words: Bearing / tilting pad / modelling / controllable / thermal / dynamics

Nomenclature

α_0	TPJB pad apperture angle (°)
Δs	TPJB pad thickness (m)
$\boldsymbol{D}_r$	proportional damping matrix of the rotor finite-element model
$\boldsymbol{D}_g$	damping matrix of the rotor-TPJBs model
μ	oil film dynamic viscosity (Pa.s)
μ_{inj}	oil injection dynamic viscosity (Pa.s)
ν	TPJB pad material Poisson ratio
Ω	rotor rotational speed (rad.s^{-1})
$\overline{x}$	pad local Cartesian coordinate system
$\overline{y}$	pad local Cartesian coordinate system
$\overline{z}$	pad local Cartesian coordinate system
ρ	oil density (kg.m^{-3})
ρ_s	TPJB pad material density (kg.m^{-3})
F	positioning function for injection holes (m^2)
C_p	oil specific heat (J.kg^{-1}.K)
d_0	diameter of the oil injection hole (m)
f_g	load vector for the rotor-TPJBs model
f_r	load vector for the rotor finite-element model
f_s	load vector for the pad finite-element model
E	TPJB pad material elasticity modulus (Pa)
EHD	elastohydrodynamic lubrication regime
$ETHD$	elastothermohydrodynamic lubrication regime
h	oil film thickness (m)
$\boldsymbol{K}_s$	stiffness matrix of the pad finite-element model
$\boldsymbol{K}_r$	stiffness matrix of the rotor finite-element model
$\boldsymbol{K}_g$	stiffness matrix of the rotor-TPJBs model
k_c	oil thermal conductivity (W.m^{-1}.K)
k_p	pad material thermal conductivity (W.m^{-1}.K)
L	TPJB pad width (m)
l_0	length of the oil injection hole (m)
$\boldsymbol{M}_s$	mass matrix of the pad finite-element model
$\boldsymbol{M}_r$	mass matrix of the rotor finite-element model
$\boldsymbol{M}_g$	mass matrix of the rotor-TPJBs model
n_0	number of injection holes on each pad
n_s	number of pads on the TPJB
p	oil film pressure (Pa)
P_{inj}	oil injection pressure (Pa)

[a] Corresponding author: acer@mek.dtu.dk

Article published by EDP Sciences

q_g	vector degrees of freedom for the rotor-TPJBs model
q_r	vector degrees of freedom for the rotor finite-element model
q_s	vector degrees of freedom for the pad finite-element model
q_s^*	vector degrees of freedom for the reduced pad finite-element model
R	rotor journal radius (m)
R_s	TPJB pad inner radius (m)
T	oil temperature (°C)
t	time (s)
THD	thermohydrodynamic lubrication regime
$TPJB$	tilting pad journal bearing
U	rotor journal tangential speed (m.s^{-1})
V_{inj}	injection velocity (m.s^{-1})
$\boldsymbol{V}_s$	pseudo modal matrix of the pad finite-element model
x	global Cartesian coordinate system
y	global Cartesian coordinate system
z	global Cartesian coordinate system

1 Introduction

Among the oil film bearing designs, the tilting-pad journal bearing is widely used due to their superior stability properties. Hence, there has been a constant interest over the years to improve the knowledge regarding the characteristics of this mechanical element. Such research effort has been carried out by means of continuous improvement the available mathematical models, as well as by experimental investigation of its static and dynamic behavior. Within the modelling effort, a number of authors have made significant contributions to the development of this area. Starting with the work from Lund [1], and later Allaire [2], the ground was set for the calculation of dynamic coefficients for this type of bearings. From there on, a number of publications have dealt with the incorporation of more effects into the modelling of the tilting-pad journal bearing. Namely, flexibility effects, coming from pad and pivot deformation due to thermal growth and presssure loading, and thermal effects, due to the temperature build-up within the oil film, are nowadays included into the modelling of tilting-pad journal bearings. Hence, the state of the art within the modelling of these bearings corresponds to an elasto-thermo-hydrodynamic ($ETHD$) formulation, such as the ones presented in [3,4]. Together with the development of the knowledge within this subject, several strategies have been formulated in order to enhace the versatility of the tilting-pad journal bearing, transforming it into a smart machine element. One approach to do it corresponds to the one presented by Santos [5], which involves the injection of pressurized oil into the bearing clearance, through holes drilled across the pads. Since the injection pressure can be modified, a controllable lubrication regime is established, which can enable to modify the dynamic properties of the bearing in order to fit the operational requirements. Many publications have dealt with the application of this concept, such as [6–12].

This work is aimed at presenting an elasto-thermo-hydrodynamic ($ETHD$) model for the tilting-pad journal bearing with controllable lubrication. Such model is used to obtain theoretical results that show the feasibility of improving the thermal and dynamic properties of such bearing by means of the controllable lubrication scheme.

2 Tilting-Pad Journal Bearing with controllable lubrication: mathematicals modelling

Previous publications on the subject of controllable lubrication have established separately a Thermo-Hydrodynamic model (THD) and an Elasto-Hydrodynamic model (EHD) for this lubrication regime. The main original contribution of this work correspond to the simultaneous implementation of both effects ($ETHD$) for the controllable lubrication Tilting-Pad Journal Bearing. For the sake of completeness, a brief presentation of such mathematical models is given here. The references provide a more complete presentation of such models.

2.1 Modified Reynolds Equation

The oil film pressure build up for the Tilting-Pad Journal Bearing has been traditionally described by means of the Reynolds Equation, based on the assumption of laminar flow and negligible effects of the fluid inertia and radial viscous shear forces. Such basic model was extended in [5], including some terms to model the effect of the oil injection into the bearing clearance. Hence, the Modified Reynolds Equation is established, as shown in Equation (1).

$$\frac{\partial}{\partial \overline{y}}\left(\frac{h^3}{\mu}\frac{\partial p}{\partial \overline{y}}\right)+\frac{\partial}{\partial \overline{z}}\left(\frac{h^3}{\mu}\frac{\partial p}{\partial \overline{z}}\right)-\frac{3}{\mu_{\text{inj}} l_0}\sum_{i=1}^{n_0} F_i\left(\overline{y},\overline{z}\right)\cdot p = 6U\frac{\partial h}{\partial \overline{y}}-12\frac{\partial h}{\partial t}-\frac{3}{\mu_{\text{inj}} l_0}\sum_{i=1}^{n_0} F_i\left(\overline{y},\overline{z}\right)\cdot P_{\text{inj}} \quad (1)$$

where $F_i\left(\overline{y},\overline{z}\right)$ is defined as follows:

$$\begin{aligned} F_i\left(\overline{y},\overline{z}\right) &= \frac{d_0^2}{4}-\left(\overline{y}-\overline{y_i}\right)^2-\left(\overline{z}-\overline{z_i}\right)^2, \\ &\quad \text{if } \left(\overline{y}-\overline{y_i}\right)^2-\left(\overline{z}-\overline{z_i}\right)^2 \leq \frac{d_0^2}{4} \\ F_i\left(\overline{y},\overline{z}\right) &= 0, \\ &\quad \text{if } \left(\overline{y}-\overline{y_i}\right)^2-\left(\overline{z}-\overline{z_i}\right)^2 \geq \frac{d_0^2}{4} \end{aligned} \quad (2)$$

A number of publications [6–12] on the subject of actively lubricated tilting pad journal bearings base the modeling of the oil film under a controllable lubrication regime on Equation (1). The reader is advised to refer specially to [8] if a complete presentation of this mathematical model is required.

From Equation (1), it can be seen that for a controllable lubrication regime, the oil film pressure field $p(\overline{y}, \overline{z})$ is a function of the injection pressure P_{inj} and the geometry of the injection hole (included into the $F_i(\overline{y}, \overline{z})$ function), as well as a function of the variables established by the traditional Reynolds Equation, namely rotor rotational speed ($U = \Omega \cdot R$), oil viscosity μ and oil film thickness h. It can be seen that the function $F_i(\overline{y}, \overline{z})$ is related to the orifices position along the pad surface, given by the coordinates $(\overline{y}_i, \overline{z}_i)$, and the orifices diameter d_0. For a passive $TPJB$, $F_i(\overline{y}, \overline{z})$ is equal to zero, hence the term P_{inj} corresponding to the oil injection pressure, vanishes. It can also be observed that the two dimensional domain for the study is defined along the axial and circumferential coordinates, in order to make room for the inclusion of the oil injection effects.

The extra terms in Equation (1) related to the oil injection are obtained as a result of the boundary conditions for the velocity field of the oil film. For a passive bearing, the oil velocity in the radial direction at the pad surface is set to be equal to the pad radial velocity, in order to respect the non-slip condition. For obtaining the Modified Reynolds Equation, one assumes that, on top of the movement of the pad, the oil velocity in the radial direction over an injection hole can be modelled using the velocity profile given by a fully developed laminar flow in a circular pipe. The integration of the continuity equation using such boundary condition entails the addition of the two extra terms to the standard Reynolds equation formulation, hence the Modified Reynolds Equation is obtained as shown in Equation (1).

2.2 Energy equation

The oil film temperature build up due to the shear and pressure forces developed within the fluid can be modelled by establishing an energy balance, which accounts for the variation of the fluid energy (kinematic and thermal) due to the work of the forces acting over it (namely pressure and shear forces). Furthermore, the effect of the oil injection into the clearance can be included as presented in [13, 14], obtaining the Energy Equation for Controllable Lubrication Regime, as given by Equation (3).

$$\begin{aligned}
&\rho C_p h \frac{\partial T}{\partial t} + k_c h \frac{\partial^2 T}{\partial \overline{y}^2} + k_c h \frac{\partial^2 T}{\partial \overline{z}^2} + k_c \left. \frac{\partial T}{\partial \overline{x}} \right|_0 F_i \\
&+ \left(\frac{\rho C_p h^3}{12\mu} \frac{\partial p}{\partial \overline{y}} - \frac{\rho C_p U h}{2} \right) \frac{\partial T}{\partial \overline{y}} + \frac{\rho C_p h^3}{12\mu} \frac{\partial p}{\partial \overline{z}} \frac{\partial T}{\partial \overline{z}} \\
&\rho C_p \left(V_{\text{inj}} - \frac{\partial h}{\partial t} \right) (T - T_{\text{inj}}) = \frac{4}{3} \frac{\mu}{h} \left(V_{\text{inj}} - \frac{\partial h}{\partial t} \right)^2 \\
&p \left(V_{\text{inj}} - \frac{\partial h}{\partial t} \right) - U^2 \frac{\mu}{h} - \frac{h^3}{12\mu} \left[\left(\frac{\partial p}{\partial \overline{y}} \right)^2 + \left(\frac{\partial p}{\partial \overline{z}} \right)^2 \right] \qquad (3)
\end{aligned}$$

The reader is advised to refer specially to [13] if a complete presentation of this mathematical model is required. The injection velocity profile V_{inj} is determined as a completely developed laminar flow inside the injection orifice, using the expression given by Equation (4):

$$V_{\text{inj}}(\overline{y}, \overline{z}) = -\frac{1}{4\mu_{\text{inj}} l_0} (P_{\text{inj}} - p) \cdot \sum_{i=1}^{n_0} F_i(\overline{y}, \overline{z}) \qquad (4)$$

Equation (3) enables to obtain the oil film temperature as a function of the oil film pressure field, bearing operational condition and oil thermal properties, as well as the injection parameters (namely, temperature and injection velocity, which is a function of the injection pressure). Physically, the extra terms corresponding to the effect of the oil injection account for the following effects: diffusive heat conduction between the oil film and the injection oil due to their temperature difference, convective heat transport of the injection oil when entering the bearing clearance, and work of the pressure and shear forces generated due to the high pressure oil injection.

It must be noted that the need of including the effect of the oil injection implies that no radial distribution for the oil film temperature is obtained, hence this formulation models the temperature field in the circumferential and axial direction, in the same way that the Modified Reynolds Equation defines the domain for the study. Secondly, the heat transfer effects between the oil film and the pad surface is included in a highly simplified way, by imposing the oil film temperature at the pad surface. Even though such boundary conditions equal to the existence of a non physical infinite heat transfer coefficient between fluid and solid, the results obtained using this model for bearings operating under laminar regime seems to be acceptable, see Section 4 of this paper. Thirdly, the boundary condition for this equation corresponds to the oil temperature at the leading edge of the pad, which is calculated by a simple mass and energy balance at the area between the pads (mixing zone).

Once the temperature field is calculated, it is possible to update the viscosity of the oil film by knowing the variation law of this parameter with the temperature, as given by Equation (5).

$$\mu = \mu^* e^{-\beta(T - T^*)} \qquad (5)$$

where the μ^* and β parameters are characteristics of the oil.

2.3 Pad flexibility

The inclusion of the pad elastic deformations due to the oil film pressure field is done by following a pseudo modal reduction scheme. This method was introduced in [3] and later implemented in [10, 11] in the context of the controllable lubrication regime. The reader is advised to refer to [10] in order to get further insights into this method. The basic idea consists of expressing the pad deformation as a linear combination of a finite number of the eigenmodes of the pads, calculated without including the presence of the oil film. The first eigenmode corresponds to the tilting motion of the pad around the pivot as a rigid body, whereas the higher modes correspond to pad elastic deformation shapes. Hence, the linear combination of such modes will generate a displacement of each point of the pad, where the elastic deformations and the tilting motion are included. Since the oil film thickness calculation is performed using that distorted shape, the solution of the Reynolds Equation and Energy Equation becomes a function of the pad flexibility effects.

In mathematical terms, by using the finite-element method the model of the pads can be expressed as:

$$\boldsymbol{M}_s\ddot{\boldsymbol{q}}_s + \boldsymbol{K}_s\boldsymbol{q}_s = \boldsymbol{f}_s \tag{6}$$

where $\boldsymbol{q}_s$ correspond to the degrees of freedom for each node of the finite element model, $\boldsymbol{M}_s$ and $\boldsymbol{K}_s$ correspond to the inertia and stiffness matrix for the pads, obtained using the finite-element method, and $\boldsymbol{f}_s$ represent the loads over the pads due to the pressure profile in the oil film. By calculating the pseudo-modal matrix $\boldsymbol{V}_s$ containing on its columns some of the eigenmodes of the pads, one can rearrange Equation (6) as follows:

$$\begin{aligned} \boldsymbol{V}_s^T\boldsymbol{M}_s\boldsymbol{V}_s\ddot{\boldsymbol{q}}_s^* + \boldsymbol{V}_s^T\boldsymbol{K}_s\boldsymbol{V}_s\boldsymbol{q}_s^* &= \boldsymbol{V}_s^T\boldsymbol{f}_s \\ \boldsymbol{q}_s &= \boldsymbol{V}_s\boldsymbol{q}_s^* \end{aligned} \tag{7}$$

By using the reduction scheme exposed in Equation (7), one ends working with a reduced system defined by the modal coordinates vector $\boldsymbol{q}_s^*$, where there are as many degrees of freedom as eigenmodes were included into the modal matrix $\boldsymbol{V}_s$. It corresponds to a pseudo-modal reduction, since only the eigenmodes which are relevant are included into the analysis. If only the first eigenmode is included, then a rigid pad model is established, and the corresponding modal coordinate measures the tilting of the pad around the pivot. The use of higher eigenmodes enables to include the flexibility of the pads into the results.

2.4 Heat Conduction through the pads and Thermal Growth

The heat conduction is modelled mathematically using the 3D form of the Fourier Heat Conduction Law, as given by Equation (8)

$$k_p\frac{\partial^2 T}{\partial x^2} + k_p\frac{\partial^2 T}{\partial y^2} + k_p\frac{\partial^2 T}{\partial z^2} = 0 \tag{8}$$

Regarding the boundary conditions, the fluid film temperature is applied as boundary condition at the fluid-pad interface. The inlet mixing temperature is applied at the pad leading edge surface and the oil supply temperature is prescribed at the back of the pad. Again, the authors stress that such simple model equals to infinite heat transfer coefficients on the pad surfaces, which corresponds to a non physical behavior. However, considering the results shown in Section 4, it is kept due to its simplicity and obtained accuracy, which is enough for the scope of this study.

Once the temperature distribution is obtained for the pad, it is possible to calculate the thermal growth and its impact on the oil film thickness. To do so, a thermal expansion rule is applied to calculate the deformation related to a certain increment in the pad material temperature, as shown in Equation (9).

$$\epsilon = \alpha \Delta T \tag{9}$$

The thermal deformation as a result of the pad temperature field are calculated using Equation (9) and imposed to the pad finite-element model, on top of the pad pivoting motion and elastic deformations due to the pressure field loading. Regarding the shaft, its temperature is assumed to be non position dependant, and it is calculated as the average of the oil film temperature. Then, its thermal expansion is calculated using Equation (9).

2.5 Numerical Implementation of the *ETHD* model

The *ETHD* model developed on this work correspond to an extension of the one presented in [10, 11]. In such work, the finite-element method was the method of choice for solving the partial differential equations corresponding to the Modified Reynolds Equation and Pad Flexibility Model using pseudo modal reduction scheme. Hence, the implementation of the oil film Energy Equation and Fourier Law for Heat Conduction on the Pads for this work is done using the finite-element method as well. The "solid" domain (pads) is discretized using tridimensional second order twenty node serendipity finite-elements. The "fluid" domain is discretized using bidimensional second order eight node quadrilateral elements, corresponding to one face of the "solid" serendipity elements. Hence, the link between the two domains is straightforward. The usage of second order elements is justified by the need of describing the pad geometry, specially the pad curvature and geometry of the injection orifice, in an accurate way.

The obtention of the weak form of the Modified Reynolds Equation and Fourier Law is done by using the Galerkin method. However, the usage of such method for the Energy equation induces numerical unstability on the solution, in the form of spurious oscillation on the obtained temperature values or "wiggle". This is a consequence of the inclusion of the oil injection terms in the Energy equation, which can be seen as the presence of a boundary condition in an upstream position, as well as the nature of the oil film flow, which exhibits a high Peclet number, in other words, strong dominance of convection effects over diffusion effects. To overcome this numerical unstability, the weak form of the Energy equation is obtained using a streamline upwind Petrov-Galerkin formulation, as presented in [15].

The dynamic behaviour of the Tilting-Pad Journal Bearing is linearized around its static equilibrium position by calculating the complete set of stiffness and damping coefficients using an analytical perturbation solution.

Such method, introduced firstly in [1] and then extended in [2], enables to couple the bearing "local" behaviour with the rotor "global" dynamic behaviour in a compact and straightforward way.

3 Rotor-Tilting Pad Journal Bearing system: mathematical modelling

The rotor is modeled using the finite-element method, using shaft elements, as proposed by Nelson [16]. Proportional damping is included in order to model the shaft internal energy dissipation processes. Thus, a damping ratio of 0.001 is imposed on the first two flexible modes of the shaft. Hence, by using this method the inertia, stiffness, gyroscopic matrices and proportional damping matrices are obtained for the shaft.

By using this method, the system can be represented mathematically as follows:

$$\boldsymbol{M}_r\ddot{\boldsymbol{q}}_r + (\boldsymbol{D}_r - \Omega\boldsymbol{G}_r)\,\dot{\boldsymbol{q}}_r + \boldsymbol{K}_r\boldsymbol{q}_r = \boldsymbol{f}_r \qquad (10)$$

In Equation (10), $\boldsymbol{q}_r$ represents the degrees of freedom of the nodes corresponding to the finite shaft model of the rotor, $\boldsymbol{M}_r$ is the rotor inertia matrix, $\boldsymbol{D}_r$ is the proportional damping matrix, $\boldsymbol{G}_r$ is the gyroscopic matrix and $\boldsymbol{K}_r$ is the rotor stiffness matrix. Related to the loading term $\boldsymbol{f}_r$, for this analysis the only loading applied to the system corresponds to the static load due to the weight of the rotor. The complete set of dynamic coefficients obtained for the Tilting-Pad Journal Bearings are assembled together with the shaft matrices, in order to obtain the global stiffness and damping matrices. By doing so, the model for the global system is defined as:

$$\boldsymbol{M}_g\ddot{\boldsymbol{q}}_g + (\boldsymbol{D}_g - \Omega\boldsymbol{G}_g)\,\dot{\boldsymbol{q}}_g + \boldsymbol{K}_g\boldsymbol{q}_g = \boldsymbol{f}_g \quad \text{where} \quad \boldsymbol{q}_g = \{\boldsymbol{q}_r\ \boldsymbol{q}_s^*\}^T \qquad (11)$$

The degrees of freedom for the global system $\boldsymbol{q}_g$ are defined by the rotor model degrees of freedom $\boldsymbol{q}_r$ and by the pads degrees of freedom $\boldsymbol{q}_s^*$, derived from the pseudo modal reduction.

The obtained global system is suitable to perform a number of analysis, such as: calculation of the Campbell diagram and stability map (eigenvalue calculation), unbalance response. To do so, the procedure to be followed, outlined in Figure 1 is depicted as follows:

1. Set the rotor rotational speed and the load applied over the bearing.
2. Determine the static equilibrium position of the rotor-bearing system by means of a Newton Raphson Scheme. The Modified Reynolds Equation is solved to obtain the pressure field, which is integrated numerically to obtain resultant forces over pads and rotor. Convergence below a given tolerance value is to be achieved for the load equilibrium over the rotor and bearing pads. Once convergence is achieved, the system state is defined by the rotor position inside the bearing, as well as a number of modal coordinates, representing the tilting angle and elastic deformation of each pad corresponding to the modes included in the analysis.
3. Calculate the temperature field using the Energy equation. Since mass and energy balance calculation is performed in the mixing zone between two adyacent pads in order to obtain the oil film leading edge temperature, it is necessary to iterate to convergence. Once convergence on the temperature field is achieved, the oil film viscosity is updated, as well as the thermal growth of the pads and shaft.
4. Repeat 2 and 3 until convergence on the oil film viscosity is achieved. Such condition implies that the system has achieved steady state regime, hence both load and thermal equilibrium is established.
5. Using the perturbation solution, determine the complete set of dynamic coefficients for each bearing.
6. Assemble the global system matrices, including the inertia, stiffness, damping and gyroscopic matrix from the rotor finite-element model, and the complete set of dynamic coefficients of the tilting-pad journal bearings.
7. Using the global system matrices, perform an eigenvalue calculation for obtaining the Campbell diagram or the stability map, or use a synchronous vibration assumption to obtain the steady state unbalance response.

4 Validation of the *ETHD* model for the Tilting-Pad Journal Bearing

The obtained *ETHD* code for the Tilting-pad Journal Bearing is validated against theoretical and experimental data coming from the literature. Among the variables to be studied are: static equilibrium position in the form of oil film thickness, oil film pressure, temperature on the surface of the pad for the steady state regime and synchronously reduced dynamic coefficients. The validation of the *ETHD* model for the controllable lubrication is being undertaken now by the authors of this work, by experimental means. Some experimental results proving the validity of the controllable lubrication model can be found in [9].

4.1 Validation against Fillon et al. [4, 17]

In [4], an *ETHD* model for the tilting-pad journal bearing is presented. An extensive experimental and theoretical study on the thermal behaviour of tilting-pad journal bearings is given in [17]. Such theoretical and experimental results are used to benchmark our code. They correspond to: oil film thickness and pressure field for the static equilibrium position, as well as temperature on the surface of the pads for the studied bearing. The comparison between those benchmark results and the ones obtained using our code are shown in (Fig. 2).

In general, close agreement is obtained between the benchmark results and the ones obtained using our *ETHD*

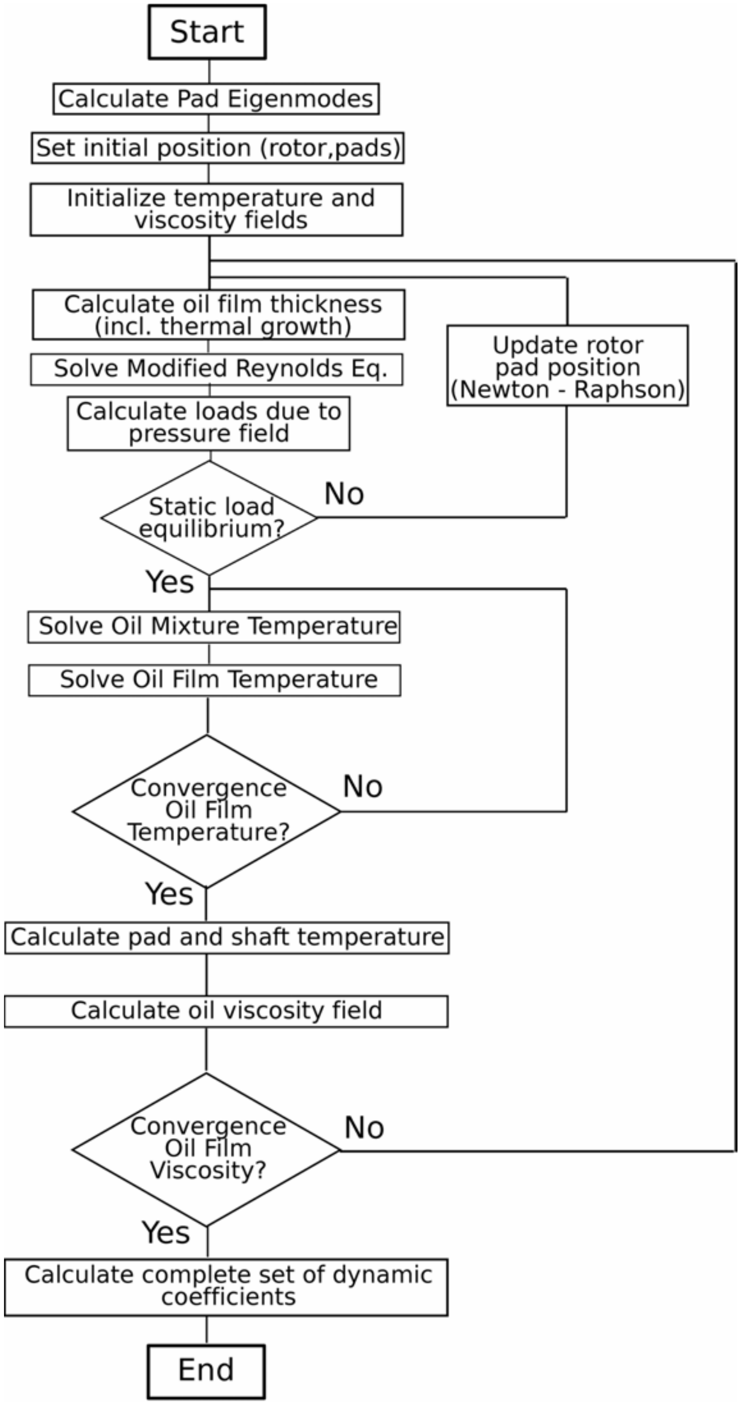

Fig. 1. Flow diagram for the model of the tilting pad journal bearing with controllable lubrication.

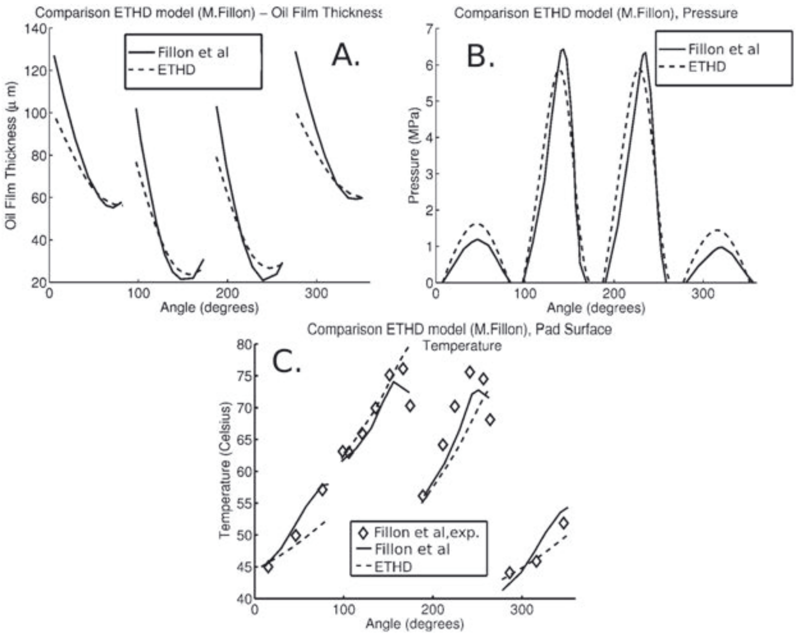

Fig. 2. Comparison between *ETHD* code and results from Fillon et al. [4,17]; the results shown correspond to oil film thickness (A), pressure profile (B) and pad surface temperature (C) at the static equilibrium position, for bearing A, as given in [17].

code. Even tough an simplified heat transfer model is assumed in our code, the results fits quite well with the provided experimental temperature data, (Fig. 2C), except for the zone towards the trailing edge. In such zone, both the experimental and theoretical benchmark results exhibit a drop in the pad surface temperature values, due to the heat transfer process taking place between the pad trailing edge and the oil bath. Since our model takes into account the heat transfer between pad and surroundings in a simplified way, it fails to reproduce the measured temperature drop.

4.2 Validation against Taniguchi et al. [18]

In [18], the authors present an analytical model and experimental results regarding the steady state pressure profile, pad surface temperature and oil film thickness for a large tilting pad journal bearing, operating in turbulent regime. Even tough such regime escapes the assumptions in which our code is based, this set of experimental data has been used by other authors, such as [17,19], to validate their "laminar" codes. Our comparison against those experimental results is given in (Fig. 3).

Close agreement is achieved between the results from our code and the theoretical and experimental results reported in [18], regarding pressure profile and oil film thickness. From the temperature results, (Fig. 3C), it is clear that the assumption of pad surface temperature to be equal to oil film temperature is not valid when a turbulent regime is reached, as it leads to an underestimation of the pad surface temperature. However, the developed code is not meant to be used for bearings operating in such condition, since no provision for turbulent regime has been implemented, so this shortcoming corresponds to an expected result. Moreover, the results obtained for oil film thickness and pressure profile indicate that the static equilibrium position is being calculated accurately.

4.3 Validation against Brockwell et al. [20]

In [20], results regarding the synchronously reduced dynamic coefficients obtained for a five shoe tilting pad journal bearing are presented. Such results are obtained both by experimental and theoretical means, using an *ETHD* code. This set of results is used to benchmark the code developed in [3]. The comparison between the results obtained using our code and the ones used as benchmark is given in (Fig. 4).

In general terms, good agreement is obtained between our results and the ones given in [20]. Closer agreement is obtained for the stiffness coefficients than for the damping ones, in a similar way to the results presented in [3], when performing the same comparison. It can also be noted that the results from our code tend to overestimate the damping characteristics of the bearing, as expected since

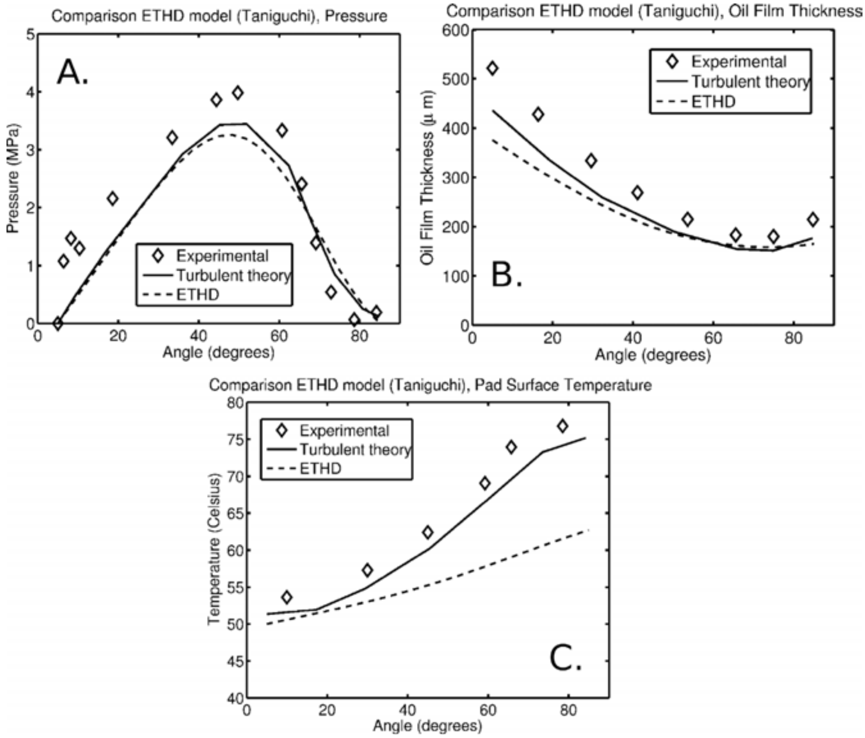

Fig. 3. Comparison between *ETHD* code and results from Taniguchi et al. [18]; pressure profile (A), oil film thickness (B) and pad surface temperature (C) for pad number 2, as given in [18].

pivot flexibility effects are not being included into the model.

5 Analysis of an industrial compressor mounted over tilting-pad journal bearings with controllable lubrication

The *ETHD* model for the tilting-pad journal bearing operating in a controllable lubrication regime is applied now to analyze an industrial rotor system. The objective is to determine the feasibility of improving the thermal behaviour of the bearing and the dynamic behaviour of a rotor mounted on such mechanical elements when pressurized oil is injected directly into the bearing clearance. These results correspond to an extension of the ones presented in [12], since those were obtained using an isothermal rigid-pads modeling assumption.

5.1 Analyzed system and scope of the analysis

The analyzed system is represented in (Fig. 5). The rotor corresponds to a gas compressor, composed of five impellers. It weighs 391 kg, and it operates normally within the range of 6942 rpm and 10 170 rpm. The rotor is supported by two identical tilting pad journal bearings. The loading due to the rotor weight acts on the negative y direction, hence pad 4 becomes the most heavily loaded one. The impellers, seals and other machine elements are considered as rigid discs and are incorporated into the model by adding inertia to the respective nodes. Hence, in the model, the impellers are at nodes 20, 24, 28, 32 and 36. Bushings are at nodes 22, 26, 30, and 34. A thrust disk sleeve is located at node 3. A balance piston is located at node 38. Seal bushes are located at nodes 12 and 46. Coupling is at node 55.

As for the TPJBs, they are located at nodes 8 (bearing 1) and 50 (bearing 2). An injection hole is located on each pad, on an axially centered position, towards the leading edge. Table 1 depicts all the parameters that define the geometry of such bearings, as well as the oil properties.

The discretization of the shaft, using beam elements, and of the pads, using tridimensional second order twenty node serendipity finite-elements, is also shown in (Fig. 5). The elements used for the pad discretization are distributed as follows: 4 elements in the radial direction, 16 elements in the axial direction and 48 elements in the circumferential direction. Only half of the pad in the axial

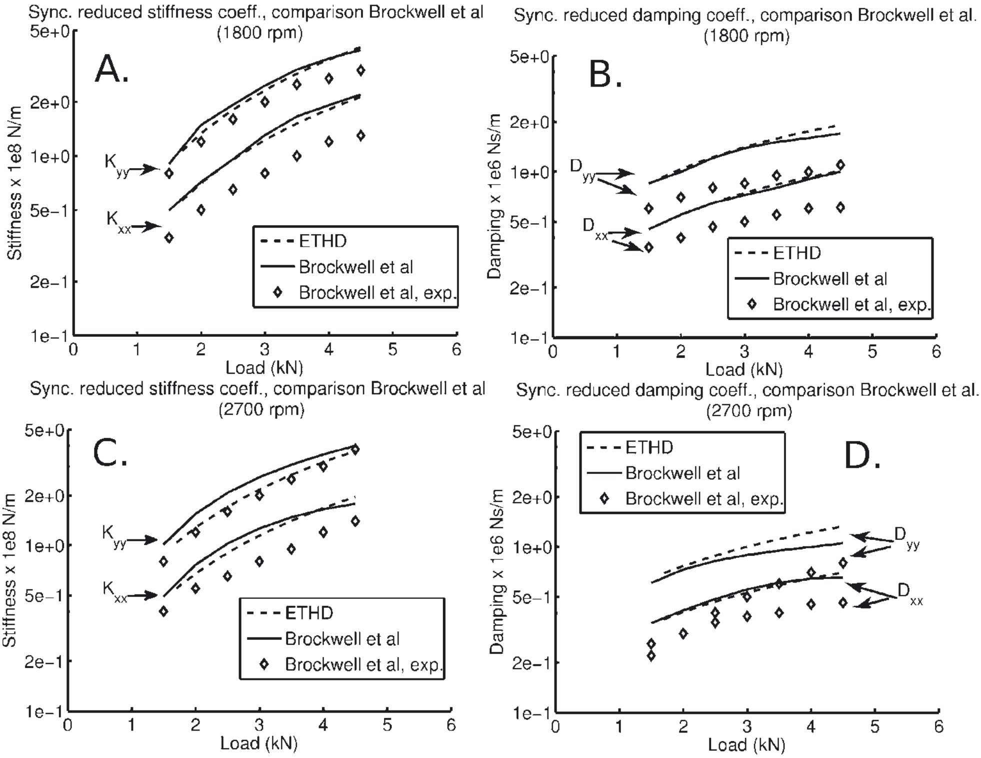

Fig. 4. Comparison between *ETHD* code and results from Brockwell et al. [20]; synchronously reduced dynamic coefficients obtained analytically and experimentally for a five shoe tilting-pad journal bearing, for two different rotational speeds.

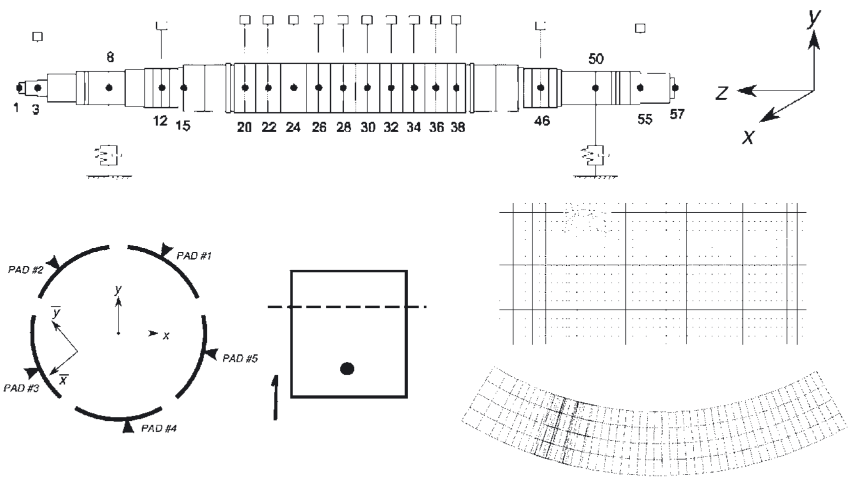

Fig. 5. Industrial compressor modeled using the finite-element method, mounted over two identical tilting-pad journal bearings. The finite-element discretization for the shaft and the pads is shown. The position of the injection hole on each pad with respect to the pivot line and leading edge is also depicted.

Table 1. Analyzed system parameters.

Parameter	Value	Units
Journal Radius (R)	50.800	mm
Number of pads (n_s)	5	–
Pad inner Radius (R_s)	50.921	mm
Pad aperture angle (α_0)	60	deg
Angular position pivot pad #1	60	deg
Angular position pivot pad #2	132	deg
Angular position pivot pad #3	204	deg
Angular position pivot pad #4	276	deg
Angular position pivot pad #5	348	deg
Offset	0.6	–
Pad width (L)	44.450	mm
Pad thickness (Δs)	10.312	mm
Pad material elasticity modulus (E)	200	GPa
Pad material Poisson ratio (ν)	0.3	–
Pad material density (ρ_s)	7800	kg.m^{-3}
Injection orifice length (l_0)	5.0	mm
Injection orifice diameter (d_0)	5.0	mm
Number of orifices per pad (n_0)	1,2	–
Assembled bearing gap (h_0)	102	μm
Oil viscosity (40 °C) (μ)	0.028	Pa s
Oil viscosity (80 °C) (μ)	0.007	Pa s
Oil density (ρ)	863.5	kg.m^{-3}
Oil specific heat (C_p)	1900	J.kg^{-1}.K
Oil thermal conductivity (k_c)	0.13	W.m^{-1}.K
Oil supply temperature	50	°C
Oil supply flow rate	0.000375	m^3.s^{-1}
Unbalance for the third impeller	720	g.mm
Unbalance for the rotor coupling	360	g.mm

direction is modeled, in order to take advantage of the axial symmetry of the pad geometry. Regarding convergence behavior for the pad model, the number of elements employed for the modeling is higher than the one used for modeling the bearings when comparing against the experimental results from the literature, as exposed in Section 4. On top of that, the guidelines obtained from the convergence analysis for the bearing model performed in [21] are taken into account.

The analysis is performed following the procedure stated in Section 3, using the validated *ETHD* code. In total, ten modes are included for the pseudo modal reduction scheme, five of them correspond to the tilting motion of each pad, and the remaining five correspond to the first bending mode of each pad. According to the results from [12], the inclusion of higher bending modes for the pads does not affect significantly the results concerning static equilibrium position and global system dynamic behavior. The results obtained allow to compare the behavior of the passive system (no injection holes are present in the bearings) against the controllable system, operating with two different injection pressures. Among the analysis performed, the oil film pressure and temperature field are compared for the two systems. Also, some tribological magnitudes are studied, such as minimum oil film thickness and oil temperature, as well as the dynamic behavior of the rotor-bearing systems, in the form of unbalance response and stability map.

5.2 Oil film pressure and temperature field

A comparison for the oil film pressure and temperature field for the passive system (no injection) and the controllable one is given in (Figs. 6 and 7). The results correspond to the static and thermal equilibrium position of bearing 2, operating at 4500 rpm and 9000 rpm. None of the pads of the bearings was cavitating for the operational conditions simulated, although the model is capable of accounting for it using Gumbel model. Two different injection pressures are applied (20 bar and 40 bar).

It can be seen that by injecting pressurized oil the pressure and the temperature field are modified. A high pressure area is created towards the leading edge of the pad, around the injection hole. When analyzing the temperature field, it can be seen that the effect of the injected oil is to generate a stream of cooler oil. The flow area affected by this stream depends on the oil film pressure gradients and injection pressure, being larger for the lightly loaded pads and for higher injection pressure.

It can also be seen that the flow area unperturbed by the stream of cooler oil develops a higher temperature towards the trailing edge, when compared to the no injection case. This is particularly evident for (Fig. 7F); in this picture, it can be seen that a high temperature zone is created toward the corners of the trailing edge. According to the analysis performed in [12], the oil injection in the leading edge induces an increase of the tilting angle of the pad. Such increase will induce a reduction of the minimum oil film thickness towards the trailing edge, hence when the oil is forced to pass through that area, it develops a higher temperature, when compared to the "no injection" case.

5.3 Minimum oil film thickness and oil temperature

As it was mentioned in Section 5.2, by injecting pressurized oil towards the leading edge, an increase on the tilting angle of the pad is obtained, which entails a reduction in the minimum oil film thickness. The results shown in (Fig. 8A) are consistent with such analysis. Also, the increase on the oil film maximum temperature with injection pressure shown in (Fig. 8B) is consistent with the analysis exposed in Section 5.2. However, when analyzing the oil film average temperature results (Fig. 8C), a clear benefit from using the controllable lubrication regime arises, since a clear reduction is obtained for the analyzed rotational speeds.

At this point, it is worth mentioning that the local increase of oil temperature towards the trailing edge can also be a consequence of the adiabatic assumption for the oil film behavior. In Section 4.1, it was noted that our model fails to reproduce the oil temperature drop towards the trailing edge observed in the experimental data. Hence, it can be argued that the negative results obtained for the oil film maximum temperature when using the controllable lubrication can be a consequence of the simplifications introduced into the model, namely the lack of the modelling of the heat transfer effects between

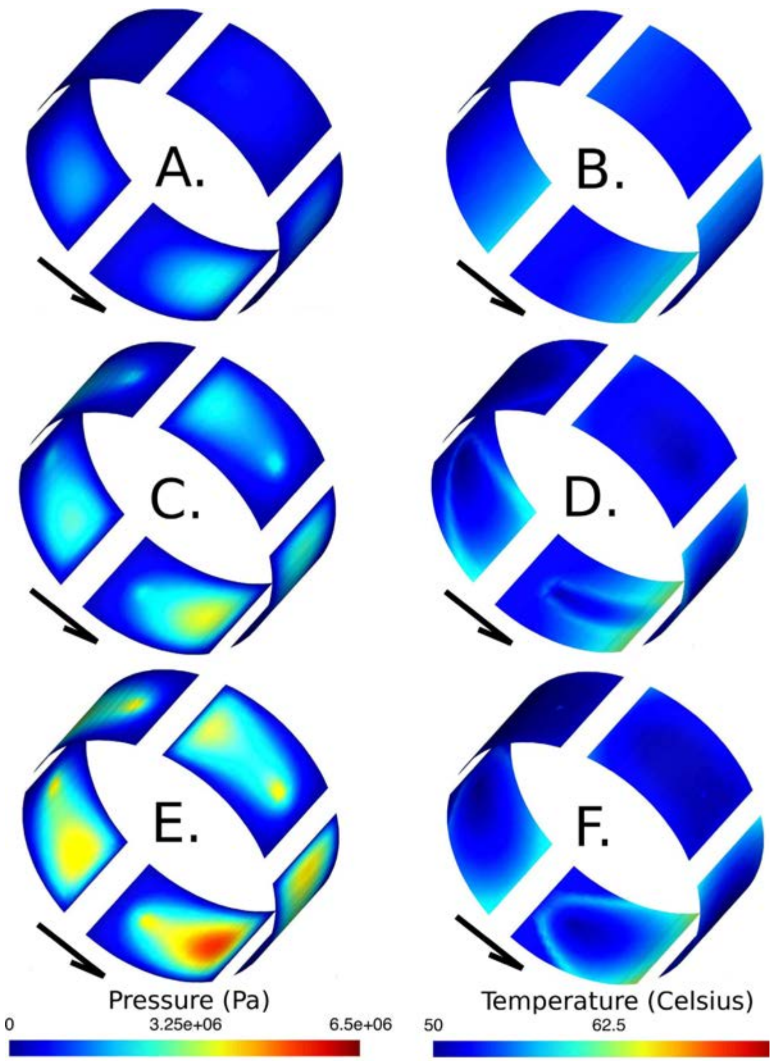

Fig. 6. Oil film pressure (A, C, E) and temperature field (B, D, F), in bearing 2, for 4500 rpm; comparison for no injection (A, B), 20 bar injection pressure (C, D), 40 bar injection pressure (E, F).

oil film and bearing pads. Experimental testing is planned to prove the validity of this hypothesis.

5.4 Dynamic behavior: rotor unbalance response and stability diagram

By imposing a controllable lubrication regime, it is possible to modify the equilibrium position of the rotor-bearing system, which entails a modification of the tilting-pad journal bearing dynamic properties. Both its stiffness and damping characteristics are modified, according to the theoretical results presented in [12]. Hence, it could be feasible to improve the performance of the rotor bearing system from the dynamic point of view, by a proper positioning of the injection orifices and proper selection of the injection pressure.

In (Fig. 9), the unbalance response amplitude for the rotor system, measured at node 28, is shown. To obtain these results, an unbalance force was applied firstly to the rotor node 28, (Figs. 9A and B), which corresponds to the position of the third impeller of the compressor, and to node 55, (Figs. 9C and D), which corresponds to the

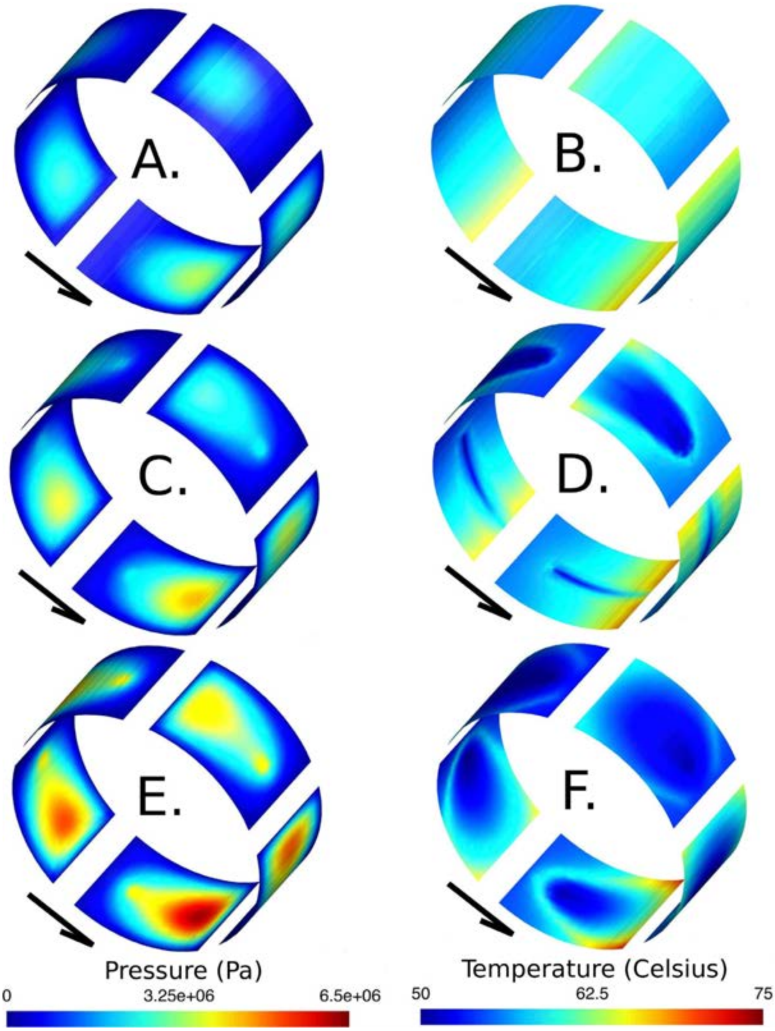

Fig. 7. Oil film pressure (A, C, E) and temperature field (B, D, F), in bearing 2, for 9000 rpm; comparison for no injection (A, B), 20 bar injection pressure (C, D), 40 bar injection pressure (E, F).

coupling. The value for the unbalance is 720 g.mm for the third impeller, and 360 g.mm for the coupling, according to API 617. In (Figs. 9A and B), it can be observed that when injecting pressurized oil the position of the resonant peak is shifted to the left, which implies a reduction in the stiffness characteristics of the bearings. This analysis is also confirmed by the amplitude response to the left of the resonant peak, which becomes higher for the controllable lubrication cases. Such reduction in the stiffness characteristics is obtained alongside an increase in the damping ratio associated to the unbalance response of the rotor, responsible for the reduction in the amplitude of the resonant peak for the controllable case. Hence, these results show that the injection of oil towards the leading edge modify the stiffness and damping characteristics of the bearing, resulting in an increase of the resulting damping ratio for the rotor-bearings system. When comparing with the admissible vibration amplitude for the rotor according to API 617, the results show that by imposing the controllable lubrication regime with injection pressure of 20 bar, it is possible to reduce the unbalance response in order to comply with the requirement of the norm.

The results obtained for the stability map shown in (Fig. 10) support the previous results. A clear increase of the instability onset speed is obtained for the controllable case, due to an increment of the damping ratio associated

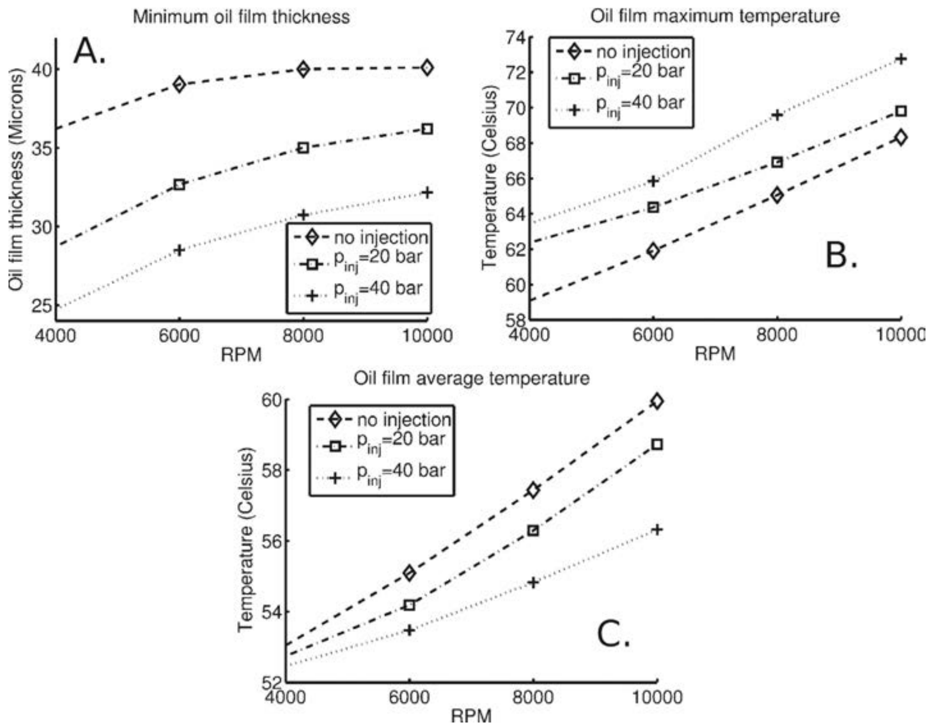

Fig. 8. Minimum oil film thickness (A), maximum (B) and average oil temperature (C) for bearing 2 operating at different rotational speeds; comparison for no injection, 20 bar and 40 bar injection case.

with the vibration mode approaching unstability, hence expanding the stable operational range of the compressor. These results confirm the ones obtained in [12], analysis that was performed using a rigid-pad isothermal model for the tilting-pad journal bearings.

With regards to the effect of changing the value of the injection pressure, the results from (Figs. 9A and B) and (Fig. 10) show opposite trends. For the unbalance response, when exciting at node 28, an increase in the injection pressure entails a reduction in the damping ratio, whereas for the stability map, an increase in the injection pressure enlarges the stable operational range, implying higher damping ratio. This apparent contradiction can be explained, since the eigenmode being excited in the unbalance response plot (excitation at the impeller) is different than the one approaching the unstability threshold in the stability map. Since each one of these two different modes associated with different modal damping ratios, it can be inferred that a change in the injection pressure value modifies in different ways the damping ratio associated with different modes.

This analysis is supported by the results shown in (Fig. 11). The damping ratio for two different modes of the rotor bearing system is calculated for the analyzed range of rotational speed. Mode 1 corresponds to the eigenmode approaching unstable behavior, as noted in (Fig. 10), whereas mode 2 is the mode excited due to the unbalance force in (Fig. 9). Firstly, the difference in the order of magnitude between the damping ratios for each mode must be noted. For both modes, it can be seen that the use of a controllable lubrication regime implies an increment in the damping ratio associated with the mode. However, for mode 1, an increase in the injection pressure value entails higher modal damping ratio, whereas for mode 2 the modal damping ratio is diminished for an increase in the injection pressure.

The analysis performed so far is valid for the unbalance response obtained when the excitation force is located at node 28, namely the third impeller, as shown in (Figs. 9A and B). The position of such node implies that the eigenmodes already shown in (Fig. 11) are preferably excited. However, when locating the unbalance force at the coupling of the rotor (node 55), namely at the end of the rotor, higher eigenmodes are excited, hence the response of the system becomes the result of the superposition of different modes. Therefore, the results shown in (Fig. 9) illustrate that the relationship between response amplitude and injection pressures seems to be altered,(Figs. 9C and D), when comparing with the case where the excitation was located at one of the impellers, (Fig. 9A and B). When exciting at the coupling, the amplitude of the resonant peak almost does not vary for the

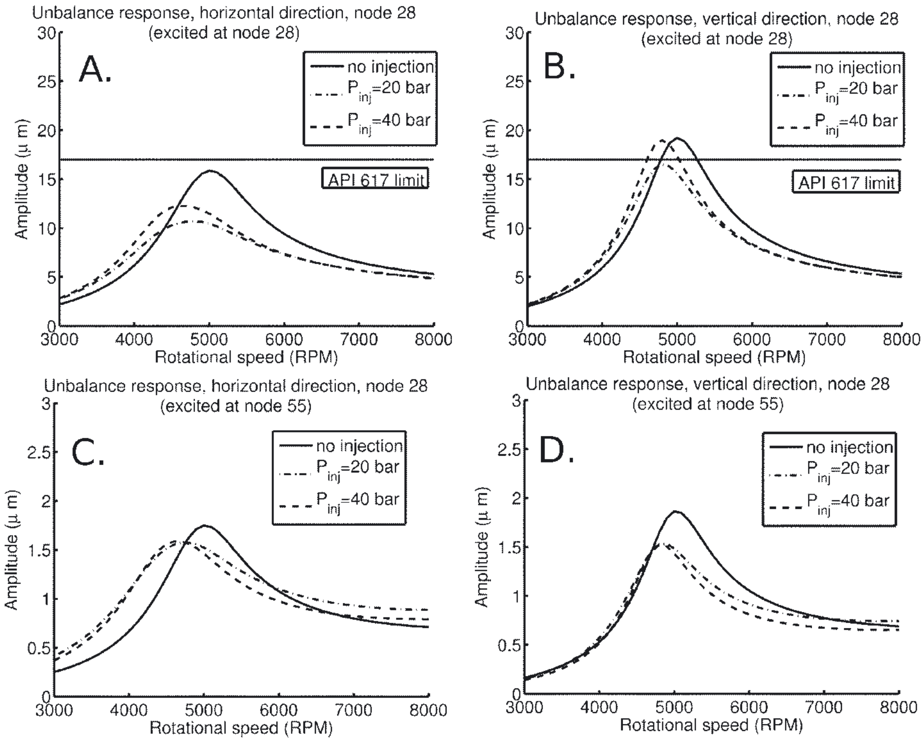

Fig. 9. Maximum amplitude for the unbalance response, measured at rotor node 28 (third impeller), for two different positions of the unbalance excitation (node 28, third impeller (A, B); node 55, coupling (C, D)); comparison for the passive case and controllable case, with different injection pressures.

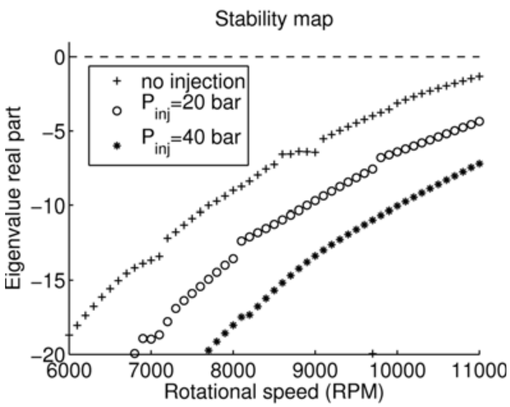

Fig. 10. Stability map of the compressor; the instability onset zone is shown for the no injection case and two different injection pressures.

imposed values of injection pressure, whereas the response outside the resonant peak does not converge towards the same value. These results show the difficulties associated with finding an optimum value for a fixed injection pressure on a practical application of the controllable (hybrid) lubrication scheme. Hence, the advantages of determining the value for the injection pressure by means of a control loop (active lubrication) become evident. Even tough in this work it has been theoretically showed that by injecting oil at a fixed pressure towards the leading edge of each pad it is possible to modify favourably the dynamic behavior of the rotor system, the achievement of the optimal results regarding reduction of the unbalance response requires varying the injection pressure according to the system state, by means of a control loop, as it was shown theoretically and experimentally in other works on these subject [9].

6 Conclusion

In this work, an Elasto-Thermo-Hydrodynamic ($ETHD$) model for the Tilting-Pad Journal Bearing has been presented. Such model includes also the effect of injecting high pressure oil directly into the bearing clearance through orifices across the bearing pads, allow-

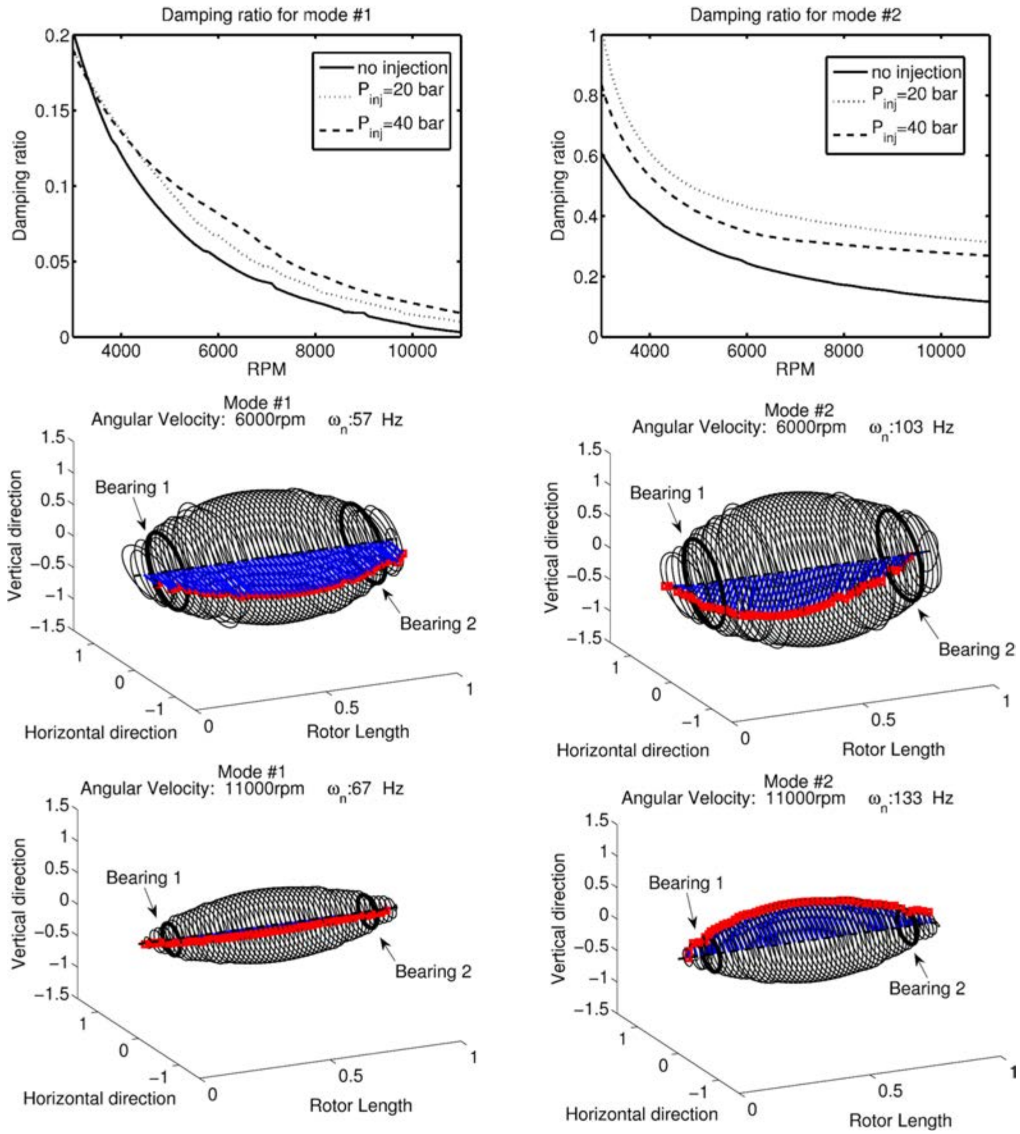

Fig. 11. Effect of the injection pressure over the damping ratio for two different modes of the rotor-bearings system; mode 1 corresponds to the mode approaching instability on (Fig. 10), whereas mode 2 is the mode excited on (Fig. 9).

ing to study the effect of imposing a controllable lubrication regime. Based on the results presented on this work, it is possible to conclude the following:

1. The developed *ETHD* model compares well to experimental and theoretical results from the literature for the passive tilting-pad journal bearing operating in laminar regime. From the validation, it is clear that improvements are possible in the form of improving the modellling of the heat transfer taking place between the oil film and the pad. On this regard, an investigation on the way of doing it will be performed, since the absence of the radial direction as part of the oil film modeling domain does not allow to apply the usual boundary conditions to include such effect.
2. The theoretical results obtained when analyzing a rotor tilting pad journal bearings system showed some clear benefits of the implementation of a controllable

lubrication regime. When injecting oil through a hole located towards the leading edge of the pads, a reduction in the oil film average temperature was observed, as well as an improvement in the damping ratio characteristics of the rotor-bearing system, expressed in the form of reduced unbalance response when crossing critical speeds and higher instability onset speed.

3. Among the drawbacks of imposing the controllable lubrication regime, a reduction in the minimum oil film thickness is observed, as well as an increase in the maximum temperature of the oil film. This last result could be a consequence of the adiabatic assumption for the oil film thermal behavior and the non-inclusion into the model of heat transfer effects between the bearing pads and the surroundings.
4. With regards to the selection of the injection pressure, the results obtained show that the resulting modification of the bearing stiffness and damping characteristics affect the damping ratio of the rotor-bearing system eigenmodes in different ways. Hence, finding an optimum value for a fixed injection pressure that enables to reduce the unbalance response at any running speed proves to be a difficult task. This difficulty can be overcome by establishing an active lubrication regime, where the injection pressure is determined by means of a control loop, as it has been shown in other works in the subject.
5. An experimental validation of the *ETHD* model including the effect of the controllable lubrication regime is on the way, in order to prove the practical validity of the promising results of this theoretical study.

References

[1] J. Lund, Spring and damping for the tilting pad journal bearings, ASLE Trans. 7 (1964) 342–352

[2] P. Allaire, J. Parsell, L. Barrett, A pad perturbation method for the dynamic coefficients of tilting-pad journal bearings, Wear 72 (1981) 29–44

[3] J. Kim, A. Palazzolo, R. Gadangi, Dynamics characteristics of tehd tilt pad journal bearing simulation including multiple mode pad flexibility, ASME J. Vib. Acoust. 117 (1995) 123–135

[4] M. Fillon, D. Souchet, J. Frêne, Influence of bearing element displacements on thermohydrodynamic characteristics of tilting-pad journal bearings, Proc. Japan International Tribology Conference, Nagoya, 1990, pp. 635–640

[5] I.F. Santos, Design and evaluation of two types of active tilting pad journal bearings, in: the active control of vibration, C.R. Burrows, P.S. Keogh (eds.) Mechanical Engineering Publications Limited, London, England, 1994, pp. 79–87

[6] I.F. Santos, Strategien fur die erhohung der dampfungsreserve von kippsegmentgelagerten rotorsystemen, in: Schwingungen in rotierenden Maschinen, H.S.H. Irretier, R. Nordmann (éd.), Vieweg Verlag, Braunschweig, Germany, 1995, Vol 3, pp. 3–12

[7] I.F. Santos, Aktive Schmierung zur Regelung von Rotorsystemen, In: Schwingungen in rotierenden Maschinen, H.S.H. Irretier, R. Nordmann, (éd.), Vieweg Verlag, Braunschweig, Germany, 1997, Vol 4, pp. 37–47

[8] I.F. Santos, F. Russo, Tilting-pad journal bearings with electronic radial oil injection, J. Tribol. ASME Trans. 120 (1998) 583–594

[9] I.F. Santos, A. Scalabrin, Control system design for active lubrication with theoretical and experimental examples, J. Eng. Gas Turbine. Power T. ASME 125

[10] A.M. Haugaard, I.F. Santos, Multi-orifice active tilting-pad journal bearings-harnessing of synergetic coupling effects, Tribol. Int. 43 (2010) 374–1391

[11] A.M. Haugaard, I.F. Santos, Stability of multi orifice active tilting-pad journal bearings, Tribol. Int. 43 (2010) 1742–1750

[12] A. Cerda, I.F. Santos, Stability analysis of an industrial gas compressor supported by tilting-pad journal bearings under different lubrication regimes, ASME J. Eng. Gas Turbine. Power T. (in print)

[13] I.F. Santos, R. Nicoletti, THD analysis in tilting-pad journal bearings using multiple orifice hybrid lubrication, J. Tribol. ASME Trans. 121 (1999) 892–900

[14] I.F. Santos, R. Nicoletti, Influence of orifice distribution on the thermal and static properties of hybridly lubricated bearings, Int. J. Solids Struct. 38 (2001) 2069–2081

[15] A. Brooks, T. Hughes, Streamline upwind/Petrov-Galerkin formulations for convection dominated flows with particular emphasis on the incompressible Navier-Stokes equation, Comput. Methods Appl. Mech. Eng. 32 (1982) 199–259

[16] H. Nelson, J. McVaugh, The dynamics of rotor-bearing systems using finite element, J. Eng. Ind. 98 (1976) 593–600

[17] M. Fillon, J.C. Bligoud, J. Frêne, Experimental study of tilting-pad journal bearings – comparison with theoretical thermoelastohydrodynamic results, J. Tribol. ASME T. 114 (1992) 579–588

[18] S. Taniguchi, T. Makino, T. Takeshita, T. Ichimura, A thermohydrodynamic analysis of large tilting-pad journal bearing in laminar and turbulent flow regimes with mixing, J. Tribol. ASME Trans. 112 (1990) 542–550

[19] J. Kim, A. Palazzolo, R. Gadangi, TEHD analysis for tilting pad journal bearings using upwind finite element method, Tribol. Trans. 37 (1994) 771–783

[20] K. Brockwell, D. Kleinbub, W. Dmochowski, Measurement and calculation of the dynamic operating characteristics of the five shoe tilting-pad journal bearing, Tribol. Trans. 33 (1989) 481–492

[21] A.M. Haugaard, On controllable elastohydrodynamic fluid film bearings, Ph.D. Thesis, Technical University of Denmark, 2010

5.3 Publication 3: On the Simplifications for the Thermal Modeling of Tilting-Pad Journal Bearings under Thermoelastohydrodynamic Regime

Proceedings of ASME Turbo Expo 2012
GT2012
June 11-15, 2012, Copenhagen, Denmark

GT2012-68329

ON THE SIMPLIFICATIONS FOR THE THERMAL MODELING OF TILTING-PAD JOURNAL BEARINGS UNDER THERMOELASTOHYDRODYNAMIC REGIME

Alejandro Cerda Varela*
Department of Mechanical Engineering
Technical University of Denmark
2800 Kgs. Lyngby, Denmark
Email: acer@mek.dtu.dk

Michel Fillon
Institut Pprime, Department GMSC
University of Poitiers
86962 Futuroscope Chasseneuil, France
Email: michel.fillon@univ-poitiers.fr

Ilmar Ferreira Santos
Department of Mechanical Engineering
Technical University of Denmark
2800 Kgs. Lyngby, Denmark
Email: ifs@mek.dtu.dk

ABSTRACT

The relevance of calculating accurately the oil film temperature build up when modeling tilting-pad journal bearings is well established within the literature on the subject. This work studies the feasibility of using a thermal model for the tilting-pad journal bearing which includes a simplified formulation for inclusion of the heat transfer effects between oil film and pad surface. Such simplified approach becomes necessary when modeling the behavior of tilting-pad journal bearings operating on controllable lubrication regime. Three different simplified heat transfer models are tested, by comparing their results against the ones obtained from an state of the art tilting-pad journal bearing model, where the heat transfer effects are throughly implemented, as well as against some experimental results from the literature. The results obtained show that the validity of the simplified heat transfer models are strongly dependent on the Reynolds number for the oil flow in the bearing. For bearings operating in laminar regime, the decoupling of the oil film energy equation solving procedure, with no heat transfer terms included, with the pad heat conduction problem, where the oil film temperature is applied at the boundary as a Dirichlet condition, showed a good balance between quality of the results, implementation easiness and reduction in calculation time. For bearings on the upper limit of the laminar regime, the calculation of an approximated oil film temperature gradient in the radial direction, as proposed by Knight and Barrett, delivered the best results.

*Address all correspondence to this author.

Nomenclature

$Br = \frac{\mu_0 \Omega^2 R^2}{k_{oil} T_0}$ Brinkman number
C radial pad clearance.
C_p oil specific heat capacity.
H convection heat transfer coefficient.
h oil film thickness.
$\overline{h} = \frac{h}{C}$ non dimensional oil film thickness.
k_{oil} oil thermal conductivity.
k_{pad} pad thermal conductivity.
L bearing length.
p oil film pressure.
$\overline{p} = \frac{pC^2}{\mu_0 \omega R^2}$ non dimensional oil film pressure.
$Pe = \frac{\rho C_p \Omega C^2}{k_{oil}}$ Peclet number
R journal radius.
$\overline{r}, \theta, \overline{z}$ non dimensional local pad reference system in cylindrical coordinates.
T oil film temperature.
T_0 oil feeding temperature.
T^{pad} pad temperature.
T^{shaft} shaft temperature.
$\overline{T} = \frac{T}{T_0}$ non dimensional oil film temperature.
$\overline{T}^{pad}$ non dimensional pad temperature.
$\overline{u}, \overline{v}, \overline{w}$ non dimensional oil velocity components in the local pad reference system.
X, Y, Z global cartesian reference system.
x, y, z local pad reference system.
$\overline{x}, \overline{y}, \overline{z}$ non dimensional local pad reference system.
μ oil viscosity.

μ_0 oil viscosity at feeding temperature.
$\overline{\mu} = \frac{\mu}{\mu_0}$ non dimensional oil viscosity.
ρ oil viscosity.
Ω journal rotational speed.

INTRODUCTION

Tilting pad journal bearings are commonly used in rotating machinery due to their superior stability properties [1] [2], when compared to other oil-film bearing designs. Hence, over the past decades there has been a constant effort regarding an improvement of the understanding of the static and dynamic properties of these mechanical components. As a result of this, the state of the art regarding the tilting-pad journal bearing modeling effort corresponds nowadays to a thermoelastohydrodynamic formulation. Among some of these works, Ettles [3] used a simple 1-D beam model to include the pad flexibility effect; Fillon [4] considered both the thermal and flexibility effects in a thorough way, including the effect of the thermal growth; Palazzolo [5, 6] used the finite element method to model both the oil film and the pads, introducing as well the use of a pseudo modal reduction method to include the pad flexibility effects. Such works focused in the steady state behaviour of the tilting-pad journal bearing; bearings operating in transient thermoelastohydrodynamic regime have also been modeled, such as in [7].

The relevance of including thermal effects into the modeling of tilting-pad journal bearings is well understood nowadays, as it is highly relevant to determine accurately the static and dynamic characteristics of the bearings. Specifically, it has been proven that by neglecting the temperature build-up within the oil film, the bearing damping characteristics are overestimated [3], which results in an erroneous calculation of the instability threshold speed of rotating machinery mounted over tilting-pad journal bearings [6] [8].

The main objective of this work is to perform a critical analysis of the results produced by the thermoelastohydrodynamic model for the tilting-pad journal bearing presented in [9], focusing specifically into the modeling of the heat transfer process between the oil film and the pad surface. The model presented in [9] has been formulated in order to assess the benefits of imposing a controllable lubrication regime, where high pressure oil is injected into the bearing clearance through holes drilled through the pads. However, the effect of the oil injection will not be included in this work, since the main focus is to study the accuracy of the oil film heat transfer modeling assumptions, phenomena that takes place regardless of the oil injection. On this matter, this study deals with the implementation of several strategies for a simplified modeling of the heat transfer process between the oil film and the bearing pads. The analysis is performed by comparison against the results from the tilting pad journal bearing model developed by the authors of [4, 7, 10], as well as experimental results from the literature. Guidelines are then obtained about the significance and consequences of following different approaches for the simplified modeling of the thermal problem in the tilting-pad journal bearing.

MODELING

On this section, two different models for the tilting-pad journal bearing are presented. The level of detail and focus of the presentation will be kept accordingly with the objectives of this study. Hence, the reader is advised to refer to the publications indicated in the text in order to get a thorough presentation.The first model corresponds to the one developed and validated by Fillon [4, 7, 10], which will be used as benchmark for this work. On the second hand, the model presented in [9] for the controllable lubrication tilting-pad journal bearing is presented. For this study, the terms corresponding to the oil injection are omitted, in order to enable the direct comparison of the results between the two models. Also, the pad elastic deformations are not included into this comparison analysis. The comparison is then restricted to bearings under thermohydrodynamic regime.

Model 1: Tilting-Pad Journal Bearing model, as developed by Fillon [4, 7, 10]

The mathematical model for obtaining the pressure field corresponds to the Reynolds Equation, which in non-dimensional form can be expressed as:

$$\frac{\partial}{\partial \theta}\left(\overline{h}^3 \overline{G} \frac{\partial \overline{p}}{\partial \theta}\right) + \left(\frac{R}{L}\right)^2 \frac{\partial}{\partial \overline{z}}\left(\overline{h}^3 \overline{G} \frac{\partial \overline{p}}{\partial \overline{z}}\right) = \frac{\partial}{\partial \theta}\left(\overline{h}\left(1 - \frac{\overline{I_2}}{\overline{J_2}}\right)\right)$$
$$\overline{I_2} = \int_0^1 \frac{\overline{y}}{\overline{\mu}} d\overline{y}$$
$$\overline{J_2} = \int_0^1 \frac{d\overline{y}}{\overline{\mu}}$$
$$\overline{G} = \int_0^1 \frac{\overline{y}}{\overline{\mu}}\left(\overline{y} - \frac{\overline{I_2}}{\overline{J_2}}\right) d\overline{y} \tag{1}$$

The thermal model determines the oil film temperature using a two dimensional domain located in the middle of the pad axial length, considering the circumferential θ and radial direction $\overline{y}$ of the bearing. It can be stated as:

$$Pe\left(\overline{u}\frac{\partial \overline{T}}{\partial \theta} + \overline{v}\frac{\partial \overline{T}}{\partial \overline{y}}\right) = \frac{1}{\overline{h}^2}\frac{\partial^2 \overline{T}}{\partial \overline{y}^2} + Br\frac{\overline{\mu}}{\overline{h}^2}\left(\frac{\partial \overline{u}}{\partial \overline{y}}\right)^2 \tag{2}$$

In Eqn.(2), the non-dimensional oil temperature $\overline{T}$ is a function of the Peclet number Pe, the Brinkman number Br, the oil velocity components $\overline{u}$ and $\overline{v}$, non-dimensional viscosity and oil film thickness. When the temperature field is calculated, the viscosity of the oil is updated by using an exponential law, as follows:

$$\overline{\mu} = \frac{\mu}{\mu_0} = e^{-\beta T_0\left(\overline{T}-1\right)} \quad (3)$$

Regarding the temperature distribution in the pad, it is obtained by solving the Fourier Law stated in polar coordinates as:

$$\frac{\partial^2 \overline{T}^{pad}}{\partial \overline{r}^2} + \frac{1}{\overline{r}}\frac{\partial \overline{T}^{pad}}{\partial \overline{r}} + \frac{1}{\overline{r}^2}\frac{\partial^2 \overline{T}^{pad}}{\partial \overline{\theta}^2} = 0 \quad (4)$$

The boundary conditions for the pressure field model stated in Eqn.(1), coupled with the thermal model defined by Eqn.(2) and Eqn.(4) are:

1. The classical Reynolds boundary conditions are applied to Eqn.(1)
2. The shaft surface temperature is fixed, and set to be equal to the value measured experimentally or determined by assuming that the global net heat flux across the shaft surface is nil.
3. At the interface between oil film and pad, the heat flux continuity condition is applied
4. At the remaining surfaces of the pads, free convection boundary condition is established
5. At the inlet zone of the pad, the oil film temperature is assumed to vary parabolically between pad and shaft temperatures. Conservation equations enable to calculate the lubricant mixing temperature at the inlet. The coefficient of recirculation is taken to be equal to 0.85, following the method used in [10]

This model also accounts for pad elastic deformations due to load applied by the pressure field and due to thermal growth. However, such features are not presented here, since they are not used for the comparison study.

Model 2: Tilting-Pad Journal Bearing model, as presented in [9]

The model presented in the previous section defines the domain for the oil film energy equation in the circumferential and radial direction. However, when it comes to model a tilting-pad journal bearing including the effect of radial oil injection, as presented in [9], such approach can not be followed. The presence of the injection hole in the pad surface entails that the domain for the analysis has to be defined in the circumferential and axial direction, if one desires to maintain a two dimensional formulation.

Taking this fact into account, this model determines the oil film pressure field in the axial direction z and circumferential direction x, using the Reynolds Equation stated for steady-state conditions as follows:

$$\frac{\partial}{\partial x}\left(\frac{h^3}{\mu}\frac{\partial p}{\partial x}\right) + \frac{\partial}{\partial z}\left(\frac{h^3}{\mu}\frac{\partial p}{\partial z}\right) = 6\Omega R\frac{\partial h}{\partial x} \quad (5)$$

For the model stated in Eqn.(5), the source term corresponds to the wedge term, which is a function of the journal rotational speed Ω.

Regarding the oil film temperature, an average value across the oil film thickness is considered. Hence, its value in the axial and circumferential direction is determined using the oil film energy equation developed in [11, 12], defined as:

$$k_{oil}h\frac{\partial^2 T}{\partial x^2} + k_{oil}h\frac{\partial^2 T}{\partial z^2} + \left(\frac{\rho C_p h^3}{12\mu}\frac{\partial p}{\partial x} - \frac{\rho C_p \Omega R h}{2}\right)\frac{\partial T}{\partial x} + \frac{\rho C_p h^3}{12\mu}\frac{\partial p}{\partial z}\frac{\partial T}{\partial z} + (\Omega R)^2\frac{\mu}{h} + \frac{h^3}{12\mu}\left(\left(\frac{\partial p}{\partial x}\right)^2 + \left(\frac{\partial p}{\partial z}\right)^2\right) + \mathbf{S}_{oil} = 0 \quad (6)$$

From Eqn.(6) , it can be seen that both the diffusion effects due the oil thermal conductivity k_{oil}, and convection effects are included into the formulation. Also, the source terms model the effect of the work due to shear and pressure forces developed within the oil film. The term $\mathbf{S}_{oil}$ is used to represent the heat transfer terms between the oil film and the pad and shaft surface.

Regarding the obtaining of the pad temperature field, the Fourier Law for the thermal conduction is employed on its 3D formulation, as follows:

$$k_{pad}\left(\frac{\partial^2 T^{pad}}{\partial X^2} + \frac{\partial^2 T^{pad}}{\partial Y^2} + \frac{\partial^2 T^{pad}}{\partial Z^2}\right) + H_\infty\left(T^{pad} - T_\infty\right)|_{boundary} + \mathbf{S}_{pad} = 0 \quad (7)$$

In Eqn. (7), the coordinates X, Y, Z correspond to the cartesian reference system that defines the domain for the pad. A source term is included in order to model the heat transfer between the pad and the surroundings, by using a free convection coefficient H_∞. On the other hand, $\mathbf{S}_{pad}$ groups the terms corresponding to the heat transfer phenomena between the pad and the oil film.

Regarding the boundary conditions for the already defined model for the tilting-pad journal bearing, they can be stated as follows:

1. Regarding Eqn.(5), the pressure value is set to be zero at the boundaries of the analyzed domain. Also, the Gumbel cavitation condition is implemented.
2. At the leading edge of the pad, the temperature of the oil is assumed to be constant in the axial direction, and it is calculated using the conservation equations in the mixing zone between two adjacent pads, as done previously in Model 1.
3. The shaft surface temperature is calculated as the average of the oil film temperature.
4. Free convection boundary condition is applied on the faces of the pads that are not in contact with the oil film responsible for the bearing load carrying capacity

Regarding the boundary conditions on the interface between oil film and pads surface, the model already expressed assumes an average value for the oil film temperature in the radial direction. This brings the advantage of including the effect of the radial oil injection without expanding the analysis into a three dimensional modeling of the oil film behavior, with the resultant save in calculation time. However, such assumption also implies that it is not possible to apply directly the heat flux continuity condition at the interface between oil film and pad surface, since the gradient in the radial distribution of the oil film temperature has been assumed to be zero. Hence, an approximate approach is to be followed in order to include the heat transfer effect between oil film and pads, while retaining the two dimensional domain for the study.

On this regard, three different approaches for modeling the heat transfer between oil film and pad surface are studied:

1. **Boundary Condition 1 (B.C. 1)**: The pad surface temperature is set to be equal to the oil film temperature calculated using Eqn.(6). In other words, an infinite heat transfer coefficient is assumed between the oil film and the pad surface. Hence, the boundary condition can be stated as:

$$\begin{aligned} \mathbf{S}_{oil} = \mathbf{S}_{pad} = 0 \\ T = T^{pad}_{boundary} \end{aligned} \tag{8}$$

   where T^{oil} corresponds to the oil film temperature field calculated using Eqn.(6), and $T^{pad}_{boundary}$ corresponds to the pad temperature at the surface in contact with the oil film.
2. **Boundary Condition 2 (B.C. 2)**: The heat transfer between the oil film and the pad surface is modeled using a convection coefficient, as follows:

$$\mathbf{S}_{pad} = -\mathbf{S}_{oil} = H_{oil-pad}\left(T - T^{pad}_{boundary}\right) \tag{9}$$

   In order to determine the order of magnitude of the convection coefficient $H_{oil-pad}$, the approach employed is to use the results delivered by Model 1. Using such model, it is possible to know the variation in the radial direction of the oil film temperature, hence it is possible to obtain the magnitude of the heat flux at the oil-pad interface. Since by using Boundary Condition 2 one is determining such heat flux as a function of the temperature difference between the two media and the convection coefficient, it is possible to state:

$$k_{oil}\frac{\partial T}{\partial y}|_{boundary} = H_{oil-pad}\left(T - T^{pad}_{boundary}\right) \tag{10}$$

   From Eqn.(10), since all the terms are available from the results delivered by Model 1, it is possible to get an estimation of the value of the convection coefficient $H_{oil-pad}$.
3. **Boundary Condition 3 (B.C. 3)**: Following the approach established by Knight and Barrett [13], the oil film temperature profile in the radial direction is assumed to be parabolic. Hence, a second order polynomial can be used to approximate the radial oil temperature distribution, as follows:

$$\begin{aligned} T_{oil}(y) = T^{pad}_{boundary} + 2\left(3T - 2T^{shaft} - 2T^{pad}_{boundary}\right)\frac{y}{h} \\ +3\left(T^{shaft} - 2T + T^{pad}_{boundary}\right)\left(\frac{y}{h}\right)^2 \end{aligned} \tag{11}$$

   Such radial temperature distribution is assumed only with the objective of estimating the heat transfer between oil and pad surface, hence the oil film energy equation presented in Eqn.(6) only determines the oil film temperature distribution in the circunferential and axial direction. Then, it is possible to apply the heat flux continuity condition at the interface between oil film and pad surface, using the assumed gradient for the oil film temperature in the radial direction, as follows:

$$\mathbf{S}_{oil} = -\mathbf{S}_{pad} = \frac{k_{oil}}{h}\left(3T - 2T^{shaft} - 2T^{pad}_{boundary}\right) \tag{12}$$

Analyzing these simplified heat transfer models solely from the calculation point of view, the usage of B.C. 1 comes with the

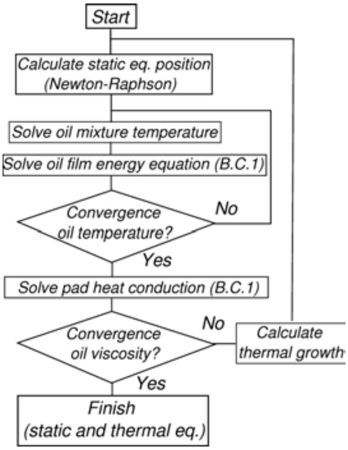

FIGURE 1. FLOWCHART DEPICTING THE OPERATIONS FOR THE CALCULATION OF THE STATIC AND THERMAL EQUILIBRIUM OF A TILTING-PAD JOURNAL BEARING, WHEN USING B.C.1

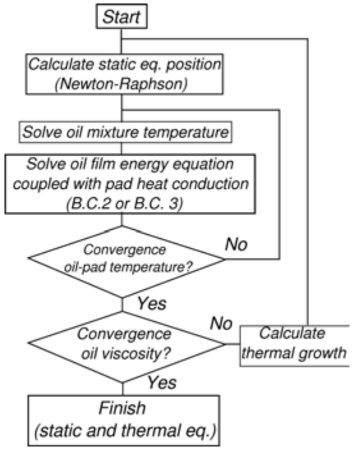

FIGURE 2. FLOWCHART DEPICTING THE OPERATIONS FOR THE CALCULATION OF THE STATIC AND THERMAL EQUILIBRIUM OF A TILTING-PAD JOURNAL BEARING, WHEN USING B.C.2 OR B.C.3

clear advantage of decoupling the solving procedure of the oil film energy equation with the calculation of the pad temperature field. The oil film energy equation must be solved iteratively in order to take into account the change of the oil film temperature in the pads leading edge due to the mixture process taking place between pads. By using B.C. 1 such iterations only involve the solving of the oil film energy equation, see Fig.1, due to the decoupling between the oil film domain and the pad domain. On the contrary, when using B.C. 2 or B.C. 3 the iterations for temperature field convergence must be performed solving the coupled system oil film-pad, see Fig.2, which of course involves the resolution of a much larger system of equations. This difference entails an increase in the time needed for calculating the static and thermal equilibrium of the bearing.

From the physical point of view, B.C. 1 entails not including heat transfer terms between oil and pads surface in the oil film energy equation, as well as assuming an infinite heat transfer coefficient between oil film and pad surface. The validity of these simplifications is tested by analyzing the results presented in the following sections.

COMPARISON FOR THD RESULTS BETWEEN THE TWO MODELS

On this section, the results delivered by the two models expressed in the previous section are compared. The results from the model developed by Fillon [4, 7, 10] (Model 1) are used as benchmark. The main objective is to determine the accuracy obtained when applying the different simplified heat transfer models into the modeling of a tilting-pad journal bearing where the oil film temperature is determined as an average in the radial direction (Model 2). Such analysis is performed by taking into account the following results:

1. Oil film temperature (obtained as an average of the oil temperature in the radial direction)
2. Pad surface temperature

Two different bearing configurations are studied. The geometry and parameters employed on each case are listed on Tab.1 and Tab.2. Configuration A corresponds to a bearing operating in laminar regime, whereas configuration B corresponds to a tilting pad journal bearing operating on the very limit of laminar regime. Since the scope of this study is set within the thermal modeling of the bearing, and in order to facilitate the comparison process, the pad flexibility and thermal growth effects are neglected. Hence, the results are obtained using a thermohydrodynamic formulation.

Results for bearing A, using B.C. 1 and B.C. 3

The results obtained for bearing A, regarding oil film and pad surface temperature, are depicted in Fig.3 and Fig.4. Generally speaking, the results for the oil film temperature shown in Fig.3 exhibit good agreement between the benchmark results and the two simplified heat transfer models.

When looking into the highly loaded pads in Fig.3, slight differences can be observed for the oil film temperature, namely a slightly higher temperature of the oil film for the simplified models, when compared to the benchmark results. Such difference is

TABLE 1. BEARING A, PARAMETERS USED FOR THE SIMULATION

Bearing radius	50	mm
Bearing length	70	mm
Radial pad clearance	0.148	mm
Preload	0.47	-
Number of pads	4	-
Pad arc	75	deg
Offset	0.5	-
Load Angle	between pads	-
Pad thickness	20	mm
Journal rotational speed	4000	RPM
Applied load	10	kN
Oil viscosity at 40 C	0.0277	Pa s
Oil viscosity at 100 C	0.0036	Pa s
Oil specific heat	2000	J/(kg K)
Oil thermal conductivity	0.13	W / (m K)
Free convection coefficient	100	W / (m^2 K)
Pad material thermal conductivity	45	W / (m K)

TABLE 2. BEARING B, PARAMETERS USED FOR THE SIMULATION

Bearing diameter	479	mm
Bearing length	300	mm
Number of pads	4	-
Pad arc	80	deg
Offset	0.5	-
Preload	0	-
Load Angle	between pads	-
Radial clearance	0.612	mm
Pad thickness	121	mm
Journal rotational speed	3000	RPM
Applied load	18	kN
Oil viscosity at 40 C	0.0277	Pa s
Oil viscosity at 100 C	0.0036	Pa s
Oil specific heat	2000	J/(kg K)
Oil thermal conductivity	0.13	W / (m K)
Free convection coefficient	115	W / (m^2 K)
Pad material thermal conductivity	45	W / (m K)

the result of different causes for the two simplified models. In the case of B.C 1, since no heat transfer term is included into the oil film energy equation, no thermal energy is transfered towards the pad or shaft, hence the oil temperature towards the pad trailing edge is higher than the benchmark result. On the contrary, when applying B.C 3 the pad temperature towards the trailing edge is higher than the benchmark result, see Fig.4, hence the heat transfer towards the oil in that zone is higher, resulting in a higher oil film temperature.

When looking into the oil film temperature in the lightly loaded pads, Fig.3 , close inspection reveals that the results delivered using the simplified models are slightly lower than the benchmark results. The explanation for this result are similar than for the loaded pads, namely no heat transfer from pad to oil when using B.C. 1, and lower pad temperature than the benchmark results when using B.C 3, as seen in Fig.4.

Regarding the pad temperature results, see Fig.4, the accuracy of the simplified models vary from the highly to the lightly loaded pads. It can be seen that, when applying B.C. 1, the pad surface temperature is underestimated in all the pads, whereas when applying B.C 3 the pad surface temperature is higher than the benchmark result for the highly loaded pads, and severely underestimated in the lightly loaded pads. On that regard, although the usage of B.C 3 on the highly loaded pads delivers excellent results, it seems that the usage of B.C. 1 offer a better overall accuracy for the pad surface temperature.

The reason for the pad surface temperature results obtained when using B.C. 3 lies in the formulation of such method. As it was explained before, this method gives an estimation of the gradient of the oil film temperature in the radial direction, in order to apply the heat flux continuity condition at pad surface-oil film interface. The value of such gradient is a function of the pad surface temperature, the oil film temperature and the shaft temperature. The shaft temperature is calculated as the average of the oil film temperature, in order to respect the assumption of nil global heat flux between shaft and oil, and in this case is equal to 52 degrees Celsius. Hence, the oil film temperature in the highly loaded pads is higher than the shaft temperature, whereas for the lightly loaded pads the opposite is true. As a result of this, the resulting approximated heat flux between oil film and pad surface produces a heating effect in the highly loaded pads, whereas it cools down the lightly loaded pads.

The results presented on this section were obtained for bearing A, which corresponds to a tilting-pad journal bearing operating in laminar regime. The results for the oil film temperature, see Fig.3, imply that the two simplified models allow to calculate accurately the effective viscosity of the oil film, with the resulting accuracy on the calculation of the static and dynamic characteristics. The fact that the oil temperature is slightly overestimated in the highly loaded pads is also beneficial, since it implicitly gives a safety factor to the calculation, as higher oil temperature implies lower viscosity and poorer dynamic characteristics. When regarding the results for the pad surface temperature, see Fig.4, B.C 3 delivers better results for the highly loaded pads, but B.C 1 offers a better overall behavior. All and all, both simplified models offer poorer characteristics for the pad temperature calculation, when compared to the oil film results, resulting in a loss of precision in the calculation of the thermal growth of the bearing pads. Since in this case a thermohydrodynamic regime was established, there is no direct impact from this result. Hence, the results for a thermoelastohydrodynamic regime expressed later on this work, should provide further insight about the validity of the approximated models.

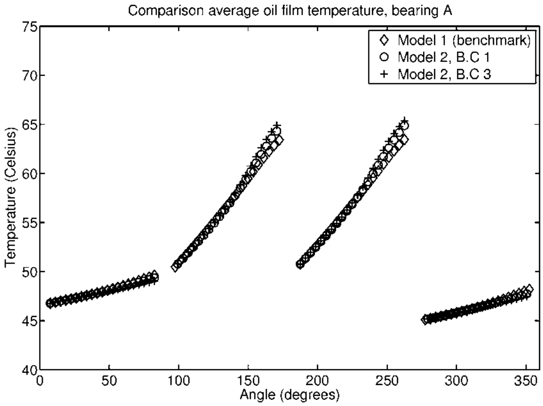

FIGURE 3. AVERAGE OIL FILM TEMPERATURE, BEARING A: COMPARISON OF RESULTS BETWEEN MODEL 1 (BENCHMARK) AND MODEL 2, WITH TWO DIFFERENT SETS OF BOUNDARY CONDITIONS FOR THE THERMAL PROBLEM

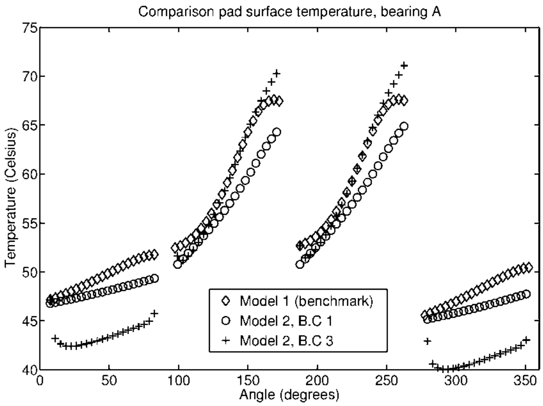

FIGURE 4. PAD SURFACE TEMPERATURE, BEARING A: COMPARISON OF RESULTS BETWEEN MODEL 1 (BENCHMARK) AND MODEL 2, WITH TWO DIFFERENT SETS OF BOUNDARY CONDITIONS FOR THE THERMAL PROBLEM

Results for bearing A, using B.C. 2

Fig.5 and Fig.6 depict the results for the oil film and pad surface temperature obtained when imposing B.C. 2 into Model 2. Three different values for the convection coefficient $H_{oil-pad}$ are tested, whose order of magnitude is obtained as a result of the analysis of the results delivered by Model 1, as it was stated previously. Such analysis revealed that the variation of the convection coefficient in the circumferential direction is important, which is a direct result of the variation of the temperature gradient in the radial direction, see Fig.7,from the pad leading edge to its trailing edge.

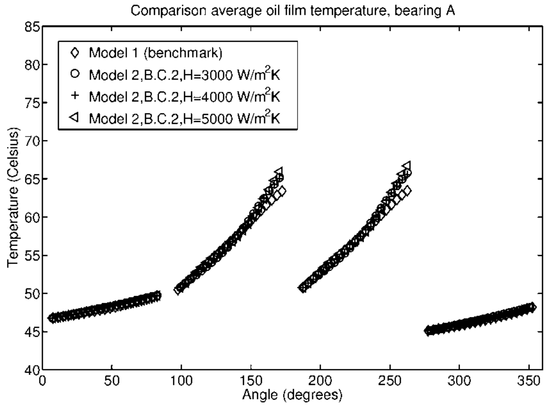

FIGURE 5. AVERAGE OIL FILM TEMPERATURE, BEARING A: COMPARISON OF RESULTS BETWEEN MODEL 1 (BENCHMARK) AND MODEL 2, USING BOUNDARY CONDITION 2 WITH DIFFERENT VALUES FOR THE CONVECTION COEFFICIENT

Such behavior in the circumferential direction, and the resulting variation in the heat flux between oil film and pad surface, make it difficult to obtain good results using a constant valued convection coefficient. Even though the results regarding the oil film temperature, Fig.5, show good coherence with the benchmark results, the results for the pad surface temperature, see Fig.6, reveal the disadvantage of applying this simplified heat transfer model. Although it is possible to obtain an acceptable agreement regarding the maximum pad surface temperature using a value of 4000 W/m^2K , the overall behavior exhibited by the results does not match the reference results. An unphysical oscillation around the benchmark results is observed, consequence of using a constant value for the convection coefficient. Hence, these results show the inadequacy of using this simplified heat transfer model with a constant value for the convection coefficient, thus such approach will not be tested any further.

Results for bearing B

The results for bearing B, regarding oil film and pad surface temperature, are expressed in Fig.8 and Fig.9 respectively. Only the results for the loaded pads are shown, since the two remaining ones are completely cavitated, condition that entails a different operational condition which lies outside of the scope of this study.

Bearing B is operating at higher limit of the laminar operational range. Hence, it corresponds to a more demanding condition from the thermal modeling point of view. In this case, the oil

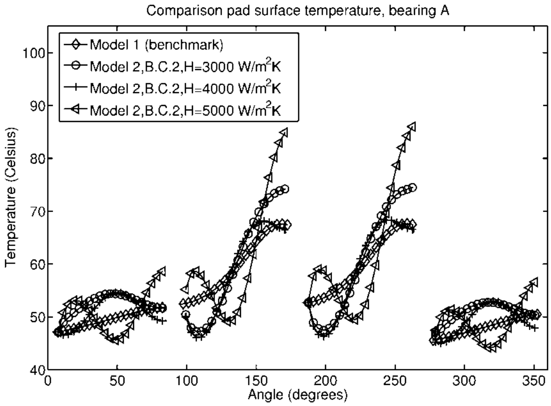

FIGURE 6. PAD SURFACE TEMPERATURE, BEARING A: COMPARISON OF RESULTS BETWEEN MODEL 1 (BENCHMARK) AND MODEL 2, USING BOUNDARY CONDITION 2 WITH DIFFERENT VALUES FOR THE CONVECTION COEFFICIENT

film temperature gradient in the radial direction is much higher than for bearing A, see Fig.7, hence some of the conclusions obtained for bearing A are no longer valid in this case. The results for oil film temperature, see Fig.8, show an overestimation of the oil film temperature value when compared to the benchmark result. Such differences are much more notorious than for bearing A, compare with Fig.3. It means that, in this case, neglecting the heat transfer between pad and oil in the oil film energy equation, as stated in B.C 1, implies a bigger error, whereas the usage of B.C. 3 entails an underestimation of the heat flux between oil film and pad surface. Such underestimation results in a higher oil film temperature, as seen in Fig.8, as well as in a lower pad surface temperature, see Fig.9, when compared to the benchmark results. However, as it was explained before, the results delivered by B.C. 3 are highly dependent in the value imposed as shaft temperature. In this case, the shaft temperature is equal to 48 degrees Celsius, calculated as the average of the oil film value. This value could be tuned in order to improve the coherence between the results, but such approach is not valid when there are no benchmark results to compare with, hence the feasibility of applying it on a real calculation is minimal.

Focusing on the pad surface temperature results, Fig.9, it can be seen than in this case the usage of B.C. 1 is not possible, as it produces an underestimation of the temperature. B.C 3 produces slightly better results, which could be improved by varying the shaft temperature, but such study is not performed for the reasons previously expressed. On this set of results, one can also observe the effect of the shaft temperature value. On the pad lying between 90 and 180 degrees, Fig.8, a reduction of the pad surface temperature is observed towards the leading edge,

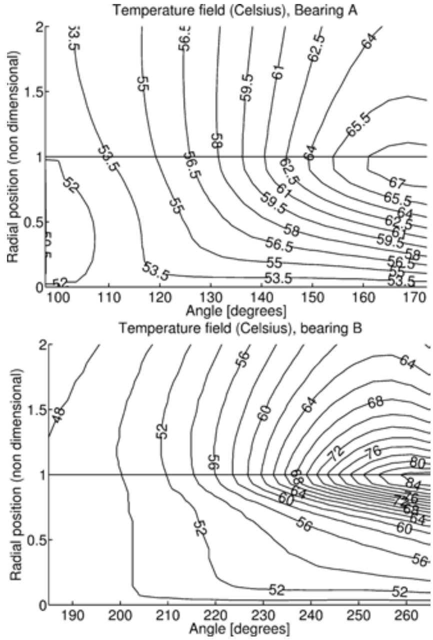

FIGURE 7. COMPARISON OF TEMPERATURE PROFILE FOR OIL FILM AND PAD IN THE AXIAL CENTRAL POSITION OBTAINED USING MODEL 1, FOR A LOADED PAD IN BEARING A AND BEARING B

whereas an increase is obtained towards the trailing edge. Such change is a consequence of the modification of the "direction" of the approximated heat flux between oil and pad, due to the value for the shaft temperature.

These results show that for a bearing operating at higher Reynolds numbers, the usage of B.C. 1 is not advisable, since it severely underestimates the pad surface temperature, with the consequent loss of precision in the temperature field calculation and resulting thermal growth. On that regard, B.C. 3 entails better results for the pad surface temperature, although its performance is function of the shaft temperature, value that is difficult to estimate theoretically. Regarding oil film temperature results, B.C. 3 entails an overestimation, characteristic that can be seen as an advantage from an engineering point of view, since it entails a safety factor in the calculation of the dynamic characteristics of the bearing.

COMPARISON AGAINST EXPERIMENTAL RESULTS FROM THE LITERATURE

On this section, the results delivered by the Model 2 are compared against some sets of experimental results available in

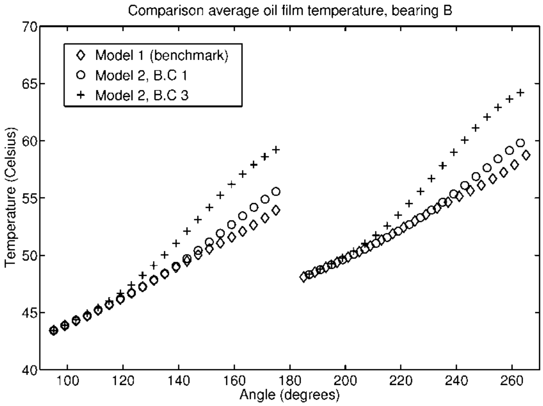

FIGURE 8. AVERAGE OIL FILM TEMPERATURE, BEARING B: COMPARISON OF RESULTS BETWEEN MODEL 1 (BENCHMARK) AND MODEL 2, WITH TWO DIFFERENT SETS OF BOUNDARY CONDITIONS FOR THE THERMAL PROBLEM

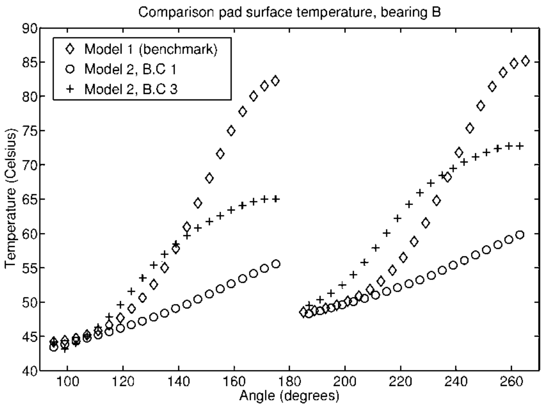

FIGURE 9. PAD SURFACE TEMPERATURE, BEARING B: COMPARISON OF RESULTS BETWEEN MODEL 1 (BENCHMARK) AND MODEL 2, WITH TWO DIFFERENT SETS OF BOUNDARY CONDITIONS FOR THE THERMAL PROBLEM

the literature. The different simplified heat transfer models are applied and the results are compared against the benchmark results. In order to perform the comparison, a thermoelastohydrodynamic assumption is established in the model. The objective is to determine the effect of applying the different simplified heat transfer models in the static and dynamic behavior of the bearing.

Regarding the modeling of the elastic deformations and thermal growth in the pads, a thorough presentation of the model can be found in [9]. In brief, it can be stated that:

1. The elastic deformations are included into the model using a pseudo modal reduction approach, as expressed throughly in [14, 15]. This method involves the calculation a priori of the eigenmodes of the pad, in order to express its deformation as a linear combination of such modes. This approach results in a significant save in calculation time, since the pad degrees of freedom are restricted to the number of modes included into the analysis. In this case, three modes are included for each pad: the tilting rigid body mode, the first bending mode and the mode related to the pivot flexibility, corresponding to a rigid body mode presenting a translation in the radial direction, whose modal stiffness is set to be equal to the pivot stiffness.
2. The thermal growth of the pads is calculated using the temperature field determined using Eqn. (7). The deformation due to thermal growth is calculated using a linear thermal expansion coefficient corresponding to the pad material.
3. The shaft thermal growth is also determined using a linear thermal expansion coefficient.

Comparison against Fillon et al [4]

The experimental results regarding pad surface temperature available in [4] correspond to a tilting-pad journal bearing with the geometry and operational characteristics listed in Tab.1. Hence, it corresponds to a bearing operating in laminar regime. Fig.10 depicts the comparison between those experimental results and the ones obtained using Model 2, on thermoelastohydrodynamic regime. In this case, both simplified heat transfer models deliver good coherence with the experimental data. In general, the usage of B.C. 1 allows to obtain a fairly good overall match with the benchmark results, whereas B.C. 3 implies an important underestimation of the temperature on the pads where the load is lower. Also, B.C. 3 tends to overestimate the temperature in the highly loaded pads, when compared to B.C. 1 and the experimental results.

One of the features that neither of the simplified heat transfer models exhibit is the temperature drop towards the trailing edge, visible on the highly loaded pads. Such temperature drop is a consequence of the heat transfer between the trailing edge of the pad and the surrounding oil bath. In the case of B.C.1, this local temperature drop is not exhibited since the temperature is fixed to be equal to the oil film temperature, which is calculated using an energy equation that does not consider heat diffusion towards the oil bath between pads. On other hand, the usage of B.C. 3 implies a high heat flux towards the trailing edge, due to the higher temperature difference between oil film and shaft temperature, hence the free convection condition established on the trailing face of the pad is not enough to produce that temperature drop.

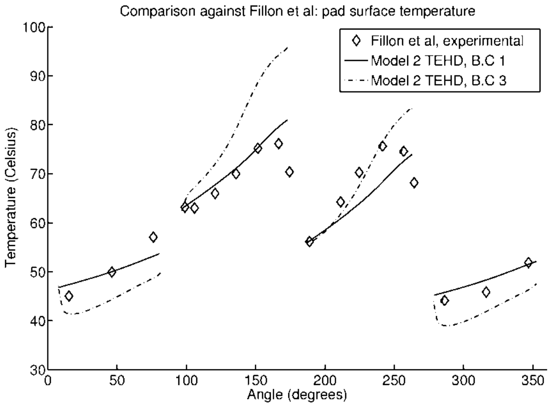

FIGURE 10. COMPARISON AGAINST FILLON ET AL [4]: EXPERIMENTAL RESULTS FOR THE PAD SURFACE TEMPERATURE, VERSUS RESULTS FROM MODEL 2 ON THERMOELASTOHYDRODYNAMIC REGIME, WITH TWO DIFFERENT SETS OF BOUNDARY CONDITIONS FOR THE THERMAL PROBLEM

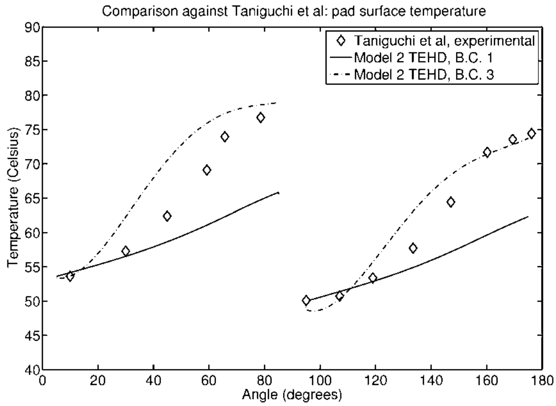

FIGURE 11. COMPARISON AGAINST TANIGUCHI ET AL [16]: EXPERIMENTAL RESULTS FOR THE PAD SURFACE TEMPERATURE, VERSUS RESULTS FROM MODEL 2 ON THERMOELASTOHYDRODYNAMIC REGIME WITH TWO DIFFERENT SETS OF BOUNDARY CONDITIONS FOR THE THERMAL PROBLEM

Comparison against Taniguchi et al [16]

The set of experimental results published by Taniguchi et al [16] corresponds to a bearing with the characteristics listed in Tab.2. Hence, it corresponds to a bearing operating on the higher limit of the laminar range.The results expressed in Fig.11 compare the experimental value for the pad surface temperature at the highly loaded pads, with the ones obtained using Model 2 in thermoelastohydrodynamic regime. Such comparison confirms that the usage of B.C. 1 on a bearing with this operational conditions entails a severe underestimation of the pad surface temperature, whereas the results obtained using B.C. 3 show good agreement with the experimental results at the trailing edge of each pad. On this case, the shaft temperature is set to be 60 degrees Celsius, following the recomendation expressed in [4] when performing the same analysis.

Comparison against Brockwell et al [17]

Experimental results regarding the obtention of dynamic coefficients for a five pad,load between pads bearings are expressed in [17]. Such bearing operates in laminar conditions, where three of the pads are completely cavitated, hence they are not included into the perturbation analysis necessary for obtaining the dynamic coefficients by theoretical means. Fig.12 and Fig.13 show the comparison for synchronously reduced stiffness and damping coefficients respectively, between experimental results, and the ones obtained using model 2 on thermoelastohydrodynamic regime.

In general, excellent agreement between model 2 and the experimental data is obtained when using B.C. 1 as the simplified heat transfer model. These results imply a significant improvement when compared to the ones presented previously in [9] when performing the same comparison. The reason for such improvement is the inclusion of the pivot flexibility on the results presented here. These results again stress the validity of using B.C. 1 when it comes to simplify the modeling of the heat transfer between oil film and pad surface for tilting-pad journal bearings on laminar regime.Moreover, these results reveal that the obtained thermoelastohydrodynamic model for the tilting-pad journal bearing is capable of calculating the equilibrium position and linearized force coefficients with sufficient accuracy. Such accuracy will be benefitial at the moment of modeling a tilting-pad journal bearing operating in controllable regime.

CONCLUSIONS AND FUTURE ASPECTS

In this work, an analysis has been performed on several simplified strategies for the thermal modeling of tilting-pad journal bearings, specifically focused on the heat transfer process between oil film and pad surface. The aim of such analysis is the application of those simplified thermal models on the theoretical modeling of tilting-pad journal bearings operating with a controllable lubrication regime (hybrid or active), regime that demands a simplified approach when it comes to model the different phenomena taking place in the different phenomena taking place in the controllable bearing as a mechatronic system. Such study has been carried out by direct comparison of the results delivered by the simplified models, with the model presented in [4, 7, 10], where the heat transfer process is thoughly modeled, as well as

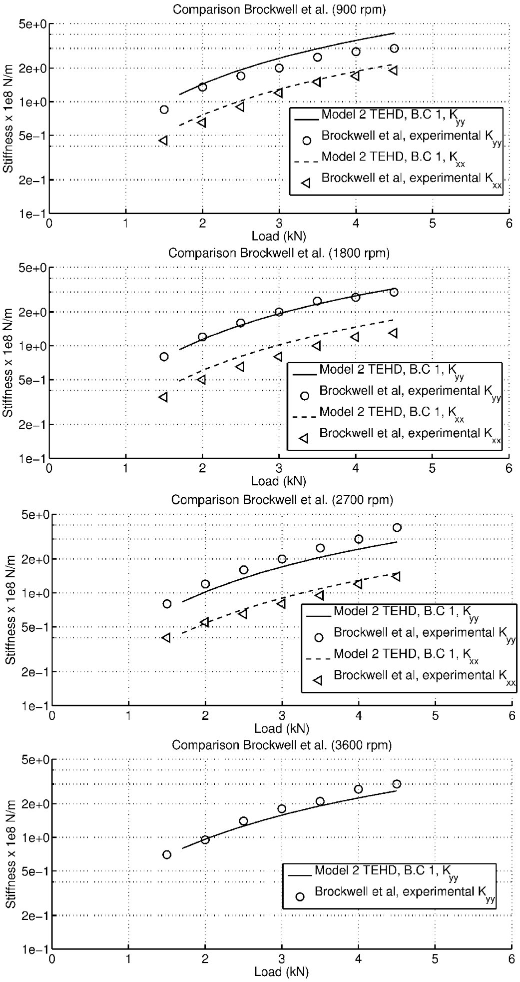

FIGURE 12. COMPARISON AGAINST BROCKWELL ET AL [17]: SYNCHRONOUSLY REDUCED STIFFNESS COEFFICIENTS, EXPERIMENTAL RESULTS VERSUS RESULTS FROM MODEL 2 ON THERMOELASTOHYDRODYNAMIC REGIME WITH BOUNDARY CONDITION 1 FOR THE THERMAL PROBLEM

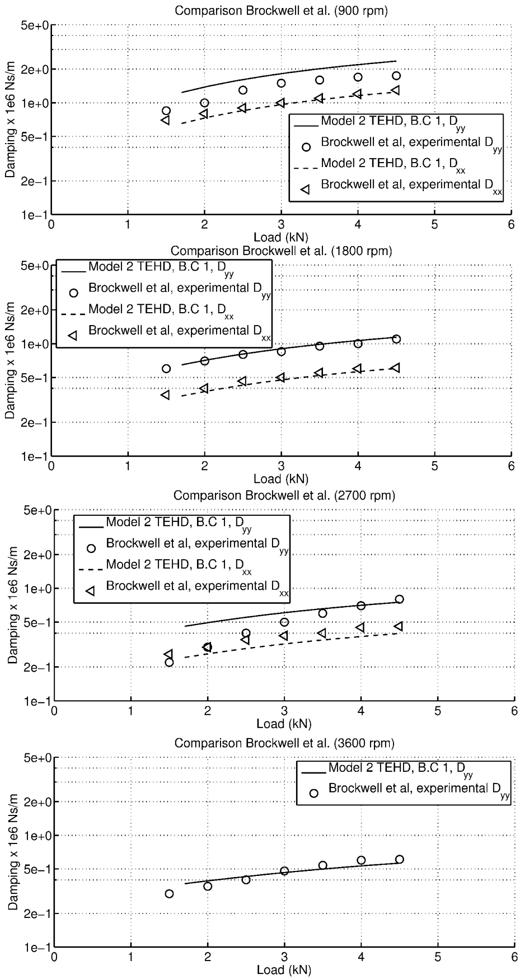

FIGURE 13. COMPARISON AGAINST BROCKWELL ET AL [17]: SYNCHRONOUSLY REDUCED DAMPING COEFFICIENTS, EXPERIMENTAL RESULTS VERSUS RESULTS FROM MODEL 2 ON THERMOELASTOHYDRODYNAMIC REGIME WITH BOUNDARY CONDITION 1 FOR THE THERMAL PROBLEM

with comparison with experimental results available in the literature. As a result of this study, it is possible to conclude the following.

1. The employment of B.C. 1, namely using an oil film energy equation formulation with no explicit heat transfer terms between oil and pads to determine the oil film temperature, which is later applied as a Dirichlet boundary conditions at the pad surface, delivers good results for tilting-pad journal bearings operating on laminar regime. This simplified approach offers a very good balance between implementation complexity, quality of the results, and calculation time. The comparison of the results delivered by the simplified model using B.C. 1 shows good agreement with benchmark model results, as well as experimental results, regarding the

static,thermal and dynamic behavior of the bearing.

2. The usage of B.C. 1 is not recommended for a tilting-pad journal bearing approaching turbulent regime. On such case, the application of this simplified model entails an important underestimation of the pad surface temperature, with the resultant accuracy loss for the thermal modeling, as well as the thermal growth calculation. In such operational regime, the implementation of B.C. 3 as stated by Knight and Barrett [13] delivers acceptable results regarding the thermal modeling of the bearing. However, when applying this simplified method two facts must be taken into account: firstly, the quality of its results varies considerably from loaded to lightly loaded pads, and secondly, its results are highly dependent on the value of the shaft temperature, parameter difficult to estimate accurately.
3. Using a constant valued convection coefficient (B.C. 2) as a tool to model the heat transfer between oil film and pad surface is not advised. The analysis of the benchmark results regarding the temperature field for the oil film and the pad surface reveals that the temperature gradient and resulting heat flux varies considerably, both in magnitude and direction, from the leading to the trailing edge of the pad. Hence, the usage of a constant valued convection coefficient delivers poor results for the pad surface temperature, which exhibit an unphysical variation around the reference results. It is necessary then to obtain a law for the variation of the convection coefficient in the circumferential direction, if one desires to apply such schemme. However, obtaining a law with the necessary degree of generality seems to be, at first glance, a difficult task.
4. The implementation of B.C. 1 enables to uncouple the solving procedure of the oil film energy equation, which must be performed iteratively due to boundary conditions related to the oil mixing temperature between two consecutive pads, with the calculation of the pads temperature field. Such feature entails an important reduction in the calculation time, when compared to the application of B.C. 3 , that demands to perform such iterations with the simultaneous calculation of the oil film and pads temperature field. For the simulations performed for this work, the reduction in the calculation time for the static and thermal equilibrium was in the order of 55%.
5. The reduction in the calculation time associated with the usage of B.C. 1 seems particularly attractive for modeling a tilting-pad journal bearing on controllable lubrication regime, which involves the coupling of the tilting-pad journal bearing model with the oil injection effects, dynamics of the servo valves and rotor system. Experimental validation of its applicability on such lubrication regime is to be undertaken by using a test rig specifically designed and built for such purpose.

REFERENCES

[1] Glienicke, J., 1987. "Stabilitatsprobleme bei Lagerung schnellaufender Wellen - Berechnung, Konstruktion und Verhalten von Mehrflchen- und Kippsegmentlagern". *Technische Akademie Wuppertal, Germany*.

[2] Flack, R. D., and Zuck, C. J., 1988. "Experiments on the Stability of Two Flexible Rotor in Tilting Pad Journal Bearing". *Tribology Trans.,* ***31***(2), pp. 251–257.

[3] Ettles, C., 1980. "The Analysis and Performance of Pivoted Pad Journal Bearings considering Thermal and Elastic Effects". *J. Lubr. Tech., ASME Trans.,* ***102***(2), pp. 182–194.

[4] Fillon, M., Bligoud, J. C., and Frêne, J., 1992. "Experimental Study of Tilting-Pad Journal Bearings – Comparison with Theoretical Thermoelastohydrodynamic Results". *Journal of Tribology, ASME Trans,* ***114***(3), pp. 579–588.

[5] Kim, J., Palazzolo, A., and Gadangi, R., 1994. "TEHD Analysis for Tilting Pad Journal Bearings using Upwind Finite Element Method". *Tribology Transactions,* ***37***(4), pp. 771–783.

[6] Kim, J., Palazzolo, A., and Gadangi, R., 1995. "Dynamics Characteristics of TEHD Tilt Pad Journal Bearing Simulation including Multiple Mode Pad Flexibility". *ASME Journal of Vibration and Acoustics,* ***117***(1), January, pp. 123–135.

[7] Monmousseau, P., Fillon, M., and Frêne, J., 1998. "Transient Thermoelastohydrodynamic Study of Tilting-Pad Journal Bearings under Dynamic Loading". *ASME Journal of Engineering for Gas Turbines and Power,* ***120***(2), pp. 405–409.

[8] Cerda, A., and Santos, I. F. "Stability Analysis of an Industrial Gas Compressor supported by Tilting-Pad Journal Bearings under Different Lubrication Regimes". *Journal of Engineering for Gas Turbines and Power, ASME Trans. (in print)*.

[9] Cerda, A., and Santos, I. F. "Performance Improvement of Tilting Pad Journal Bearings by means of Controllable Lubrication". *Mecanique et Industries (accepted for publication)*.

[10] Fillon, M., Souchet, D., and Frêne, J., 1990. "Influence of Bearing Element Displacements on Thermohydrodynamic Characteristics of Tilting-Pad Journal Bearings". *Proceedings of the Japan International Tribology Conference, Nagoya 1990*, pp. 635–640.

[11] Santos, I. F., and Nicoletti, R., 1999. "THD Analysis in Tilting-Pad Journal Bearings using Multiple Orifice Hybrid Lubrication". *Journal of Tribology, ASME Trans.,* ***121***, pp. 892–900.

[12] Santos, I. F., and Nicoletti, R., 2001. "Influence of Orifice Distribution on the Thermal and Static Properties of Hybridly Lubricated Bearings". *International Journal of Solids and Structures,* ***38***, pp. 2069–2081.

[13] Knight, J., and Barrett, L., 1988. "Analysis of Tilting Pad

Journal Bearings with Heat Transfer Effects". *ASME Journal of Tribology,* ***110***, January, pp. 128–133.
[14] Haugaard, A., and Santos, I. F., 2010. "Multi-orifice Active Tilting-Pad Journal Bearings-Harnessing of Synergetic Coupling Effects". *Tribology International,* ***43***(8), pp. 1374–1391.
[15] Haugaard, A., and Santos, I. F., 2010. "Stability of Multi Orifice Active Tilting-Pad Journal Bearings". *Tribology International,* ***43***(9), pp. 1742–1750.
[16] Taniguchi, S., Makino, T., Takeshita, T., and Ichimura, T., 1990. "A Thermohydrodynamic Analysis of Large Tilting-Pad Journal Bearing in Laminar and Turbulent Flow Regimes With Mixing". *Journal of Tribology, ASME Trans.,* ***112***, July, pp. 542–550.
[17] Brockwell, K., Kleinbub, D., and Dmochowski, W., 1989. "Measurement and Calculation of the Dynamic Operating Characteristics of the Five Shoe Tilting-Pad Journal Bearing". *Tribology Transactions,* ***33***(4), pp. 481–492.

5.4 Publication 4: Steady State Characteristics of a Tilting Pad Journal Bearing with Controllable Lubrication: Comparison between Theoretical and Experimental Results

Tribology International 58 (2013) 85–97

Contents lists available at SciVerse ScienceDirect

Tribology International

journal homepage: www.elsevier.com/locate/triboint

Steady state characteristics of a tilting pad journal bearing with controllable lubrication: Comparison between theoretical and experimental results

Alejandro Cerda Varela *, Bo Bjerregaard Nielsen, Ilmar Ferreira Santos

Department of Mechanical Engineering, Technical University of Denmark, 2800 Kgs. Lyngby, Denmark

ARTICLE INFO

Article history:
Received 1 August 2012
Received in revised form
8 October 2012
Accepted 12 October 2012
Available online 23 October 2012

Keywords:
Bearing
Tilting-pad
Controllable
Steady state

ABSTRACT

This paper is aimed at presenting results regarding the static and thermal behavior of a tilting-pad journal bearing operating under controllable regime. The bearing is rendered controllable by injecting high pressure oil into the clearance using holes drilled across the bearing pads in the radial direction. The modification of the injection pressure enables to modify the bearing static and dynamic properties according to the operational needs. The results presented are obtained using a theoretical model, which considers all the effects that determine the bearing behavior (controllable elastothermohydrodynamic lubrication regime), as well as using a test rig designed and built to this effect. The comparison between experimental and theoretical results provides solid ground to determine the accuracy of the available model for the the prediction of the steady-state behavior of the tilting-pad bearing with controllable lubrication. Among the parameters considered for the study are: oil film temperature field, resulting forces over rotor and pads, and rotor equilibrium position. The results obtained show good agreement between theory and experiment, as long as the assumptions on which the model is based are respected. Also, it is shown that some improvements are possible when it comes to model the steady-state behavior of the controllable bearing with the injection system turned off.

1. Introduction

Tilting-pad journal bearings are widely used within the industry, due to their superior stability characteristics when compared to other oil film bearing designs. Their successful application for industrial purposes is a direct result of the current level of knowledge regarding their static and dynamic properties. Such knowledge is the result of many publications available within the literature, which deal both with the theoretical modeling of these mechanical elements, as well as with experimental investigations of the tilting-pad bearings operational characteristics.

The state of the art regarding the modeling of tilting-pad bearings establishes the need for including several effects within the model formulation. Namely, one has to consider the oil film pressure build-up or hydrodynamic effect, the thermal effects related to temperature build up within the oil film and the bearing pads, and the flexibility effects associated with the elastic deformations of the pads and pivots due to the loads exerted over them. Hence, an elastothermohydrodynamic (ETHD) lubrication regime must be established within the model in order to represent accurately the static and dynamic properties of the tilting-pad bearing. Such conclusion is the direct result of the work of several authors regarding bearing modeling, such as Ettles [1,2], Brockwell and Dmochowski [3], Fillon et al. [4,5], Kim and Palazzolo [6,7], among others.

The continuous development of more sophisticated models for the tilting-pad bearing is a direct result of the critical review of the results of such models by comparison with experimental results available in the literature. Such sets of results deal mainly with the static and thermal properties of these bearings, as well as with the obtention of bearing dynamic coefficients by experimental means. Regarding steady state static and thermal properties of tilting-pad bearings, the experimental results obtained by Brockwell and Kleinbub [8], Taniguchi et al. [9], Fillon et al. [4,5,10] are good examples. Concerning the experimental identification of dynamic coefficients for the tilting-pad bearing, one should refer to the results published by Brockwell [11], Dmochowski [12], Wygant et al. [13], Ha and Yang [14], Childs [15], among others.

The versatility of the tilting-pad journal bearing design can be further expanded by modifying its basic configuration, with the aim of transforming it into a "smart" machine element. Such modifications involve the inclusion of additional elements or variables within the original design, which can be controlled directly during the bearing operation, resulting in the adjustment of the static and dynamic properties of the bearing according to the operational demands. With this objective in mind, Santos [16]

* Corresponding author.
E-mail addresses: acer@mek.dtu.dk (A. Cerda Varela), ifs@mek.dtu.dk (I.F. Santos).

0301-679X/$ - see front matter © 2012 Elsevier Ltd. All rights reserved.
http://dx.doi.org/10.1016/j.triboint.2012.10.004

introduced the concept of an active lubrication system for the tilting-pad bearing, which considers the injection of high pressure oil directly into the bearing clearance, through holes drilled across the pad in the radial direction. The injection pressure can be modified during the bearing operation using a servovalve, enabling to alter the pressure field within the oil film. Hence, the bearing equilibrium position can be altered, resulting in a modification of the system behaviour depending on the requirements at hand.

Since the introduction of this technology, there has been a constant effort dealing with the improvement of the model for the actively lubricated tilting-pad bearing. Firstly, Santos and Russo [17] presented in a thorough way the Modified Reynolds Equation for Active Lubrication, which enables to calculate the oil film pressure field considering the effect of the radial oil injection. A rigid-pad, isothermal modeling assumption was established for the analysis performed in such work. Then, Santos and Nicoletti [18,19] introduced an energy equation for the calculation of the oil film temperature field, including the effect of the oil injection. Such model assumed an adiabatic regime for the oil film temperature calculation, thus neither heat transfer towards the pad or shaft, nor resulting thermal growth of those elements was considered. The rigid-pad assumption was kept at that time. Hence, the bearing model achieved a controllable thermohydrodynamic regime. Later on, Haugaard and Santos [20,21] developed a finite element model for the fluid and solid domain of the active bearing, which enabled to include the pad flexibility effects using a pseudo modal reduction scheme. No thermal effects were included at that point, hence such model considered a controllable elastohydrodynamic regime. Hertzian local deformations in the surface of the pad are not considered for the analysis. Cerda and Santos [22] coupled the previously exposed models, by expanding the finite element model developed by Haugaard and Santos [20,21] in order to include oil film temperature build up and thermal growth for the pads and journal. Also, the pivot flexibility was included in such work, taking advantage of the pseudo modal reduction scheme already implemented within the model. Regarding thermal effects, such model included the heat transfer process between the oil film and the pad surface using a highly simplified approach, by assuming an infinite heat transfer coefficient between oil film and pad surface. Hence, the oil film temperature was calculated using the energy equation as stated in [18,19], with no explicit heat transfer terms, which is decoupled from the pad heat conduction model. Later on, the oil film temperature is imposed as a Dirichlet boundary condition in the pad surface when solving the Fourier law for heat conduction in the pads. This simplified approach for modeling the thermal effects was modified in [23]. Here, the oil film energy equation and Fourier law implementation were modified to include explicitly heat flux terms to model the heat transfer process between oil film and pad surface, by assuming a parabolic oil temperature distribution in the radial direction, as originally proposed by Knight and Barrett [24].

Thus, the state of the art regarding the modeling of a tilting-pad bearing with controllable lubrication considers a controllable elastothermohydrodynamic (ETHD) lubrication regime. The model has been validated [22,23] on its standard configuration (no injection holes) against experimental results available in the literature, regarding static, thermal and dynamic properties of tilting-pad journal bearings operating within laminar regime. By performing such validation, it is now possible to state that the available model is capable to capture all the relevant effects taking place within the tilting-pad bearing, which entails an accurate prediction of its static and dynamic properties. However, the validation of the modeling approach used for including the effect of the oil injection that renders the bearing “active” remains pending until now.

The benefits of employing the actively lubricated tilting-pad bearing in an industrial application have been demonstrated by several studies. The potential of the active lubrication system for reducing the bearing oil film average temperature, as well as for extending the stable operational range of an industrial compressor and reducing its unbalance response when crossing critical speeds has been shown using the available ETHD model [25,22]. The feasibility of modifying the tilting-pad bearing dynamic coefficients using the active lubrication system was proven experimentally in [26]. In this work, a comparison against theoretical results using the model available at the time (controllable hydrodynamic lubrication regime) was presented, which yielded better results for the prediction of the stiffness coefficients than for the damping coefficients. On the other hand, the experimental results shown in [27,28] depict the feasibility of modifying the frequency response function as well as to reduce the vibrations amplitude of a rotor test rig using the actively lubricated bearing as the actuator of a control loop.

In order to apply this technology in a real industrial application, it is mandatory to be able to predict accurately the static and dynamic behavior of the rotating machine where the actively lubricated bearing is being installed. For doing so, it is necessary to achieve a high level of confidence in the results delivered by the available theoretical model for the bearing, considering its static and thermal behavior, as well as its dynamic properties. Such confidence can only be achieved by validating the existing model using experimental data. The first step in this direction is to determine the accuracy of the model regarding the prediction of equilibrium position of the system under steady state conditions, which will depend on the quality of the available models for the hydrodynamic, thermal and flexibility effects. The tilting-pad journal bearing, in both its standard and controllable configuration, exhibits non-linear behaviour, hence the linearization of the oil film forces for rotor design purposes via dynamic coefficients will produce good results only if the steady state equilibrium position is determined accurately.

The main original contribution of this paper is to present a comparison between experimental and theoretical results, regarding the steady state properties of the tilting-pad journal bearing with controllable lubrication. Among the parameters to be studied are the journal equilibrium position, oil film temperature field and resulting forces over pads and rotor. As a result of this study, the validation of the available ETHD model for tilting-pad journal bearings with controllable lubrication will be achieved, in terms of the steady state behavior of such system.

2. Tilting-pad journal bearing with controllable lubrication: mathematical modeling

In this section, the mathematical model for the modeling of the tilting-pad journal bearing with controllable lubrication is presented briefly. The reader is advised to refer to the cited publications [16–21] in order to get a more complete presentation of the model.

2.1. Oil film pressure build-up: Modified Reynolds Equation for controllable lubrication

The oil film pressure build up for the tilting-pad journal bearing has been traditionally described by means of the Reynolds Equation, based on the assumption of laminar flow and negligible effects of the fluid inertia and radial viscous shear forces. Such basic model was extended in [16,17], including some terms to model the effect of the oil injection into the bearing clearance using n_0 orifices. Hence, the Modified Reynolds

Equation for Controllable Lubrication is established, as shown in Eq. (1).

$$\frac{\partial}{\partial \bar{y}}\left(\frac{h^3}{\mu}\frac{\partial p}{\partial \bar{y}}\right)+\frac{\partial}{\partial \bar{z}}\left(\frac{h^3}{\mu}\frac{\partial p}{\partial \bar{z}}\right)-\frac{3}{\mu_{inj} l_0}\sum_{i=1}^{n_0} F_i(\bar{y},\bar{z})\cdot p$$
$$=6U\frac{\partial h}{\partial \bar{y}}-12\frac{\partial h}{\partial t}-\frac{3}{\mu_{inj} l_0}\sum_{i=1}^{n_0} F_i(\bar{y},\bar{z})\cdot P_{inj} \quad (1)$$

where $F_i(\bar{y},\bar{z})$ is defined as follows:

$$F_i(\bar{y},\bar{z})=\frac{d_0^2}{4}-(\bar{y}-\bar{y}_i)^2-(\bar{z}-\bar{z}_i)^2,\ \text{ if } (\bar{y}-\bar{y}_i)^2-(\bar{z}-\bar{z}_i)^2 \le \frac{d_0^2}{4}$$
$$F_i(\bar{y},\bar{z})=0,\ \text{ if } (\bar{y}-\bar{y}_i)^2-(\bar{z}-\bar{z}_i)^2 \ge \frac{d_0^2}{4} \quad (2)$$

From Eq. (1), it can be seen that for a controllable lubrication regime, the oil film pressure field $p(\bar{y},\bar{z})$ is a function of the injected oil pressure P_{inj} and viscosity μ_{inj}, as well as the geometry of the injection hole (included into the $F_i(\bar{y},\bar{z})$ function shown in Eq. (2)), on top of the variables established by the traditional Reynolds Equation, namely rotor tangential speed ($U=\Omega\cdot R$), oil viscosity μ and oil film thickness h . The two dimensional domain for the study is defined along the axial $\bar{z}$ and circumferential $\bar{y}$ coordinates, see (Fig. 1), in order to make room for the inclusion of the oil injection effects. It can be seen that the function $F_i(\bar{y},\bar{z})$ is related to the orifices position along the pad surface, given by the coordinates $(\bar{y}_i,\bar{z}_i)$, and the orifices diameter d_0 and length l_0. For a passive TPJB, $F_i(\bar{y},\bar{z})$ is equal to zero, hence the term P_{inj} corresponding to the oil injection pressure vanishes.

2.2. Thermal effects: the oil film energy equation for controllable lubrication and Fourier law for heat conduction in the pads

The oil film temperature build up due to the shear and pressure forces developed within the fluid can be modelled by establishing an energy balance, which accounts for the variation of the fluid energy (kinematic and thermal) due to the work of the forces acting over it (namely pressure and shear forces). Furthermore, the effect of the oil injection into the clearance can be included as presented in [18,19], obtaining the Oil Film Energy Equation for Controllable Lubrication Regime, as given by Eq. (3)

$$\rho C_p h\frac{\partial T}{\partial t}+k_c h\frac{\partial^2 T}{\partial \bar{y}^2}+k_c h\frac{\partial^2 T}{\partial \bar{z}^2}+k_c\left.\frac{\partial T}{\partial \bar{x}}\right|_0 F_i$$
$$+\left(\frac{\rho C_p h^3}{12\mu}\frac{\partial p}{\partial \bar{y}}-\frac{\rho C_p U h}{2}\right)\frac{\partial T}{\partial \bar{y}}+\frac{\rho C_p h^3}{12\mu}\frac{\partial p}{\partial \bar{z}}\frac{\partial T}{\partial \bar{z}}$$

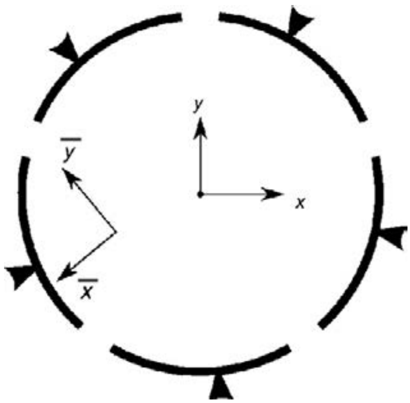

Fig. 1. Reference coordinate systems used for the bearing model.

$$\rho C_p\left(V_{inj}-\frac{\partial h}{\partial t}\right)(T-T_{inj})+\mathbf{S}_{oil}=\frac{4}{3}\frac{\mu}{h}\left(V_{inj}-\frac{\partial h}{\partial t}\right)^2$$
$$p\left(V_{inj}-\frac{\partial h}{\partial t}\right)-U^2\frac{\mu}{h}-\frac{h^3}{12\mu}\left[\left(\frac{\partial p}{\partial \bar{y}}\right)^2+\left(\frac{\partial p}{\partial \bar{z}}\right)^2\right] \quad (3)$$

The injection velocity profile V_{inj} is determined as a completely developed laminar flow inside the injection orifice, using the expression given by Eq. (4)

$$V_{inj}(\bar{y},\bar{z})=-\frac{1}{4\mu_{inj} l_0}(P_{inj}-p)\cdot\sum_{i=1}^{n_0} F_i(\bar{y},\bar{z}) \quad (4)$$

Eq. (3) assumes a constant oil temperature value across the radial direction. It enables to obtain the oil film temperature in the circumferential and axial direction, as a function of the oil film pressure field, bearing operational condition and oil thermal properties. Aditionally, some parameters related to the the oil injection are included (namely, temperature and injection velocity, which is a function of the injection pressure). Physically, the extra terms corresponding to the effect of the oil injection account for the following effects: diffusive heat conduction between the oil film and the injection oil due to their temperature difference, convective heat transport of the injected oil when entering the bearing clearance, and work of the pressure and shear forces generated due to the high pressure oil injection. On the other hand, the term $\mathbf{S}_{oil}$ groups the terms corresponding to the modeling of the heat transfer between oil film and pad surface.

Regarding the obtention of the pad temperature field, the Fourier Law for the thermal conduction is employed on its 3D formulation, as follows:

$$k_{pad}\left(\frac{\partial^2 T^{pad}}{\partial x^2}+\frac{\partial^2 T^{pad}}{\partial y^2}+\frac{\partial^2 T^{pad}}{\partial z^2}\right)+H_\infty\left(T^{pad}-T_\infty\right)|_{boundary}+\mathbf{S}_{pad}=0 \quad (5)$$

In Eq. (5), the coordinates x,y,z correspond to the tridimensional cartesian reference system that defines the domain for the pad, see Fig. 1. In order to model the heat transfer between the pad and the surroundings, a free convection coefficient H_∞ is employed. On the other hand, $\mathbf{S}_{pad}$ groups the terms corresponding to the heat transfer phenomena between the pad surface and the oil film.

Since the oil film energy equation does not include the radial direction explicitly within the analysis domain, some simplifying assumption must be established in order to model the radial temperature gradient and resulting heat flux between the oil film and the pad surface, while keeping a two dimensional domain for the analysis. A thorough study on this issue was carried out in [23]. As a result of it, the simplified model presented by Knight and Barrett [24] was implemented. According to this model, the oil film temperature profile in the radial direction is assumed to be parabolic, and can be characterized by the surface temperature of the shaft T_{shaft}, determined as the average oil film temperature, the mean oil film temperature T at the middle of the oil film thickness, determined using Eq. (3), and the pad surface temperature $T^{pad}_{boundary}$. Hence, a second order polynomial can be used to approximate the radial oil temperature distribution, as follows:

$$T(\bar{x})=T^{pad}_{boundary}+2\left(3T-2T^{shaft}-2T^{pad}_{boundary}\right)\frac{\bar{x}}{h}$$
$$+3\left(T^{shaft}-2T+T^{pad}_{boundary}\right)\left(\frac{\bar{x}}{h}\right)^2 \quad (6)$$

Such radial temperature distribution is assumed only with the objective of estimating the heat transfer between oil and pad surface, hence the oil film energy equation presented in Eq. (3) only determines the oil film temperature distribution in the circunferential and axial direction. Then, it is possible to apply the heat flux continuity condition at the interface between oil film and pad surface, using the assumed gradient for the oil film temperature in the radial direction, resulting in heat transfer terms defined as follows:

$$\mathbf{S}_{oil} = -\mathbf{S}_{pad} = \frac{k_{oil}}{h}(3T - 2T^{shaft} - 2T^{pad}_{boundary}) \tag{7}$$

The presence of the heat transfer terms $\mathbf{S}_{oil}$ and $\mathbf{S}_{pad}$ in Eqs. (3) and (5) entails that the oil film energy equation and pad heat conduction model are coupled, hence they must be solved simultaneously. Once the oil film temperature field is calculated, it is possible to update the viscosity of the oil film by knowing the variation law of this parameter with the temperature, as given by Eq. (8)

$$\mu = \mu^* e^{-\beta(T - T^*)} \tag{8}$$

where the μ^*, T^* and β parameters are characteristics of the oil.

2.3. Flexibility effects: the pseudo modal reduction scheme and thermal growth calculation

The inclusion of the pad elastic deformations due to the oil film pressure field is done by following a pseudo modal reduction scheme. This method was introduced by Palazzolo et al. [7] and later implemented by Haugaard and Santos [20,21] in the context of the controllable lubrication regime. This model does not account for local Hertzian deformations in the surface of the pad. The basic idea consists of expressing the pad deformation as a linear combination of a finite number of the eigenmodes of the pads, calculated without including the presence of the oil film. It corresponds to a pseudo reduction, since only the modes that are relevant for the analysis are considered. The first eigenmode corresponds to the tilting motion of the pad around the pivot as a rigid body, whereas the higher modes correspond to pad elastic deformation shapes. Also, an additional mode corresponding to a rigid body radial displacement of the pad can be used to include the pivot flexibility effects. The modal stiffness in this case is set to be equal to the pivot stiffness. Hence, the linear combination of such modes will generate a displacement of each point of the pad, where the elastic deformations of the pad and pivot, plus the pad tilting motion, are included. Since the oil film thickness calculation is performed using that distorted shape, the solution of the Reynolds Equation and Energy Equation becomes a function of the pad flexibility effects. In mathematical terms, using the finite element method the model of the pads can be expressed as:

$$\mathbf{M}_s \ddot{\mathbf{q}}_s + \mathbf{K}_s \mathbf{q}_s = \mathbf{f}_s \tag{9}$$

where $\mathbf{q}_s$ correspond to the degrees of freedom for each node of the finite element model, $\mathbf{M}_s$ and $\mathbf{K}_s$ correspond to the inertia and stiffness matrix for the pads, obtained using the finite element method, and $\mathbf{f}_s$ represent the loads over the pads due to the pressure profile in the oil film. By calculating the pseudo-modal matrix $\mathbf{V}_s$ containing on its columns some of the eigenmodes of the pads, one can rearrange Eq. (9) as follows:

$$\begin{aligned} \mathbf{V}_s^T \mathbf{M}_s \mathbf{V}_s \ddot{\mathbf{q}}_s^* + \mathbf{V}_s^T \mathbf{K}_s \mathbf{V}_s \mathbf{q}_s^* &= \mathbf{V}_s^T \mathbf{f}_s \\ \mathbf{q}_s &= \mathbf{V}_s \mathbf{q}_s^* \end{aligned} \tag{10}$$

Using the reduction scheme exposed in Eq. (10), one ends working with a reduced system defined by the modal coordinates vector $\mathbf{q}_s^*$, where there are as many degrees of freedom as eigenmodes were included into the modal matrix $\mathbf{V}_s$. It corresponds to a pseudo-modal reduction, since only the eigenmodes which are relevant are included into the analysis. If only the first eigenmode is included, then a rigid pad model is established, and the corresponding modal coordinate measures the tilting of the pad around the pivot. The use of higher eigenmodes enables to include the flexibility of the pads and pivot into the results.

Regarding the thermal growth of the pads, once its temperature distribution is obtained by solving Eq. (5), it is possible to calculate the thermal growth and its impact on the oil film thickness. To do so, a thermal expansion rule is applied to calculate the deformation related to a certain increment in the pad material temperature, as shown in Eq. (11)

$$\epsilon = \alpha \Delta T \tag{11}$$

The thermal deformation as a result of the pad temperature field are calculated using Eq. (11) and imposed to the pad finite element model, on top of the pad pivoting motion and elastic deformations due to the pressure field loading. The thermal growth of the shaft is also calculated using Eq. (11).

2.4. Numerical implementation of the model

The finite element method is the method of choice for solving the partial differential equations corresponding to the Modified Reynolds Equation, Oil Film Energy Equation, Fourier Law for Heat Conduction and Pad Flexibility Model using pseudo modal reduction scheme. The implementation is based on the one used in [20,21]. The 'solid' domain (pads) is discretized using tridimensional second order twenty node serendipity finite elements. The 'fluid' domain (oil film) is discretized using bidimensional second order eight node quadrilateral elements, corresponding to one face of the 'solid' serendipity elements. Hence, the link between the two domains is straightforward. The usage of second order elements is justified by the need of describing the pad geometry, specially the pad curvature and geometry of the injection orifice, in an accurate way. To take advantage of the pad axial symmetry, only half of the pad in the axial direction is modelled.

The obtention of the weak form of the Modified Reynolds Equation, Fourier Law and Pad Flexibility equations is done using the Galerkin method. However, the usage of such method for the Oil Film Energy Equation induces numerical unstability on the solution, in the form of spurious oscillation on the obtained temperature values or 'wiggle'. This is a consequence of the inclusion of the oil injection and heat transfer terms in the Energy equation, which can be seen as the presence of a boundary condition in an upstream position, as well as the nature of the oil film flow, which exhibits a high Peclet number, in other words, strong dominance of convection effects over diffusion effects. To overcome this numerical unstability, the weak form of the Oil Film Energy equation is obtained using a streamline upwind Petrov–Galerkin formulation, as presented in [29]. Also, a finer discretization of the finite element mesh around the injection hole is established.

2.5. Calculation of the steady state equilibrium position

The calculation of the steady state equilibrium position of the tilting-pad journal bearing with controllable lubrication under certain operational conditions (namely, journal rotational speed, load and injection pressure) is performed using the scheme depicted as follows

1. Using the finite element model for the bearing pads, calculate the eigenmodes to be included in the pseudo modal reduction scheme.
2. Set an initial guess for the equilibrium position of the journal, as well as for the modal coordinates representing each one of the pads eigenmodes included in the calculation. Initialize the

oil film and bearing pads temperature field, setting it to be equal to the oil supply temperature. Calculate the initial viscosity for the oil film and the initial thermal growth of the bearing pads and journal.
3. Using the Newton Raphson method, iterate until static equilibrium is achieved, while keeping the oil viscosity constant in the process. The static equilibrium position will be defined by the journal position, as well as the modal coordinates representing the tilting angle and elastic deformation of the bearing pads and pivots.
4. Solve the oil film energy equation and Fourier law for heat conduction in the pads, considering the equilibrium position calculated in step 3. These equations are coupled by the heat transfer terms between oil film and pad surface, hence they must be solved simultaneously. As a result, the oil film and pads temperature fields, as well as the shaft temperature are calculated.
5. Update the oil film viscosity using the calculated oil film temperature field. Calculate the pad and journal thermal growth, using the calculated temperature for these elements.
6. Repeat steps 3–5 until convergence in the viscosity field is achieved. Then, the static and thermal equilibrium of the system has been achieved.

The boundary conditions established for the model are established as follows:

1. Modified Reynolds Equation: the pressure is set to be zero at the boundaries of the oil film domain. Also, the Gumbel condition is applied if cavitation is occurring.
2. Pad flexibility model: the nodes around the pivot of each pad are restricted to rotate around it, as explained thoroughly in [20].
3. Oil Film Energy Equation: the oil film temperature at the leading edge of each pad is assumed to be constant in the axial direction, and it is set to be equal to the experimentally measured value. The shaft temperature is also assumed constant and it can be calculated as the average of the oil film temperature or set to be equal to the experimentally obtained value. At the interface between oil film and pad, the heat flux is prescribed as discussed previously in Section 2.2.
4. Fourier Law for heat conduction: a free convection boundary condition is applied in the pad surfaces not related to the load carrying capacity. The heat flux continuity condition is applied in the face in contact with the oil film, following the analysis presented in Section 2.2.

3. Experimental setup

The test rig, which is shown in (Fig. 2), consists of a test bearing and a rigid rotor supported by a tilting frame. The rotor is driven by a belt transmission connected to an electric motor. The electric motor is equipped with a frequency converter and speed control. The fixed dimensions for the test rig are stated in Table 1.

The test bearing consists of two tilting pads located above and below of the rotor, which support it in the vertical direction. The rotor is prevented from movement in the horizontal direction, due to the frame in which the rotor is mounted. Since the frame is allowed to tilt around its pivoting point, a single degree of freedom is required to describe the position of the rotor, related to its vertical displacement. This can be measured by means of a displacement sensor. Also, it is possible to fix the vertical position of the rotor using an adjustment screw located at the frame free end, and to measure the resulting forces over it, using a load cell associated with the adjustment screw.

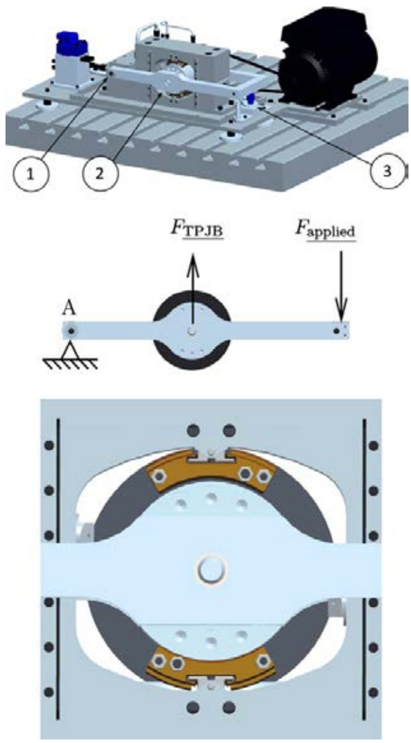

Fig. 2. Test rig for the tilting-pad bearing with controllable lubrication; the arrangement consists of a test bearing with two tilting-pads and a rigid rotor (2), supported by a tilting frame pivoted in one end (1). The frame free end can be used to apply load over the bearing, or to fix the rotor vertical position using an adjustment screw (3).

Table 1
Dimensions, oil properties and parameters used for modeling the test rig bearing.

Pad inner radius	49.923	mm
Journal radius	49.692	mm
Bearing axial length	100	mm
Assembly radial clearance	0.140	mm
Preload	0.39	–
Number of pads	2	–
Pad arc	69	deg.
Offset	0.5	–
Load angle	On pad	-
Pad thickness	12	mm
Injection nozzle radius	3	mm
Injection nozzle length	10	mm
Oil viscosity at 40 °C	0.01892	Pa s
Oil viscosity at 100 °C	0.004	Pa s
Oil specific heat	1900	J/(kg K)
Oil thermal conductivity	0.13	W / (m K)
Free convection coefficient	100	W/(m^2 K)
Pad material thermal conductivity	109	W/(m K)
Pad material Young Modulus	100	GPa
Pad material Poisson ratio	0.3	–
Pad material density	8400	kg/m^3

The bearing case is divided in a top and a bottom half, with a tilting pad resting on each one of them through a rocker pivot. Calibrated separation plates are installed between these two halves, enabling to control the clearance and resulting preload on the test bearing. The bearing case was designed with an open configuration. This design does not retain the lubricant from escaping the bearing after it has passed through the bearing

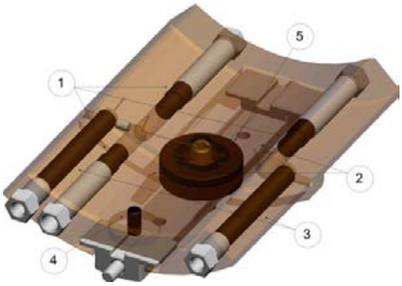

Fig. 3. Tilting pad installed in the test rig, and the position for the different sensors installed on it; numbers 1–3 show the position of the thermocouples, number 4 show the position for displacement sensor (not installed), and number 5 show the location of the load cell and high pressure injection nozzle.

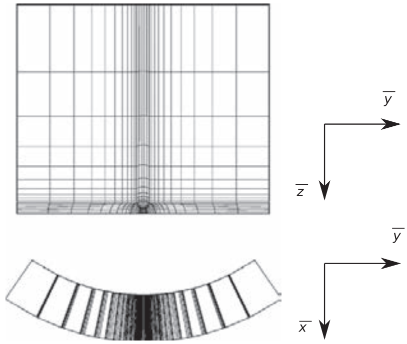

Fig. 4. The finite element mesh used for modeling the bearing pads.

gap. Since such design does not allow generating an oil bath between pads, sprinklers are used to supply the low-pressure oil to the pads leading edges, entailing a reduced effect of hot lubricant carryover from one pad to the next one.

A closer view of the tilting pad and its instrumentation can be seen in Fig. 3. They are instrumented using thermocouples, which are mounted according to [30], and a force transducer in the back of the pad, enabling to measure the resulting forces in the radial direction over the pad. The most important component within the tilting pads design is the nozzle, through which high pressure lubricant can be injected into the gap between the tilting pad and the rotor, rendering the bearing controllable. The oil flow towards the nozzle in each tilting pad is controlled by means of a single servo valve, which is connected to a high pressure oil supply pump. Among the parameters that are feasible to be modified within the test rig are: load, preload, rotational speed, pad and pivot geometry. Among the parameters that are feasible to be measured within the test rig are:oil film temperature distribution, using thermocouples located in the pads; resulting forces over the pads in the radial direction, using force transducers installed in the back of the pad; resulting forces over the rotor, using load cell and adjustment screw mounted at the end of the rotor frame; rotor position, using displacement sensor.

4. Comparison between theoretical and experimental results

In this section, the validity of the available model for the tilting-pad journal bearing with controllable lubrication is verified by comparing its results against the experimental data obtained using the test rig depicted in the previous section. The study is restricted to static and thermal properties of the bearing.

Regarding the experimental setup, three different configurations were employed:

1. *Configuration* 1 (*Single pad*, *rotor free*): in this case, only the bottom pad is installed in the test rig, and it is instrumented using thermocouples. This configuration is aimed at obtaining data regarding the oil film temperature distribution, in order to validate the thermal model for the bearing.
2. *Configuration* 2 (*Two pads*, *rotor fixed*): both pads are installed, and the rotor is fixed into a certain position, using the screw and load cell installed at the end of the rotor arm. The objective of this test is to measure the resulting forces over rotor and pads for a certain rotor position, depending on the imposed operational conditions. By comparing these results with the ones coming from the model, its accuracy for predicting the oil film resultant forces is to be tested.
3. *Configuration* 3 (*Two pads*, *rotor free*): both pads are installed, while the rotor arm is not constrained. Hence, the rotor should converge to a certain equilibrium position depending on the imposed operational conditions. The comparison of these experimental results with the theoretical ones provides insight on the capability of the model to predict the equilibrium position of the system.

Regarding the modeling of the tested bearing, the finite element mesh used for modeling the bearing pads is depicted in Fig. 4. Only half of the pad in the axial direction is modeled, taking advantage of the pad symmetry. The mesh contains 450 second order serendipity elements, distributed so that a finer discretization is obtained in the vicinity of the injection hole. The number of elements was chosen so that a compromise between calculation speed and accuracy is obtained. To ensure this, a convergence test was performed. The relative error for the relevant magnitudes (pressure and temperature fields) obtained using this mesh was below 0.1%, when compared to the results achieved using a much finer discretization (1600 elements), hence it was considered suitable for the analysis to be performed. The boundary conditions correspond to the ones presented in Section 2.5. Regarding the pad and pivot flexibility model, three eigenmodes for each pad are included for the pseudo modal reduction scheme, namely: pad rigid-body tilting motion mode, pad first bending mode, and pad rigid-body radial translation mode, corresponding to the pivot flexibility effect. The omission of other pad bending modes is justified by the results presented in [25], where convergent behavior was observed when including higher bending modes. Regarding the pivot stiffness, it was obtained by means of a direct mechanical test performed on the test rig. A value of $2 \times 10^7 (\mathrm{N/m})$ was obtained.

Uncertainty analysis is applied to both experimental and theoretical results, following the guidelines given in [31]. For the experimental results, the reported uncertainty interval is related to random error, and it is calculated using multisample analysis with a 95% confidence range. The uncertainty on the theoretical results is related to the effect of the geometrical tolerances in the test rig, calculated using root-sum-square method. Since such tolerances do not have a significant effect on the obtained temperature results, the uncertainty related to those theoretical results is not reported.

4.1. Results for Configuration 1: validation of the thermal model

The relevance of including the thermal effects within the modeling of the tilting-pad journal bearing is well established by the literature on the subject. In order to predict accurately both the static and dynamic properties of the bearing, it is necessary to take into account the oil viscosity change due to the temperature build-up, as well as the thermal growth of bearing pads and journal. The model presented in this work has already been validated against experimental results regarding temperature distribution in "passive" tilting-pad bearings

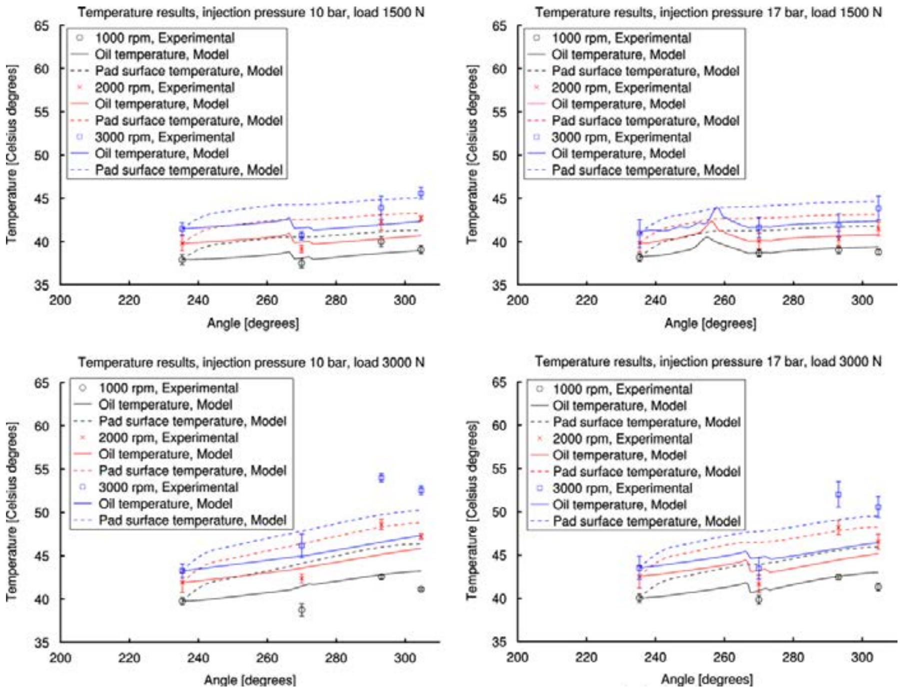

Fig. 5. Oil temperature distribution, comparison between theoretical and experimental results for different applied loads and rotational speeds; injection system turned on.

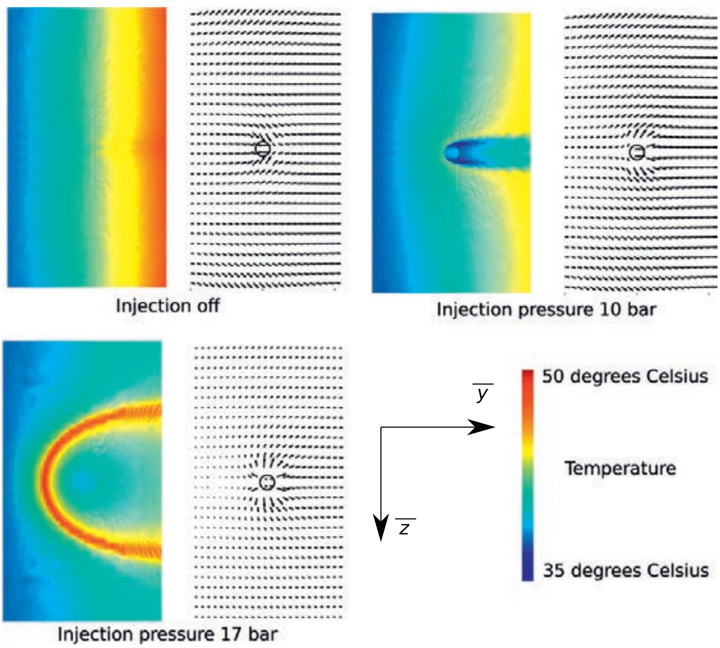

Fig. 6. Theoretical oil temperature distribution and flowlines, comparison between the injection off case, and the injection on case, with two different values for the injection pressure.

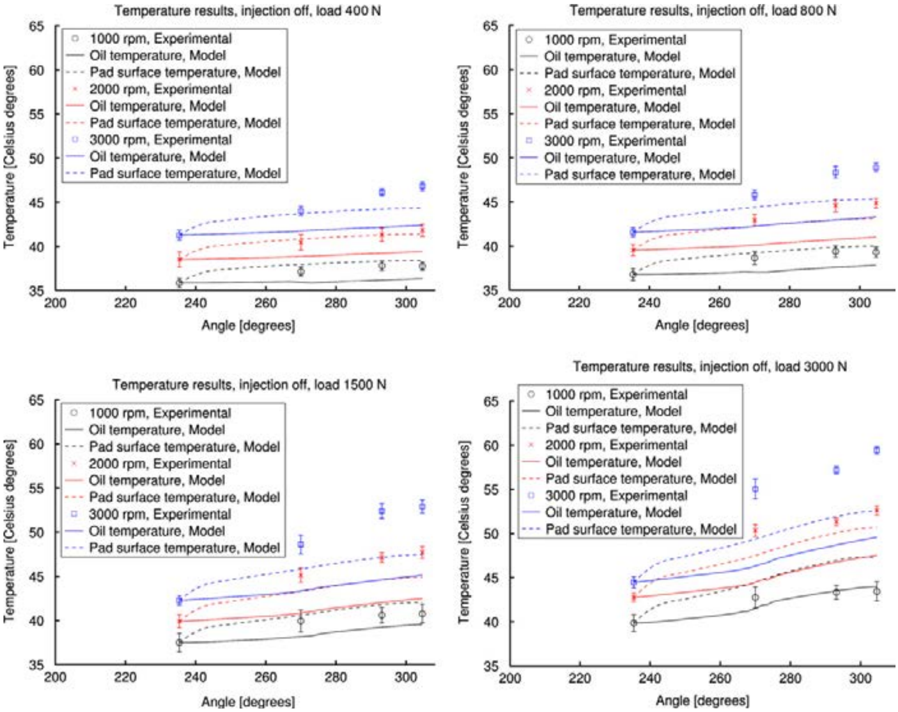

Fig. 7. Oil temperature distribution, comparison between theoretical and experimental results; injection system turned off.

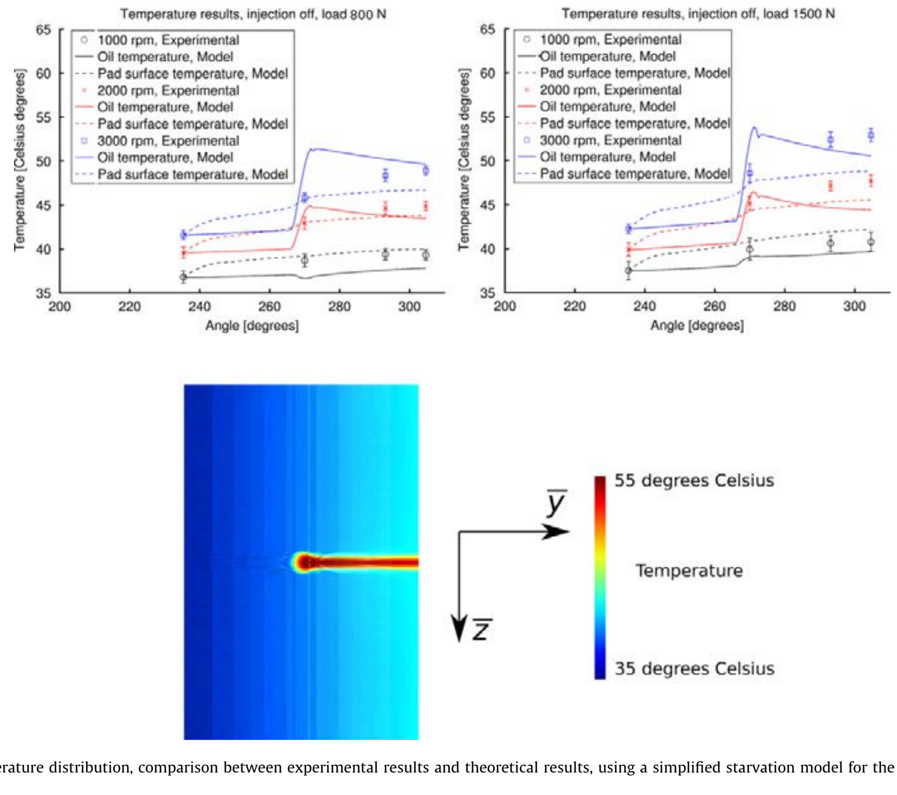

Fig. 8. Oil temperature distribution, comparison between experimental results and theoretical results, using a simplified starvation model for the injection off case.

(without injection holes) [22,23]. Hence, the question to be asked at this point is whether it also provides a good representation of the perturbation introduced within the oil film temperature field by the presence of the high pressure injection hole. To answer such question, Configuration 1 was established within the test rig, in order to obtain experimental results regarding the oil film temperature distribution. Since the oil supply at the leading edge of the pads in the test rig is provided using sprinklers, there is not an oil bath between the two pads. Hence, the oil temperature on the pad leading edge cannot be calculated using an energy and mass balance in the space between pads, as it is the usual practice for tilting-pad bearings. Consequently, the oil film leading edge temperature is set to be equal to the experimentally measured one when obtaining the theoretical results. An experimental value of the shaft surface temperature obtained using a laser temperature sensor is also applied to the model, since this result is considered to be more accurate than the usual estimation using the average of the oil film temperature.

The theoretical results reported include the oil film temperature and pad surface temperature, calculated by the coupled solution of Eqs. (3) and (5). The parameters modified included the value for the injection pressure, the load applied over the bearing, and the journal rotational speed. When comparing experimental and theoretical results, one must be aware that the oil film temperature as delivered by the model corresponds to an average value in the radial direction, whereas in practice the experimentally measured temperature value corresponds to an average oil temperature in the radial direction, due to the mixing effect taking place inside the measurement capilar hole where the thermocuple is mounted. Hence, a good correlation between theory and experiment is achieved when the experimental value lies closer to the theoretical oil temperature than to the pad

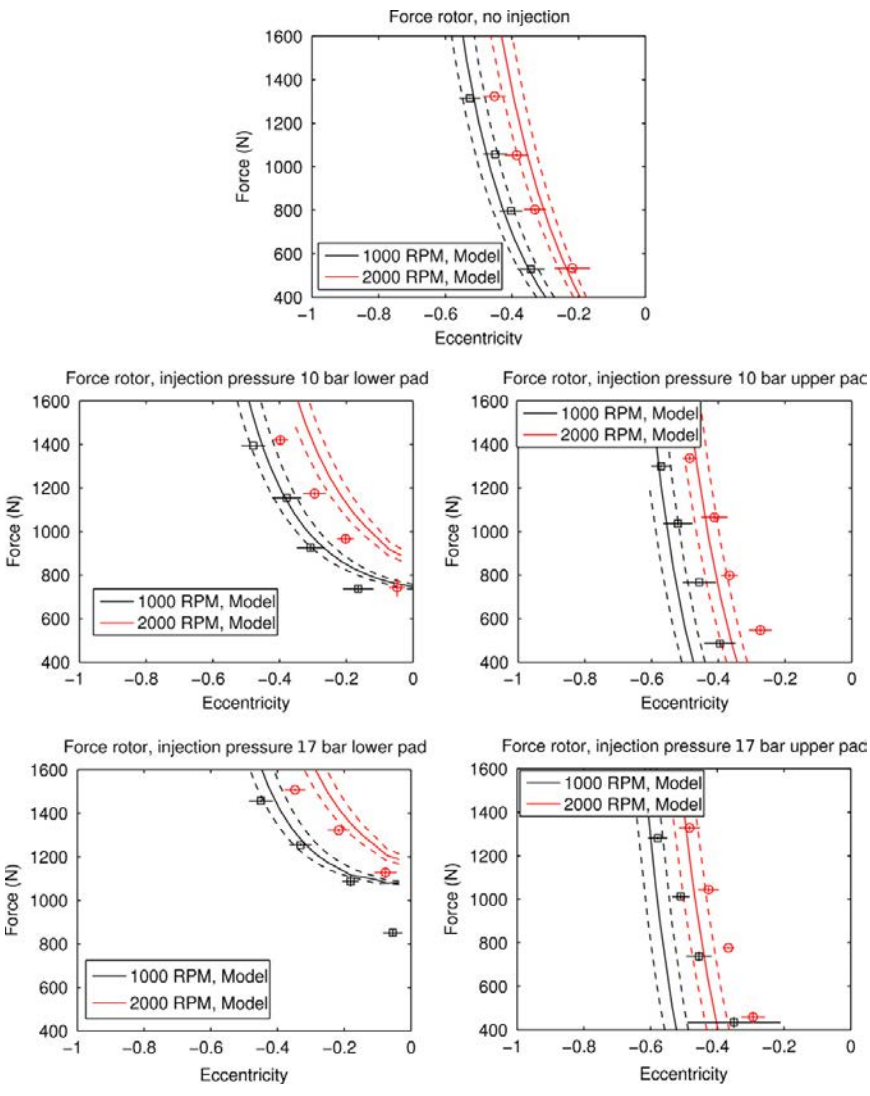

Fig. 9. Resultant vertical force over rotor versus rotor eccentricity, comparison between experimental and theoretical results for different operational conditions.

surface temperature. Fig. 5 depicts the comparison between theoretical and experimental results regarding temperature distribution when the injection system is turned on. These results must be analyzed in terms of the actual flow of injected oil coming into the bearing clearance. The injection process was included within the oil film energy equation mainly using a convective term representing the heat transport of the injected oil when coming into the bearing clearance. Such convection effect is evidently proportional to the injected oil mass flow entering the clearance, hence when it is dominant enough within the bearing, very good coherence is achieved between theory and experiment.

The injected oil mass flow coming into the clearance is a function of the difference between the injection pressure and the hydrodynamic pressure developed in bearing clearance. Hence, better agreement between theory and experiment is observed for those operational conditions where such difference is maximized, namely: higher injection pressure, lower journal applied load, lower rotational speed. When analyzing the axial distribution of the oil film temperature as depicted in Fig. 6, it can be observed that the effect of the injection system is to generate a stream of cool oil from the injection hole to the pad trailing edge. Also, it can be noted that a region of higher temperature is generated in a position upstream from the injection hole. The severity of the temperature rise in this zone, as well as its position are a function of the injection pressure. This result can be explained by taking a look at the flowlines shown in Fig. 6. It can be seen that oil film velocity field gets significantly affected around the injection hole when turning on the injection system. When looking in the area upstream from the injection hole, it can be seen that the direction of the flow in circumferential direction is even reverted for an injection pressure of 17 bar. Such reversion of the oil flow entails higher viscous forces acting within the fluid, which explains the observed upstream local heating.

It is also important to analyze the accuracy of the available thermal model when predicting the oil film temperature field at the moment that the injection system is turned off. Fig. 7 depicts the comparison between experimental and theoretical results for such operational condition. In general, the theoretical results underestimate the oil temperature downstream from the injection hole, and such underestimation is more pronounced for higher rotational speeds and higher applied journal load. These results call for an analysis of the model. The modeling approach used for obtaining both the Reynolds Equation for the pressure field and the oil film energy equation for temperature field assumes that there is a continuous oil film layer all over the surface of the pad. Also, the thermal model is posed so that the effect of an oil stream entering the clearance through the injection hole is considered. Such conditions are respected when the injection system is on, but they do not necessarily hold when the injection system is turned off. An important amount of oil exits the bearing clearance through the injection hole, due to the pressure build up in the clearance. Such “sink” effect can be observed by taking a look at the flowlines pointing towards the injection hole for the injection off case, as depicted in Fig. 6. As a consequence of this, oil starvation can take place in the zone located downstream from the injection hole, resulting in higher oil temperature, due to the reduction in the convection effect responsible for carrying heat away from the bearing clearance.

Modeling this local starvation effect seems like a difficult task. A very simple approach is proposed, whose results are depicted in Fig. 8. A reduction of the oil film density is established for those elements located in the injection hole area. Since the thermal model only includes the circumferential and axial direction, such reduction in the oil density is aimed at modeling the oil flow exiting the clearance through the injection hole. In the zone located downstream from the injection hole, no density reduction was imposed, considering that the oil film is reformed in that area, as the flowlines from the injection off case in Fig. 6 suggest. The results from this simplified approach deliver better agreement with the experimental data, as shown in Fig. 8. However, as shown in the axial temperature distribution depicted in Fig. 8

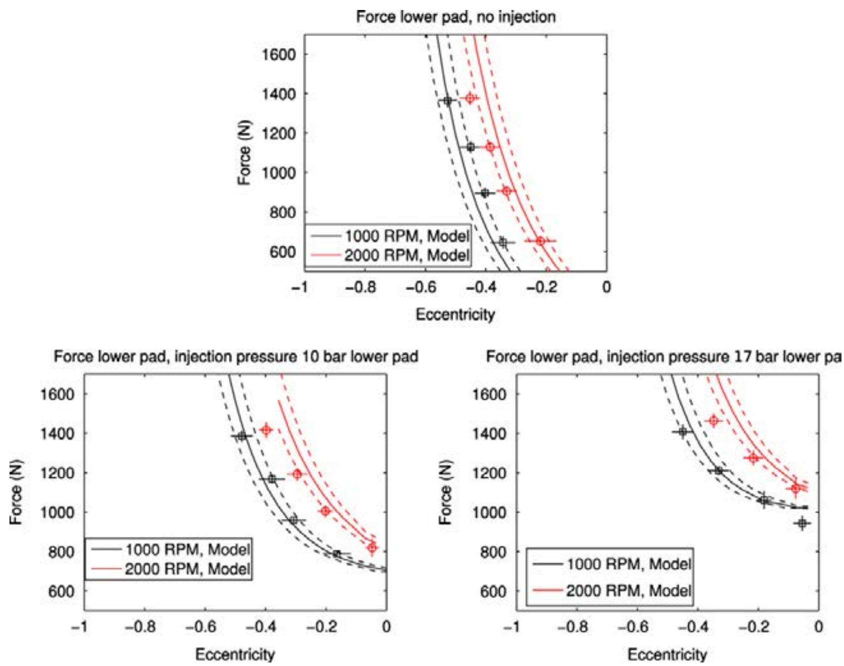

Fig. 10. Resultant radial force over lower pad versus rotor eccentricity, comparison between experimental and theoretical results for different operational conditions.

only the area downstream from the injection hole is affected by this starvation effect. Putting this result in context, the idea of obtaining an accurate thermal model is to be able to model the oil film viscosity reduction, resulting in an accurate prediction of the bearing equilibrium position. Hence, the question arises whether this localized downstream heating has relevant effects on the equilibrium position prediction. Such question is analyzed in the following sections.

4.2. Results for configuration 2: resultant forces over bearing pads and rotor

The test rig used during this investigation enables to impose a certain eccentricity over the rotor, fixing it in a certain position, in order to measure simultaneously the forces over rotor and pads originated by the pressure build-up taking place within the oil film. The results depicted in Figs. 9 and 10 correspond to the experimentally measured forces compared to the theoretical results. The theoretical results marked with full line correspond to the ones obtained using nominal geometry, whereas the dashed line indicates the uncertainty in the results coming from geometrical tolerances in the test rig.

In general, good agreement is observed between theory and experiment, regarding the prediction of resulting oil film forces. The discrepancies seem to be higher when increasing the rotational speed of the journal and when the oil injection takes place in the upper pad. The same injection pressure value was set in both injection holes when running the simulations, which is not necessarily true, due to the different geometry of the lines connecting the injection holes with the servovalve regulating the flow direction. Also, the position of the displacement sensor could explain this discrepancy. Since it was located on top of the upper half of the bearing case for this test, the results would be sensitive to the resulting radial load over the upper pad, and the resulting elastic deformation of the case. When injecting oil from the upper pad or when decreasing the rotor eccentricity, the resulting oil film forces over the upper pad increases, hence the chances of perturbing the results by introducing a relative movement between the upper case and the rotor also increase.

4.3. Results for configuration 3: equilibrium position of the rotor

The final set of experimental results deal with the verification of the accuracy of the model for predicting the equilibrium position of the system. Obtaining good results on this regard is fundamental for an accurate estimation of the dynamic coefficients of the bearing. According to Brockwell [11], among other authors, when performing an experimental identification of dynamic coefficients for the tilting-pad journal bearing, the amplitude of the rotor movement should be kept within 20% of the radial clearance, in order to comply with the requirement of keeping the oil film forces behaving as linearly as possible. Thus, this value would also give a good estimate of the allowable error when determining the rotor eccentricity using the available ETHD model.

Fig. 11 and Table 3 depict the comparison between theoretical and experimental results, regarding the rotor eccentricity obtained when different operational conditions are imposed in the test rig, as detailed in Table 2. The theoretical results represent in a good way the physical behavior of the system studied, as they can predict the change of the rotor position when imposing different conditions for the injection system. It becomes clear that the model exhibits better agreement for the cases where injection is taking place, when compared to the cases where the injection system is turned off. When looking into the magnitude of the difference between theoretical and experimental results, the maximum error corresponds to 27% of the radial clearance, obtained when the injection system is turned off at 3000 RPM. For the cases where the injection system is working, the error is kept lower or equal than 20% of the radial clearance.

5. Conclusion

In this work, the analysis of the accuracy of the model for the tilting-pad journal bearing with controllable lubrication under

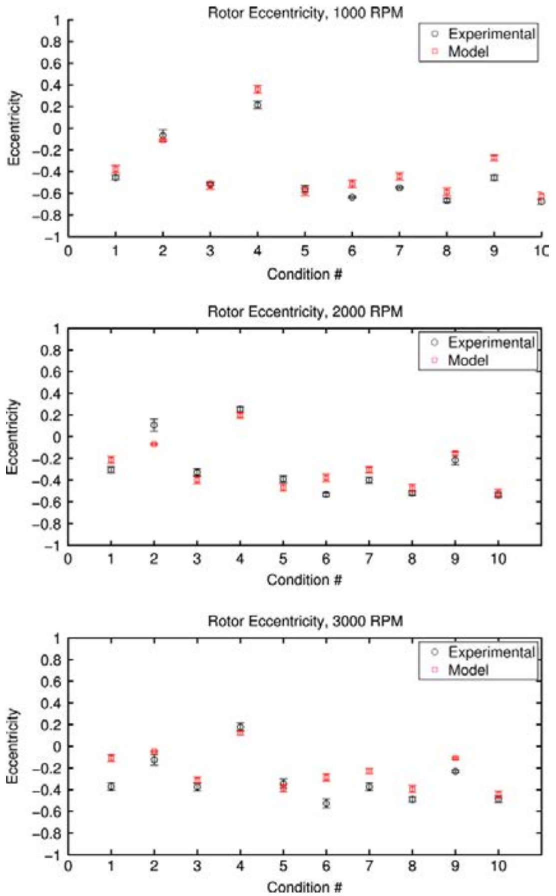

Fig. 11. Rotor eccentricity, comparison between experimental and theoretical results for different operational conditions.

Table 2
Operational conditions for the results shown in Fig. 11.

Condition	Load (N)	Injection status	Injection pressure
1	800	Off	–
2	800	On	10 bar lower pad
3	800	On	10 bar upper pad
4	800	On	17 bar lower pad
5	800	On	17 bar upper pad
6	1500	Off	–
7	1500	On	10 bar lower pad
8	1500	On	10 bar upper pad
9	1500	On	17 bar lower pad
10	1500	On	17 bar upper pad

Table 3
Summary of the eccentricity results depicted in Fig. 11.

Condition	Ecc. theory 1000 RPM	Ecc. exp. 1000 RPM	Error (% radial clearance)
1	−0.46	−0.38	8
2	−0.07	−0.11	4
3	−0.52	−0.52	0
4	0.21	0.36	15
5	−0.58	−0.59	1
6	−0.64	−0.51	13
7	−0.55	−0.45	10
8	−0.67	−0.59	8
9	−0.46	−0.27	19
10	−0.68	−0.63	5
Condition	Ecc. theory 2000 RPM	Ecc. exp. 2000 RPM	Error (% radial clearance)
1	−0.30	−0.21	9
2	0.11	−0.07	18
3	−0.33	−0.40	7
4	0.25	0.20	5
5	−0.39	−0.47	8
6	−0.53	−0.38	15
7	−0.40	−0.30	10
8	−0.52	−0.47	5
9	−0.21	−0.15	6
10	−0.54	−0.52	2
Condition	Ecc. theory 3000 RPM	Ecc. exp. 3000 RPM	Error (% radial clearance)
1	−0.37	−0.10	27
2	−0.12	−0.05	7
3	−0.37	−0.31	6
4	0.18	0.12	6
5	−0.34	−0.39	5
6	−0.53	−0.28	25
7	−0.37	−0.22	15
8	−0.49	−0.39	10
9	−0.23	−0.11	12
10	−0.49	−0.45	4

steady-state conditions was performed. Such analysis was carried out by direct comparison with the experimental results obtained using a test rig designed to this purpose. As a result of this work, it can be stated that:

1. The ETHD model for the tilting-pad bearing with controllable lubrication provides sufficient accuracy for predicting the static and thermal behavior of the bearing under steady state conditions. The comparison with the experimental results shows good agreement regarding oil film temperature field, resulting forces over rotor and pads and equilibrium position of the system. Furthermore, the experimental results show the possibility of modifying the rotor equilibrium position using the controllable lubrication system. This entails implicitly the feasibility of modifying the dynamic properties of the bearing, namely stiffness and damping, using this system. Such investigation is currently being carried out.
2. As a result of the analysis performed, it becomes clear that there is room for improvement when it comes to model the tilting-pad bearing with controllable lubrication operating with the injection system turned off. Since the modeling approach used for including the oil injection effects always considers a pressurized oil flow coming into the bearing clearance, it is reasonable that the model exhibits poorer performance when used for a condition that it is not fully considered in its formulation.
3. The accuracy of the ETHD model for predicting the oil film forces and the equilibrium position of the rotor provides a solid foundation to start working in the experimental validation of the dynamic model for the tilting-pad bearing with controllable lubrication.

References

[1] Ettles C. The analysis and performance of pivoted pad journal bearings considering thermal and elastic effects. Journal of Lubrication Technology, ASME Transactions 1980;102(2):182–94.
[2] Ettles C. The analysis of pivoted pad journal bearing assemblies considering thermoelastic deformation and heat transfer effects. STLE Tribology Transactions 1992;35(1):156–62.
[3] Brockwell K, Dmochowski W. Thermal effects in the tilting pad journal bearing. Journal of Physics DApplied Physics. 1992;25:384–92.
[4] Fillon M, Bligoud JC, Frêne J. Influence of bearing element displacements on thermohydrodynamic characteristics of tilting-pad journal bearings. In: Proceedings of the Japan international tribology conference, Nagoya; 1990. p. 635–40.
[5] Fillon M, Bligoud JC, Frêne J. Experimental study of tilting-pad journal bearings—comparison with theoretical thermoelastohydrodynamic results. ASME Journal of Tribology 1992;114:579–88.
[6] Kim J, Palazzolo A, Gadangi R. TEHD analysis for tilting pad journal bearings using upwind finite element method. Tribology Transactions 1994;37(4): 771–83.
[7] Kim J, Palazzolo A, Gadangi R. Dynamics characteristics of TEHD tilt pad journal bearing simulation including multiple mode pad flexibility. ASME Journal of Vibration and Acoustics 1995;117(1):123–35.
[8] Brockwell K, Kleinbub D. Measurements of the steady state operating characteristics of the five shoe tilting pad journal bearing. STLE Tribology Transactions 1989;32(2):267–75.
[9] Taniguchi S, Makino T, Takeshita T, Ichimura T. A thermohydrodynamic analysis of large tilting-pad journal bearing in laminar and turbulent flow regimes with mixing. Journal of Tribology, ASME Transactions 1990;112: 542–50.
[10] Bouchoule C, Fillon M, Nicolas D, Barresi F. Experimental study of thermal effects in tilting-pad journal bearings at high operating speeds. ASME Journal of Tribology 1996;118:532–8.
[11] Brockwell K, Kleinbub D, Dmochowski W. Measurement and calculation of the dynamic operating characteristics of the five shoe tilting-pad journal bearing. STLE Tribology Transactions 1989;33(4):481–92.
[12] Dmochowski W. Dynamic properties of tilting-pad journal bearings: experimental and theoretical investigation of frequency effects due to pivot flexibilityASME Journal of Engineering for Gas Turbines and Power 2007;129: 865–9.
[13] Wygant D, Flack R, Barrett L. Measured performance of tilting-pad journal bearings over a range of preloads - Part II: dynamic operating conditionsSTLE Tribology Transactions 2004;47:585–93.
[14] Ha H, Yang S. Excitation frequency effects on the stiffness and damping coefficients of a five pad tilting pad journal bearing. ASME Journal of Tribology 1999;121(3):517–22.
[15] Childs D, Carter C. Rotordynamics characteristics of a five pad, Rocker-Pivot, tilting pad bearing in a load-on-pad configuration: comparisons to predictions and load-between-pad results. ASME Journal of Engineering for Gas Turbines and Power 2011;133.
[16] Santos IF. Design and evaluation of two types of active tilting pad journal bearings. In: Burrows CR, Keogh PS, editors. The active control of vibration. London, England: Mechanical Engineering Publications Limited; 1994. p. 79–87.
[17] Santos IF, Russo F. Tilting-pad journal bearings with electronic radial oil injection. Journal of Tribology, ASME Transactions 1998;120(3):583–94.
[18] Santos IF, Nicoletti R. THD analysis in tilting-pad journal bearings using multiple orifice hybrid lubrication. Journal of Tribology, ASME Transactions 1999;121:892–900.
[19] Santos IF, Nicoletti R. Influence of orifice distribution on the thermal and static properties of hybridly lubricated bearings. International Journal of Solids and Structures 2001;38:2069–81.
[20] Haugaard AM, Santos IF. Multi-orifice active tilting-pad journal bearings-harnessing of synergetic coupling effects. Tribology International 2010;43(8): 1374–91.
[21] Haugaard AM, Santos IF. Stability of multi orifice active tilting-pad journal bearings. Tribology International 2010;43(9):1742–50.
[22] Cerda A, Santos IF. Performance improvement of tilting-pad journal bearings by means of controllable lubrication. Mechanics & Industry 2012;13:17–32.
[23] Cerda A, Fillon M, Santos IF. On the simplifications for the thermal modeling of tilting–pad journal bearings under thermoelastohydrodynamic regime. In: Proceedings of the ASME Turbo Expo 2012, GT2012-68329. Presented at: ASME Turbo Expo 2012, Copenhagen; 2012.
[24] Knight J, Barrett L. Analysis of tilting pad journal bearings with heat transfer effects. ASME Journal of Tribology 1988;110:128–33.
[25] Cerda A, Santos IF. Stability analysis of an industrial gas compressor supported by tilting-pad journal bearings under different lubrication regimes. Journal of Engineering for Gas Turbines and Power, ASME Transactions 2012;134(2).

[26] Santos IF. Theoretical and experimental identification on the stiffness and damping coefficients of active-tilting pad journal bearings. In: Friswell M, Mottershead J, editors. Identification in engineering systems. Swansea, Great Britain: The Cromwell Press Ltd.; 1996. p. 325–34.
[27] Santos IF, Scalabrin A. Control system design for active lubrication with theoretical and experimental examples. Journal of Engineering for Gas Turbines and Power, ASME Transactions 2003;125:75–80.
[28] Nicoletti R, Santos I. Frequency response analysis of an actively lubricated rotor/tilting-pad bearing system. ASME Journal of Engineering for Gas Turbines and Power 2005;127:638–45.
[29] Brooks A, Hughes T. Streamline upwind/Petrov–Galerkin formulations for convection dominated flows with particular emphasis on the incompressible Navier–Stokes equation. Computer Methods in Applied Mechanics and Engineering 1982;32:199–259.
[30] Glavatskih SB. A method of temperature monitoring in fluid film bearings. Tribology International 2004;37:143–8.
[31] Moffat R. Describing the uncertainties in experimental results. Experimental Thermal and Fluid Science 1988;1:3–17.

5.5 Publication 5: Actively Lubricated Bearings Applied as Calibrated Shakers to Aid Parameter Identification in Rotordynamics

Proceedings of ASME Turbo Expo 2013
TE2013
June 3-7, 2013, San Antonio, Texas, USA

GT2013-95674

ACTIVELY LUBRICATED BEARINGS APPLIED AS CALIBRATED SHAKERS TO AID PARAMETER IDENTIFICATION IN ROTORDYNAMICS

Ilmar Ferreira Santos*

Department of Mechanical Engineering
Technical University of Denmark
2800 Kgs. Lyngby, Denmark
Email: ifs@mek.dtu.dk

Alejandro Cerda Varela

Department of Mechanical Engineering
Technical University of Denmark
2800 Kgs. Lyngby, Denmark
Email: acer@mek.dtu.dk

ABSTRACT

The servo valve input signal and the radial injection pressure are the two main parameters responsible for dynamically modifying the journal oil film pressure and generating active fluid film forces in controllable fluid film bearings. Such fluid film forces, resulting from a strong coupling between hydrodynamic, hydrostatic and controllable lubrication regimes, can be used either to control or to excite rotor lateral vibrations. An accurate characterization of the active oil film forces is of fundamental importance to elucidate the feasibility of applying the active lubrication as non-invasive perturbation forces, or in other words, as a "calibrated shaker", to perform in-situ rotordynamic tests. The main original contributions of this paper are three: a) the experimental characterization of the active fluid film forces generated in an actively-lubricated tilting-pad journal bearing in the frequency domain and the application of such a controllable bearing as a calibrated shaker aiming at determining the frequency response function (FRF) of rotordynamic systems; b) experimental quantification of the influence of the supply pressure and servo valve input signal on the FRF of rotor-journal bearing systems; c) experimental indication of how small such active fluid film forces (perturbation forces) should be, in order to perturb the rotor-journal bearing system without significantly changing its dynamic characteristics. To validate the experimental procedure and results obtained via actively-lubricated bearing, similar experimental tests are carried out using an electromagnetic shaker. Very good agreements between the two experimental approaches are found. Maximum values of the main input parameters, namely servo valve voltage and radial injection pressure, are experimentally identified/suggested with the objective of obtaining non-invasive perturbation forces.

NOMENCLATURE

ALB Actively Lubricated Bearing
$C(f)$ ALB active force calibration function
$F(f)$ Force function
FRF Frequency response function
$H(f)$ Frequency response function
$X(f)$ Displacement function

INTRODUCTION

For several decades, bearings were seen as basic mechanical parts mostly used as the building blocks in the design of machines. Bearings were standarized to common sizes. In special applications, considering loads and relative velocity among components, such elements have to be redesigned and optimized to satisfy predefined design requirements. During the last decades, we have faced a rapid and fascinating development of electronics, followed by a miniaturization and integration of circuit components such as resistors, capacitors and transistors. Such a development of electronic components, as sensors and actuators, for example, has also been supported by multidisciplinary optimization techniques, exploring chemical, piezoelectric and magnetic

*Address all correspondence to this author.

properties of materials, among others. This development has led to more reliable and cheaper sensors and actuators, which are nowadays integrated into many different mechanical systems to yield mechatronic products, allowing for monitoring and controlling system conditions. Thus, the integration of bearings (Mechanics) with sensors and actuators (Electronics) controlled via computers and dedicated software (Informatics) enables the development of new smart bearings, able to deal with multi-objective functions and capability of self-adjustments, depending on operation conditions, i.e. loading and relative velocity among components. The synergy among different areas of mechanics, electronics, control techniques and informatics enables significant improvements and balancing of various contradictory properties, associated to one or several interactive machine components. Moreover, the integration of bearings, electronics and control (Mechatronics) add a new dimension to the problem of optimization of system performance and open new possibilities of innovation in machine element design.

A modern vision of bearings should also incorporate electronics and software, i.e. bearings should be seen as basic mechanical, electrical and software parts to be used as the building blocks in the design of machines. In this vision, the optimization of system performance can occur, for example, by simply optimizing feedback gains of controllers, easily implementable in practice by means of software. The mechatronic structure of the machine, the built-in control, its sensors, processors, actuators, and above all, its software, will enable these novel features. This is a way to design and optimize machines and bearings with higher performance, less maintenance costs, longer lifetime, and an enhanced customer attraction.

One representative of this modern vision is the active magnetic bearing [1], used as smart machine element to control vibrations and aid rotordynamic tests [2–8] among other multi-objective functions. In the same framework actively-lubricated bearings [9] and externally-pressurized bearings [10, 11] have a much shorter history and are still under research and development phases. They have been extensively investigated during the last two decades, theoretically as well as experimentally. Most of the results presented are focused on vibration control [9–11], enhancing of bearing damping properties [12], stability of rigid [13] and flexible rotor lateral dynamics [14, 15], and finally compensation of thermal effects [16–18].

Journal bearings operating under active lubrication regime (ALB) are controlled by servo valves and well-tuned feedback control laws. The servo valve input signal and the supply pressure are the two main parameters responsible for the dynamic modification of the journal pressure distribution, generating active fluid film forces. Such active fluid film forces can be used either to control or to excite rotor lateral vibrations. An accurate characterization of the active oil film forces is of fundamental importance. Such a characterization aids the development of accurate mathematical models and allows the optimization and the improvement of bearing design under critical operational conditions. Moreover, such a characterization elucidates the feasibility of using the active lubrication as a "calibrated shaker", which would be extremely useful towards "in-situ" rotordynamic testing, identification of machine parameters and aid fault diagnose procedures in the near future. The idea of using controllable fluid film bearings as a calibrated shaker has been mentioned in [19] but not yet fully exploited. In this special context the main original contributions of this work are: a) the experimental characterization of the active fluid film forces generated in an actively-lubricated tilting-pad journal bearing in the frequency domain and the application of the ALB as a calibrated shaker aiming at determining the frequency response function (FRF) of a rotordynamic system; b) experimental quantification of the influence of the supply pressure and servo valve input signal on the FRF of rotor-journal bearing systems; c) experimental indication of how small such active fluid film forces (perturbation forces) might be, in order to perturb the rotor-journal bearing system without significantly chancing its dynamic characteristic. The experimental analyzes are carried out by using a special test rig, designed to investigate the behaviour of tilting-pad bearings under actively-controlled lubrication. In order to validate the experimental procedure and results obtained via actively-lubricated bearing, similar tests are carried out using an electromagnetic shaker coupled to a force transducer. Very good agreements between the two experimental approaches are found. The maximum values of the two main input parameter, namely servo valve voltage and injection pressure, are experimentally found and suggested, having the focus on building non-invasive perturbation forces. With non-invasive forces we have in mind small perturbation forces built by the controllable radial oil injection which do not significantly alter the fluid film dynamics, i.e. the stiffness and damping properties of the film, but still perceptible and measurable, allowing for measurements of frequency response functions with high values of coherence.

PRESENTATION OF THE EXPERIMENTAL SETUP

The ALB Test Rig

The Actively Lubricated Bearing (ALB) test rig, which is shown in Fig.1, consists of a test bearing and a rigid rotor supported by a tilting frame. The rotor is driven by a belt transmission connected to an electric motor. The electric motor is equipped with a frequency converter and speed control. The fixed dimensions for the test rig are stated in Table 1.

The bearing case is divided in a top and a bottom half, with a tilting pad resting on each one of them through a rocker pivot. Calibrated separation plates are installed between these two halves, enabling to control the clearance and resulting preload on the test bearing. The test bearing itself consists of two tilting pads located above and below the rotor, which support it in the vertical direction. The rotor is prevented from movement in the

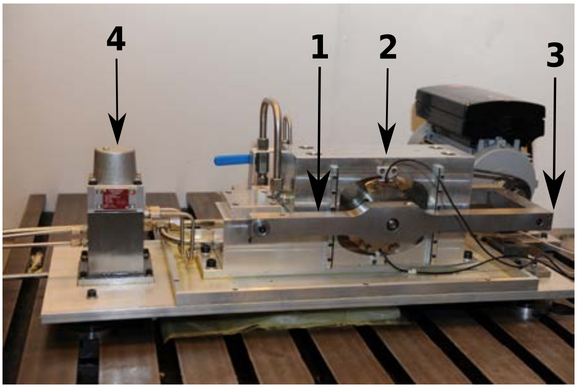

FIGURE 1. Test rig for the tilting-pad bearing with active lubrication; the arrangement consists of a test bearing with two tilting-pads and a rigid rotor (2), supported by a tilting frame pivoted in one end (1). The tilting frame free end (3) can be used to apply load over the bearing, or to fix the rotor vertical position using an adjustment bolt. A servovalve (4) controls the pressurized oil flow towards the injection nozzle on each pad.

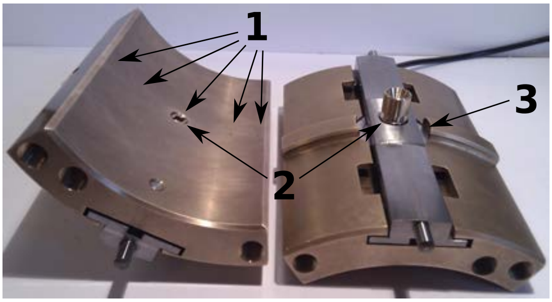

FIGURE 2. Tilting pads installed in the test rig; (1) shows the position of the thermocouples or pressure transducers measurement points, (2) shows the high pressure injection nozzle, (3) shows the location of the load cell for measuring oil film resulting radial force

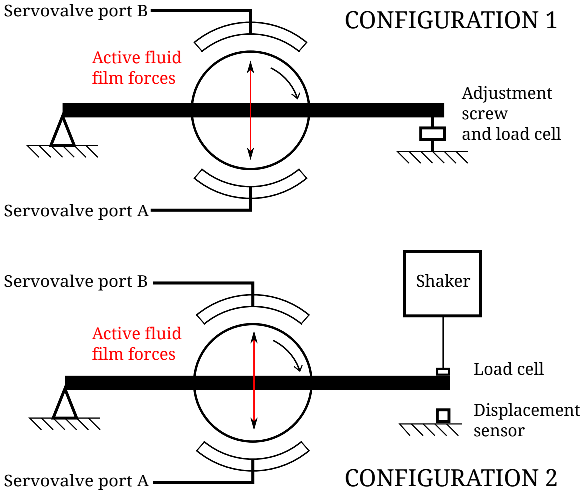

FIGURE 3. The two configurations of the test rig used for this study: measurement of the ALB active forces (Configuration 1, upper), and experimental FRF measurement using the shaker or the calibrated ALB as the excitation source (Configuration 2, lower)

horizontal direction, by the frame in which the rotor is mounted. Since the frame is allowed to tilt around its pivoting point, only a single degree of freedom is required to describe the position of the rotor, related to its vertical displacement. This can be measured by means of a displacement sensor. Furthermore, it is possible to fix the vertical position of the rotor by using an adjustment bolt located at the frame free end, and to measure the resulting forces over it, using a load cell associated with the adjustment bolt.

A closer view of the tilting pad and its instrumentation can be seen in Fig.2. It can be equipped with thermocouples, pressure transducers and a force transducer in the back of the pad, enabling the measurement of the resulting forces in the radial direction over the pad. The most important component within the tilting pads design is the nozzle, through which high pressure oil can be injected into the gap between the tilting pad and the rotor, thus rendering the bearing controllable. The oil flow towards the injection nozzle in each tilting pad is controlled by means of a single servo valve, which is connected to a high pressure oil supply pump. The position of the servovalve spool can be measured using its built-in displacement transducer.

Experimental procedure

In order to experimentally determine the frequency response function of a mechanical system, it is necessary to simultaneously measure the excitation force applied to it, and the output, in terms of resulting displacement or acceleration. Hence, in the frequency domain, the FRF can be defined as:

$$H(f) = \frac{X(f)}{F(f)} \tag{1}$$

When using an electromagnetic shaker or an impulse hammer to excite the system, the measurement of the applied force can be performed directly by using a piezoelectric load cell. Hence, the input forcing function $F(f)$ is readily available, as well as the system response $X(f)$. However, when using the ALB as the exciter, the force applied over the structure can not be obtained directly. In this case, the magnitudes that can be measured directly are the resulting displacement or acceleration of the system $X(f)$, as well as the control signal $U(f)$ sent to the servovalve. Consequently, a "pseudo" frequency response function can be directly obtained:

$$\hat{H}(f) = \frac{X(f)}{U(f)} \tag{2}$$

In order to determine the "true" frequency response function of the system using the ALB, the relationship $C(f)$ between servovalve control signal and active force applied over the rotor must be previously determined, as follows:

$$C(f) = \frac{F(f)}{U(f)} \tag{3}$$

Once the calibration function for the ALB $C(f)$ is determined, the frequency response function of the system can be obtained using the following relationship:

$$H(f) = \frac{X(f)}{U(f)} \cdot \frac{U(f)}{F(f)} = \hat{H}(f) \cdot C(f)^{-1} \tag{4}$$

The determination of the ALB calibration function $C(f)$ can be performed using a theoretical model or an experimental approach. For the work presented here, a purely experimental approach is followed, using the test rig described in the previous section. For doing so, the test rig is arranged in the manner described in Fig.3, see Configuration 1. The procedure can be stated as follows:

1. Set the rotational speed of the rotor and the pressure for the high pressure supply system, responsible for providing oil flow to the injection nozzles in the bearings pads.
2. Using the adjustment bolt located at the end of the tilting frame, the rotor vertical position is set in order to apply an static load over the bearing.
3. A chirp signal of known amplitude is generated and sent to the servovalve. Such signal produces a displacement of the servovalve spool, which changes the resulting oil flow into the injection nozzle of each pad. As a result of this, an active force is generated in the ALB and applied over the rotor.
4. The active force originated in the ALB can be related to the force measured using the load cell located at the end of the tilting frame, by simple equilibrium of moments with respect to the tilting frame pivot point. The usage of this relationship is validated by checking that the relevant system dynamics take place in frequencies well above the analyzed frequency range.
5. The ALB calibration function $C(f)$ is determined using Eqn.(3), where $U(f)$ is the chirp signal sent to the servovalve, and $F(f)$ is measured using the load cell. Since both signals are simultaneously measured, $C(f)$ contains the calibration data in amplitude and phase of the ALB active force with respect to the servovalve control signal, for any frequency within the analyzed range.

Once the ALB calibration function $C(f)$ has been determined experimentally, the frequency response function $H(f)$ of the rotor-bearing system is determined by using Configuration 2, see Fig.3. The following procedure is used:

1. Set the rotational speed of the rotor and the pressure for the high pressure supply system, responsible for providing oil flow to the injection nozzles in the bearings pads. This supply system is turned on at all times, meaning that the leakage flow passing through the servovalve is constantly being fed into the pads injection nozzle.
2. A static load is applied over the bearing, by placing calibrated weights on top of the tilting frame free end.
3. The rotor-bearing arrangement is excited by using the shaker whose stinger is connected at the tilting frame free end. The resulting displacement of the frame free end $X(f)$ is measured using a displacement probe. The applied force $F(f)$ is measured using a piezoelectric load cell. The frequency response function $H(f)$ obtained by this method is used as reference for evaluating the quality of the results obtained using the ALB as the system shaker.
4. The rotor-bearing arrangement is excited using the ALB active forces generated by sending a chirp signal to the servovalve. Both the chirp control signal $U(f)$ and the resulting tilting frame free end displacement $X(f)$ are simultaneously measured. Hence, the "pseudo" frequency response function of the system $\hat{H}(f)$ is determined.
5. Using $\hat{H}(f)$, the ALB calibration function $C(f)$ and Eqn.(4), the frequency response function $H(f)$ can be determined. Its validity is evaluated by direct comparison

with the reference frequency response function determined in step 3.

RESULTS

Experimental Measurement of the ALB Active Force

As it was explained in the previous section, the first step necessary to employ the ALB as a calibrated shaker is to measure the relationship between control signal and resulting active force generated by it, by means of an experimentally determined calibration function $C(f)$. This procedure was repeated for all the operational conditions tested, defined by the following parameters: rotor rotational speed, pressure value set at the high pressure supply pump, amplitude of the chirp signal sent to the servovalve. Only some representative results are shown here, to demonstrate the dependency of the ALB calibration function with those operational parameters.

The comparison of the results shown in Fig.4 and Fig.5 enables to determine the effect of changing the value of the injection pressure over the ALB active force, for a rotational speed of 1000 RPM. In general, it can be seen that by increasing the supply pressure value from 40 bar to 80 bar, the amplitude of the obtained ALB active force is also increased, within the analyzed frequency range. This is consistent with the fact that an increase of the supply pressure value will also increase the pressurized oil flow through the injection nozzle into the bearing clearance, with the resulting modification of the oil film pressure field.

Three different amplitudes of the servovalve control signal were tested for obtaining the results depicted in Fig.4 and Fig.5. It can be seen that by increasing its magnitude, the coherence between control signal and resulting ALB active force increases. Also, from these results it is noted that by increasing the amplitude of the chirp signal above 2.5% of the servovalve maximum control voltage (10 V), the amplitude of the ALB active force tend to decrease. This behavior can be explained in terms of the actual pressurized oil flow coming through the injection nozzle. By increasing the amplitude of the servovalve control signal above a critical level, the assumed "linear" behavior for this device is no longer valid, meaning that the relationship between amplitude of the control signal and resulting flow is not direct anymore [20]. Moreover, by increasing the amplitude of the control signal, the amplitude of the servovalve spool movement increases, which implies that the pressure transients within the servovalve and connecting pipeline are stronger, with the resulting modification of the oil flow due to compressibility effects. These effects modify the pressurized oil flow arriving to the pad injection nozzle, with the corresponding reduction of the ALB active force.

The effect of increasing the rotor rotational speed can be assessed by analyzing the results shown in Fig.6 and Fig.7. When the rotational speed is set to 2000 RPM, the amplitude of the ALB active force decreases, compared to the values obtained for 1000 RPM and similar supply pressures. For a higher rotational speed, the pressure developed in the oil film due to hydrodynamic effect is increased, hence a larger value for the injection pressure is required in order to make the pressurized oil flow enter the bearing clearance through the injection nozzle. Consequently, if the injection pressure is maintained and the hydrodynamic pressure is increased due to an increment in the rotor speed, a lower injection flow is obtained, with the resulting reduction in the ALB active force.

Regarding the frequency dependency of the ALB active force, it can be noted that both its amplitude and phase are modified by the frequency of the control signal. Moreover, its phase with respect to the servovalve control signal tends to increase linearly over the analyzed frequency range. Since the active force is a function of the pressurized oil flow coming through the injection nozzles in the pads, it becomes clear that there is a frequency dependant transfer function between servovalve control signal and pressurized oil flow coming into the bearing clearance.

The available theoretical model for determining the active forces generated in the ALB [9, 21] accounts for this effect, by stating that it is originated due to the well established servovalve frequency dependency between control signal and resulting flow. This relationship between servovalve input signal and resulting flow on its output ports, can be modelled based on an equivalent second order linear differential equation [22], which enables capturing in a simplified way the amplitude and phase shift relationship between those magnitudes. By introducing this simplified servovalve model within the ALB mathematical model, one obtains a frequency dependency between servovalve control signal and the active force applied over the rotor.

Fig.8 depicts the experimentally measured frequency response function between servovalve control signal and resulting spool displacement in the servovalve. Since the servovalve output flow is proportional to its spool displacement [20], this result provides an approximation to the transfer function between servovalve control signal and output flow. The comparison between Fig.8 and Fig.4, specially regarding the phase shift behavior, reveals that the servovalve dynamics are not the only cause for the frequency dependency between the ALB active force and control signal. An additional transfer function is present in the system, resulting in the modification of the injected flow in the pad with respect to ouput flow in the servovalve port. These experimental results reveal the need for updating the available ALB mathematical model to include these additional dynamics.

FRF Measurements using the ALB as a calibrated shaker

When the frequency response function of a mechanical system is determined using a shaker as the excitation source, some constraints need to be respected regarding the magnitude of the excitation force used to perturb the system. Firstly, the excitation

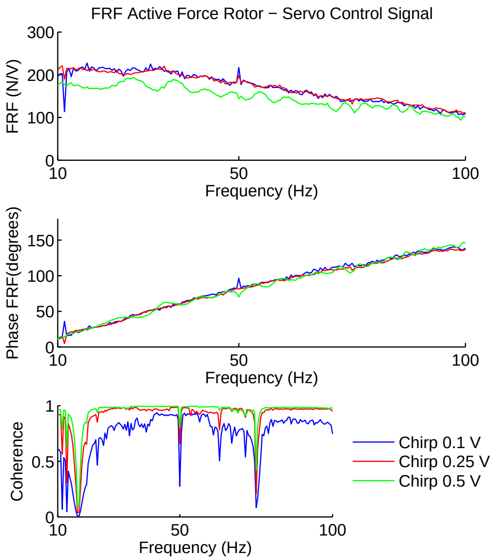

FIGURE 4. Calibration function of the ALB active force: results for 1000 RPM, 40 bar injection pressure, and different amplitudes of the chirp signal used to control the servovalve

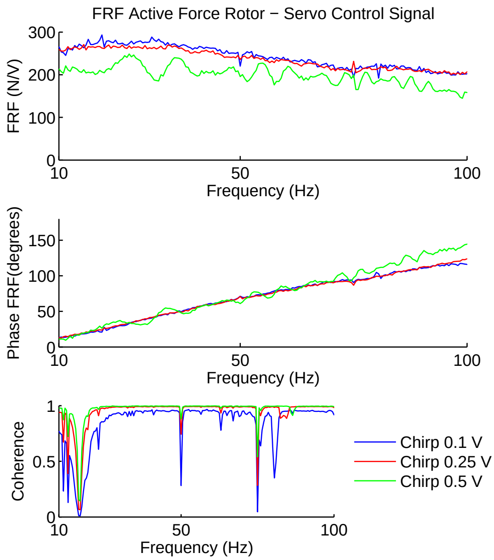

FIGURE 5. Calibration function of the ALB active force: results for 1000 RPM, 80 bar injection pressure, and different amplitudes of the chirp signal used to control the servovalve

force must be strong enough, so that the measured displacement signal exhibits a good signal to noise ratio, which entails a good coherence for the obtained frequency response function. Secondly, if the frequency response function is measured in order to determine the equivalent linearized dynamic coefficients of the studied mechanical system, the reduction from the real system to a linearized one is only valid for small perturbations around the static equilibrium position. Consequently, the upper limit for the magnitude of the excitation force is dictated by the maximum admissible amplitude for the resulting displacements in the structure, so that the linear behavior assumption is respected.

When the ALB is used for exciting the rotor-bearing system, the previously exposed constraints are still valid, but an additional constraint must be introduced. In this case, the forces used for exciting the mechanical system are generated by modifying the oil film pressure field within the bearing clearance. This modification is obtained by using the oil injection system. Since the dynamic behavior of the rotor-bearing system is a function of such pressure field, care must be taken in keeping the perturbation caused by the oil injection within admissible levels, so that the original dynamic behavior of the studied system is preserved. Hence, the experimental parameter identification using the ALB as the excitation source must be planned taking into account three constraints: (I) good coherence in the resulting FRF; (II) small rotor displacements around the equilibrium position; (III) negligible modification of the dynamic behavior of the original rotor-bearing system. In other words, the perturbation introduced by the oil film active force must be as small as possible in order to obtain a "non-invasive" testing technique.

Among the parameters that must be chosen in order to use the ALB as the excitation source, one can name: the amplitude of the chirp signal generated to control the servovalve, and the supply pressure for the oil injection system. The experimental results shown in this section provide insight about the feasibility of using the ALB as a calibrated shaker in the studied system, as well as the effect over the obtained FRF results of chosing different parameters for controlling the ALB.

Effect of the servovalve leakage flow over the system dynamics The first effect to be analyzed corresponds to the influence of the servovalve leakage flow on the dynamics of the studied system. Even when no control signal is sent to the servovalve and its spool is centered, a leakage flow occurs through its output ports, due to manufacturing clearances. This is due to the design of the servovalve, which corresponds to an underlapped one [20]. Such flow is a function of the pressure of the supply system, as well as the pressure in the load, in this case the bearing pads. Fig.9 depicts the influence of adjusting

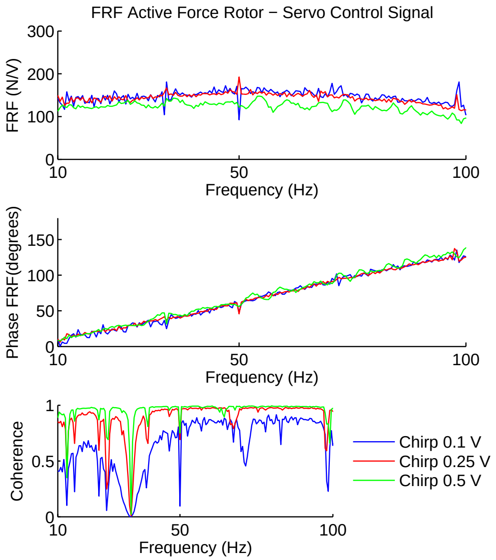

FIGURE 6. Calibration function of the ALB active force: results for 2000 RPM, 40 bar injection pressure, and different amplitudes of the chirp signal used to control the servovalve

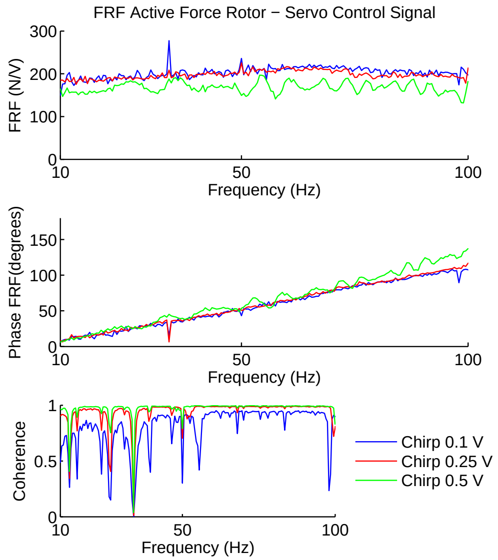

FIGURE 7. Calibration function of the ALB active force: results for 2000 RPM, 80 bar injection pressure, and different amplitudes of the chirp signal used to control the servovalve

the pressure of the supply system for the FRF results in amplitude, obtained using the electromagnetic shaker as the excitation source. No control signal is sent to the servovalve. For both rotational speeds, it can be seen that by increasing the supply pressure for the injection system, the resonant peak amplitude decreases and the system response in the low frequency range remains the same. This is equivalent to state that the stiffness characteristics stays unaffected, but the damping is increased. By increasing the supply pressure, the leakage flow is also increased. This increase in the damping characteristic is consistent with the disruption of the oil film velocity field due to the leakage flow entering the bearing clearance.

Comparison of FRF results using electromagnetic shaker and ALB as excitation source The following set of results, presented in Fig.10,11,12, correspond to the FRF of the studied rotor-bearing system obtained using the shaker or the ALB as the excitation source. The results obtained using the shaker, plotted in thick blue line, are considered as the reference results. For this set of results, the rotor rotational speed is set to 1000 RPM, and the supply pressure for the injection system is set to 20 bar, 40 bar and 80 bar respectively. The behavior of the reference FRF in amplitude and phase shows that the studied system behaves as a single degree of freedom system within the analyzed frequency range, with a resonance zone around 60 Hz. Such dynamic behavior corresponds physically to the rigid body movement of the rotor-tilting frame arrangement, pivoting with respect to its support point.

One can observe that in general lines the FRF obtained using the ALB show good correlation with the reference results. Regarding the requirement of preserving the dynamics of the original system, it can be seen that in general the usage of the ALB induces a higher response in the lower frequency range, which corresponds to a slight reduction in the stiffness of the system. Regarding damping, since the resonant zone exhibits a highly damped shape, it is difficult to extract conclusions in this case. Regarding coherence in the obtained FRF results, it can be seen that better results are obtained by increasing the injection pressure and the amplitude of the chirp signal.

A clearer idea about the effect of using the ALB injection system over the original system dynamics can be obtained by exciting a system which exhibits a clearly defined resonant peak in the studied frequency range. This can be obtained by increasing the rotor rotational speed, which entails a reduction of damping provided by the oil film. Fig.13,14,15 depict the FRF results obtained for 3000 RPM and injection pressure set to 20 bar, 40 bar and 80 bar respectively. The reference results obtained using the shaker as the excitation source show a more visible resonant peak, when

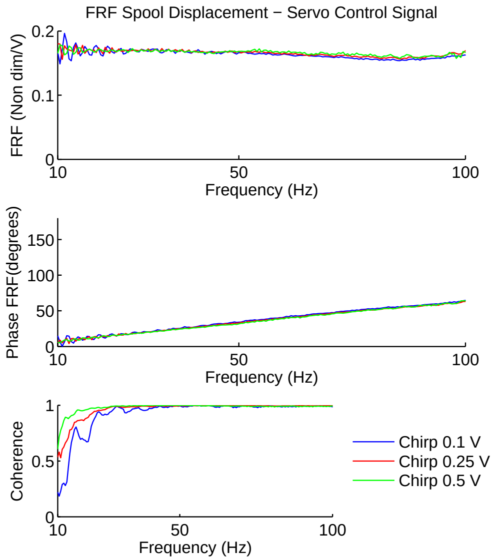

FIGURE 8. FRF between the spool displacement of the servovalve and the control signal for the servovalve: results for 1000 RPM, 40 bar injection pressure, and different amplitudes of the chirp signal

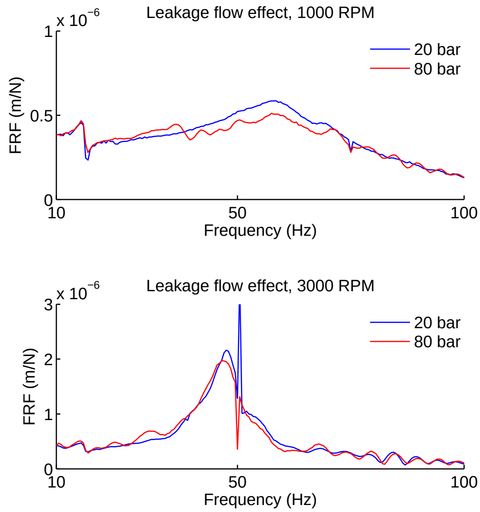

FIGURE 9. Effect of the servovalve leakage flow over the FRF reference results obtained using the shaker: results for two rotational speeds (1000 RPM and 3000 RPM) and two different injection pressures (20 bar and 80 bar)

compared to the results obtained for 1000 RPM.
In this case, it can be clearly observed the delicate balance between obtaining good coherence in the FRF, and keeping the original system dynamics, when using the ALB as the excitation source. In general, a better coherence is obtained by increasing the injection pressure and the amplitude of the chirp signal. Particularly, in Fig.13 it can be seen that poor coherence is obtained when using 20 bar as the supply pressure for the injection system. When the rotational speed is set to 3000 RPM, the hydrodynamic pressure increases, hence a higher injection pressure is required in order to inject oil into the bearing clearance and to obtain oil film active forces. Consequently, the results obtained with 40 bar and 80 bar, Fig.14 and Fig.15, exhibit much better coherence.
On the other hand, using a higher injection pressure and a higher amplitude of the chirp signal entails a stronger modification of the original system dynamics. Such modification is evidenced by an increase of the system response in the low frequency range, which is equivalent to a reduction of the stiffness, and a reduction of the amplitude and frequency of the resonant peak, which entails an increase of the system damping. The damping introduced into the system by the oil film is a consequence of the energy dissipation taking place in the oil due to the viscous forces. These viscous forces are a function of the oil film velocity field. It can be infered that the more pressurized oil is injected into the clearance, the more disrupted is the velocity field, with the corresponding modification of the resulting damping characteristics. This characteristic is highly desirable when using the ALB to control the rotor vibrations, but not convenient when using it as an excitation source for the determining the dynamic properties of the studied system.
For the two different operational conditions that were analyzed, it can be observed that using a chirp amplitude between 0.25 V and 0.5 V provides the best balance between good coherence in the FRF results, and keeping the system dynamics as unaltered as possible. Regarding the pressure of the supply system for the injection nozzles, this value should be set so that the pressurized flow can be injected into the bearing clearance. Hence, it is a function of the hydrodynamic pressure in the oil film, which is in turn a function of the applied load and rotational speed for the rotor-bearing arrangement.

CONCLUSIONS AND FUTURE ASPECTS

In this work, the feasibility of using an actively lubricated tilting-pad journal bearing as a calibrated shaker for parameter identification purposes has been experimentally shown, using a test rig designed and built for this purpose. Based on the obtained experimental results, the following conclusions can be stated:

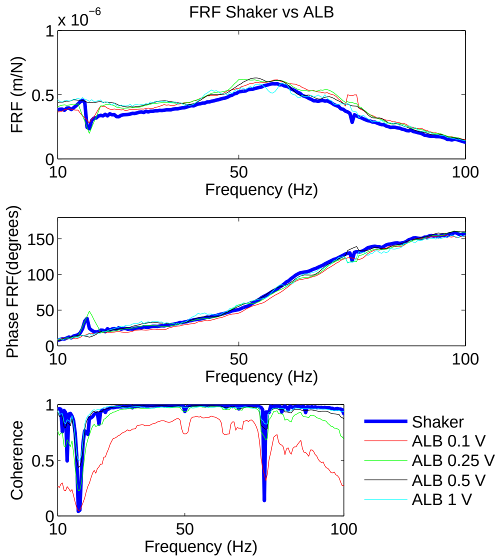

FIGURE 10. Comparison of experimentally obtained FRFs using shaker and the calibrated ALB as the excitation source: results for 1000 RPM, 20 bar injection pressure, and different amplitudes of the chirp signal sent to the servovalve

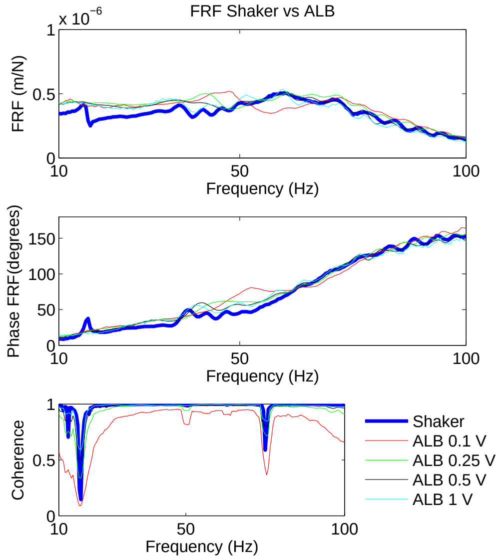

FIGURE 11. Comparison of experimentally obtained FRFs using shaker and the calibrated ALB as the excitation source: results for 1000 RPM, 40 bar injection pressure, and different amplitudes of the chirp signal sent to the servovalve

1. When using the ALB as a calibrated shaker, three constraints must be observed in order to obtain reliable results for the frequency response function of the studied system: (I) good coherence between applied excitation and resulting displacement; (II) small displacements around the equilibrium position; (III) negligible modification of the original system dynamic behavior, due to the oil injection into the bearing clearance, i.e. “non-invasive” perturbation forces.
2. A good coherence for the obtained FRF is obtained if the supply pressure for the injection system and the amplitude of the chirp signal for controlling the servovalve are set so that the resulting pressurized flow is capable of entering the bearing clearance. On the other hand, an increase in the supply pressure and chirp amplitude entails a stronger modification of the original system dynamics, regarding its equivalent stiffness and damping. Hence, a balance between these two conditions must be carefully achieved in order to obtain reliable results.
3. Considering the previously stated constraints, good quality for the FRF results was achieved by setting the amplitude of the chirp signal between 2.5% and 5 % of the maximum servovalve voltage for the test rotor-ALB system. Regarding the injection pressure, this value must be set depending on the hydrodynamic pressure developed in the oil film, which is a function of the rotational speed and applied load. In practical terms, the injection pressure should be incremented in small steps, until good coherence between applied ALB active force and resulting vibration of the system is achieved.
4. The experimental work was carried out in a test rig which can be set up to directly measure the ALB active force calibration function. For an industrial application of this technology, an accurate modeling of the active force generated in the ALB would be required, due to the practical difficulties of directly measuring the active force on a real rotating machine. The experimental results regarding the ALB calibration function show the need for including the dynamics of the oil within the pipeline into the existing theoretical model, in order to predict accurately the oil flow being injected into the bearing clearance, and the resulting active force. Consequently, an update of the available controllable elastothermohydrodynamic model for the actively lubricated tilting-pad journal bearing [23] is required to incorporate these new findings.

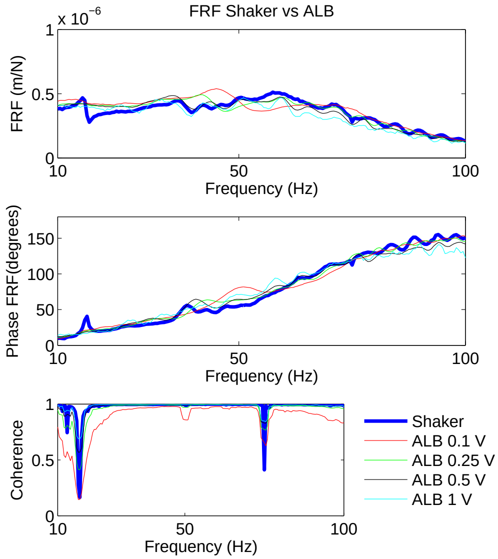

FIGURE 12. Comparison of experimentally obtained FRFs using shaker and the calibrated ALB as the excitation source: results for 1000 RPM, 80 bar injection pressure, and different amplitudes of the chirp signal sent to the servovalve

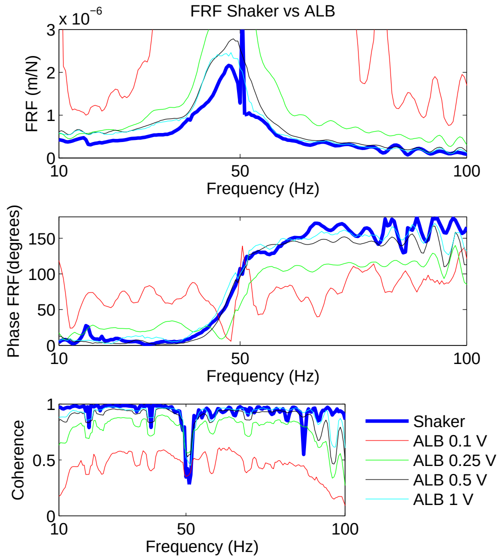

FIGURE 13. Comparison of experimentally obtained FRFs using shaker and the calibrated ALB as the excitation source: results for 3000 RPM, 20 bar injection pressure, and different amplitudes of the chirp signal sent to the servovalve

TABLE 1. Dimensions, oil properties and parameters for the test rig bearing

Pad inner radius	49.923	mm
Journal radius	49.692	mm
Bearing axial length	100	mm
Assembly radial clearance	0.075	mm
Number of pads	2	-
Pad arc	69	deg
Offset	0.5	-
Load Angle	on pad	-
Pad thickness	12	mm
Injection nozzle radius	3	mm
Injection pipeline length	700	mm
Injection nozzle length	10	mm
Oil type	ISO VG22	-
Pad material	Brass	-
Pivot insert material	Steel	-

REFERENCES

[1] Schweitzer, G., Traxler, A., and Bleuler, H., 1994. *Active Magnetic Bearings - Basics, Properties and Applications of Active Bearings*. Springer Verlag, Berlin, Heidelberg, New York.

[2] Ulbrich, H., 1988. "New Test Techniques using Active Magnetic Bearings". *Proceedings of the First International Symposium on Magnetic Bearings*.

[3] Gähler, C., and Förch, P., 1994. "A Precise Magnetic Bearing Exciter for Rotordynamic Experiments". *Proceedings of the Fourth International Symposium on Magnetic Bearings*.

[4] Gähler, C., 1998. "Rotor Dynamic Testing and Control with Active Magnetic Bearings". PhD Thesis, ETH Zürich.

[5] Aenis, M., Knoph, E., and Nordmann, R., 2002. "Active Magnetic Bearings for the Identification and Fault Diagnosis in Turbomachinery". *Mechatronics,* ***12***(8), pp. 1011–1021.

[6] Knoph, E., and Nordmann, R., 1994. "Active Magnetic Bearings for the Identification of Dynamic Characteristics of Fluid Bearings - Calibration Results". *Proceedings of the Fourth International Symposium on Magnetic Bearings*.

[7] Kjølhede, K., and Santos, I., 2007. "Experimental Contribution to High-Precision Characterization of Magnetic Forces in Active Magnetic Bearings". *ASME Journal of Engineering for Gas Turbines and Power,* ***129***, pp. 503–

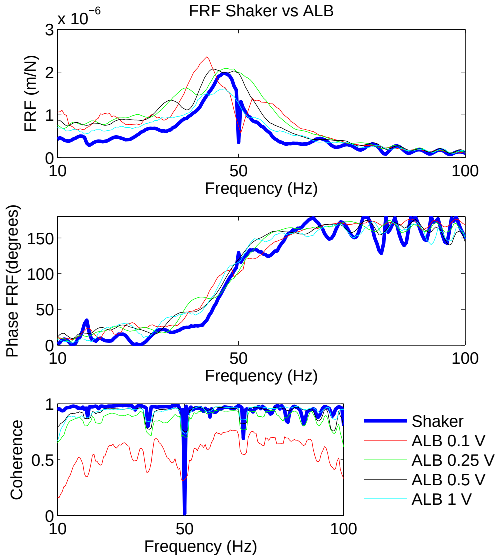

FIGURE 14. Comparison of experimentally obtained FRFs using shaker and the calibrated ALB as the excitation source: results for 3000 RPM, 40 bar injection pressure, and different amplitudes of the chirp signal sent to the servovalve

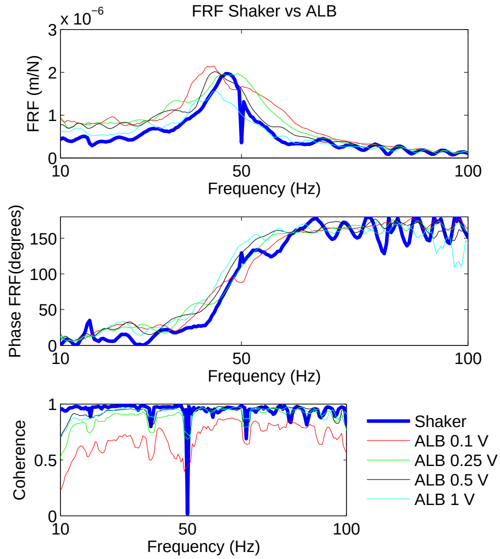

FIGURE 15. Comparison of experimentally obtained FRFs using shaker and the calibrated ALB as the excitation source: results for 3000 RPM, 80 bar injection pressure, and different amplitudes of the chirp signal sent to the servovalve

509.
[8] Voigt, A., and Santos, I., 2012. "Theoretical and Experimental Investigation of Force Estimation Errors using Active Magnetic Bearings with Embedded Hall Sensors". *Proceedings of ASME Turbo Expo 2012*.
[9] Santos, I. F., 1994. "Design and Evaluation of Two Types of Active Tilting Pad Journal Bearings". In *The Active Control of Vibration*, C.R.Burrows and P.S.Keogh, eds. Mechanical Engineering Publications Limited, London, England, pp. 79–87.
[10] Bently, D., Grant, J., and Hanifan, P., 2000. "Active Controlled Hydrostatic Bearings for a New Generation of Machines". *ASME/IGTI International Gas Turbine and Aeroengine Congress and Exhibition*.
[11] Bently, D., Eldridge, T., Jensen, J., and Mol, P., 2001. "Externally Pressurized Bearings allow Rotor Dynamic Optimization". *VDI-Berichte*(1640), pp. 49–61.
[12] Santos, I. F., 1996. "Theoretical and Experimental Identification on the Stiffness and Damping Coefficients of Active-Tilting Pad Journal Bearings". In *Identification in Engineering Systems*, M. Friswell and J. Mottershead, eds. The Cromwell Press Ltd., Swansea, Great Britain, pp. 325–334.
[13] Santos, I. F., and Scalabrin, A., 2003. "Control System Design for Active Lubrication with Theoretical and Experimental Examples". *Journal of Engineering for Gas Turbines and Power, ASME Trans.*, ***125***, January, pp. 75–80.
[14] Santos, I. F., and Watanabe, F., 2004. "Compensation of Cross-Coupling Stiffness and Increase of Direct Damping in Multirecess Journal Bearings using Active Hybrid Lubrication - Part i: Theory". *ASME Trans. Journal of Tribology,* ***126***(1), pp. 146–155.
[15] Cerda, A., and Santos, I. F., 2012. "Stability Analysis of an Industrial Gas Compressor supported by Tilting-Pad Journal Bearings under Different Lubrication Regimes". *Journal of Engineering for Gas Turbines and Power, ASME Trans.,* ***134***(2).
[16] Santos, I. F., and Nicoletti, R., 1999. "THD Analysis in Tilting-Pad Journal Bearings using Multiple Orifice Hybrid Lubrication". *Journal of Tribology, ASME Trans.,* ***121***, pp. 892–900.
[17] Santos, I. F., and Nicoletti, R., 2001. "Influence of Orifice Distribution on the Thermal and Static Properties of Hybridly Lubricated Bearings". *International Journal of Solids and Structures,* ***38***, pp. 2069–2081.
[18] Cerda, A., and Santos, I. F., 2012. "Performance Improvement of Tilting-Pad Journal Bearings by means of Control-

lable Lubrication". *Mechanics & Industry,* ***13***, pp. 17–32.
[19] Santos, I. F. "Trends in Controllable Oil Film Bearings". *IUTAM Symposium on Emerging Trends in Rotor Dynamics (in print, Springer Verlag)*.
[20] Merritt, H., 1967. *Hydraulic Control Systems*. Wiley and Sons, Inc.
[21] Santos, I. F., and Russo, F., 1998. "Tilting-Pad Journal Bearings with Electronic Radial Oil Injection". *Journal of Tribology, ASME Trans.,* ***120***(3), pp. 583–594.
[22] Thayer, W., 1965. "Transfer Functions for MOOG Servovalves". *MOOG Technical Bulletin,* ***103***, pp. 1–11.
[23] Cerda.A, Bjerregaard Nielsen, B., and Santos, I., 2012. "Steady State Characteristics of a Tilting Pad Journal Bearing with Controllable Lubrication: Comparison between Theoretical and Experimental Results". *Tribology International (in print) http://dx.doi.org/10.1016/j.triboint.2012.10.004*.

CHAPTER 6

Controllable TPJB: Characterization of Dynamic Behavior

In order to employ the controllable TPJB as the actuator in a control loop, it is mandatory to characterize accurately the active forces generated by it. The frequency dependent transfer function between servovalve control signal and active force over the rotor must be determined, by experimental or theoretical means. This function describes both the amplitude of the active force, as well as the phase lag or time delay of the active force with respect to the servovalve control signal. Furthermore, the frequency dependency of amplitude and phase of the active force must be thoroughly defined.

In the previous chapter, the results shown in Publication 5, see section 5.5, provided the first set of results regarding the experimental characterization of the controllable TPJB active forces in the frequency domain. Prior to the start of this research project, it was considered that the only component that introduced a frequency dependent transfer function between control signal and resulting active force over the rotor was the servovalve [29, 34]. However, the experimental results presented in Publication 5, see section 5.5, show that there are additional dynamics within the controllable TPJB setup. In other words, the servovalve dynamics is not the only contribution to the time delay between control signal and resulting active force.

This chapter is focused on presenting an experimental study regarding the characterization of the transfer function between servovalve control signal and bearing active force. The main objective is to identify as clearly as possible the contribution from each component of the controllable TPJB to the studied transfer function. Consequently, the validity of the available mathematical model for the controllable bearing can be evaluated.

6.1 Experimental Setup and Procedure

The theoretical analysis of the controllable TPJB presented in Chapter 2 reveals that this system presents non linear behavior. However, if the system reaches an equilibrium state and its operation is characterized by small perturbations around that equilibrium, then it is possible to analyze it as a linearized system. This operation mode is desirable not only because of the advantages it presents regarding its mathematical analysis, but also because of its benefits regarding the mechanical "health" of the system, since it entails low vibration amplitudes and low magnitude of the generated dynamic forces. Consequently, it is possible to apply linear systems theory to describe the controllable bearing behavior, as it is explained here.

The relationship between servovalve control signal u_V and active force over the rotor F_{active} can be expressed in the frequency domain by means of a transfer function $\mathbf{G}(f)$, defined as:

$$\mathbf{G}(f) = \frac{F_{active}(f)}{u_V(f)} \tag{6.1}$$

The transfer function defined in Equation (6.1) can be obtained experimentally, by measuring simultaneously the servovalve control signal $u_V(t)$ and active force over the rotor $F_{active}(t)$, and applying the following relationship [66]:

$$\mathbf{G}(f) = \frac{S_{FF}(f)}{S_{uF}(f)} \tag{6.2}$$

where S_{FF} is the power spectral density of the measured active force $F_{active}(t)$, and S_{uF} is the cross spectral density between the active force $F_{active}(t)$ and the servovalve control signal $u_V(t)$.

The transfer function $\mathbf{G}(f)$ results from the contribution of every component of the controllable TPJB to the overall system dynamics. Mathematically, this can be stated as:

$$\mathbf{G}(f) = G_1(f) \cdot G_2(f) \cdot G_3(f) \cdot ... \cdot G_i(f) \tag{6.3}$$

where $G_i(f)$ represents the transfer function from each component of the controllable TPJB that contributes to the overall transfer function $\mathbf{G}(f)$. Consequently, the objective of this experimental study is to determine each one of the "component" transfer functions $G_i(f)$.
The setup employed for performing this experimental study is depicted in Figure 6.1. It corresponds to the test rig designed and constructed by Nielsen and Santos [46], described briefly in the introduction of this thesis.
The configuration is similar to the one used in Publication 5, see section 5.5, to characterize experimentally the active forces generated by the controllable TPJB. The difference in this case stems from the number of sensors and signal considered for the analysis, as well as the parameters varied for the study. A schematic of the experimental setup is depicted in Figure 6.1. Among the magnitudes to be measured during the experimental tests are: servovalve control signal $u_V(t)$, servovalve spool position $x_V(t)$, pressure in the injection nozzle $p_{inj}(t)$, pressure in one point inside the bearing clearance $p_{clear}(t)$ and active force acting over the rotor $F_{active}(t)$.
The effect of the upper pad oil injection is negligible over the experimental measurements presented here, as a result of the clearance between the upper pad and the rotor. For all tests, a "negative" rotor eccentricity was imposed (the rotor is moved towards the lower pad). This effect was checked by repeating each experimental test while cutting the high pressure flow towards the upper pad. No significant change in the measurements was observed.
Concerning the operational conditions for the servovalve, a constant supply pressure of 100 bar is imposed, and the control signal corresponds to a chirp signal of amplitude 0.2 Volts. The supply pressure is set to the highest possible value of the available pump, in order to obtain good signal to noise ratio in the piezoelectric pressure transducers, whereas the amplitude of the control signal is determined based on the experience gathered in Publication 5, see section 5.5.
The experimental procedure can be stated as follows:

1. Set the rotational speed and eccentricity of the rotor, using the adjustment bolt located at the end of the tilting frame.

2. A chirp signal $u_V(t)$ of amplitude 0.2 Volts is generated and sent to the servovalve. This signal produces a displacement of the servovalve spool, which modifies the resulting oil flow into the injection nozzle of each pad. As a result of this, an active force is generated in the controllable TPJB and applied over the rotor.

3. The active force originated in the controllable TPJB can be related to the force measured using the load cell located at the end of the tilting frame, by simple equilibrium of moments with respect to the tilting frame pivot point. The usage of this relationship is validated by checking that the relevant system dynamics take place in frequencies well above the

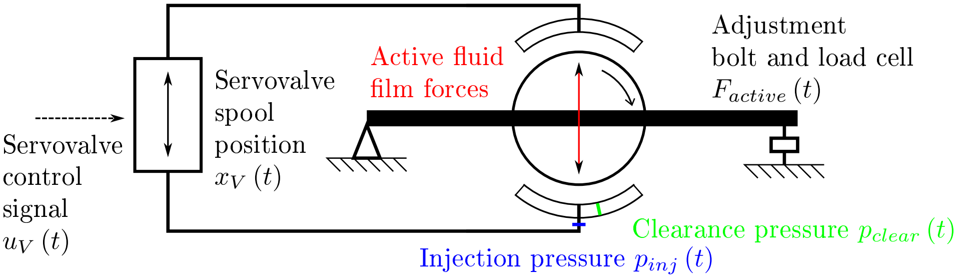

Figure 6.1: *The experimental setup for determining the contribution of each component transfer function $G_i(f)$ to the global transfer function of the controllable bearing $\mathbf{G}(f)$*

analyzed frequency range. This is done by repeating the same test with a calibrated weight of 10 Kg over the tilting frame and observing whether the added mass introduces any change in the studied frequency range.

4. By measuring simultaneously the servovalve control signal $u_V(t)$, spool position $x_V(t)$, injection pressure $p_{inj}(t)$, bearing clearance pressure $p_{clear}(t)$ and active force $F_{active}(t)$, it is possible to calculate the frequency response function of each component $G_i(f)$ by using Equation (6.2).

Uncertainty analysis is applied to the experimentally obtained transfer functions $G_i(f)$, following the guidelines given in [67]. The reported uncertainty for magnitude, phase and coherence quantifies the effect of random errors affecting the repeatibility of the results, and it is calculated using multisample analysis with a 95% confidence range. A total of five independant tests were obtained for each operational condition, in order to determine the uncertainty interval.

6.2 Experimental Results: Transfer Functions Characterization

6.2.1 Servovalve Transfer Function $G_1(f)$

The first element to be analized is the servovalve. As it was stated in Chapter 2, it is well established that this electromechanical device introduces a transfer function between input control signal u_V and output flow towards the load, in

this case, the injection points in the pads.
Although the experimental setup does not allow the direct measurement of the output flow, it is possible to measure a voltage signal $x_V(t)$ proportional to the servovalve spool displacement. Consequently, the servovalve transfer function $G_1(f)$ is defined as:

$$G_1(f) = \frac{x_V(f)}{u_V(f)} \tag{6.4}$$

Figure 6.2 depicts the experimentally obtained $G_1(f)$, with magnitude units $\left[\frac{V}{V}\right]$. The servovalve manufacturer measures and report the transfer function between input signal and output flow for "no load" condition, see Chapter 2. Comparing those results with the ones given here, it can be observed that measuring the spool displacement gives a good qualitative approximation of the dynamic behavior of the servovalve output flow. Furthermore, it can be noted that the servovalve transfer function is not qualitatively affected by the operational conditions of the bearing, such as eccentricity or rotational speed (results not included here, for the sake of briefness). However, it must be kept in mind that the actual magnitude of the output flow is a function of the load pressure, resulting from rotor eccentricity and rotational speed. This effect is accounted for within the mathematical model, using the K_{pq} linearized coefficient, see Chapter 2.

6.2.2 Pipeline Transfer Function $G_2(f)$

The characterization of the pipeline dynamics is given by the transfer function defined as:

$$G_2(f) = \frac{p_{inj}(f)}{x_V(f)} \tag{6.5}$$

Figure 6.3, Figure 6.4, Figure 6.5 depict the experimentally measured $G_2(f)$, for different rotor eccentricities and rotational speeds. Although the behavior of the transfer function amplitude shows weak frequency dependency, making it difficult to identify resonances in the system, the analysis of the phase plots provides insight on this issue. A phase shift from 0^o to 180^o indicates the existence of a natural frequency. A sharp transition between those values indicates low damping for the mode related to that natural frequency, whereas a smooth transition indicates high damping.
Taking into account these guidelines, it can be noted that the pipeline transfer function is highly dependent on the bearing operational conditions. In general, it can be noted that higher rotational speeds and higher rotor eccentricity entails an increment in the value of the system natural frequency. Furthermore,

the damping associated with the acoustic mode is incremented with higher rotor eccentricities. This is equivalent to state that an increase in the system natural frequency and associated damping ratio is observed for operational conditions where the hydrodynamic pressure developed in the oil film is incremented.
Although it is clear that further theoretical and experimental investigations are necessary in order to pinpoint the physical origin of the observed behavior, some temptative explanations can be stated as hypotheses for analyzing it. Regarding the shift in the natural frequency of the pipeline system, the theoretical analysis presented in Chapter 2 states that the natural frequencies are a function of the equivalent bulk modulus of the oil flow. This parameter is highly sensitive to the amount of air in the system, since the air is much more compressible than the oil. The increase in the pipeline natural frequency for higher rotor eccentricies suggests an increase of the equivalent bulk modulus, which is equivalent to a reduction in the amount of air within the pipeline. Physically, this could be related to the increase of the hydrodynamic pressure in the oil film, which could expel the air, preventing it from entering the pipeline.
Regarding the observed change in the damping properties, these are a function of the losses within the system. By imposing a higher rotor eccentricity, the clearance in the injection point is diminished. The transition of the flow from the pipeline to the bearing clearance entails the occurrence of significant losses, which are a function of the geometry of the clearance. A smaller clearance implies higher restriction for the oil flow, with the resulting increase in damping properties.

6.2.3 Oil Film Transfer Function $G_3\left(f\right)$

By injecting pressurized oil into the bearing clearance, the oil film pressure is modified, with the resulting change of the active force over the rotor. Consequently, a transfer function between the injection pressure p_{inj} and active force F_{active} can be defined as:

$$G_3\left(f\right) = \frac{F_{active}\left(f\right)}{p_{inj}\left(f\right)} \tag{6.6}$$

Figure 6.6, Figure 6.7, Figure 6.8 depict the experimental results related to the characterization of the oil film transfer function, for different rotor rotational speeds and eccentricities. Analyzing the phase plots, it can be seen that a significant phase lag exists between the injection pressure and the resulting force over the rotor. This phase lag seems to be weakly dependent on the rotational speed and eccentricity, hence it can be inferred that the effect of the pad dynamics is not dominant in this phenomena. Physically, this delay can be related to dynamic effects taking place within the oil flow in the injection nozzle and bearing clearance. It is well known that the resulting force magnitude is not only a function of the oil film pressure, but also from the area. Consequently, the maximum force over the rotor is obtained when the pressure perturbation has affected the entire surface of the oil film covering the pad. This explanatory hypothesis is supported by Figure 6.9. Here, the transfer function between injection pressure and pressure in one point inside the clearance p_{clear} is depicted. This point is located in an intermediate angular position, between the injection nozzle and the pad leading edge. By comparing the phase plot with the one shown in Figure 6.7, it can be seen that the delay between p_{inj} and p_{clear} is slightly smaller than between p_{inj} and F_{active}.

6.2.4 Global Transfer Function $\mathbf{G}(f)$

The resulting global transfer function $\mathbf{G}(f)$ between control signal u_V and active force over the rotor F_{active} is given in Figure 6.10, Figure 6.11 and Figure 6.12. Comparing the phase plots obtained in this case with the one corresponding to the servovalve transfer function $G_1(f)$, see Figure 6.2, it becomes evident that it is not possible to assume that the servovalve is the only element introducing a time delay between control signal and active force over the rotor. In the light of the results previously shown, an accurate prediction of this global transfer function can be obtained by including the effect of the servovalve, pipeline, injection point and oil film dynamics.

Regarding the **amplitude of the active force**, it can be observed that it exhibits weak frequency dependency below 100 Hz. In previous experimental studies [44, 45], the authors performed the calibration of the magnitude of the active force using a quasi-static approach, i.e a constant valued control signal was fed into the servovalve. In other words, those authors determined the force magnitude for zero frequency. The results shown here prove the validity of that approach, entailing that it is possible to use a static method to determine the amplitude of the active force, and then extrapolate that result in a wider frequency range. When looking at the entire frequency range analyzed, some local increments of the amplitude of the active force can be observed, located on frequencies that coincide with the resonant areas determined in the pipeline dynamics transfer function $G_2(f)$, see Figure 6.3, Figure 6.4 and Figure 6.5.

Regarding the **phase lag of the active force**, it can be seen that it exhibits a linear increment in the frequency range below 100 Hz. This can be justified by analyzing the phase plots for the servovalve $G_1(f)$, see Figure 6.2, and the oil film transfer function $G_3(f)$, see Figure 6.6, Figure 6.7 and Figure 6.8. Equation (6.3) entails that the phase lag of the global transfer function is obtained as the sum of the partial phase lags. Both $G_1(f)$ and $G_3(f)$ exhibit linear increment of the phase lag with the frequency, consequently $\mathbf{G}(f)$ also features that characteristic. The deviations from the linear increment behavior of the phase lag can be explained by the effect of the pipeline dynamics. It can be seen that the deviations in the phase plot for the global transfer function $\mathbf{G}\left(f\right)$ coincide with the resonant areas observed in the phase plot for the pipeline transfer function $G_2\left(f\right)$, see Figure 6.3, Figure 6.4 and Figure 6.5.

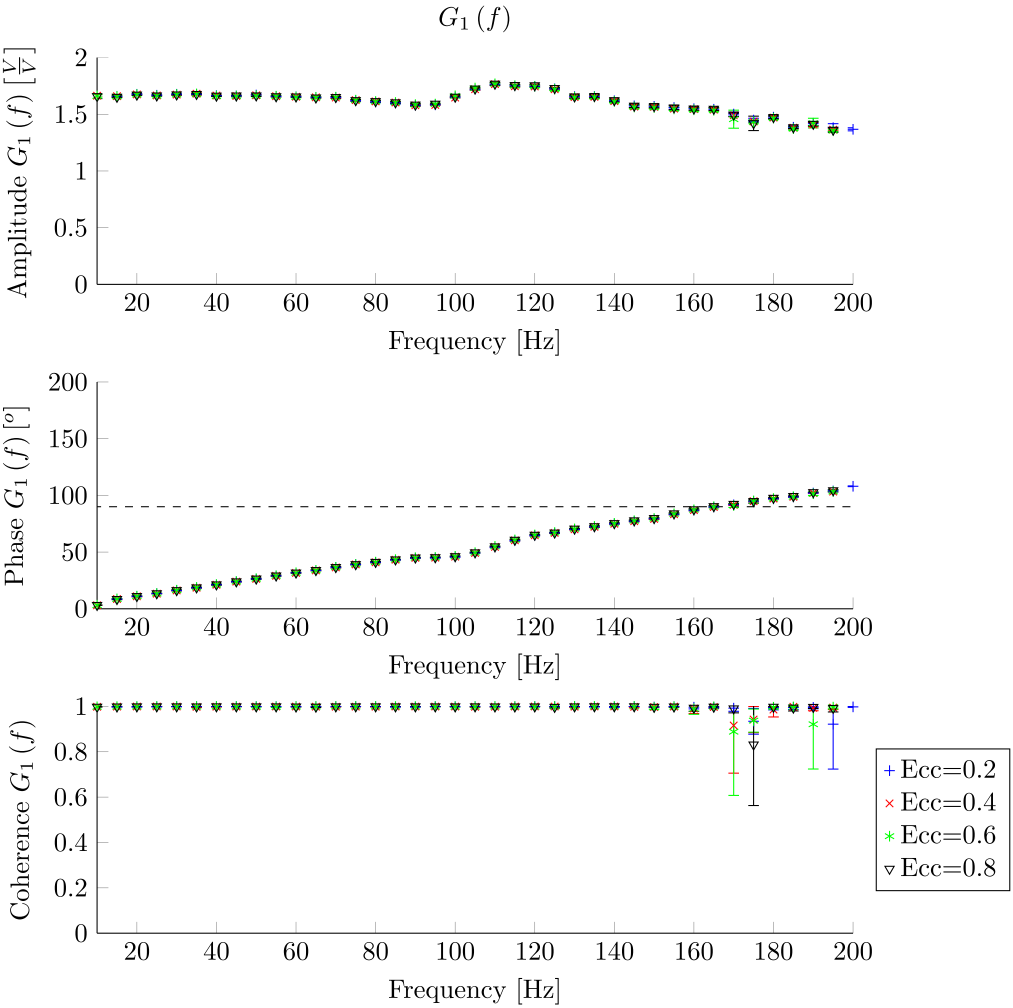

Figure 6.2: *Servovalve transfer function $G_1(f)$; results for different rotor eccentricities (segmented line in the phase plot indicates the 90^o phase lag)*

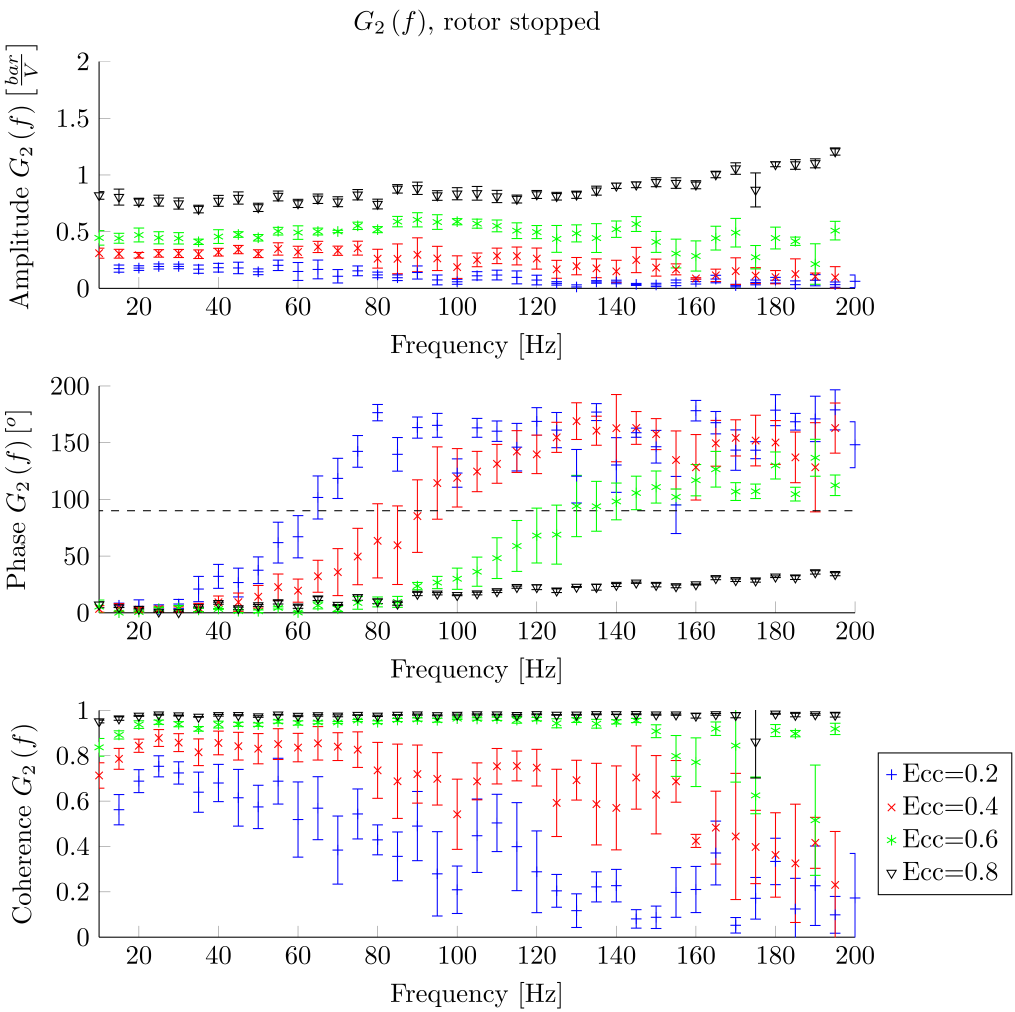

Figure 6.3: *Pipeline transfer function $G_2(f)$; results for different rotor eccentricities, rotor stopped (segmented line in the phase plot indicates the 90^o phase lag)*

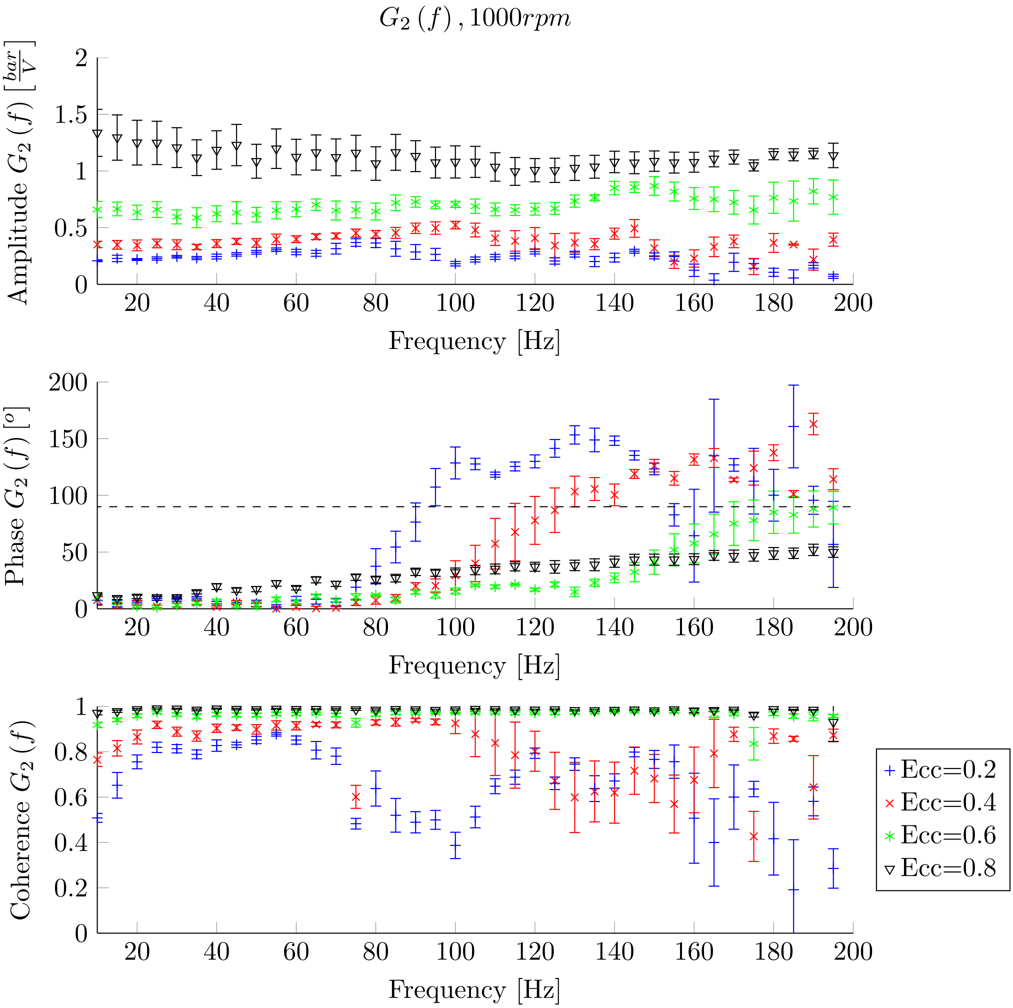

Figure 6.4: *Pipeline transfer function $G_2(f)$; results for different rotor eccentricities, 1000 rpm (segmented line in the phase plot indicates the 90^o phase lag)*

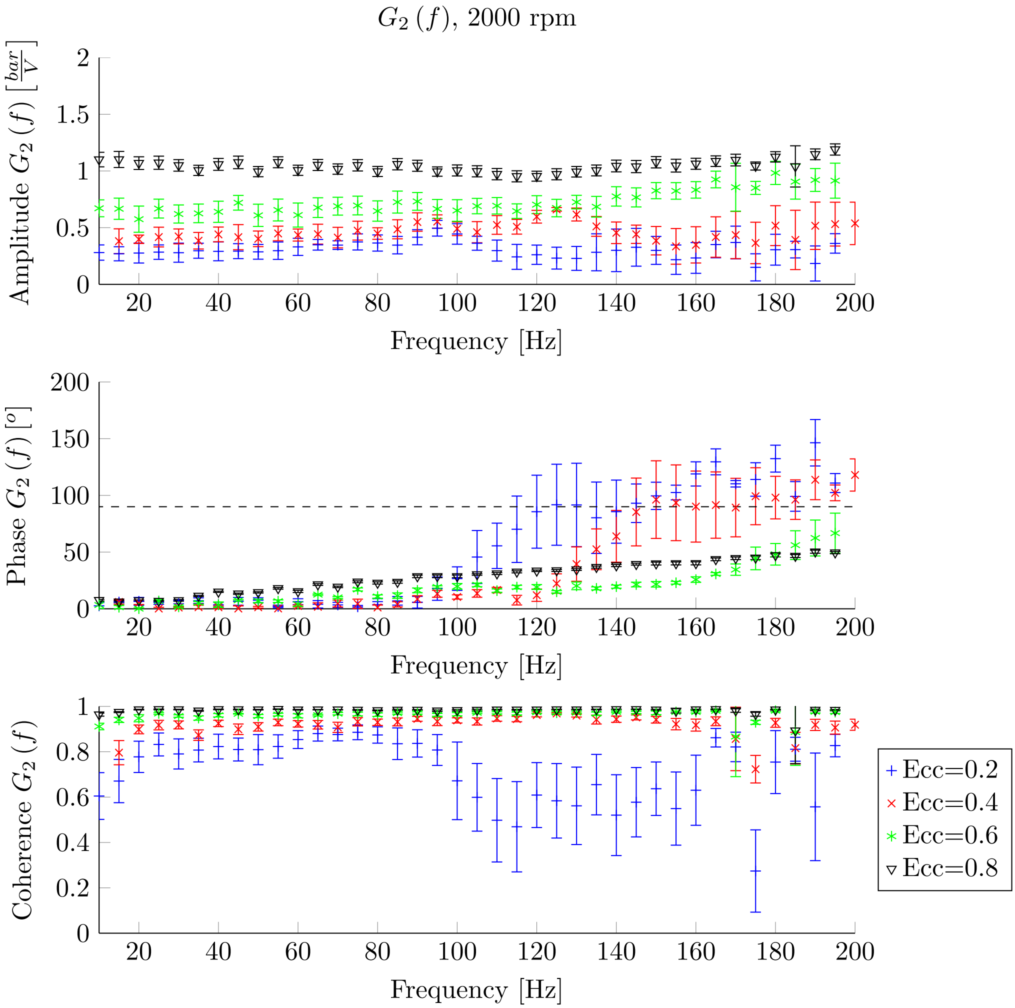

Figure 6.5: *Pipeline transfer function $G_2(f)$; results for different rotor eccentricities, 2000 rpm (segmented line in the phase plot indicates the 90^o phase lag)*

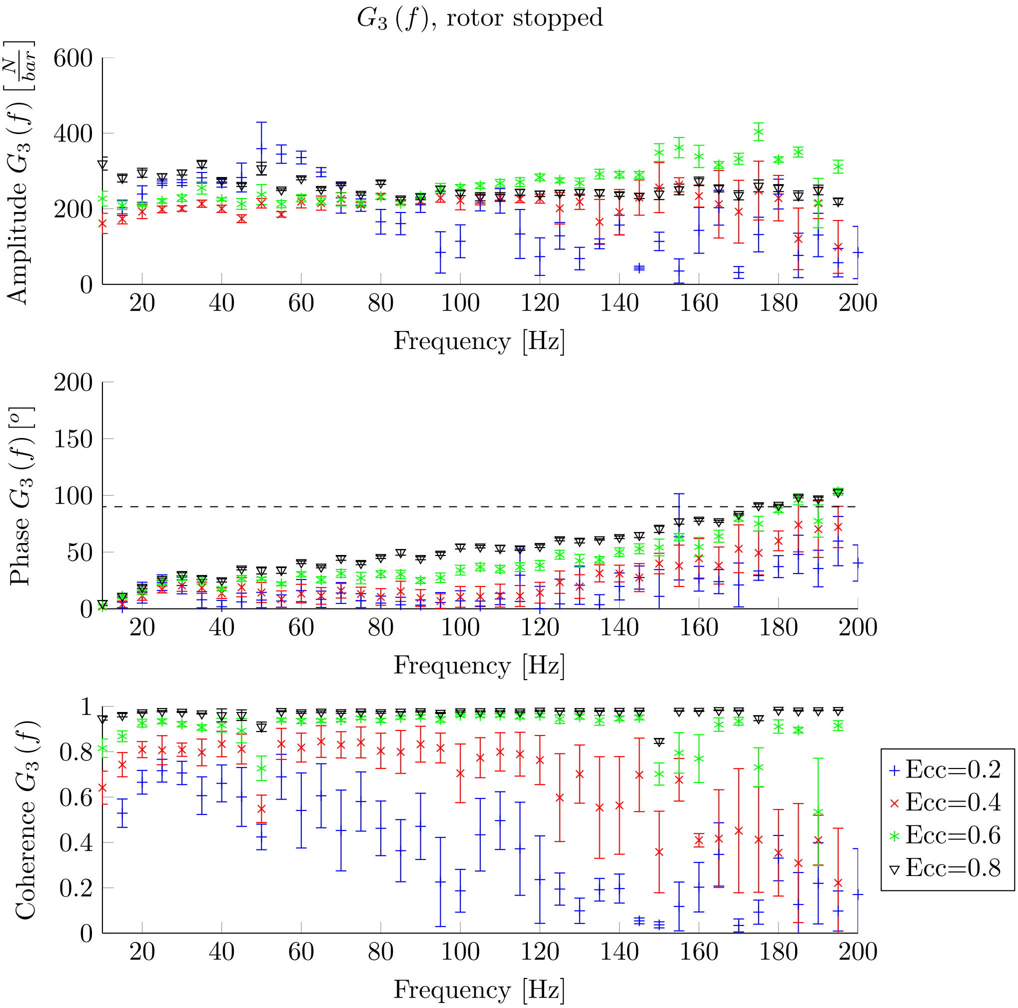

Figure 6.6: *Oil film transfer function $G_3(f)$; results for different rotor eccentricities, rotor stopped (segmented line in the phase plot indicates the 90^o phase lag)*

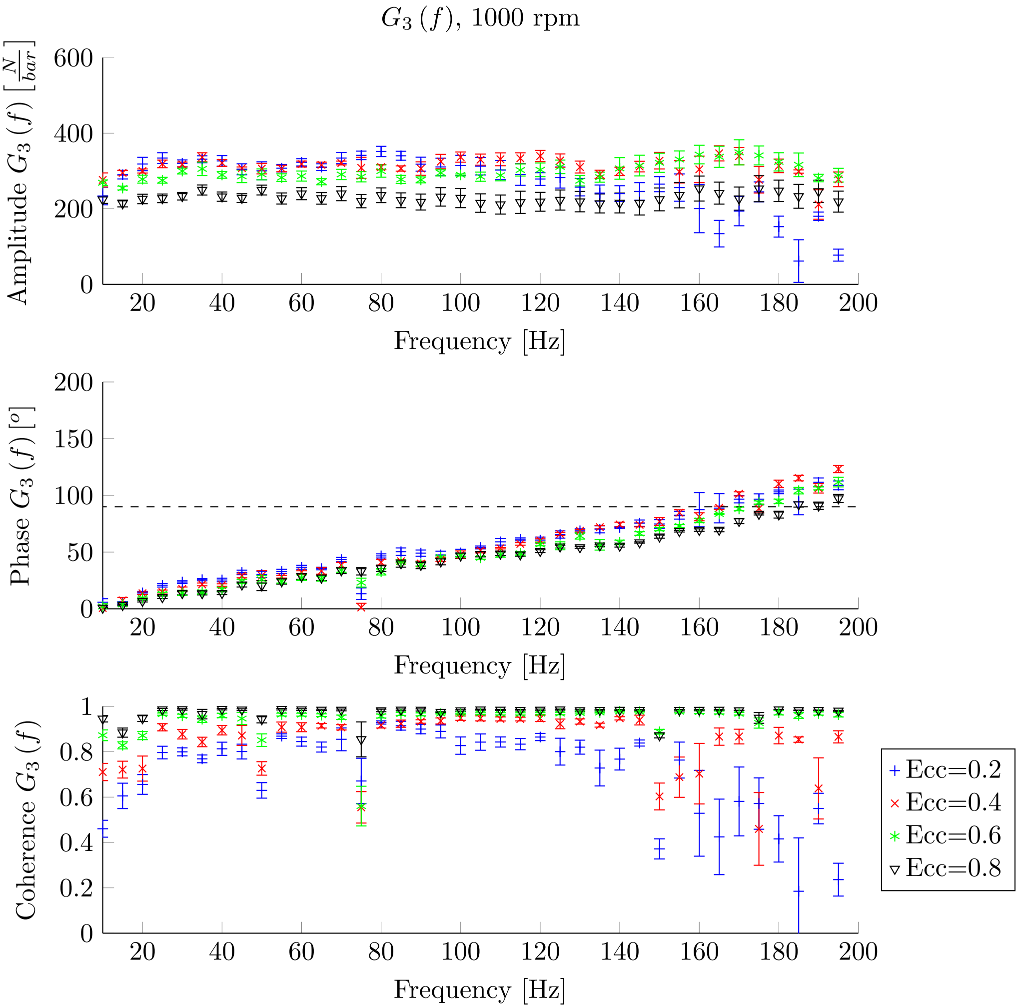

Figure 6.7: *Oil film transfer function $G_3(f)$; results for different rotor eccentricities, 1000 rpm (segmented line in the phase plot indicates the 90^o phase lag)*

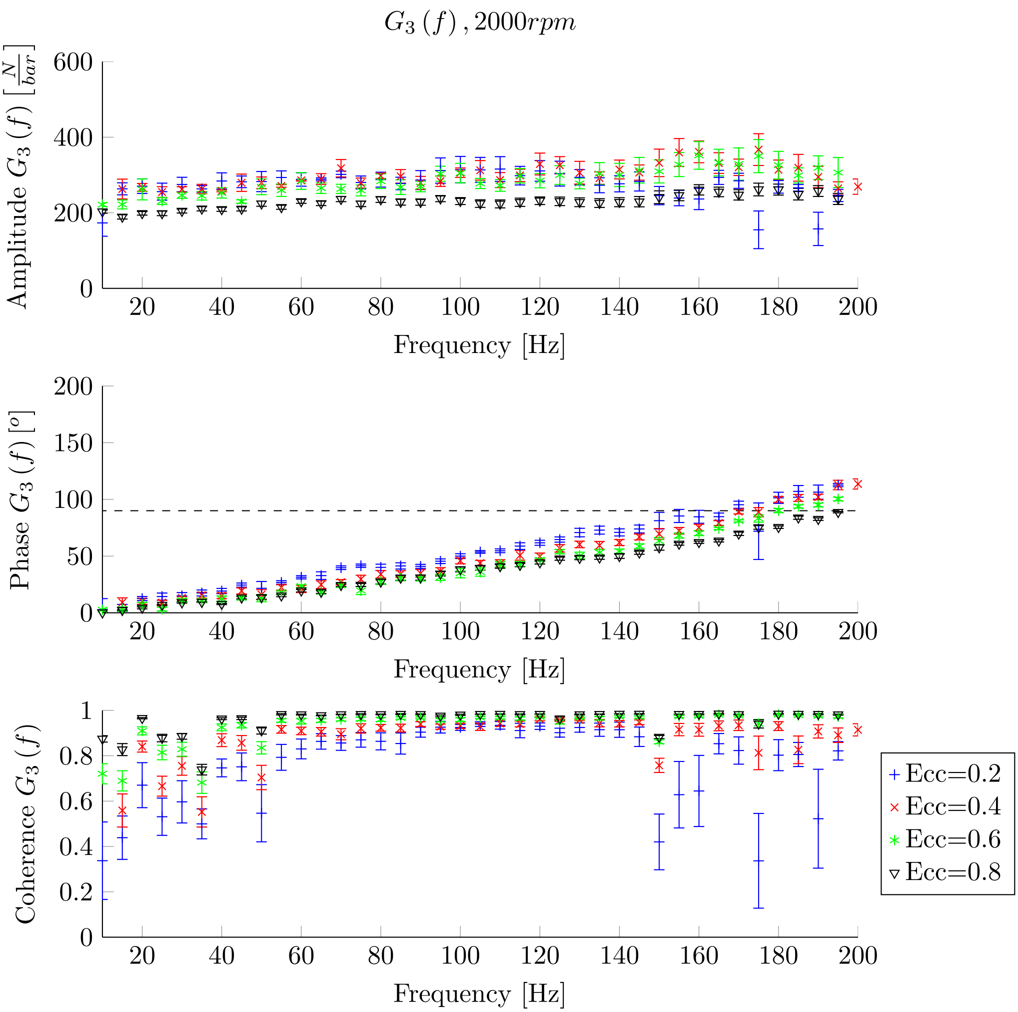

Figure 6.8: *Oil film transfer function $G_3(f)$; results for different rotor eccentricities, 2000 rpm (segmented line in the phase plot indicates the 90^o phase lag)*

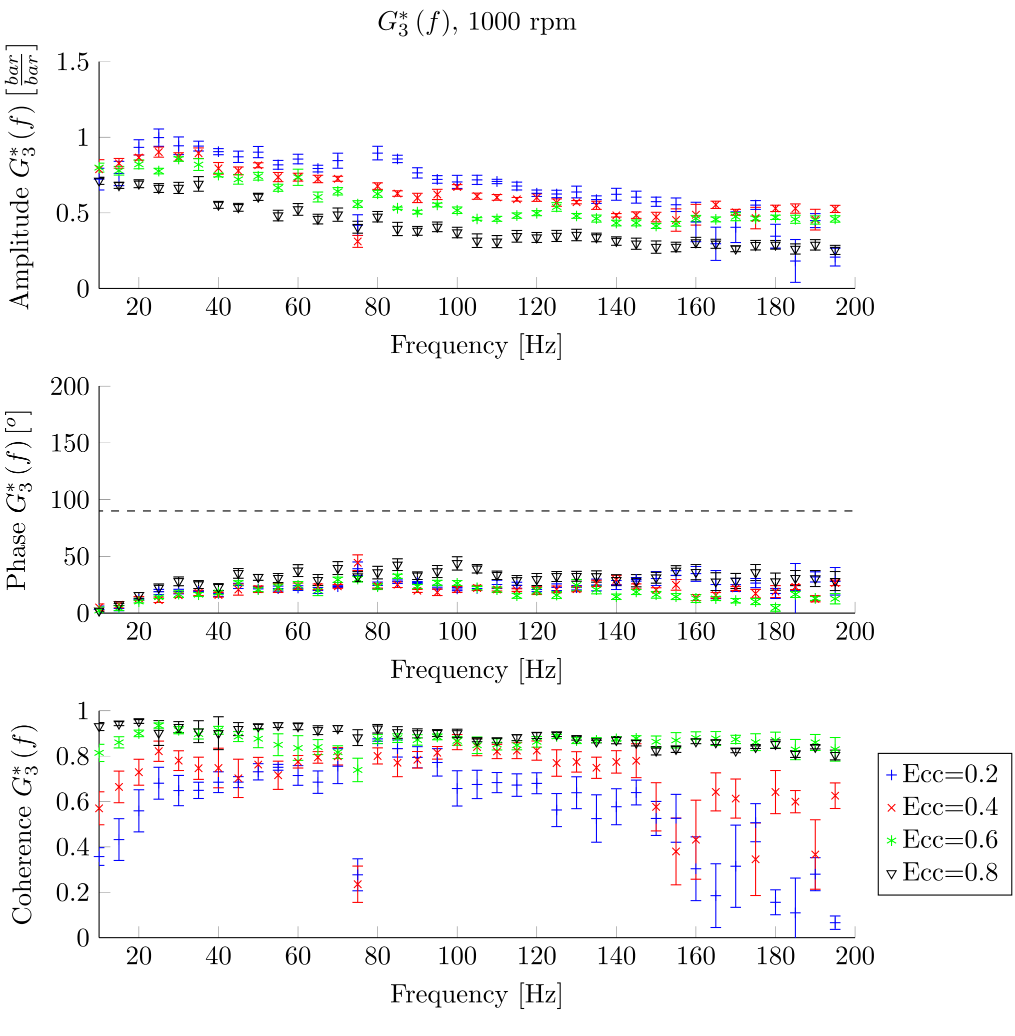

Figure 6.9: *Oil film transfer function $G_3^*(f)$; results for different rotor eccentricities, 1000 rpm (segmented line in the phase plot indicates the 90^o phase lag)*

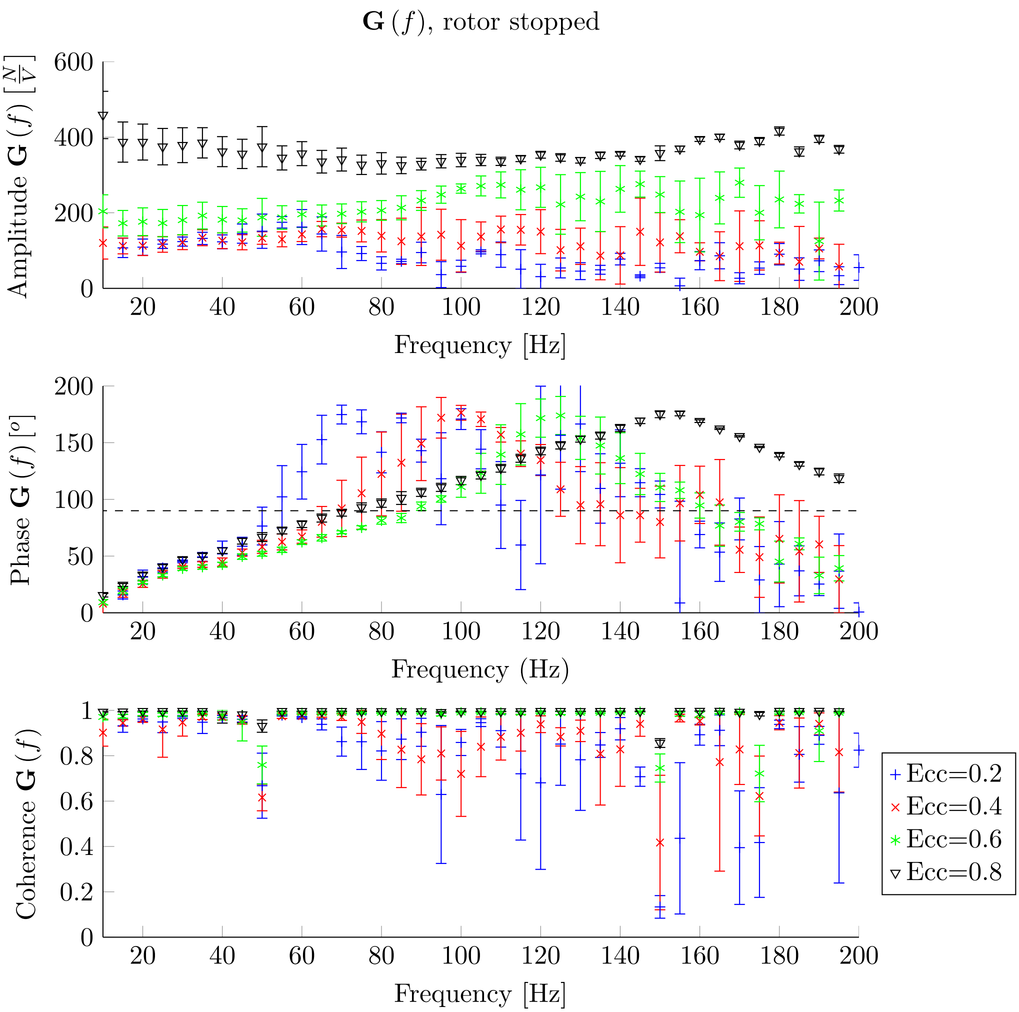

Figure 6.10: *Global transfer function $\boldsymbol{G}(f)$; results for different rotor eccentricities, rotor stopped (segmented line in the phase plot indicates the 90^o phase lag)*

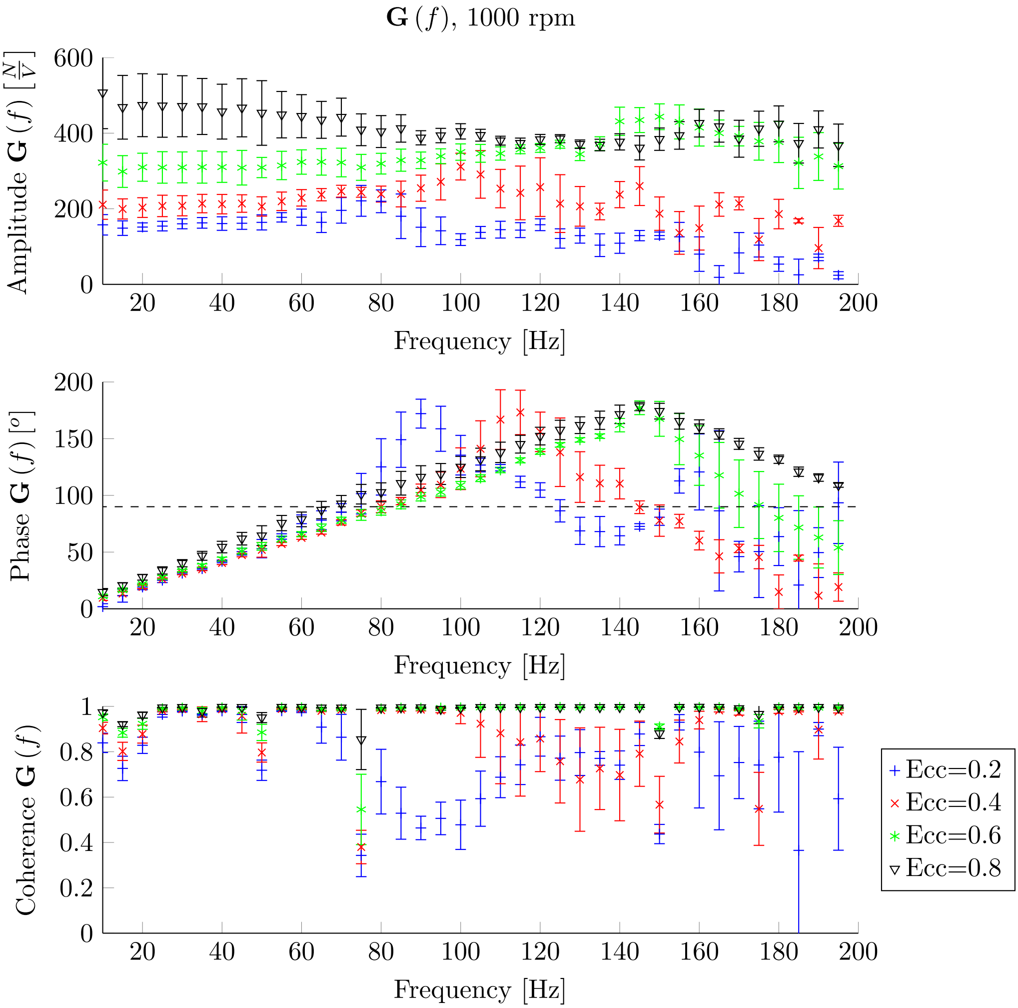

Figure 6.11: *Global transfer function $\boldsymbol{G}(f)$; results for different rotor eccentricities, 1000 rpm (segmented line in the phase plot indicates the 90^o phase lag)*

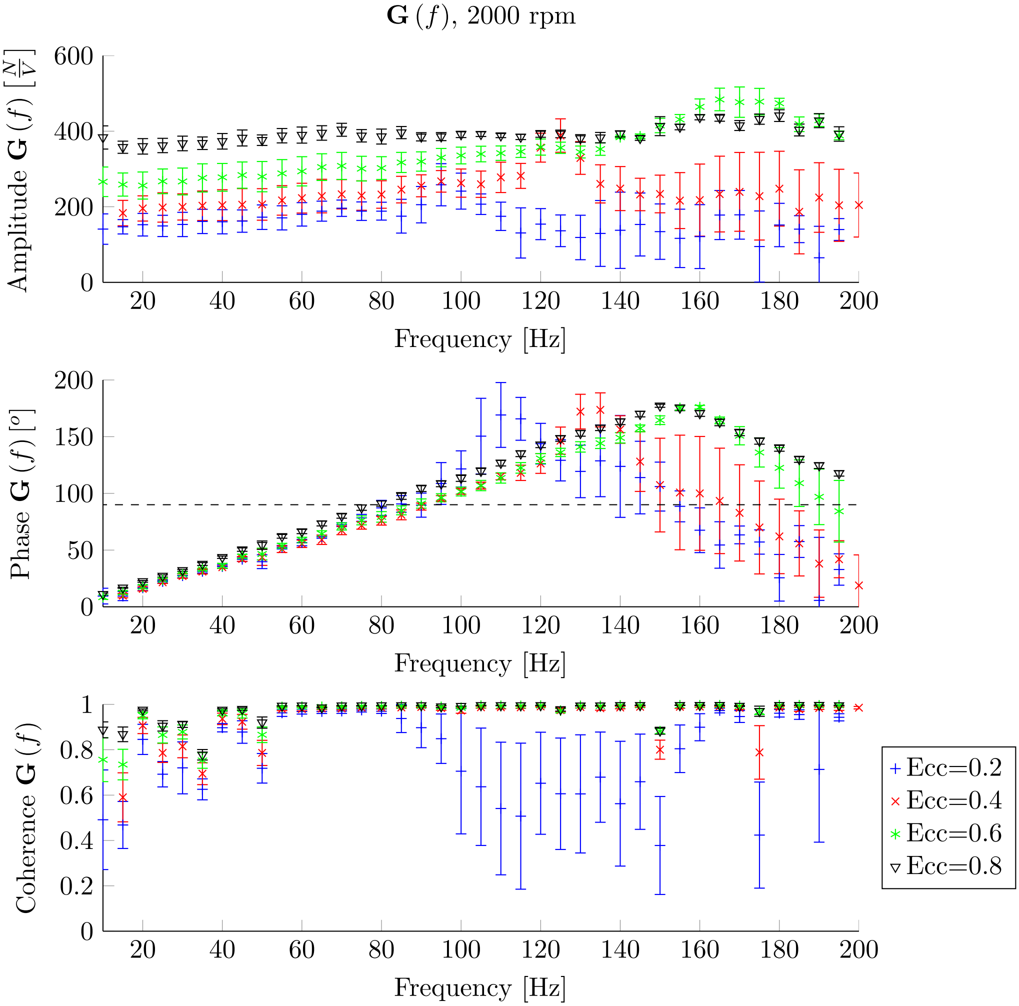

Figure 6.12: *Global transfer function $\boldsymbol{G}(f)$; results for different rotor eccentricities, 2000 rpm (segmented line in the phase plot indicates the 90^o phase lag)*

6.3 Closure

In the light of the experimental results contained in this chapter, a revision of the available mathematical model for the controllable TPJB is required. The validity of this model to predict the static and thermal behavior of the studied bearing was proved in Publication 4, see section 5.4. However, some additional considerations must be taken into account to describe accurately the dynamic behavior of the controllable bearing.

Whenever a system is modeled in order to predict its dynamic behavior, the resulting mathematical representation is valid within a certain frequency range. This general statement is also valid when modeling the controllable TPJB. From the obtained experimental results, it can be seen that if the usage of the controllable bearing is restricted to a narrow band in the low frequency range, it is possible to neglect the dynamic effects arising from the pipeline and oil film transfer functions. In this case, the sole inclusion of the servovalve dynamics should guarantee acceptable precision when predicting the transfer function between control signal and active force over the rotor. However, if the controllable bearing is intended to be used to excite or control vibrations in a wider frequency range, then it becomes necessary to include additional dynamics (pipeline and oil film) into its theoretical model, if an adequate prediction of the amplitude and phase lag of the active force is desired.

It has been proven experimentally that the pipeline can influence significantly the controllable bearing dynamics. Furthermore, its influence is a function of the loading and rotational speed imposed over the rotor, being more relevant in the lower frequency range for lightly loaded pads and lower rotational speeds. Although this effect has been already included in the mathematical model of the controllable bearing using a modal approach, an analytical formulation to obtain the equivalent acoustic natural frequencies and damping factors is missing, specially after verifying that these magnitudes are dependant on the rotor ecccentricity and rotational speed. From the practical point of view, a simple design solution to avoid including this effect into the system dynamics would be to shorten up the length of the pipeline, thus increasing the value of the acoustic natural frequencies above the frequency range desired for the controllable bearing actives forces. A similar effect would be obtained if the controllable bearing system is designed so that the amount of air within the oil flow is minimized.

Additionally, it has been shown that a significant phase lag effect exists between the injection pressure in the nozzle and the active force obtained over the rotor. This effect is not accounted for in the current mathematical model of the controllable bearing. The modeling of the oil film pressure field is based on the Reynolds Equation assumptions, entailing that the perturbation of the pressure due to the injection process occurs simultaneously in the entire oil film domain. Consequently, the active over the rotor is in phase with the pressure in the injection point. Further theoretical investigations are required in order to pinpoint the source of the observed phase lag effect, since it could arise from dynamic effects in the injection nozzle or within the oil film itself.

Chapter 7

Conclusions and Future Aspects

The conclusions obtained from the development of this research project can be stated as follows:

1. A study on the implementation of a controllable lubrication system within the tilting-pad journal bearing design has been performed, by theoretical and experimental means. Two different approaches for employing this technology have been tested. The first one entails the usage of the controllable bearing operating in a "static" configuration, featuring a constant oil pressure within the injection nozzles. In this case, the variable to be controlled in order to modify the bearing characteristics is the supply pressure for the oil injection system. The second configuration is related to the "dynamic" application of the technology, featuring the usage of a servovalve to modify the pressurized oil flow towards the injection nozzles. When operating in this configuration, the bearing characteristics are controlled by means of the control signal sent to the servovalve.

2. The theoretical model of the controllable bearing, featuring a controllable elastothermohydrodynamic regime, has been validated for the "static" configuration of the studied system. The validation was performed by direct comparison of its results against the experimental data gathered in the

test facilities used during this research project. As a result, the feasibility of predicting the static and thermal characteristics of the controllable bearing operating in "static" configuration with sufficient accuracy has been proven. The theoretical model developed in this work has also been employed to theoretically demonstrate the benefits of applying the controllable bearing technology in "static" configuration for industrial rotating machinery. Among the benefits are: reduction of unbalance response when crossing critical speeds, increase of the stable operational margin of the rotor.

3. Regarding the application of the controllable bearing technology in "dynamic" configuration, the possibility of using the bearing as a calibrated actuator for control and parameter identification purposes has been demonstrated by experimental means. The experimental measurement of the active oil film forces generated by the controllable bearing prove the feasibility of employing the studied system to excite system dynamics up to at least 200 Hz. Furthermore, the modification of the original bearing dynamics due to the pressurized oil injection has been experimentally assessed. As a result, it has been shown that a careful election of the controllable TPJB operational parameters (supply pressure and amplitude of the chirp control signal) must be performed, in order to perform parameter identification procedures without significantly modifying the original system dynamics.

4. Regarding the theoretical prediction of the active forces generated by the controllable TPJB, it has been experimentally shown that the sole inclusion of the servovalve transfer function does not guarantee an accurate description of the global transfer function, between control signal and active force over the rotor. Consequently, a theoretical model for the pipeline dynamics have been developed and included in the controllable TPJB dynamic model. Furthermore, additional dynamics arising from the oil flow within the injection nozzle and bearing clearance, must be thoroughly studied and included in the theoretical model in order to predict accurately the global transfer function.

The future aspects for the improvement of the knowledge related to the studied technology are:

1. A theoretical study on the oil flow dynamics, considering the injection nozzle and the oil film within the bearing clearance, must be carried out, in order to pinpoint the physical phenomena behind the measured phase lag between injection pressure and active force over the rotor. Considering the results of this study, an expansion of the controllable TPJB theoretical model must be performed, to take into account the new findings.

2. An experimental study on the influence of the design of the hydraulic system associated with the controllable bearing over the transfer function between control signal and active force. Among the variables that must be included are: amount of air within the oil flow, length of the pipelines.

3. An experimental study on the identification of the dynamic coefficients of the controllable TPJB must be performed, in order to validate the theoretical prediction of these coefficients in "static" and "dynamic" configuration.

APPENDIX A

Derivation of the Reynolds Equation

In this appendix, the procedure for obtaining the Reynolds Equation is detailed. As it was already stated in Chapter 2, the Reynolds Equation corresponds to a particular case of the well-known Navier-Stokes set of equations.
Let $\mathbf{v}(\hat{x}, \hat{y}, \hat{z}, t) = [v_{\hat{x}}, v_{\hat{y}}, v_{\hat{z}}]$ be the oil velocity field within the bearing clearance in the curvilinear reference frame. Assuming an incompressible newtonian fluid behavior for the oil, the Navier-Stokes equations are stated as:

$$
\begin{aligned}
\rho\left(\frac{\partial v_{\hat{x}}}{\partial t}+v_{\hat{x}}\frac{\partial v_{\hat{x}}}{\partial \hat{x}}+v_{\hat{y}}\frac{\partial v_{\hat{x}}}{\partial \hat{y}}+v_{\hat{z}}\frac{\partial v_{\hat{x}}}{\partial \hat{z}}\right) &= S_{\hat{x}}-\frac{\partial p}{\partial \hat{x}} \\
&+\frac{\partial}{\partial \hat{x}}\left(2\mu\frac{\partial v_{\hat{x}}}{\partial \hat{x}}-\frac{2}{3}\mu\left(\frac{\partial v_{\hat{x}}}{\partial \hat{x}}+\frac{\partial v_{\hat{y}}}{\partial \hat{y}}+\frac{\partial v_{\hat{z}}}{\partial \hat{z}}\right)\right) \\
&+\frac{\partial}{\partial \hat{y}}\left(\mu\left(\frac{\partial v_{\hat{x}}}{\partial \hat{y}}+\frac{\partial v_{\hat{y}}}{\partial \hat{x}}\right)\right)+\frac{\partial}{\partial \hat{z}}\left(\mu\left(\frac{\partial v_{\hat{x}}}{\partial \hat{z}}+\frac{\partial v_{\hat{z}}}{\partial \hat{x}}\right)\right) \\
\rho\left(\frac{\partial v_{\hat{y}}}{\partial t}+v_{\hat{x}}\frac{\partial v_{\hat{y}}}{\partial \hat{x}}+v_{\hat{y}}\frac{\partial v_{\hat{y}}}{\partial \hat{y}}+v_{\hat{z}}\frac{\partial v_{\hat{y}}}{\partial \hat{z}}\right) &= S_{\hat{y}}-\frac{\partial p}{\partial \hat{y}} \\
&+\frac{\partial}{\partial \hat{y}}\left(2\mu\frac{\partial v_{\hat{y}}}{\partial \hat{y}}-\frac{2}{3}\mu\left(\frac{\partial v_{\hat{x}}}{\partial \hat{x}}+\frac{\partial v_{\hat{y}}}{\partial \hat{y}}+\frac{\partial v_{\hat{z}}}{\partial \hat{z}}\right)\right) \\
&+\frac{\partial}{\partial \hat{x}}\left(\mu\left(\frac{\partial v_{\hat{x}}}{\partial \hat{y}}+\frac{\partial v_{\hat{y}}}{\partial \hat{x}}\right)\right)+\frac{\partial}{\partial \hat{z}}\left(\mu\left(\frac{\partial v_{\hat{y}}}{\partial \hat{z}}+\frac{\partial v_{\hat{z}}}{\partial \hat{y}}\right)\right) \\
\rho\left(\frac{\partial v_{\hat{z}}}{\partial t}+v_{\hat{x}}\frac{\partial v_{\hat{z}}}{\partial \hat{x}}+v_{\hat{y}}\frac{\partial v_{\hat{z}}}{\partial \hat{y}}+v_{\hat{z}}\frac{\partial v_{\hat{z}}}{\partial \hat{z}}\right) &= S_{\hat{z}}-\frac{\partial p}{\partial \hat{z}} \\
&+\frac{\partial}{\partial \hat{z}}\left(2\mu\frac{\partial v_{\hat{z}}}{\partial \hat{z}}-\frac{2}{3}\mu\left(\frac{\partial v_{\hat{x}}}{\partial \hat{x}}+\frac{\partial v_{\hat{y}}}{\partial \hat{y}}+\frac{\partial v_{\hat{z}}}{\partial \hat{z}}\right)\right) \\
&+\frac{\partial}{\partial \hat{x}}\left(\mu\left(\frac{\partial v_{\hat{x}}}{\partial \hat{z}}+\frac{\partial v_{\hat{z}}}{\partial \hat{x}}\right)\right)+\frac{\partial}{\partial \hat{x}}\left(\mu\left(\frac{\partial v_{\hat{y}}}{\partial \hat{z}}+\frac{\partial v_{\hat{z}}}{\partial \hat{y}}\right)\right)
\end{aligned}
\tag{A.1}
$$

The Navier-Stokes equations, see Equation (A.1), correspond to the application of Newton Second Law for a fluid control volume. Basically, they state the balance of the variation of fluid linear momentum (the inertia terms on the left side of the equations), with the forces acting over it, namely viscous forces, pressure forces and body forces S_i (right side of the equations).
For the thin fluid film developed within the bearing clearance, a dimensional analysis [47] enables to neglect some terms in Equation (A.1). Firstly, for laminar regime the contribution from the inertia terms can be neglected. Secondly, the body forces are negligible compared to the pressure and viscous forces. Hence, Equation (A.1) is reduced to:

$$
\begin{aligned}
\frac{\partial p}{\partial \hat{x}} &= \frac{\partial}{\partial \hat{x}}\left(2\mu\frac{\partial v_{\hat{x}}}{\partial \hat{x}} - \frac{2}{3}\mu\left(\frac{\partial v_{\hat{x}}}{\partial \hat{x}} + \frac{\partial v_{\hat{y}}}{\partial \hat{y}} + \frac{\partial v_{\hat{z}}}{\partial \hat{z}}\right)\right) \\
&\quad + \frac{\partial}{\partial \hat{y}}\left(\mu\left(\frac{\partial v_{\hat{x}}}{\partial \hat{y}} + \frac{\partial v_{\hat{y}}}{\partial \hat{x}}\right)\right) + \frac{\partial}{\partial \hat{z}}\left(\mu\left(\frac{\partial v_{\hat{x}}}{\partial \hat{z}} + \frac{\partial v_{\hat{z}}}{\partial \hat{x}}\right)\right) \\
\frac{\partial p}{\partial \hat{y}} &= \frac{\partial}{\partial \hat{y}}\left(2\mu\frac{\partial v_{\hat{y}}}{\partial \hat{y}} - \frac{2}{3}\mu\left(\frac{\partial v_{\hat{x}}}{\partial \hat{x}} + \frac{\partial v_{\hat{y}}}{\partial \hat{y}} + \frac{\partial v_{\hat{z}}}{\partial \hat{z}}\right)\right) \\
&\quad + \frac{\partial}{\partial \hat{x}}\left(\mu\left(\frac{\partial v_{\hat{x}}}{\partial \hat{y}} + \frac{\partial v_{\hat{y}}}{\partial \hat{x}}\right)\right) + \frac{\partial}{\partial \hat{z}}\left(\mu\left(\frac{\partial v_{\hat{y}}}{\partial \hat{z}} + \frac{\partial v_{\hat{z}}}{\partial \hat{y}}\right)\right) \\
\frac{\partial p}{\partial \hat{z}} &= \frac{\partial}{\partial \hat{z}}\left(2\mu\frac{\partial v_{\hat{z}}}{\partial \hat{z}} - \frac{2}{3}\mu\left(\frac{\partial v_{\hat{x}}}{\partial \hat{x}} + \frac{\partial v_{\hat{y}}}{\partial \hat{y}} + \frac{\partial v_{\hat{z}}}{\partial \hat{z}}\right)\right) \\
&\quad + \frac{\partial}{\partial \hat{x}}\left(\mu\left(\frac{\partial v_{\hat{x}}}{\partial \hat{z}} + \frac{\partial v_{\hat{z}}}{\partial \hat{x}}\right)\right) + \frac{\partial}{\partial \hat{y}}\left(\mu\left(\frac{\partial v_{\hat{y}}}{\partial \hat{z}} + \frac{\partial v_{\hat{z}}}{\partial \hat{y}}\right)\right)
\end{aligned}
\tag{A.2}
$$

In Equation (A.2), only the terms related to fluid pressure and viscous forces are kept. Concerning these last terms, the dimensional analysis [47] reveals that some viscous forces terms are negligible. The relevant viscous forces are related to the gradients of the fluid velocity $v_{\hat{x}}$ and $v_{\hat{z}}$ in the radial direction $\hat{y}$. Furthermore, since the viscous forces are negligible in the radial direction, then the pressure gradient in that direction is also negligible. Hence, Equation (A.2) can be simplified to:

$$
\begin{aligned}
\frac{\partial}{\partial \hat{y}}\left(\mu\frac{\partial v_{\hat{x}}}{\partial \hat{y}}\right) &= \frac{\partial p}{\partial \hat{x}} \\
\frac{\partial}{\partial \hat{y}}\left(\mu\frac{\partial v_{\hat{y}}}{\partial \hat{y}}\right) &= 0 \\
\frac{\partial}{\partial \hat{y}}\left(\mu\frac{\partial v_{\hat{z}}}{\partial \hat{y}}\right) &= \frac{\partial p}{\partial \hat{z}}
\end{aligned}
\tag{A.3}
$$

Assuming that the oil viscosity μ does not vary in the radial direction $\hat{y}$, and integrating over that direction, one obtains:

$$\begin{aligned}
\mu\left(\frac{\partial v_{\hat{x}}}{\partial \hat{y}}\right) &= \frac{\partial p}{\partial \hat{x}}\hat{y} + A_1 \\
\mu\left(\frac{\partial v_{\hat{y}}}{\partial \hat{y}}\right) &= B_1 \\
\mu\left(\frac{\partial v_{\hat{z}}}{\partial \hat{y}}\right) &= \frac{\partial p}{\partial \hat{z}}\hat{y} + C_1
\end{aligned} \tag{A.4}$$

Integrating again:

$$\begin{aligned}
v_{\hat{x}} &= \frac{1}{\mu}\left(\frac{\partial p}{\partial \hat{x}}\frac{\hat{y}^2}{2} + A_1\hat{y} + A_2\right) \\
v_{\hat{y}} &= \frac{1}{\mu}\left(B_1\hat{y} + B_2\right) \\
v_{\hat{z}} &= \frac{1}{\mu}\left(\frac{\partial p}{\partial \hat{z}}\frac{\hat{y}^2}{2} + C_1\hat{y} + C_2\right)
\end{aligned} \tag{A.5}$$

In Equation (A.5), analytical expressions for the oil velocity in the three directions are obtained, as a function of the radial coordinate $\hat{y}$. The following oil velocity boundary conditions, corresponding to the non-slip condition, are applied in order to obtain the integration constants A_i, B_i, C_i:

$$\begin{aligned}
v_{\hat{x}}\left(\hat{x}, \hat{y}=0, \hat{z}, t\right) &= 0 \\
v_{\hat{x}}\left(\hat{x}, \hat{y}=h, \hat{z}, t\right) &= \Omega R \\
v_{\hat{y}}\left(\hat{x}, \hat{y}=0, \hat{z}, t\right) &= 0 \\
v_{\hat{y}}\left(\hat{x}, \hat{y}=h, \hat{z}, t\right) &= \frac{\partial h}{\partial t} \\
v_{\hat{z}}\left(\hat{x}, \hat{y}=0, \hat{z}, t\right) &= 0 \\
v_{\hat{z}}\left(\hat{x}, \hat{y}=h, \hat{z}, t\right) &= 0
\end{aligned} \tag{A.6}$$

Consequently, Equation (A.5) becomes:

$$
\begin{aligned}
v_{\hat{x}} &= \frac{1}{\mu}\left(\frac{\partial p}{\partial \hat{x}}\frac{\hat{y}^2}{2} + \left(\frac{\mu \Omega R}{h} - \frac{\partial p}{\partial \hat{x}}\frac{h}{2}\right)\hat{y}\right) \\
v_{\hat{y}} &= \frac{\partial h}{\partial t}\frac{\hat{y}}{h} \\
v_{\hat{z}} &= \frac{1}{2\mu}\frac{\partial p}{\partial \hat{z}}\left(\hat{y}^2 - h\hat{y}\right)
\end{aligned}
\tag{A.7}
$$

To relate the velocity field component on each direction given in Equation (A.7), the mass conservation principle stated as the continuity equation for an incompressible fluid can be used:

$$
\frac{\partial v_{\hat{x}}}{\partial \hat{x}} + \frac{\partial v_{\hat{y}}}{\partial \hat{y}} + \frac{\partial v_{\hat{z}}}{\partial \hat{z}} = 0 \tag{A.8}
$$

Integrating it over the domain $\hat{y} = [0, h]$, and inserting Equation (A.7), one obtains:

$$
\begin{gathered}
\int_0^h \left(\frac{\partial v_{\hat{x}}}{\partial \hat{x}} + \frac{\partial v_{\hat{y}}}{\partial \hat{y}} + \frac{\partial v_{\hat{z}}}{\partial \hat{z}}\right) d\hat{y} = 0 \\
\frac{\partial}{\partial \hat{x}}\left(\frac{h^3}{12\mu}\frac{\partial p}{\partial \hat{x}}\right) + \frac{\partial}{\partial \hat{z}}\left(\frac{h^3}{12\mu}\frac{\partial p}{\partial \hat{z}}\right) = \frac{\partial h}{\partial t} + \frac{R\Omega}{2}\frac{\partial h}{\partial \hat{x}}
\end{gathered}
\tag{A.9}
$$

Equation (A.9) corresponds to the Reynolds Equation for an incompressible, laminar flow. A similar approach is followed to obtain the Modified Reynolds Equation for a controllable TPJB, being the only difference the boundary conditions stated in Equation (A.6). In order to include the effect of the radial oil injection in the orifice, the boundary conditions are slightly modified as follows:

$$
\begin{aligned}
v_{\hat{x}}\left(\hat{x},\hat{y}=0,\hat{z},t\right) &= 0\\
v_{\hat{x}}\left(\hat{x},\hat{y}=h,\hat{z},t\right) &= \Omega R\\
v_{\hat{y}}\left(\hat{x},\hat{y}=0,\hat{z},t\right) &= v_{inj}\\
v_{\hat{y}}\left(\hat{x},\hat{y}=h,\hat{z},t\right) &= \frac{\partial h}{\partial t}\\
v_{\hat{z}}\left(\hat{x},\hat{y}=0,\hat{z},t\right) &= 0\\
v_{\hat{z}}\left(\hat{x},\hat{y}=h,\hat{z},t\right) &= 0
\end{aligned}
\tag{A.10}
$$

Using this new set of boundary conditions, the rest of the procedure stays just the same.

Appendix B

Derivation of the Oil Film Energy Equation

In this appendix, the mathematical procedure for obtaining the Oil Film Energy Equation for an incompressible fluid is presented. The first principle to be invoked for this analysis is the conservation of energy. It can be stated in general as:

$$\begin{gathered}\textit{Rate of variation of internal energy} = \\ \textit{Heat flux through boundaries} + \textit{Work of surface and body forces}\end{gathered} \tag{B.1}$$

Each one of the physical phenomena stated in Equation (B.1) must be stated in mathematical terms, for the $(\hat{x}, \hat{y}, \hat{z})$ domain corresponding to the oil film flow within the bearing clearance.

B.1 Rate of variation of internal energy

The rate of variation of internal energy can be defined using a total derivative as:

$$\rho \frac{D}{Dt}\left(e + \frac{|\mathbf{v}|^2}{2}\right) \tag{B.2}$$

Where e corresponds to the internal energy per unit mass, and $\frac{|\mathbf{v}|^2}{2}$ corresponds to the kinematic energy of the fluid.
Regarding the total derivative of the internal energy per unit of mass e, for an incompressible fluid it can be written as function of the fluid temperature $T(\hat{x}, \hat{y}, \hat{z})$ using the thermal capacity of the fluid C_p:

$$\rho \frac{De}{Dt} = \rho C_p \frac{DT}{dt} = \rho C_p \left(\frac{\partial T}{\partial t} + v_{\hat{x}} \frac{\partial T}{\partial \hat{x}} + v_{\hat{y}} \frac{\partial T}{\partial \hat{y}} + v_{\hat{z}} \frac{\partial T}{\partial \hat{z}}\right) \tag{B.3}$$

For obtaining an expression for the kinematic energy, Newton Second Law is applied to the fluid flow on each direction, considering that the forces acting over it correspond to pressure forces and shear forces due to viscous effects. Hence, body forces are neglected. For each direction one has:

$$\begin{aligned}
\rho \frac{Dv_{\hat{x}}}{Dt} &= -\frac{\partial p}{\partial \hat{x}} + \frac{\partial \tau_{\hat{x}\hat{x}}}{\partial \hat{x}} + \frac{\partial \tau_{\hat{y}\hat{x}}}{\partial \hat{y}} + \frac{\partial \tau_{\hat{z}\hat{x}}}{\partial \hat{z}} \\
\rho \frac{Dv_{\hat{y}}}{Dt} &= -\frac{\partial p}{\partial \hat{y}} + \frac{\partial \tau_{\hat{x}\hat{y}}}{\partial \hat{x}} + \frac{\partial \tau_{\hat{y}\hat{y}}}{\partial \hat{y}} + \frac{\partial \tau_{\hat{z}\hat{y}}}{\partial \hat{z}} \\
\rho \frac{Dv_{\hat{z}}}{Dt} &= -\frac{\partial p}{\partial \hat{z}} + \frac{\partial \tau_{\hat{x}\hat{z}}}{\partial \hat{x}} + \frac{\partial \tau_{\hat{y}\hat{z}}}{\partial \hat{y}} + \frac{\partial \tau_{\hat{z}\hat{z}}}{\partial \hat{z}}
\end{aligned} \tag{B.4}$$

Since $|\mathbf{v}|^2 = v_{\hat{x}}^2 + v_{\hat{y}}^2 + v_{\hat{z}}^2$, the total derivative of the kinematic energy is given by:

$$\rho \frac{D}{Dt}\left(\frac{|\mathbf{v}|^2}{2}\right) = -v_{\hat{x}}\frac{\partial p}{\partial \hat{x}} - v_{\hat{y}}\frac{\partial p}{\partial \hat{y}} - v_{\hat{z}}\frac{\partial p}{\partial \hat{z}} + v_{\hat{x}}\left(\frac{\partial \tau_{\hat{x}\hat{x}}}{\partial \hat{x}} + \frac{\partial \tau_{\hat{y}\hat{x}}}{\partial \hat{y}} + \frac{\partial \tau_{\hat{z}\hat{x}}}{\partial \hat{z}}\right)$$
$$+ v_{\hat{y}}\left(\frac{\partial \tau_{\hat{x}\hat{y}}}{\partial \hat{x}} + \frac{\partial \tau_{\hat{y}\hat{y}}}{\partial \hat{y}} + \frac{\partial \tau_{\hat{z}\hat{y}}}{\partial \hat{z}}\right) + v_{\hat{z}}\left(\frac{\partial \tau_{\hat{x}\hat{z}}}{\partial \hat{x}} + \frac{\partial \tau_{\hat{y}\hat{z}}}{\partial \hat{y}} + \frac{\partial \tau_{\hat{z}\hat{z}}}{\partial \hat{z}}\right) \tag{B.5}$$

B.2 Heat flux through boundaries

The heat flux through the boundaries can be modelled using the thermal conductivity of the fluid κ and the temperature gradients as follows:

$$\kappa\left(\frac{\partial^2 T}{\partial \hat{x}^2} + \frac{\partial^2 T}{\partial \hat{y}^2} + \frac{\partial^2 T}{\partial \hat{z}^2}\right) \tag{B.6}$$

B.3 Work of surface forces

Considering pressure effect and viscous shear stresses, this effect can be modelled as follows:

$$\frac{\partial\left(v_{\hat{x}}\tau_{\hat{x}\hat{x}}\right)}{\partial \hat{x}} + \frac{\partial\left(v_{\hat{x}}\tau_{\hat{y}\hat{x}}\right)}{\partial \hat{y}} + \frac{\partial\left(v_{\hat{x}}\tau_{\hat{z}\hat{x}}\right)}{\partial \hat{z}} + \frac{\partial\left(v_{\hat{y}}\tau_{\hat{x}\hat{y}}\right)}{\partial \hat{x}} + \frac{\partial\left(v_{\hat{y}}\tau_{\hat{y}\hat{y}}\right)}{\partial \hat{y}} + \frac{\partial\left(v_{\hat{y}}\tau_{\hat{z}\hat{y}}\right)}{\partial \hat{z}}$$
$$+ \frac{\partial\left(v_{\hat{z}}\tau_{\hat{x}\hat{z}}\right)}{\partial \hat{x}} + \frac{\partial\left(v_{\hat{z}}\tau_{\hat{y}\hat{z}}\right)}{\partial \hat{y}} + \frac{\partial\left(v_{\hat{z}}\tau_{\hat{z}\hat{z}}\right)}{\partial \hat{z}} - \frac{\partial\left(v_{\hat{x}}p\right)}{\partial \hat{x}} - \frac{\partial\left(v_{\hat{y}}p\right)}{\partial \hat{y}} - \frac{\partial\left(v_{\hat{z}}p\right)}{\partial \hat{z}} \tag{B.7}$$

B.4 Energy Equation for the Passive TPJB

For the thin fluid film in the bearing clearance, the oil temperature T, viscosity μ and pressure field p are assumed as constant in the radial direction $\hat{y}$. A dimensional analysis [47] reveal that the relevant viscous forces terms correspond to the variation in the radial direction of $\tau_{\hat{y}\hat{x}}$ and $\tau_{\hat{y}\hat{z}}$. Hence, the formulation for the energy conservation principle can be reduced in steady state condition to:

$$\rho C_p\left(v_{\hat{x}}\frac{\partial T}{\partial \hat{x}}+v_{\hat{z}}\frac{\partial T}{\partial \hat{z}}\right)-v_{\hat{x}}\frac{\partial p}{\partial \hat{x}}-v_{\hat{z}}\frac{\partial p}{\partial \hat{z}}+v_{\hat{x}}\frac{\partial \tau_{\hat{y}\hat{x}}}{\partial \hat{y}}+v_{\hat{z}}\frac{\partial \tau_{\hat{y}\hat{z}}}{\partial \hat{y}}= \\ \kappa\left(\frac{\partial^2 T}{\partial \hat{x}^2}+\frac{\partial^2 T}{\partial \hat{z}^2}\right)+\frac{\partial\left(v_{\hat{x}}\tau_{\hat{y}\hat{x}}\right)}{\partial \hat{y}}+\frac{\partial\left(v_{\hat{z}}\tau_{\hat{y}\hat{z}}\right)}{\partial \hat{y}}-\frac{\partial\left(v_{\hat{x}}p\right)}{\partial \hat{x}}-\frac{\partial\left(v_{\hat{z}}p\right)}{\partial \hat{z}} \tag{B.8}$$

For a Newtonian fluid $\tau_{\hat{y}\hat{x}}=\mu\frac{\partial v_{\hat{x}}}{\partial \hat{y}}$ and $\tau_{\hat{y}\hat{z}}=\mu\frac{\partial v_{\hat{z}}}{\partial \hat{y}}$, hence:

$$\rho C_p\left(v_{\hat{x}}\frac{\partial T}{\partial \hat{x}}+v_{\hat{z}}\frac{\partial T}{\partial \hat{z}}\right)-v_{\hat{x}}\frac{\partial p}{\partial \hat{x}}-v_{\hat{z}}\frac{\partial p}{\partial \hat{z}}+v_{\hat{x}}\mu\frac{\partial}{\partial \hat{y}}\left(\frac{\partial v_{\hat{x}}}{\partial \hat{y}}\right)+v_{\hat{z}}\mu\frac{\partial}{\partial \hat{y}}\left(\frac{\partial v_{\hat{z}}}{\partial \hat{y}}\right)= \\ \kappa\left(\frac{\partial^2 T}{\partial \hat{x}^2}+\frac{\partial^2 T}{\partial \hat{z}^2}\right)+\mu\frac{\partial}{\partial \hat{y}}\left(v_{\hat{x}}\frac{\partial v_{\hat{x}}}{\partial \hat{y}}\right)+\mu\frac{\partial}{\partial \hat{y}}\left(v_{\hat{z}}\frac{\partial v_{\hat{z}}}{\partial \hat{y}}\right)-\frac{\partial\left(v_{\hat{x}}p\right)}{\partial \hat{x}}-\frac{\partial\left(v_{\hat{z}}p\right)}{\partial \hat{z}} \tag{B.9}$$

Reducing similar terms:

$$\rho C_p\left(v_{\hat{x}}\frac{\partial T}{\partial \hat{x}}+v_{\hat{z}}\frac{\partial T}{\partial \hat{z}}\right)-\kappa\left(\frac{\partial^2 T}{\partial \hat{x}^2}+\frac{\partial^2 T}{\partial \hat{z}^2}\right)=\mu\left(\left(\frac{\partial v_{\hat{x}}}{\partial \hat{y}}\right)^2+\left(\frac{\partial v_{\hat{z}}}{\partial \hat{y}}\right)^2\right) \tag{B.10}$$

In Equation (B.10), the terms related to convection effect, diffusion effect and source term related to viscous forces can be distinguished. The oil film velocity field $\mathbf{v}$ is already defined, see Appendix A, by considering non-slip boundary conditions at $\hat{y}=0$ and $\hat{y}=h$:

$$\begin{aligned} v_{\hat{x}} &= \frac{1}{\mu}\left(\frac{\partial p}{\partial \hat{x}}\frac{\hat{y}^2}{2}+\left(\frac{\mu\Omega R}{h}-\frac{\partial p}{\partial \hat{x}}\frac{h}{2}\right)\hat{y}\right) \\ v_{\hat{y}} &= \frac{\partial h}{\partial t}\frac{\hat{y}}{h} \\ v_{\hat{z}} &= \frac{1}{2\mu}\frac{\partial p}{\partial \hat{z}}\left(\hat{y}^2-h\hat{y}\right) \end{aligned} \tag{B.11}$$

Replacing the velocity components given in Equation (B.11) into Equation (B.10), and integrating over the domain $\hat{y} = [0, h]$, one obtains:

$$\kappa h \frac{\partial^2 T}{\partial \hat{x}^2} + \kappa h \frac{\partial^2 T}{\partial \hat{z}^2} + \left(\frac{\rho C_p h^3}{12\mu} \frac{\partial p}{\partial \hat{x}} - \frac{\rho C_p \Omega R h}{2} \right) \frac{\partial T}{\partial \hat{x}} + \frac{\rho C_p h^3}{12\mu} \frac{\partial p}{\partial \hat{z}} \frac{\partial T}{\partial \hat{z}} + (\Omega R)^2 \frac{\mu}{h} + \frac{h^3}{12\mu} \left(\left(\frac{\partial p}{\partial \hat{x}} \right)^2 + \left(\frac{\partial p}{\partial \hat{z}} \right)^2 \right) = 0 \quad \text{(B.12)}$$

B.5 Energy Equation for the Controllable TPJB

For the case of the controllable TPJB, Equation (B.12) still holds, but some extra terms must be included in order to model the effect of the radial oil injection within the orifice. The oil injection effect can be included by analyzing the energy conservation in the radial direction $\hat{y}$ within the injection orifice. It is assumed then that the convection, diffusion and viscous disipation effect in the circumferential and axial direction can be modelled in the same way, in the injection orifice and in the rest of the oil film domain.
Taking this simplication into account, in the radial direction of the injection orifice S_0 one can state the energy conservation principle as:

$$\rho C_p v_{\hat{y}} \frac{\partial T}{\partial \hat{y}} - v_{\hat{y}} \frac{\partial p}{\partial \hat{y}} + v_{\hat{y}} \frac{\partial \tau_{\hat{x}\hat{y}}}{\partial \hat{x}} + v_{\hat{y}} \frac{\partial \tau_{\hat{y}\hat{y}}}{\partial \hat{y}} + v_{\hat{y}} \frac{\partial \tau_{\hat{z}\hat{y}}}{\partial \hat{z}} = \kappa \frac{\partial^2 T}{\partial \hat{y}^2} + \frac{\partial \left(v_{\hat{y}} \tau_{\hat{x}\hat{y}} \right)}{\partial \hat{x}} + \frac{\partial \left(v_{\hat{y}} \tau_{\hat{y}\hat{y}} \right)}{\partial \hat{y}} + \frac{\partial \left(v_{\hat{y}} \tau_{\hat{z}\hat{y}} \right)}{\partial \hat{z}} - \frac{\partial \left(v_{\hat{y}} p \right)}{\partial \hat{y}} \quad \text{(B.13)}$$

Since within the injection orifice the flow is considered to be purely radial, the relevant shear stresses are $\tau_{\hat{x}\hat{y}}$ and $\tau_{\hat{z}\hat{y}}$, hence Equation (B.13) can be reduced to:

$$\rho C_p v_{\hat{y}} \frac{\partial T}{\partial \hat{y}} - v_{\hat{y}} \frac{\partial p}{\partial \hat{y}} + v_{\hat{y}} \frac{\partial \tau_{\hat{x}\hat{y}}}{\partial \hat{x}} + v_{\hat{y}} \frac{\partial \tau_{\hat{z}\hat{y}}}{\partial \hat{z}} = \kappa \frac{\partial^2 T}{\partial \hat{y}^2} + \frac{\partial \left(v_{\hat{y}} \tau_{\hat{x}\hat{y}} \right)}{\partial \hat{x}} + \frac{\partial \left(v_{\hat{y}} \tau_{\hat{z}\hat{y}} \right)}{\partial \hat{z}} - \frac{\partial \left(v_{\hat{y}} p \right)}{\partial \hat{y}} \quad \text{(B.14)}$$

Reducing similar terms:

$$\rho C_p v_{\hat{y}} \frac{\partial T}{\partial \hat{y}} = \kappa \frac{\partial^2 T}{\partial \hat{y}^2} + \tau_{\hat{x}\hat{y}} \frac{\partial v_{\hat{y}}}{\partial \hat{x}} + \tau_{\hat{z}\hat{y}} \frac{\partial v_{\hat{y}}}{\partial \hat{z}} - p \frac{\partial v_{\hat{y}}}{\partial \hat{y}} \tag{B.15}$$

For a Newtonian fluid $\tau_{\hat{x}\hat{y}} = \mu \frac{\partial v_{\hat{y}}}{\partial \hat{x}}$ and $\tau_{\hat{z}\hat{y}} = \mu \frac{\partial v_{\hat{y}}}{\partial \hat{z}}$, hence:

$$\rho C_p v_{\hat{y}} \frac{\partial T}{\partial \hat{y}} = \kappa \frac{\partial^2 T}{\partial \hat{y}^2} + \mu \left(\left(\frac{\partial v_{\hat{y}}}{\partial \hat{x}} \right)^2 + \left(\frac{\partial v_{\hat{y}}}{\partial \hat{z}} \right)^2 \right) - p \frac{\partial v_{\hat{y}}}{\partial \hat{y}} \tag{B.16}$$

Equation (B.16) contains a convection term, a diffusion term, and source terms corresponding to the work performed by viscous and pressure forces. Considering that the interest is focused in modeling the energy transfer from the injection point towards the oil film, Equation (B.16) can be simplified to the following terms:

$$\rho C_p v_{inj} \left(T_{inj} - T \right) + \kappa \frac{T_{inj} - T}{l_0} + \frac{4}{3} \frac{\mu}{h} v_{inj}^2 + p v_{inj} = 0 \tag{B.17}$$

Which are inserted into the oil film energy equation in order to include the oil injection effect.

Appendix C

Mathematical Model of the Pipeline Dynamics

In this appendix, the procedure for obtaining the mathematical model for the pipeline dynamics is presented. The solution presented here is based on the one presented in [62].

C.1 Governing equations: The Continuity and Navier-Stokes Equations

Consider Figure C.1 for the following analysis. A one-dimensional domain is defined for the analysis, taking into account the longitudinal coordinate x. Then, the state of the flow within the pipeline can be defined by its pressure $p(x,t)$ and volumetric flow $q(x,t)$. Considering that the density ρ of the fluid remains essentially constant along the pipeline, the continuity equation can be stated as follows [62]:

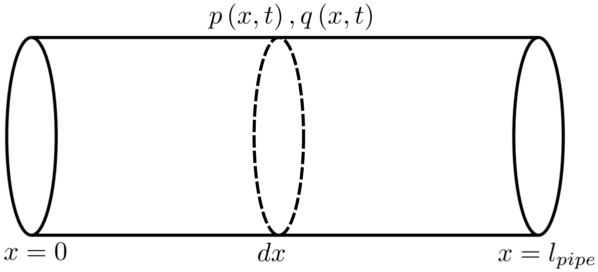

Figure C.1: *Mathematical model for the pipeline dynamics*

$$\frac{\partial p}{\partial t} + \frac{\rho c_0^2}{A_{pipe}} \frac{\partial q}{\partial x} = \frac{\rho c_0^2}{A_{pipe}} S_q$$
$$c_0 = \sqrt{\frac{\beta}{\rho}} \tag{C.1}$$

In Equation (C.1), the continuity equation for a differential pipeline element is stated as follows: the variation of flow in the longitudinal direction is equal to the flow put in or taken out of the system by the sinks or sources S_q, minus the variation of the fluid volume within the differential pipe element due to compressibility effects. Some parameters are introduced, such as the cross section area of the pipe A_{pipe} and the speed of sound c_0, which is a function of the equivalent bulk modulus of the flow β, calculated as:

$$\beta = \left[\frac{1-r}{\beta_{oil}} + \frac{r}{\beta_{air}} + C_{pipe} \right]^{-1} \tag{C.2}$$

Where r is the percentage of air in the total volume of fluid, β_{air} and β_{oil} the bulk modulus of air and oil respectively, and C_{pipe} the radial compliance of the pipe.
Applying the Navier-Stokes equation to the analyzed domain, they can be reduced to the following form [62]:

$$\frac{\partial q}{\partial t} + \frac{A_{pipe}}{\rho} \frac{\partial p}{\partial x} = \frac{F_{ext}}{\rho} \tag{C.3}$$

In Equation (C.3), it is stated that the variation of linear momentum of the fluid flow is due to the gradient of pressure in the longitudinal direction, and due to the action of externally applied forces per unit length F_{ext}. Consequently, the dynamic behavior of the oil within the pipeline can be determined by solving simultaneously the following set of equations (continuity and reduced Navier Stokes):

$$\begin{aligned} \frac{\partial p}{\partial t} + \frac{\rho c_0^2}{A_{pipe}} \frac{\partial q}{\partial x} &= \frac{\rho c_0^2}{A_{pipe}} S_q \\ \frac{\partial q}{\partial t} + \frac{A_{pipe}}{\rho} \frac{\partial p}{\partial x} &= \frac{F_{ext}}{\rho} \end{aligned} \tag{C.4}$$

C.2 Introducing the Boundary Conditions

Having defined the governing equations for the analyzed domain, it becomes necessary to apply a set of boundary conditions. In this case, they correspond to the volumetric flow q or pressure p at each end of the pipeline, namely, $x = 0$ and $x = l_{pipe}$.

It must be noted that it is not possible to impose simultaneously flow and pressure at one end of the pipeline, since these physical magnitudes are not independant from each other.

The analyzed pipeline in this case is the one existing in the controllable TPJB, i.e. it corresponds to the one connecting the servovalve with the injection point in the pad. For this configuration, the following set of boundary conditions are obtained:

$$\begin{aligned} q(x = 0, t) &= q_{servo} \\ p(x = l_{pipe}, t) &= p_{inj} \end{aligned} \tag{C.5}$$

Hence, one imposes the flow at the servovalve end of the pipeline ($x = 0$), by making it equal to the volumetric flow leaving/returning to the servovalve q_{servo}, and the pressure in the injection nozzle p_{inj} , at the end of the pipe connected with the bearing pad ($x = l_{pipe}$).

In order to introduce the boundary conditions in Equation (C.4), the sink/source term S_q and external forces F_{ext} terms can be stated using the delta Dirac function δ as follows:

$$\begin{aligned} F_{ext}(x,t) &= -\rho d_{pipe} q(x,t) - A_{pipe}\, p_{inj}\, \delta(x - l_{pipe}) \\ S_q(x,t) &= q_{servo}\, \delta(x) \end{aligned} \tag{C.6}$$

In Equation (C.6), the external forces arise from viscous losses effects, assumed to be proportional to the flow through the pipeline by the constant d_{pipe}, and from the pressure p_{inj} applied at $x = l_{pipe}$. On the other hand, the source term S_q includes the flow coming from the servovalve q_{servo} at $x = 0$.
Hence, Equation (C.4) can be rewritten taking into account the boundary conditions, as follows:

$$\begin{aligned} \frac{\partial p}{\partial t} + \frac{\rho c_0^2}{A_{pipe}} \frac{\partial q}{\partial x} &= \frac{\rho c_0^2}{A_{pipe}} q_{servo}\, \delta(x) \\ \frac{\partial q}{\partial t} + \frac{A_{pipe}}{\rho} \frac{\partial p}{\partial x} &= -d_{pipe} q(x,t) - \frac{A_{pipe}}{\rho} p_{inj}\, \delta(x - l_{pipe}) \end{aligned} \tag{C.7}$$

The continuity and reduced Navier-Stokes equation in Equation C.7 can be reduced into a single equation in terms of the volumetric flow rate $q(x,t)$:

$$\frac{\partial^2 q}{\partial t^2} + c_0^2\, q_{servo} \frac{\partial \delta(x)}{\partial x} - c_0^2 \frac{\partial^2 q}{\partial x^2} + d_{pipe} \frac{\partial q}{\partial t} + \frac{A_{pipe}}{\rho} \frac{d p_{inj}}{dt} \delta(x - l_{pipe}) = 0 \tag{C.8}$$

C.3 Solution by using the Separation of Variables method

The separation of variables method states that the flow rate function can be expressed as:

$$q(x,t) = \sum_{i=1}^{\infty} H_i(x)\, \gamma_i(t) \tag{C.9}$$

The first step is to determine the normal modes $H_i(x)$. Since these modes are a function of the system, independant from the boundary conditions, one sets $q_{servo} = 0$ and $p_{inj} = 0$. Replacing Equation (C.9) in Equation (C.8), one obtains the following relationship:

$$\frac{\ddot{\gamma}_i}{\gamma_i} + d_{pipe}\frac{\dot{\gamma}_i}{\gamma_i} = c_0^2\frac{H_i''}{H_i} = -\omega_i^2 \tag{C.10}$$

Where . denotes time differentiation and $'$ represents a derivative with respect to x. The normal modes $H_i(x)$ must satisfy Equation (C.10) and the following boundary conditions:

$$\begin{aligned} q\left(x=0,t\right) &= 0 \\ p\left(x=l_{pipe},t\right) &= \frac{\partial q}{\partial x}\left(x=l_{pipe},t\right) = 0 \end{aligned} \tag{C.11}$$

These constraints are satisfied using the following normal modes [62]:

$$\begin{aligned} H_i\left(x\right) &= sin\left(\frac{\omega_i x}{c_0}\right) \\ \omega_i &= \frac{\left(2i-1\right)\pi c_0}{2l_{pipe}} \end{aligned} \tag{C.12}$$

Consequently, the normal modes $H_i(x)$ and their corresponding acoustic natural frequencies ω_i are defined.
Introducing the separation of variables, Equation (C.9), in Equation (C.8), one obtains:

$$\sum_{i=1}^{\infty} H_i\ddot{\gamma}_i + c_0^2\, q_{servo}\frac{\partial\delta\left(x\right)}{\partial x} - c_0^2\sum_{i=1}^{\infty} H_i''\gamma_i + d_{pipe}\sum_{i=1}^{\infty} H_i\dot{\gamma}_i + \frac{A_{pipe}}{\rho}\dot{p}_{inj}\delta\left(x-l_{pipe}\right) = 0 \tag{C.13}$$

Multiplying Equation (C.13) by H_j and integrating it over the domain $x = [0, l_{pipe}]$, the following expression is obtained:

$$\begin{aligned} \ddot{\gamma}_j + d_{pipe}\dot{\gamma}_j + \omega_j^2\gamma_j &= c_0\,\omega_j\,q_{servo} - \frac{A_{pipe}}{\rho}\dot{p}_{inj}\left(-1\right)^{j+1} \\ \omega_j &= \frac{\left(2j-1\right)\pi c_0}{2l_{pipe}} \end{aligned} \tag{C.14}$$

By solving the second order differential equation stated in Equation (C.14), one can obtain the modal flow γ_j associated with each acoustic normal mode H_j. Then, Equation (C.9) enables to determine the flow rate $q(x,t)$ within the pipeline.

Even though the exact solution for $q(x,t)$ is determined by considering an infinite amount of acoustic modes and modal flows, this solution can be truncated to a finite number of modes depending on the frequency range of interest for the analysis. The number of relevant modes for the analysis is determined by determining which acoustic natural frequencies ω_j fall within the analyzed range.

Bibliography

[1] J. Glienicke, “Stabilitatsprobleme bei Lagerung schnellaufender Wellen - Berechnung, Konstruktion und Verhalten von Mehrflchen- und Kippsegmentlagern,” *Technische Akademie Wuppertal, Germany*, 1987.

[2] R. D. Flack and C. J. Zuck, “Experiments on the Stability of Two Flexible Rotor in Tilting Pad Journal Bearing,” *Tribology Trans.*, vol. 31, no. 2, pp. 251–257, 1988.

[3] J. Lund, “Spring and Damping for the Tilting Pad Journal Bearings,” *ASLE Trans.*, vol. 7, no. 4, pp. 342–352, 1964.

[4] J. Nicholas, “Lund’s Tilting Pad Journal Bearing Pad Assembly Method,” *ASME Journal of Vibrations and Acoustics*, vol. 125, pp. 448–454, October 2003.

[5] P. Allaire, J. Parsell, and L. Barrett, “A Pad Perturbation Method for the Dynamic Coefficients of Tilting-Pad Journal Bearings,” *Wear*, vol. 72, pp. 29–44, 1981.

[6] T. Dimond, A. Younan, and P. Allaire, “Comparison of Tilting-Pad Journal Bearing Dynamic Full Coefficient and Reduced Order Models Using Modal Analysis,” *ASME Journal of Vibration and Acoustics*, vol. 132, October 2010.

[7] T. Dimond, A. Younan, and P. Allaire, “The Effect of Tilting Pad Journal Bearing Dynamic Models on the Linear Stability Analysis of an 8-Stage Compressor,” *ASME Journal of Engineering for Gas Turbines and Power*, vol. 134, May 2012.

[8] J. Wilkes and D. Childs, "Tilting Pad Journal Bearings: A Discussion on Stability Calculation, Frequency Dependence, and Pad and Pivot Flexibility," *Proceeding of ASME Turbo Expo 2012*, 2012.

[9] T. Dimond, P. Sheth, P. Allaire, and M. He, "Identification methods and test results for tilting pad and fixed geometry journal bearing dynamic coefficients - A review," *Shock and Vibration*, vol. 16, pp. 13–43, 2009.

[10] K. Brockwell, D. Kleinbub, and W. Dmochowski, "Measurement and Calculation of the Dynamic Operating Characteristics of the Five Shoe Tilting-Pad Journal Bearing," *STLE Tribology Transactions*, vol. 33, no. 4, pp. 481–492, 1989.

[11] H. Ha and S. Yang, "Excitation Frequency Effects on the Stiffness and Damping Coefficients of a Five Pad Tilting Pad Journal Bearing," *ASME Journal of Tribology*, vol. 121, no. 3, pp. 517–522, 1999.

[12] W. Dmochowski, "Dynamic Properties of Tilting-Pad Journal Bearings: Experimental and Theoretical Investigation of Frequency Effects due to Pivot Flexibility," *ASME Journal of Engineering for Gas Turbines and Power*, vol. 129, pp. 865–869, July 2007.

[13] D. Childs and C. Carter, "Rotordynamics Characteristics of a Five Pad, Rocker-Pivot, Tilting Pad Bearing in a Load-on-Pad Configuration; Comparisons to Predictions and Load-Between-Pad Results," *ASME Journal of Engineering for Gas Turbines and Power*, vol. 133, August 2011.

[14] J. Lund, "The Influence of Pad Flexibility on the Dynamic Coefficients of a Tilting Pad Journal Bearing," *ASME Journal of Tribology*, vol. 109, pp. 65–70, 1987.

[15] C. Ettles, "The Analysis and Performance of Pivoted Pad Journal Bearings considering Thermal and Elastic Effects," *J. Lubr. Tech., ASME Trans.*, vol. 102, no. 2, pp. 182–194, 1980.

[16] C. Ettles, "The Analysis of Pivoted Pad Journal Bearing Assemblies considering Thermoelastic Deformation and Heat Transfer Effects," *STLE Tribology Transactions*, vol. 35, no. 1, pp. 156–162, 1992.

[17] K. Brockwell and W. Dmochowski, "Thermal Effects in the Tilting Pad Journal Bearing," *J.Phys.D: Appl.Phys*, vol. 25, pp. 384–392, 1992.

[18] M. Fillon, J. C. Bligoud, and J. Frêne, "Influence of Bearing Element Displacements on Thermohydrodynamic Characteristics of Tilting-Pad Journal Bearings," *Proceedings of the Japan International Tribology Conference, Nagoya 1990*, pp. 635–640, 1990.

[19] M. Fillon, J. C. Bligoud, and J. Frêne, "Experimental Study of Tilting-Pad Journal Bearings – Comparison with Theoretical Thermoelastohydrodynamic Results," *ASME Journal of Tribology*, vol. 114, pp. 579–588, 1992.

[20] L. Earles, A. Palazzolo, and R. Armentrout, "A Finite Element Approach to Pad Flexibility Effects in Tilting Pad Journal Bearings: Part I - Single Pad Analysis," *ASME Journal of Tribology*, vol. 112, pp. 169–177, 1990.

[21] L. Earles, A. Palazzolo, and R. Armentrout, "A Finite Element Approach to Pad Flexibility Effects in Tilting Pad Journal Bearings: Part II - Assembled Bearing and System Analysis," *ASME Journal of Tribology*, vol. 112, pp. 178–182, 1990.

[22] J. Kim, A. Palazzolo, and R. Gadangi, "TEHD Analysis for Tilting Pad Journal Bearings using Upwind Finite Element Method," *Tribology Transactions*, vol. 37, no. 4, pp. 771–783, 1994.

[23] J. Kim, A. Palazzolo, and R. Gadangi, "Dynamics Characteristics of TEHD Tilt Pad Journal Bearing Simulation including Multiple Mode Pad Flexibility," *ASME Journal of Vibration and Acoustics*, vol. 117, pp. 123–135, January 1995.

[24] C. Bouchoule, M. Fillon, D. Nicolas, and F. Barresi, "Experimental Study of Thermal Effects in Tilting-Pad Journal Bearings at High Operating Speeds," *ASME Journal of Tribology*, vol. 118, pp. 532–538, 1996.

[25] K. D. Wygant, R. D. Flack, and L. Barrett, "Influence of Pad Pivot Friction on Tilting-Pad Journal Bearing Measurements - Part I: Steady Operating Position," *Tribology Trans.*, vol. 42, no. 1, pp. 210–215, 1999.

[26] K. D. Wygant, R. D. Flack, and L. Barrett, "Influence of Pad Pivot Friction on Tilting-Pad Journal Bearing Measurements - Part II: Dynamic Coefficients," *Tribology Trans.*, vol. 42, no. 1, pp. 250–256, 1999.

[27] S. Kim and K. Kim, "Influence of pad pivot friction on tilting pad journal bearing," *Tribology International*, vol. 41, pp. 694–703, 2008.

[28] H. Ulbrich and J. Althaus, "Actuator Design for Rotor Control," *ASME Design Technical Conference: Proceedings of the 12th Bienial Conference on Mechanical Vibration and Noise*, pp. 17–22, 1989.

[29] I. F. Santos, "Design and Evaluation of Two Types of Active Tilting Pad Journal Bearings," in *The Active Control of Vibration* (C.R.Burrows and P.S.Keogh, eds.), pp. 79–87, London, England: Mechanical Engineering Publications Limited, 1994.

[30] I. Santos, "On the Adjusting of the Dynamic Coefficients of Tilting-Pad Journal Bearings," *STLE Tribology Transactions*, vol. 38, no. 3, pp. 700–706, 1995.

[31] D. Deckler, R. Veillette, M. Braun, and F. Choy, "Simulation and Control of an Active Tilting-Pad Journal Bearing," *STLE Tribology Transactions*, vol. 47, no. 3, pp. 440–458, 2004.

[32] A. Wu and M. De Queiroz, "A New Active Tilting-Pad Bearing: Non Linear Modeling and Feedback Control," *STLE Tribology Transactions*, vol. 53, no. 5, pp. 755–763, 2010.

[33] A. Wu, Z. Cai, and M. De Queiroz, "Model-Based Control of Active Tilting Pad Bearings," *IEEE/ASME Transactions on Mechatronics*, vol. 12, pp. 689–695, December 2007.

[34] I. F. Santos and F. Russo, "Tilting-Pad Journal Bearings with Electronic Radial Oil Injection," *Journal of Tribology, ASME Trans.*, vol. 120, no. 3, pp. 583–594, 1998.

[35] I. F. Santos and R. Nicoletti, "THD Analysis in Tilting-Pad Journal Bearings using Multiple Orifice Hybrid Lubrication," *Journal of Tribology, ASME Trans.*, vol. 121, pp. 892–900, 1999.

[36] I. F. Santos and R. Nicoletti, "Influence of Orifice Distribution on the Thermal and Static Properties of Hybridly Lubricated Bearings," *International Journal of Solids and Structures*, vol. 38, pp. 2069–2081, 2001.

[37] A. M. Haugaard and I. F. Santos, "Multi-orifice Active Tilting-Pad Journal Bearings-Harnessing of Synergetic Coupling Effects," *Tribology International*, vol. 43, no. 8, pp. 1374–1391, 2010.

[38] A. M. Haugaard and I. F. Santos, "Stability of Multi Orifice Active Tilting-Pad Journal Bearings," *Tribology International*, vol. 43, no. 9, pp. 1742–1750, 2010.

[39] I. F. Santos and A. Scalabrin, "Control System Design for Active Lubrication with Theoretical and Experimental Examples," *Journal of Engineering for Gas Turbines and Power, ASME Trans.*, vol. 125, pp. 75–80, January 2003.

[40] R. Nicoletti and I. Santos, "Frequency Response Analysis of an Actively Lubricated Rotor/Tilting-Pad Bearing System," *ASME Journal of Engineering for Gas Turbines and Power*, vol. 127, pp. 638–645, July 2005.

[41] R. Nicoletti and I. Santos, "Linear and Non-Linear Control Techniques Applied to Actively Lubricated Journal Bearings," *Journal of Sound and Vibration*, vol. 260, no. 5, pp. 927–947, 2003.

[42] R. Nicoletti and I. Santos, "Control System Design for Flexible Rotors Supported by Actively Lubricated Bearings," *Journal of Vibration and Control*, vol. 14, no. 3, pp. 347–374, 2008.

[43] I. F. Santos, "Theoretical and Experimental Identification on the Stiffness and Damping Coefficients of Active-Tilting Pad Journal Bearings," in *Identification in Engineering Systems* (M. Friswell and J. Mottershead, eds.), pp. 325–334, Swansea, Great Britain: The Cromwell Press Ltd., 1996.

[44] J. Andersen and E. Bureau, "Flexible Rotors Supported by Active Lubricated Journal Bearings: Observer Design," Master Thesis, Technical University of Denmark, 2009.

[45] A. Greve and S. Warburg, "Control Design for Flexible Rotors Supported by Controllable Oil Film Bearings," Master Thesis, Technical University of Denmark, 2010.

[46] B. B. Nielsen, "Creation of a Mechatronic Tilting Pad Test Rig," Master Thesis, Technical University of Denmark, 2010.

[47] B. Hamrock, *Fundamentals of Fluid Film Lubrication.* McGraw-Hill, 1994.

[48] S. Taniguchi, T. Makino, T. Takeshita, and T. Ichimura, "A Thermohydrodynamic Analysis of Large Tilting-Pad Journal Bearing in Laminar and Turbulent Flow Regimes With Mixing," *Journal of Tribology, ASME Trans.*, vol. 112, pp. 542–550, July 1990.

[49] J. Knight and L. Barrett, "Analysis of Tilting Pad Journal Bearings with Heat Transfer Effects," *ASME Journal of Tribology*, vol. 110, pp. 128–133, 1988.

[50] A. M. Haugaard, "On Controllable Elastohydrodynamic Fluid Film Bearings," PhD Thesis, Technical University of Denmark, 2010.

[51] R. Cook, *Concepts and Applications of Finite Element Analysis.* Wiley and Sons, Inc., 1974.

[52] H. Merritt, *Hydraulic Control Systems.* Wiley and Sons, Inc., 1967.

[53] I. F. Santos, "Active Tilting Pad Bearings - Theory and Experiment," *VDI Fortschritt-Berichte, Reihe 11: Schwingungstechnik*, no. 189, 1993.

[54] F. Edelmann, "High-Response Servovalves and their applications," *Ölhydraulik und Pneumatik*, no. 30, pp. 1–6, 1986.

[55] W. Thayer, "Transfer Functions for MOOG Servovalves," *MOOG Technical Bulletin*, vol. 103, pp. 1–11, 1965.

[56] B. Datta, S. Akella, and S. G.L., "Effect of Entrained Air on Dynamic Characteristics of Hydraulic Servosystem with Asymmetric Linear Motor," *Meccanica*, vol. 21, pp. 51–57, 1986.

[57] J. Watton, "The Generalized Response of Servovalve Controlled, Single Rod, Linear Actuators and the Influence of Transmission Line Dynamics," *ASME Journal of Dynamic Systems, Measurement and Control*, vol. 106, pp. 157–162, June 1984.

[58] P. FitzSimons and J. Palazzolo, "Part I: Modeling of a One Degree of Freedom Active Hydraulic Mount," *ASME Journal of Dynamic Systems, Measurement and Control*, vol. 118, pp. 439–442, September 1996.

[59] R. Anderson and P. Li, "Mathematical Modeling of a Two Spool Flow Control Servovalve Using a Pressure Control Pilot," *ASME Journal of Dynamic Systems, Measurement and Control*, vol. 124, pp. 420–427, September 2002.

[60] J. Watton and M. Tadmori, "A comparison of techniques for the analysis of transmission line dynamics in electrohydraulic control systems," *Appl. Math. Modelling*, vol. 12, pp. 457–466, October 1988.

[61] D. Matko, G. Geiger, and W. Gregoritza, "Pipeline Simulation Techniques," *Mathematics and Computers in Simulation*, vol. 52, pp. 211–230, 2000.

[62] L. Yang, J. Hals, and T. Moan, "Comparative Study of Bond Graph Models for Hydraulic Transmission Lines with Transient Flow Dynamics," *ASME Journal of Dynamic Systems, Measurement and Control*, vol. 134, May 2012.

[63] A. Brooks and T. Hughes, "Streamline Upwind/Petrov-Galerkin Formulations for Convection Dominated Flows with Particular Emphasis on the Incompressible Navier-Stokes Equation," *Computer Methods in Applied Mechanics and Engineering*, vol. 32, pp. 199–259, 1982.

[64] T. Someya, *Journal Bearing Databook*. Berlin, Heidelberg: Springer-Verlag, 1989.

[65] J. Nicholas, E. Gunter, and A. P.E., "Stiffness and Damping Coefficients for the Five-Pad Tilting-Pad Bearing," *ASLE Transactions*, vol. 22, no. 2, pp. 113–124, 1979.

[66] D. Inman, *Engineering Vibration*. Prentice Hall, 2001.

[67] R. Moffat, "Describing the Uncertainties in Experimental Results," *Experimental Thermal and Fluid Science*, vol. 1, pp. 3–17, 1988.